PERFORMANCE OF VEGETATION, ON MINED SANDS

by

L.C. Bliss (ed.)
Department of Botany
University of Alberta

for

ALBERTA OIL SANDS ENVIRONMENTAL RESEARCH PROGRAM

Project VE 6.1

1979

TABLE OF CONTENTS

ABSTRACT

This report, covering the results of the 1977 research, adds significantly to the earlier findings. It is always difficult to predict long term plant responses on only a few years of data; in this case, only two years.

Climatically the two summers (May - August) were very similar, with the mean monthly temperatures averaging 0.2°C lower in 1977. Precipitation was ≈20% higher in 1977, cloud cover was also greater, and as a result, diffuse radiation was higher. Short wave and net radiation were similar to the previous year. Net radiation increased from 70W m^{-2} in early March to a maximum 207W m^{-2} in mid-June. Photosynthetically active radiation (PHAR) was about 50% of incoming radiation, similar to other temperate region studies.

Summer climate of the Richardson Lookout Station is similar to the long term summer climate at Fort McMurray. Temperatures for May through August were slightly warmer (0.4 to 1.3°C) at Richardson and precipitation is ≈20 mm less than at Fort McMurray. There are also fewer summer days with precipitation at the research site (44 vs. 55 days).

As found the previous year, little precipitation runs off these porous sands. During spring thaw, water runs down slope within the soil. about the frozen soil layer. About 50% of total precipitation moves out of the rooting zone to greater soil depths and is therefore unavailable for plant growth. The

Jack Pine forest and its limited understory use only 170-200 mm of water per year, yet soil water potentials seem to not drop below 1.0 MPa.

Microclimate within a forest canopy is difficult to measure and this is further complicated by working on a slope. As in 1976, gradients of temperature, water vapour and wind were small within the forest canopy. The exchange surfaces for heat and water vapour are diffuse due to openness of the canopy and its slope position. In spite of this, the canopy acts as a "surface layer" for radiation. On nights with little cloud cover and light winds (0.5 to 0.8 m s^{-1}) cold air drainage was greatest, resulting in temperature differences of 3.5 to 7.0°C between the mid-slope and bottom-slope sites.

Soit heat flux amounted to 7% of ned radiation measured above the canopy. Soils were naturally warmest near the surface, decreasing in heat with depth. At 200 cm soils were generally 8 to 10°C cooler than at -2 cm and the time lag for heat transfer to the deepest level measured was 3-4 days.

As observed in 1976, interception of precipitation by the tree canopy and trunk is high in storms with little precipitation and rains of low intensity predominate. On average, 53% of all precipitation was absorbed by the trees. Interception was greatest (44%) near the tree base (25 cm) and significantly less (17%) at a distance of 1 m.

As a result of increased turbulent exchange within

the forest canopy a more homogeneous environment of temperature, water vapour, and air movement results. This, however, makes it more difficult to establish the actual sources and sinks within a Jack Pine forest.

The field and laboratory data on young and mature Jack Pine show how well this tree species is adapted to high water stress environments. As with other conifers, this species has relatively low maximum net assimilation rates (6 to 8 mg dm^{-2} h^{-1}). After two drying cycles, maximum rates were 4.5 mg dm^{-2} h^{-1}. This indicates some supression of photosynthetic capacity following severe drought yet an ability for considerable recovery. Net assimilation reached zero at -2.2 MPa leaf water potential, again indicating a considerable adaptation to stressful environments.

Trees avoid winter and spring drought stress by maintaining high leaf resistances; the stomates remain closed when the soils are frozen. In winter cavitation does not occur and as a result, water columns are maintained in the xylem and therefore a better water balance.

In summer the stomates are sensitive to atmospheric VPD and close prior to xylem tension or ψ leaf triggered closure. Considerable osmotic adjustment also occurs which permits further water uptake as ψ soil increases. The lethal limit for ψ leaf is at least -3.5 to -4.0 MPa. Under extreme drought conditions the more photosynthetically active needles survive at the expense of the young ones.

All of these data contribute to a more complete understanding of why Jack Pine is so well adapted to these cold winter and warm droughty summer conditions that dominate these porous sands.

The mycorrhizal studies showed that 14 species of fungi formed mycorrhizae with Jack Pine under synthetic conditions. From this work and the field studies, it appears that no small group of fungi dominate the below ground symbiotic system. In the field 57 species of fungi were found associated with Jack Pine within a limited area. The synthesis test showed that a variety of fungi produce the non-descript associations found in the field.

Mycorrhizal fungi were studied in relation to *Arctostaphylos uva-ursi* and all of the infections were of the ectendomycorrhizal type.

Fifteen species of mycorrhizal fungi were grown at different osmotic potentials using NaCl and sucrose. All species grew the most at high osmotic potentials (-0.16 and -0.61 MPa). This differs from other studies for the fungi grew most at lower potentials (-1.5 to 5.8 MaPa).

In summary this second year of limited field work but intensive laboratory and greenhouse studies contribute to a much fuller understanding of the factors related to the very successful growth of Jack Pine and its associated lichen understory on these deep sands.

1. LONG TERM PREDICTION OF VEGETATION PERFORMANCE ON MINED SANDS

L. C. Bliss
Department of Botany
University of Alberta

1.1 INTRODUCTION

The original objective of studying both native and agronomic species that might be of use in stabilizing mined sands was not achieved because the project was terminated without studying the performance of species planted on the GCOS dike. However, the performance of the major native species inhabiting sand slope, Jack pine, was thoroughly studied and provides considerable insight into how plants survive on nutrient-poor drought prone sands. The implications of these results are discussed on page of the physiology section.

This report is meant to be added to the original report. There is little if any overlap between the two reports. The organization is the same as the previous report, therefore if there is nothing further to report, the section will just state "See previous report".

2. SITE DESCRIPTION

L. C. Bliss and D. W. A. Whitfield
Department of Botany
University of Alberta

"See previous report"

3. CLIMATE AND MICROMETEOROLOGY

C. Labine and K. Hage
Division of Meteorology, Department of Geography
University of Alberta

3.1 INTRODUCTION

There have been several major studies of the meteorology within forest canopies in the past few years (Baumgartner 1965, Gay 1972, Landsberg and Thom 1971, Landsberg and Jarvis 1973, Mukammal 1971, Stewart and Thom 1973 and Thom et al. 1975). Because of the complex structure of the canopy, the actual micrometeorology of the forest is still not fully understood (Jarvis et al. 1976). In fact a recent workshop on forest meteorology (Hutchison 1979) stresses that "lack of knowledge and understanding of the mechanisms involved in turbulent exchanges of sensible heat, mass and momentum within forests and across forest-atmosphere interfaces is, without doubt, the most critical current problem of forest meteorology". Knowledge is not totally lacking, however. We have some understanding of unique features of the forest canopy such as the air flow within the trunk space area. From a number of studies involving flux-profile relationships it was found that the simple similarity relationships of other vegetated surfaces could not be applied to the forest canopy. The radiative properties of the forest are perhaps better understood than the turbulent processes. Several radiation components can be determined by means of mathematical models and computer techniques and several studies have elucidated the variations of radiation within the canopy as well as the spectral properties of the leaves themselves. The major area which needs further research

in forest radiation is the role of the structure and geometry of forests and validation of radiation theory and modelling with real data.

Nevertheless, in spite of the complexities of the forest canopy and the gaps in our present understanding a field research program was undertaken to support the main objectives of the revegetation-modelling project. The purpose of the project (see Bliss, this report) was to provide management with information on our ability to predict the success or failure of different kinds of vegetation on raw sands. A first and practical revegetation problem was a tailings dike. This forced the selection of a sloped site with slope, aspect and orientation similar to those of the G.C.O.S. dike. The choice of a sloped site eliminated all possibilities of having horizontal uniformity and consequently eliminated the use of flux-profile techniques and measurements which otherwise could have been used to understand some of the micrometeorological processes within the forest canopy.

The field site was at the Richardson Fire Tower in northeastern Alberta. The main site characteristics as well as plant community structure have previously been described (Bliss and Whitfield 1977). Briefly, the site is a pine-lichen woodland having open stands of *Pinus banksiana* with a ground cover of lichens, mostly *Cladina mitis*, scattered dwarf shrubs of *Arctostaphylos uva-ursi* and a few forbs characteristic of the dry sandy soils in northeastern Alberta and northern Saskatchewan. The site was chosen because it is representative of pine-lichen woodland, and because its slope is similar to that of a west-southwest sand dike slope. Such a site represents a severe environment for plant growth and one that is expected to be difficult to revegetate. The hill slope

(2.3:1 rise, 19° slope and 20° south of west aspect) has a porous sand surface. The mean tree height is approximately 6 m with an average density of 72 trees per 100 m^2.

In a multi-disciplinary study such as this it is necessary to describe the state of the atmosphere to which living organisms are exposed; this was accomplished by describing the characteristics of the climate of the area as well as the microclimate within the plant canopy. In this section we describe the microclimate of the jack pine forest with emphasis on the distribution of radiation, temperature, wind and water vapour within the canopy. A second equally-important objective of the field measurement program was to provide long-term atmospheric driving variables for the air-plant-soil computer model component of the project (Mehlenbacher and Whitfield 1977).

In order to meet these objectives large field-measurement and data-processing programs were undertaken. Apart from the problems associated with a sloped study area, many of the usual problems related to field projects in remote areas were encountered. Lack of an A.C. power line required the use of a portable generator and the operation of a generator in such a dusty and hot environment occasionally led to problems and loss of data. The dusty environment also necessitated frequent sensor and equipment maintenance. In spite of the accessibility of the site by airplane, any instrument problems were compounded by the longer turn-around time between leaving the site and returning from the manufacturer. Finally, budget restraints made it impossible to use enough sensors and measurement sites to guarantee fully representative measurement samples from a site of such complex structure.

3.2 METHODS AND MATERIALS

The general approach to the measurement program reflected the dual purposes of the microclimate study. At one level a long term collection of some standard meteorological variables was undertaken in order to describe the climate and microclimate of the area and also to furnish the computer model with some essential atmospheric driving variables. At a second more detailed level, frequent short-term measurements were undertaken during the so-called intensive runs. The purpose of these intensive runs, which were normally of 24 to 48 hour duration, was to monitor the response of the trees and lichens to environmental conditions at key seasonal plant development stages (spring snow melt, spring growth, mid and late summer, fall initial dormancy and winter dormancy). These intensive runs also allowed us to better describe the plant-atmosphere relationships and to assist in verifying and correcting the model.

Two special-purpose experiments were also conducted to help clarify the relationships between tree and canopy geometry and the unique atmospheric properties which are found within the forest canopy. The major experiment involved a series of radiation transects at several heights within the canopy and at two sites on the slope. Details of the radiation transect experiments are discussed in a separate section. The other special-purpose experiment involved measurements of precipitation interception by the forest canopy.

The first field season went from May, 1976 through to early January, 1977. The second and final field season took place from March to August, 1977. Table 1 gives information on the time spans and dates

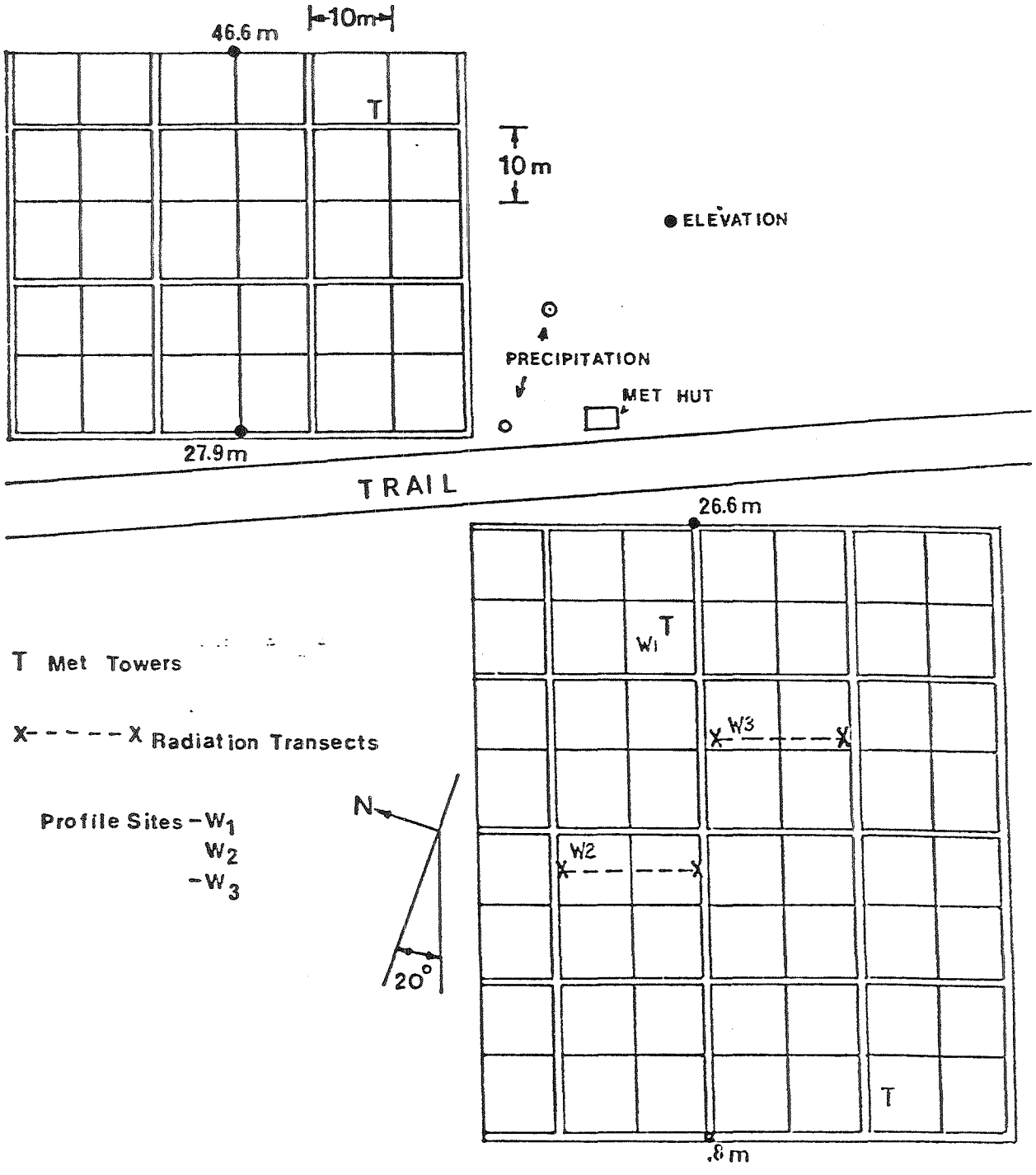

Figure 1. Site of measurements on hillside. Distribution of plots and meteorological instruments is shown .

Table 1. Record of Field Measurements

1976 Field Season: May 1 - December 31 1976
1977 Field Season: January 1977, March 7 - August 15 1977

Intensive Runs *:

April 3-4 1976	May 9-11 1976
June 2-3 1976	June 29-30 1976
July 20-23 1976	Aug. 17-20 1976
Sept. 24-27 1976	June 1-5 1977

Radiation Transects :

April 16 1977	May 1 1977
May 27 1977	June 6 1977
June 17 1977	June 18 1977
June 19 1977	June 28 1977
July 31 1977	Aug. 1 1977
Aug. 2 1977	Aug. 10 1977
Aug. 14 1977	

Wind, Air Temperature and Dew Point Temperature Profile Measurements :

(Date and Time Periods in hours are shown)

June 1 1977 8 h	June 3 1977 12 h
June 4 " 14 h	June 5 " 7 h
June 8 " 3 h	June 11 " 2 h
June 12 " 2 h	June 15 " 3 h
June 16 " 2 h	June 17 " 2 h
June 20 " 4 h	June 21 " 4 h
June 23 " 8 h	June 24 " 10 h
June 27 " 8 h	June 28 " 3 h
June 30 " 2 h	July 1 " 6 h
July 8 " 3 h	July 9 " 2 h
July 12 " 4 h	July 14 " 6 h
July 16 " 3 h	July 18 " 2 h
July 19 " 3 h	July 22 " 3 h
July 24 " 3 h	July 26 " 3 h
July 27 " 4 h	July 29 " 2 h
July 30 " 6 h	Aug. 1 " 3 h
Aug. 6 " 8 h	Aug. 7 " 8 h
Aug. 8 " 8 h	Aug. 9 " 9 h
Aug. 10 " 6 h	Aug. 11 " 7 h
Aug. 12 " 6 h	Aug. 13 " 3 h

Table 2. Continuous data logging system and sensors used to measure and produce atmospheric driving variables.

SENSOR	PARAMETER MEASURED
Eppley Precision pyronometer (280-2850 nm)	Global Incoming Radiation
Eppley Infra Red Radiometer (3500-50,000 nm)	Long Wave Incoming Radiation
Eppley Precision pyranometer (with filter 695-2850 nm)	Near Infra Red Radiation
Kipp and Zonen solarimeter (with shadow band)	Diffuse Sky Radiation
Kahlisco Radiation Balance Probe (300-6000 nm)	All Wave Incoming & All Wave Outgoing Radiation
Copper-Constantan Thermocouples	Air Temperature at 8 m Air Temperature at 0.05 m
Lambrecht Pernix Humidity Transmitter	Relative Humidity at 8 m Relative Humidity at 0.05 m
Climet Model 011-2b Anemometer	Wind Speed at 8 m
Stewart Electric Wind Vane	Wind Direction at 8 m
Weather Measure Tipping Bucket	Precipitation
Other Variables	
C.S.I.R.O. Soil Heat Flux Plate	Soil Heat Flux
Copper-Constantan Thermocouples	Air Temperature near top of slope Air Temperature at bottom of slope Soil Temperatures at 0.02,0.08,.25 and 2.0
Lambda Quantum Sensor (400-700 nm)	Photosynthetically Active Radiation

Data Logger: Campbell Scientific CR5 Digital Recorder
Data Recorder: D. C. Operated Facit 4070 Paper Tape Punch
Sampling Time: Integrated values over 30 min. period,printed every 30 min.

Table 3. Data logging system and sensors used during intensive runs.

SENSOR	PARAMETER MEASURED
Eppley Precision pyronometer (280-2850 nm)	Global Incoming Radiation
Eppley Infra Red Radiometer (3500-50,000 nm)	Long Wave Incoming Radiation
Eppley Precision pyranometer (with filter 695-2850 nm)	Near Infra Red Radiation
Kipp and Zonen solarimeter (with shadow band)	Diffuse Sky Radiation
Kahlisco Radiation Balance Probe (300-6000 nm)	All Wave Incoming & All Wave Outgoing Radiation
Copper-Constantan Thermocouples	Air Temperature 0.25, 0.5, 1.0, 2.0 3.0, 4.0, 5.0, 6.0 m Soil Temperatures 0.01, 0.02, 0.04, 0.08, 0.125, 0.25, 2.0, 6.0 m

Data Logger: A.C. Operated Fluke 2240A
Data Recorder: A.C. Operated Facit 4070 Paper Tape Punch

Sampling Time: Every three minutes during intensive runs.

of the field measurements of the continuous system, the intensive runs, and the profile and interception measurements. Figure 1 shows the location of the measuring sites on the hill as well as the general location of the hill.

As mentioned previously, two main types of data acquisition systems were used in order to fulfill the two objectives of the meteorological phase of the project. The first, labelled as the continuous system, was used to measure the model driving variables and long-term climatic variables and is described in Table 2. The second, labelled as the intensive run system, was used for several short periods and is summarized in Table 3.

In addition to the automatic acquisition of data during the intensive runs, vertical profiles of wind and water vapour were measured and recorded manually; every 14 minutes for the wind and every 15 minutes for the dew point. Sensitive RIMCO three-cup anemometers were installed at several heights and at three sites on the slope for wind profile measurements. There were some variations in anemometer-heights because it was not always possible to place the anemometers at exactly the same level at each site due to interference by branches. Specific heights are included with tables of results but generally the anemometers were at 0.5, 1.0, 1.5, 2.0, 3.0, 4.0, 5.0, 6.0 and 8.0 m. For water-vapour profiles a model 880 dew point hygrometer (Environmental Equipment Division) with four sensors was used. These sensors were installed at 0.5, 2.0, 4.0 and 6.0 m at each of the three profile measuring sites. Both anemometers and dew point hygrometers were on loan from the Meteorology Division, University of Alberta.

Precipitation measurements were made automatically using a Weather Measure tipping bucket raingauge attached to the Campbell data logger, and manually using a Taylor Clear View raingauge read at 0900h. Special investigations of precipitation interception by the canopy were also undertaken. Juice cans (48 oz) were used to measure interception at 11 sites on the hill. Whistance-Smith (1973) found that these were accurate raingauges. One can was placed in a clearing to measure the total amount of rainfall and two cans were placed at 0.5 m from the trunk of a tree. In addition, four trees were intensively sampled using radial lines of cans from near the trunk to the extremities of the branches. Cans were spaced at 0.25, 0.50, 0.75 and 1.0 m from the trunk along these lines. This allowed us to look at the variability of precipitation interception under the canopy.

3.3 RESULTS AND DISCUSSION

3.3.1 Climate

The climate of the oil sands area has been described recently by Longley and Janz (1978) as continental. Data from the Richardson Lookout station operated by the Alberta Forestry Service and the site of the measurements described here, were included in their analyses.

Long-term records and recent five-year means show that generally, Richardson Lookout is a warmer site than Fort McMurray Airport (Fig. 2) The long-term normals show that in May, there is little difference in temperature between the two sites; Richardson is only 0.4^{o}C cooler than Fort McMurray (8.6 vs. 9.0^{o}C, respectively). During the summer months, however, Richardson Lookout remains consistently warmer than Fort

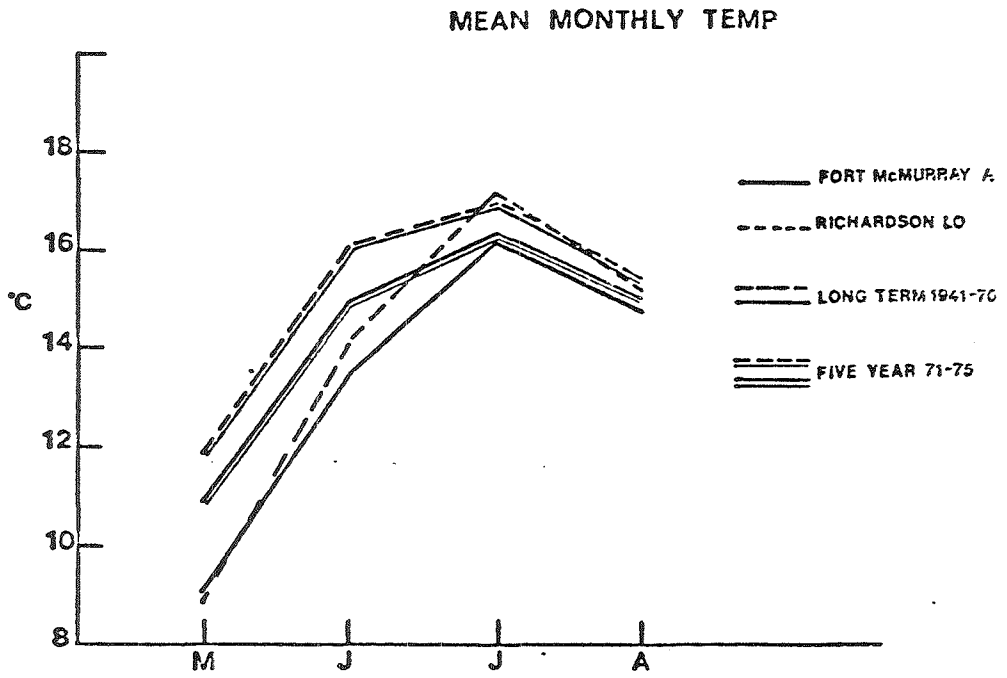

Figure 2. Mean monthly temperatures for Fort McMurray Airport and and Richardson Lookout. Long term and recent five year means are shown .

McMurray, although by only 1°C. Recent five-year means show a slightly larger difference; Richardson is still the warmer site (Fig. 2). The greatest difference occurred in June (ΔT 1.3°C) while May showed Richardson being 1° warmer as opposed to the long-term records. July and August had essentially the same pattern for the recent five-year normals as for the long-term pattern.

Long-term precipitation data show that Richardson receives less rainfall than Fort McMurray Airport (Table 4) for all summer months except August. On a total basis for the months of May to August, Richardson Lookout had 20.1 mm less precipitation than Fort McMurray for the long-term mean. Longley and Janz (1978) further point out that Richardson Lookout was an anomaly with 44 days with precipitation for the five warm months as opposed to 55 days at Fort McMurray, a further indication of the drier nature of the Richardson area.

In conclusion, one could simply say that Richardson is slightly warmer and drier than Fort McMurray during the growing season.

3.3.2 The Climates of 1976 and 1977

Monthly climatic summaries for the 1976 and 1977 summer field seasons are presented in Table 5.

The global incoming shortwave radiation regime shows many similarities in the two years. May 1976 had almost the same amount of incoming solar radiation as May 1977; the same was true for July. June 1977 had slightly more incoming radiation than June 1976. The largest observed difference occurred in August with 1976 receiving 50 Wm^{-2} more than in 1977.

Table 4. Total monthly precipitation data for Richardson, Richardson L. O. and Ft. McMurray Airport (mm).

STATION	MAY	JUNE	JULY	AUG.	TOTAL
Ft. McMurray A. (1941-1970)	33.0	61.5	73.7	64.0	232.2
Richardson (L. O.) (1941-1970)	24.9	56.6	57.4	73.4	212.3
Richardson (our site) (1976)	22.3	71.9	67.7	33.3	195.2

Table 5. Monthly climatic summary (1976,1977)

PARAMETER		MAY	JUNE	JULY	AUG.	
Mean daily Incoming Radiation (Wm^{-2})	1976	216	213	194	229	
	1977	200	229	204	180	
Mean daily Diffuse Radiation (% Incoming)	1976	34	39	37	23	
	1977	40	40	40	44	
Mean daily Longwave Radiation (Wm^{-2})	1976	323	335	391	288	
	1977	391	432	427	404	
Mean daily Net Radiation (Wm^{-2})	1976	156	177	151	190	
	1977	154	176	163	M	
Temperature (C)	1976	13.8	17.3	17.5	17.6	
	1977	13.7	16.2	16.2	13.4	
Wind speed (ms^{-1})	1976	1.96	1.91	1.76	1.59	
	1977	1.62	1.77	1.49	1.65	
Total Precipitation (mm)	1976	22.3	71.9	67.7	33.3	TOTAL 195.2
	1977	57.7	43.2	85.4	46.0	233.1

The percentage of diffuse radiation to incoming radiation was consistently greater in 1977 because of the higher amounts of cloud cover that field season; the differences ranged from only 1.5% in June, which is usually the month of maximum precipitation, to 20% in August. Longwave incoming radiation values also showed consistently higher fluxes in 1977, again as a result of cloud cover. With overcast sky conditions, the sky radiant temperature is higher and therefore the amount of emitted longwave thermal energy is greater.

The net radiation values are the differences between incoming and outgoing radiation and therefore are strongly dependent on the radiative properties of the surface. Since the surface did not change, the net radiation values were quite similar in May, June and July in both years. Net radiation values for August 1977 are not available due to instrument problems.

The temperature regime depends to a large extent on the radiation regime. The mean monthly temperatures for both years in May were almost the same (13.8 vs. 13.7^{o}C). June and July of 1977 were approximately 1^{o}C cooler than in 1976 a further indication of the greater amount of clouds in 1977. August 1977 was cooler by more than 4^{o}C than August 1976 which is not surprising since the incoming radiation was lower by 21% in August 1977 from the previous year.

The precipitation values reveal substantial month-to-month and year-to-year variability. On a total basis for both field seasons, 1977 had 28 mm of rain more than 1976, while on a month-to-month basis May, July and August had more precipitation in 1977 while only June had less precipitation in 1977 than 1976.

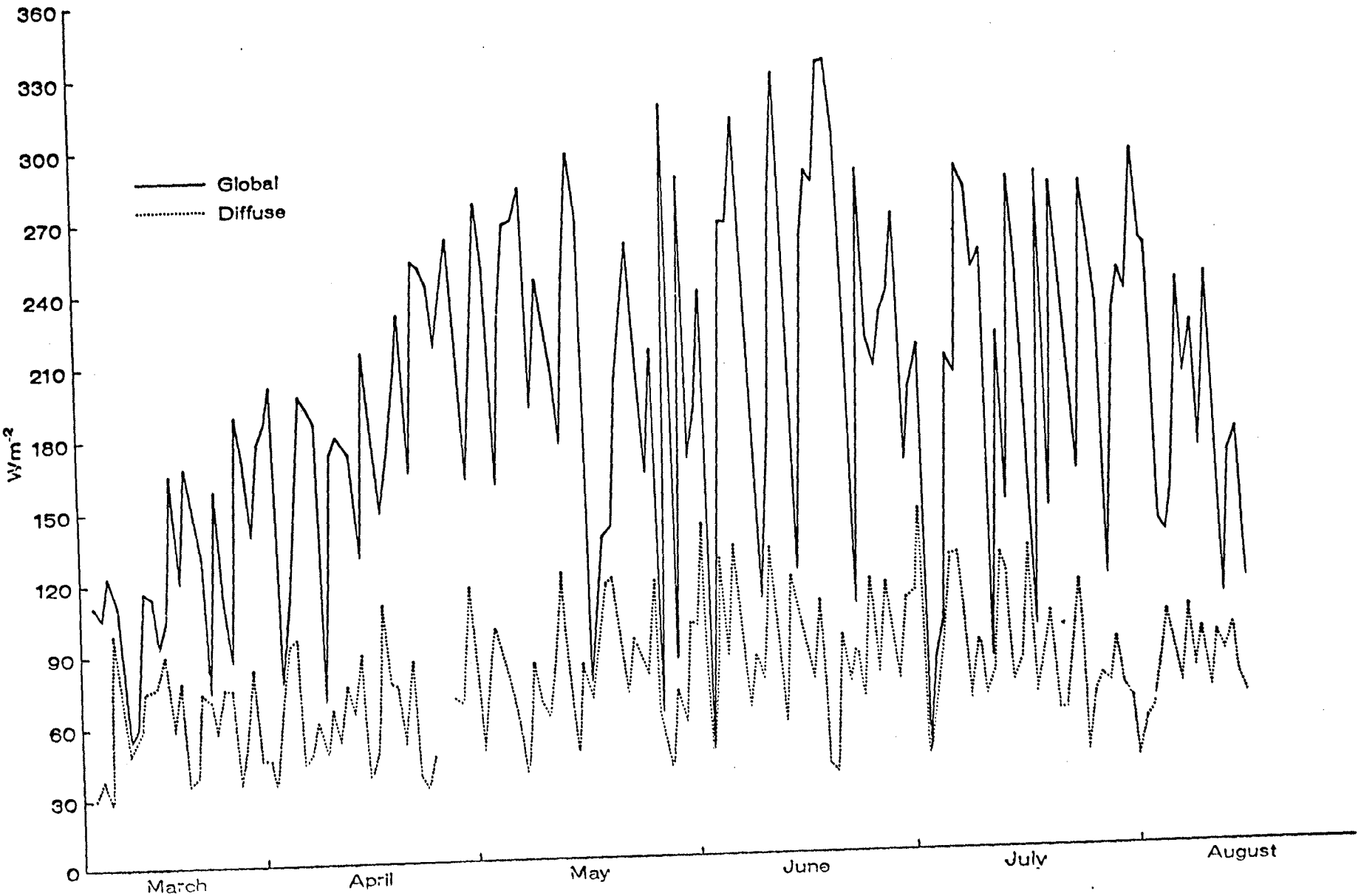

Figure 3. Mean daily values for global incoming direct shortwave radiation and incoming diffuse radiation .

Mean wind speeds were quite low in all months with a range from 1.5 to 2.0 ms^{-1}. Average speeds for the four-month field season were slightly lower in 1977 than in 1976.

Daily climatic information for the 1976 field season has been previously reported (Hage, Labine and Reynolds 1977) and therefore only the 1977 climatic summaries will be presented. Fig. 3 shows the incoming solar radiation regime (both direct and diffuse components). From early mean daily values of 110-140 Wm^{-2} in March, there was a gradual increase to a peak of 300-330 Wm^{-2} in June, and then a slow decrease after solstice to 200 Wm^{-2} in early to mid-August. Diffuse radiation did not vary as much as the direct + diffuse (i.e., total) radiation components. Diffuse radiation varied from a mean of 60 Wm^{-2} in March to 80-90 Wm^{-2} in May and June. The lower values in the early part of the season may have resulted from the drier Arctic air masses, shorter day lengths, and low sun angles of early spring. On the average, diffuse radiation was found to be 40% of the total incoming shortwave radiation. However, during the passages of low pressure systems accompanied by the corresponding cloud patterns, one finds diffuse radiation values to be almost 100% of the total incoming radiation. Examples of this occurred in early April, mid-May, end of May, early July, and mid-July, 1977.

Fig. 4 illustrates the two main components of net radiation, namely, all-wave incoming (shortwave plus longwave) and all-wave outgoing radiation. All-wave incoming radiation was very similar to the global shortwave radiation previously discussed. The all-wave outgoing radiation was much smaller and less variable because it is controlled by the surface and is not sensitive to cloudiness. The area between the two

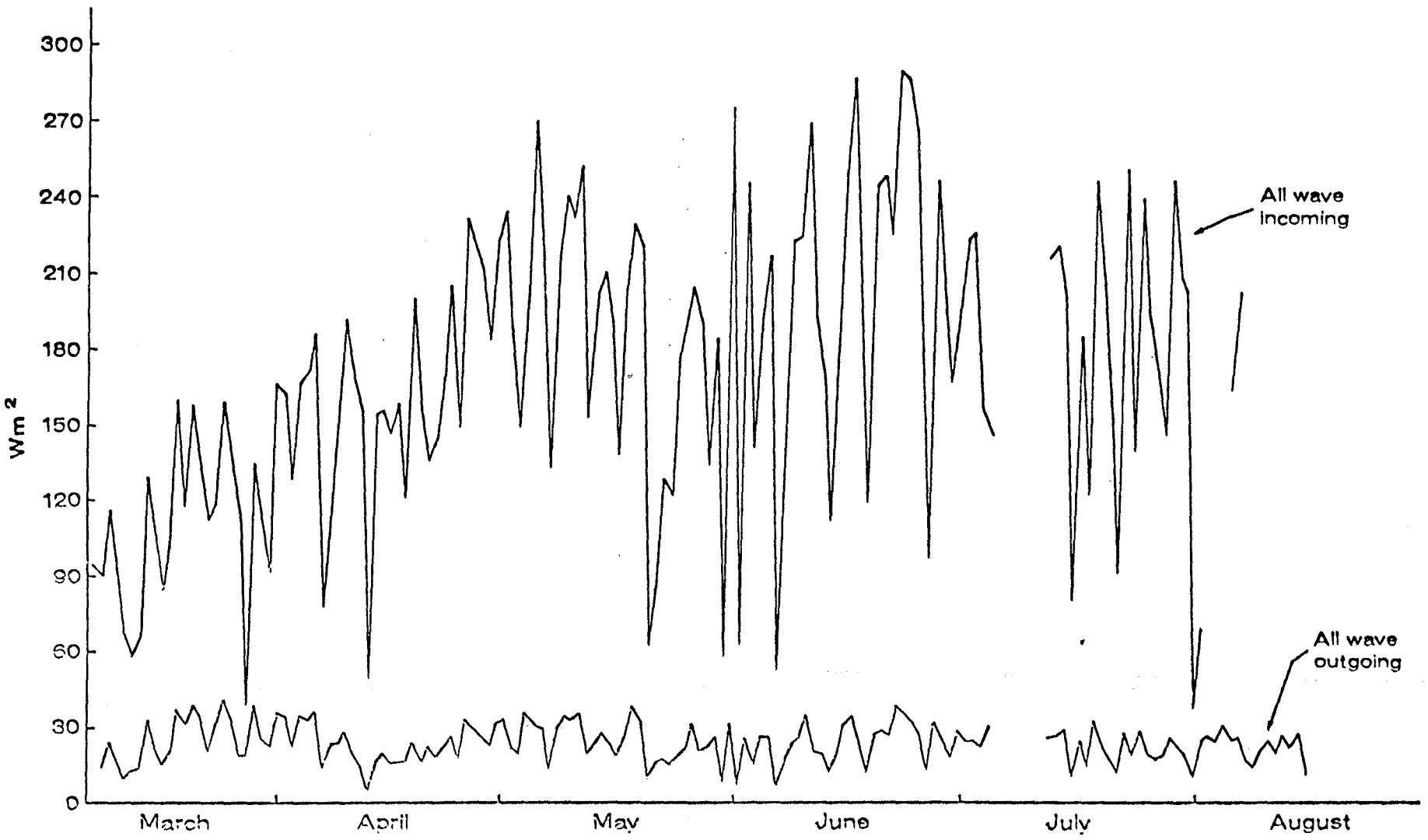

Figure 4. Mean daily values for All Wave (300-6000 nm) Incoming radiation and All Wave Outgoing radiation.

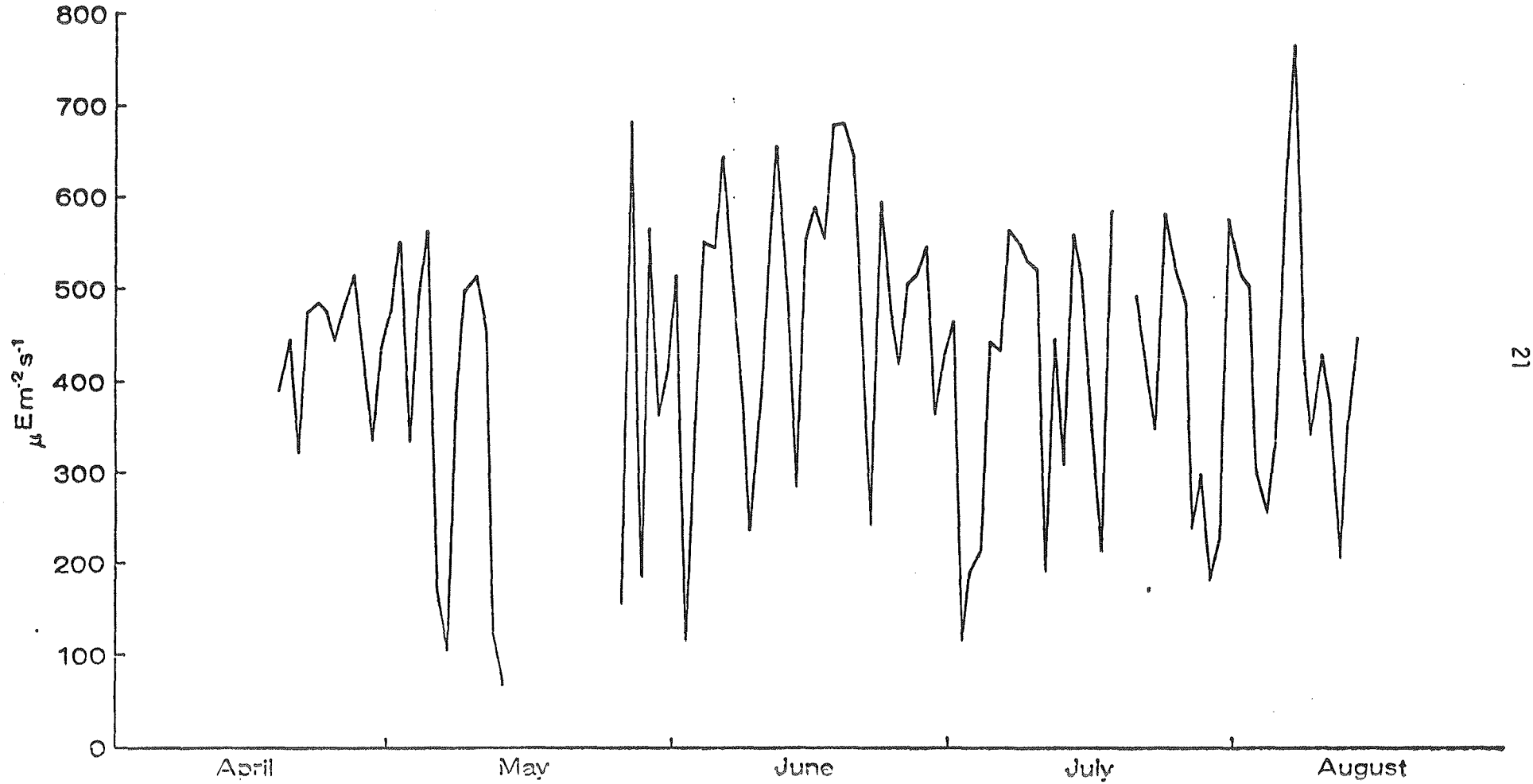

Figure 5. Mean daily values for Photosynthetically Active Radiation (400-700 nm) .

curves is the net or absorbed radiation. Net radiation values started at 70 Wm^{-2} in early March, increased to 145 Wm^{-2} in mid-April, 180 Wm^{-2} in mid-May and reached a mean maximum of 207 Wm^{-2} in mid-June followed by a gradual decline.

Photosynthetically-active radiation (P.A.R.) (400-700 nm) is one of the most important components of radiation which can be measured in a plant process study such as this one. A review of the literature shows that few long-term measurements of this component are available. Galoux (1971) points out that the energy available in the range of P.A.R. is usually 50% of the incoming solar radiation. Fig. 5 shows the distribution of P.A.R. during the 1977 field season. From mid-April to early May the mean daily value was 400 $\mu Em^{-2}\ s^{-1}$. Mean values then increased to 500 $\mu Em^{-2}\ s^{-1}$ in mid-June, and then decreased to 300-400 $\mu Em^{-2}\ s^{-1}$ by mid-July. As expected, P.A.R. exhibited the same seasonal pattern and day-to-day variations as solar incoming radiation because its wavelength range of 0.4-0.7 μm is well within that of the solar radiation.

The temperature regime for the 1977 season is shown in Fig. 6. Daily mean values have been plotted for three sites which represent a transect from the bottom of the hill, through the mid-slope main tower site and further to the upper slope near the top of our plot distribution. The temperature differences between the sites will be discussed later and only the general seasonal trends will be looked at now.

The field season started in early March with unusually high temperatures. For the first few days of measurement the mean daily temperatures were above freezing. This was followed by a fresh outbreak of cold Arctic air which brought mean temperatures down near $-20^{0}C$.

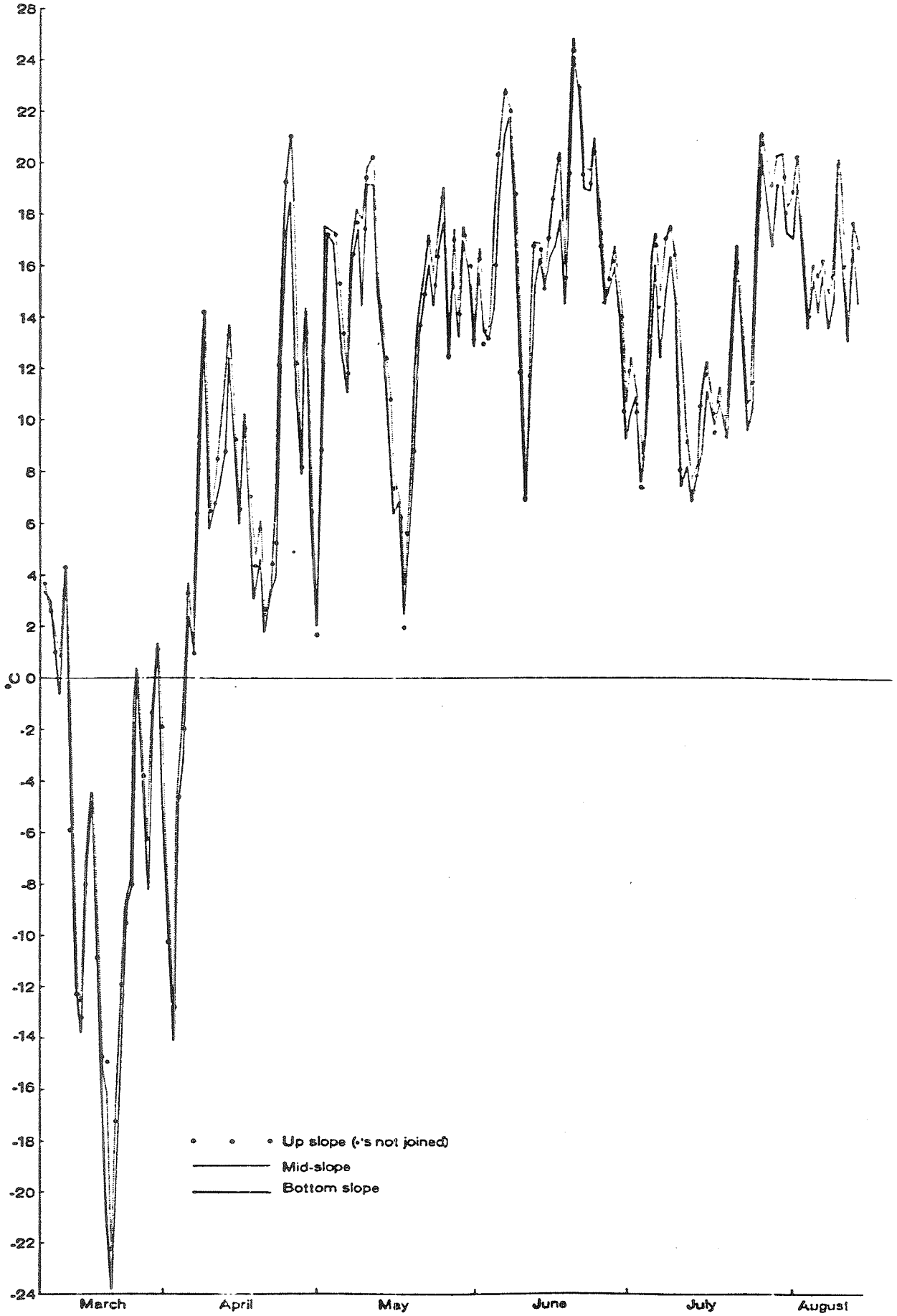

Figure 6. Mean daily temperatures for the top, middle and bottom sites on the hill .

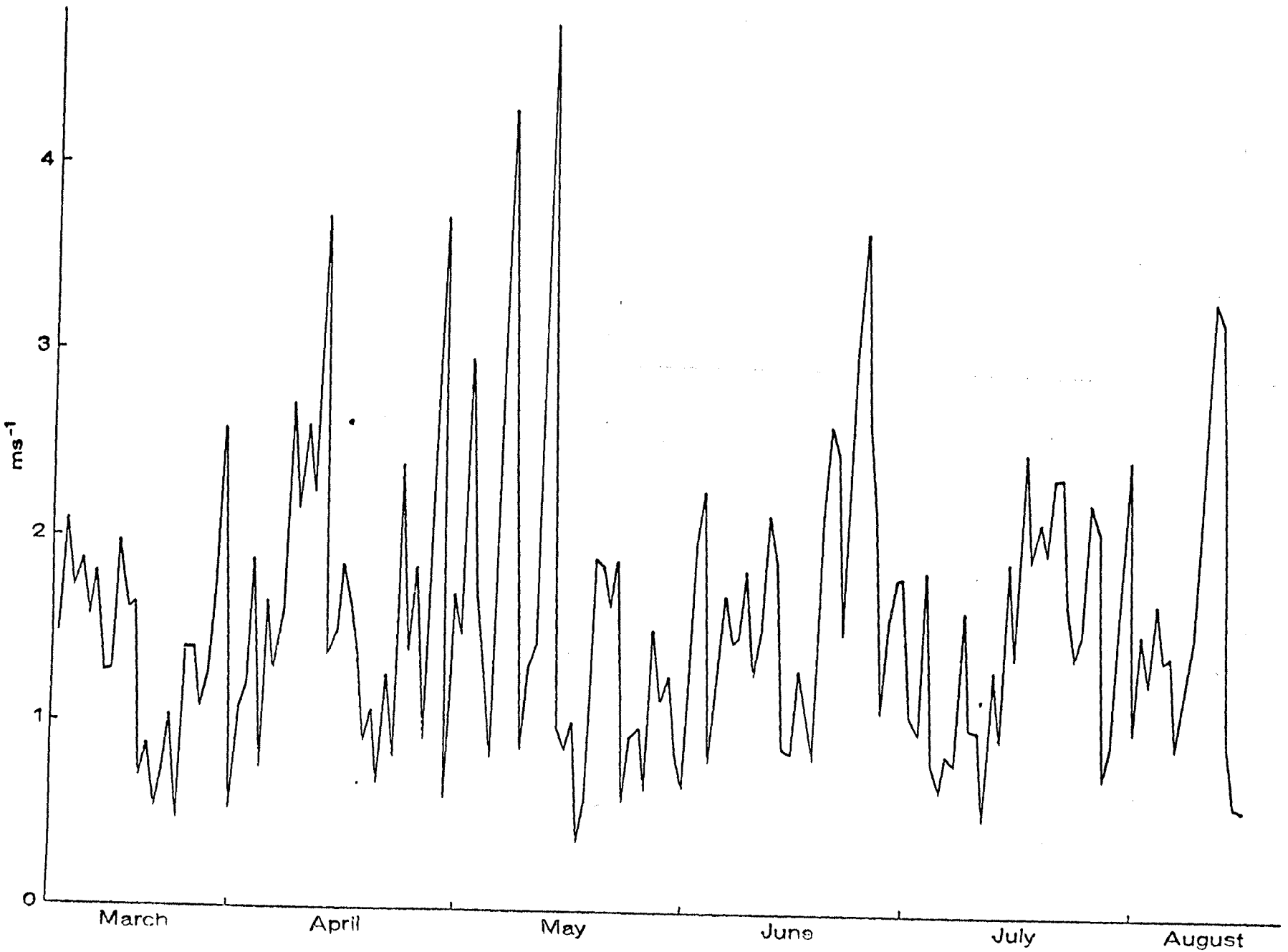

Figure 7. Mean daily windspeed measured at 8 m at the middle site.

After this initial cold spell a gradual increase of temperature can be observed but with irregular additional outbreaks of cold air on March 28, April 1, and April 2. Temperatures rose above the freezing level permanently on April 5 as the general seasonal warming continued. The highest mean daily temperature was reached on June 20 (24.9°C) preceded by several outbreaks of cool air from the north. However, temperatures did not go below freezing during these outbreaks because the air masses had been modified and warmed after leaving their northern source regions. The most obvious of these occurred on April 20 (2.5°C), April 30 (2.3°C), May 17 (2.6°C), and June 10 (7.5°C). Following the maximum temperature in mid-June there was a cool period from July 11 to July 19. From July 19 to early August the temperatures were again seasonal (18°C) followed by cooler temperatures till the end of the field season.

The wind regime for 1977 is shown in Fig. 7. Daily means ranged from maximum values of 3.0 to 5.2 ms^{-1} to minimum values of 0.4 to 0.6 ms^{-1}. The mean winds at Richardson were very light with an average value of 1.6 ms^{-1} for the entire season. Wind speeds in March were close to the mean until the third week when they dropped to 0.7 ms^{-1}. These light winds were associated with the outbreak of Arctic air and the stable conditions associated with the cold high pressure system. The period from early April to mid-May generally had above-average windspeeds possibly as a result of the frequent north-south passage of the front and associated low pressure. After mid-May wind speeds returned to average values except for high winds experienced on June 23-25 in mid-July and in early August. These periods of higher winds were associated with the passage of frontal waves.

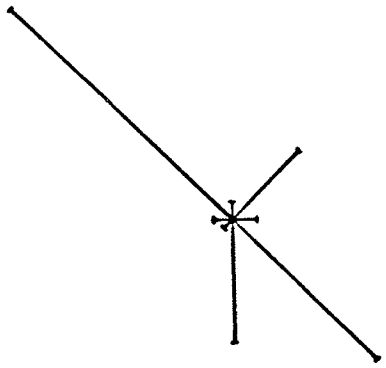

March

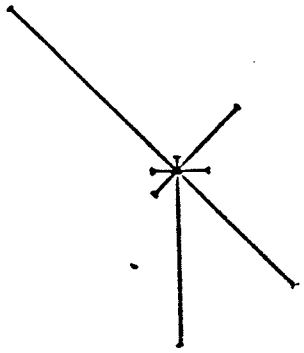

April

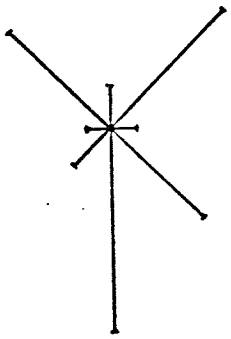

May

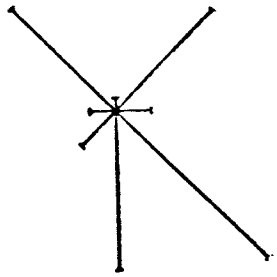

June

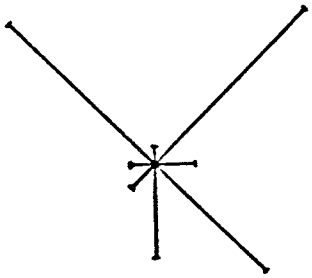

July

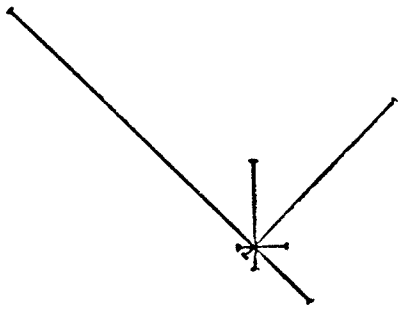

August

Figure 8. Monthly windroses showing the frequency of wind direction. Data are from the middle site.

Since our wind direction measurements were made on the western side of the hill it is understandable that no strong east component was ever measured and that there was an almost even distribution between the NE and SE. The mean monthly wind roses are shown in Fig. 8. In March the major wind component is from the NW with secondary prevailing directions from the SE, NE and S. The same is true for April, although the prevailing NW direction is not as strong and there is a major southerly component; the NE and SE components are still present. Although May has a predominantly south wind direction, it is quickly followed in rank by prevailing winds from the NW, NE and SE, again, a reflection of the frequent passage of the polar front. June and July also show uniform distribution of wind directions. June has a major component in the SE with secondaries in the NE, NW and S, while July has a major northerly component in the NE and NW with a secondary in the SE. Finally, August had a strong wind direction component from the NW with a secondary in the NE. Longley and Janz (1978) also show that the months of May and June have an eastward component.

As is usual for the area, the precipitation was very light in the early part of the season (March and April). Snow cover was also average for that time of year with 32 cm of snow on the hillslope at the start of the field season on March 3rd. A small decrease in snow cover to 28 cm followed, with the advent of higher temperatures in early March. Following precipitation in mid-March, snow cover again increased to a maximum of 47 cm in the third week of the month. From then on, with increasing temperatures and initiation of snowmelt, there was a steady decrease in snow depth, from 35 cm on April 5 to 28 cm on April 8, and to 18 cm on April 9. The slope was clear of snow on

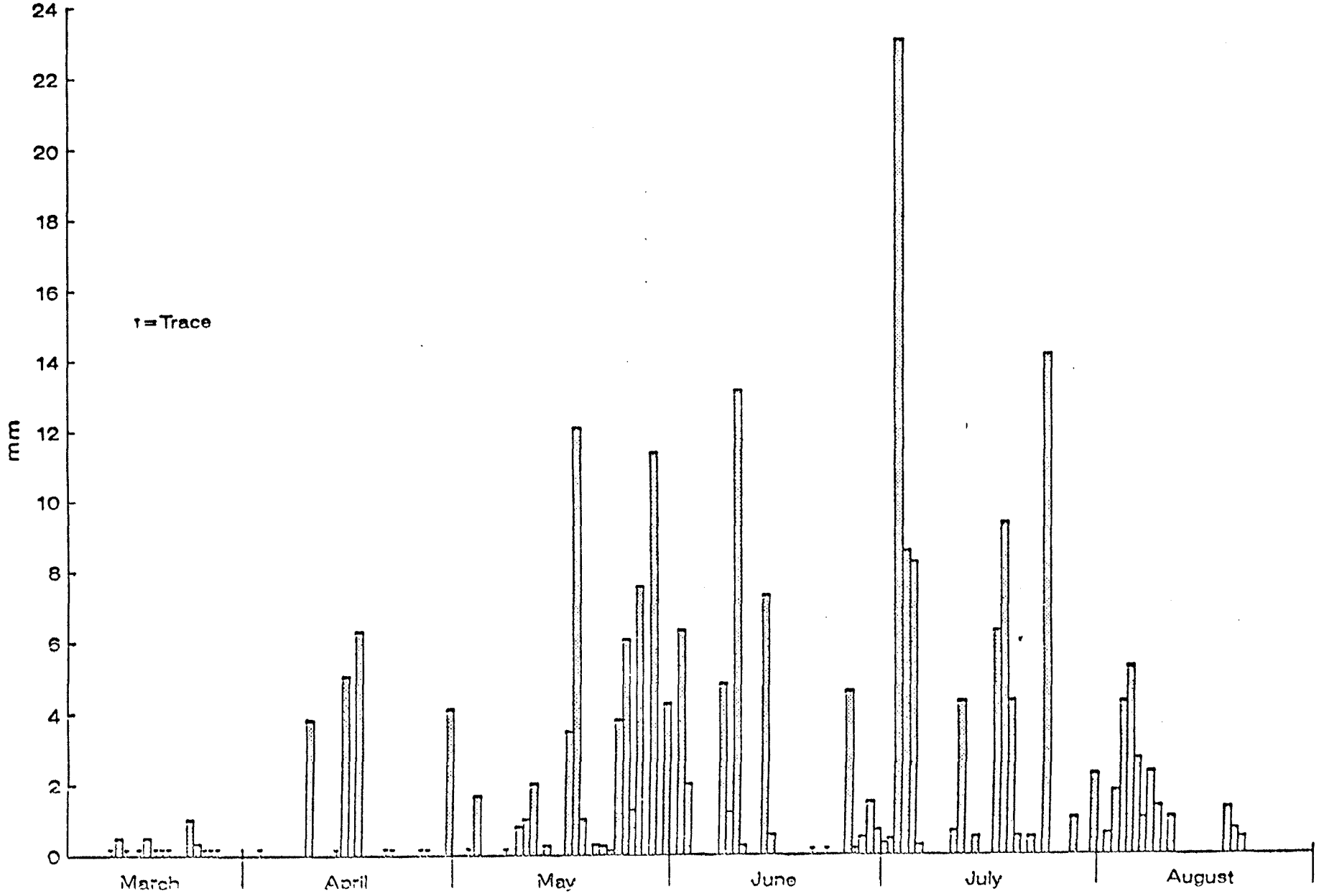

Figure 9. Total daily precipitation for the 1977 field season.

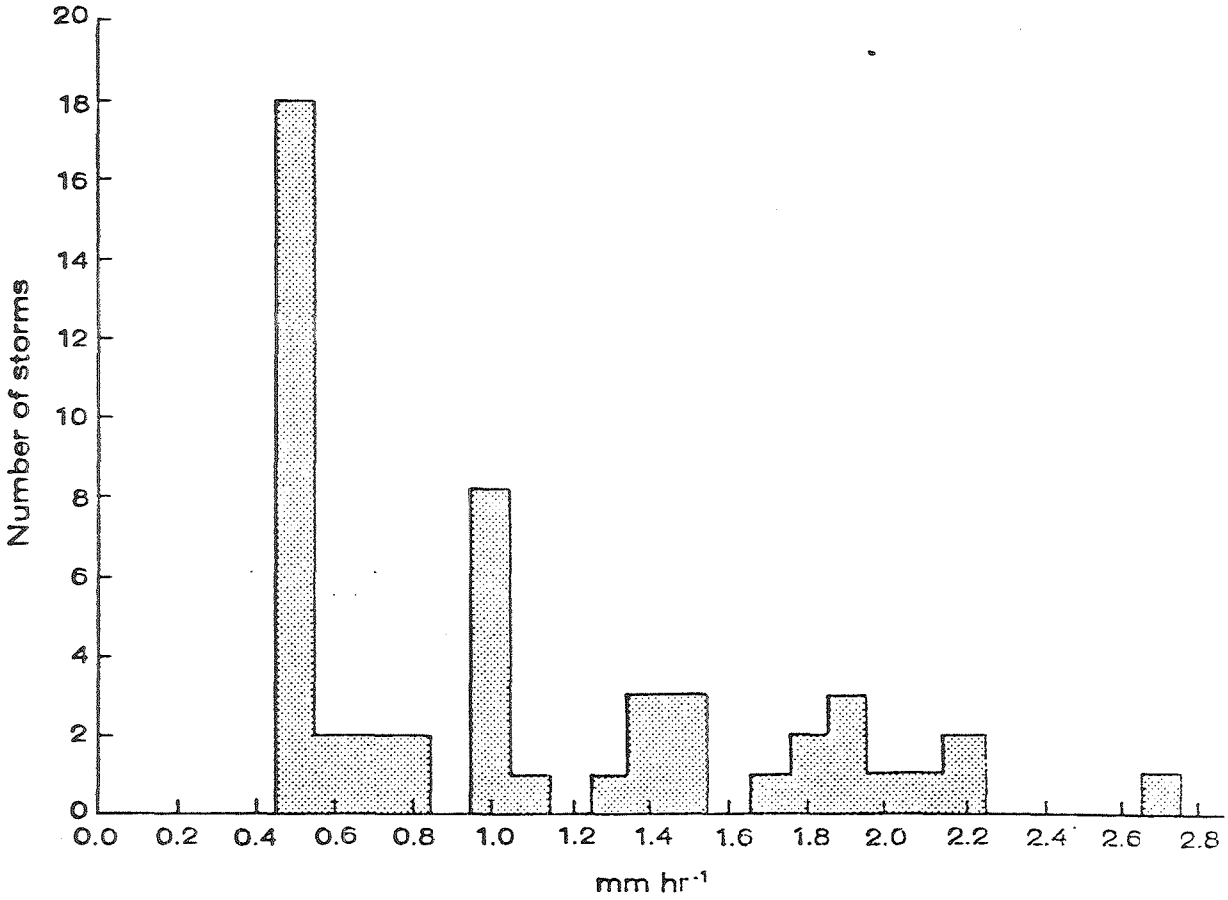

Figure 10. Histogram showing the distribution of storms according to precipitation intensity .

April 11, while snow persisted on the flats and in the forest for a few more days. The entire area, except for sheltered snow patches, was snow-free by April 15.

Following generally light precipitation in March and April, heavier falls started in early May and maximum amounts occurred in July. As stated earlier, August was a wetter month than usual (Fig. 9). Fig. 10 shows the manner in which precipitation falls at Richardson. The histogram clearly shows that most of the storms were of low intensity (0.5 mm h^{-1}). The rest of the storms consisted of 2-3 storms with 1.4-1.5 mm h^{-1} and 1.8-1.9 mm h^{-1}. Two strong "cloud bursts" resulted in high intensity rainfall. One occurred on July 5 and had an intensity of 17.8 mm h^{-1} and the other was on July 24 where 14.2 mm fell in 30 minutes, resulting in an intensity of 28.4 mm h^{-1}.

3.3.3 The Microclimate of the Jack Pine Canopy

Forests are the most complex of plant canopies and this complexity has been one of the main reasons for the rarity of integrated studies of the micro-environment within the forest canopy. In a recent review of the subject, Jarvis et al. (1976) discusses the problem and presents a synthesis of most, if not all, major forest meteorology projects.

Our own research was further complicated by the fact that it was conducted on a slope and not within a level uniform forest. All commonly-used methods of estimating the exchanges of mass, energy, and water vapour between the atmosphere and the earth's surface assume stationary and horizontally homogeneous conditions. These assumptions were clearly not satisfied in the jack pine canopy on the Richardson slope. Nevertheless, it is hoped that th. microclimatological observations

that were taken will shed some light on the nature of the exchange processes and other physical characteristics of the canopy environment.

Profile measurements of temperature, water vapour and wind within the canopy were presented earlier for the 1976 season and the same characteristic curves were found to exist in the 1977 season. Gradients of temperature, vapour concentration and wind were small within the forest canopy even though the transfer of energy and mass may have been proceeding at high rates. It is believed that small gradients resulted from turbulent mixing induced by the rough canopy surface. Our site was further complicated by the slope and by the irregular open spaces of the forest. Furthermore, the exchange surfaces were distributed through a considerable canopy depth so that the sources of heat and water vapour were diffuse rather than concentrated at a mean height as in dense canopies of field crops or other low vegetation. Fig. 11 shows "daily mean" wind profiles from three sites on the slope for several days during the field season. The "daily means", however, are for 24 hours, but for the time periods during which 15-minute wind runs were taken. The number of wind runs during a period varied from day to day but there were generally from 10 to 25 wind runs per mean daily period.

The variability of the individual profiles themselves is the main indication of the roughness and turbulence within the canopy. There is a gradual increase in wind with height at all three sites. The strongest changes in windspeed occur both near the ground and the top of the canopy. Near the top of the trees the wind shear is as a result of the wind regime changing from free air laminar flow to the turbulent flow of the irregular canopy. The slight bulge or increase which occurs near the surface is due to the greater ease of airflow in the trunk area free

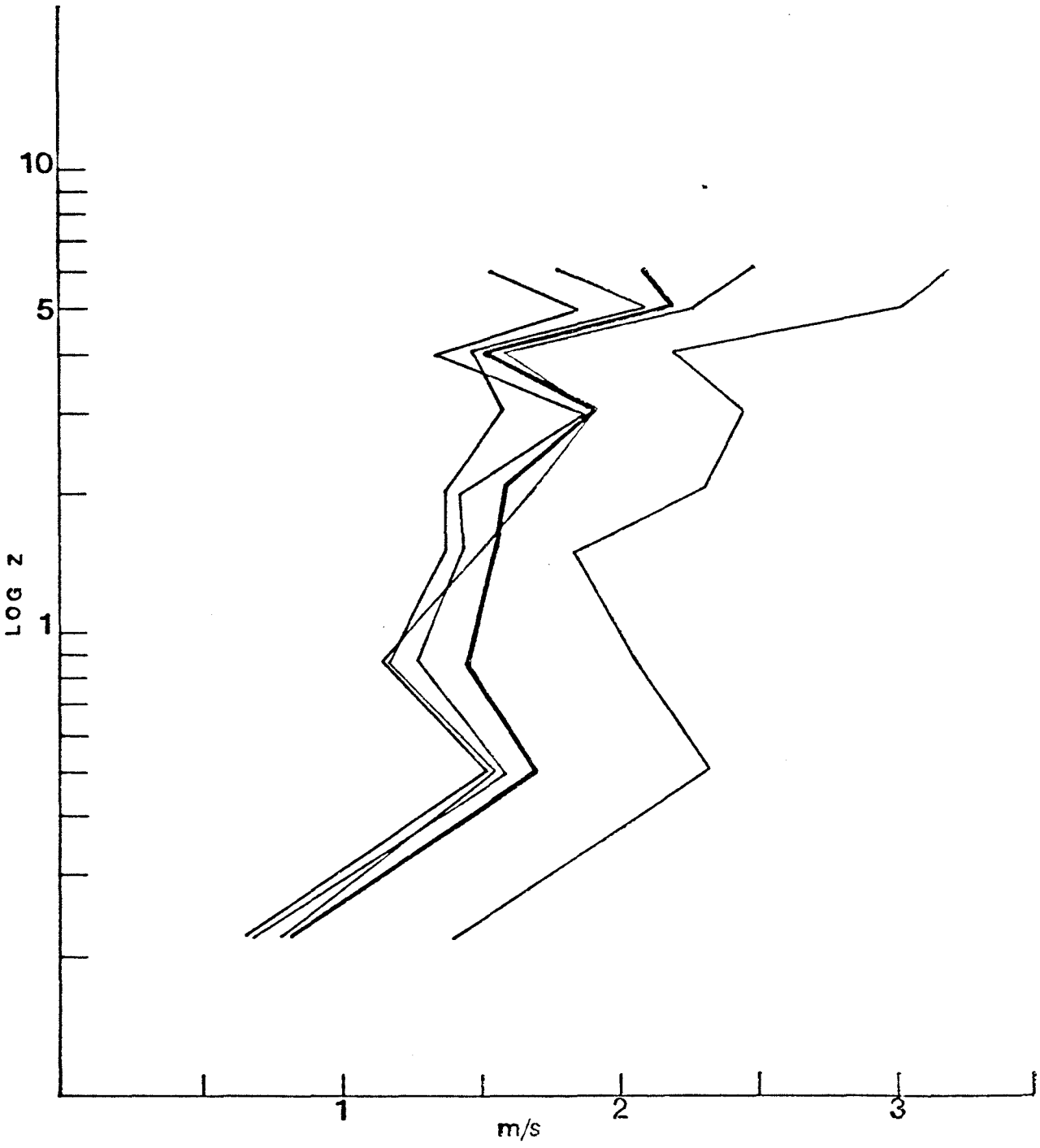

Figure 11a. Windprofiles measured at the W1 profile site. Heavy line is the mean for the measurement period while the lighter lines represent hourly values.

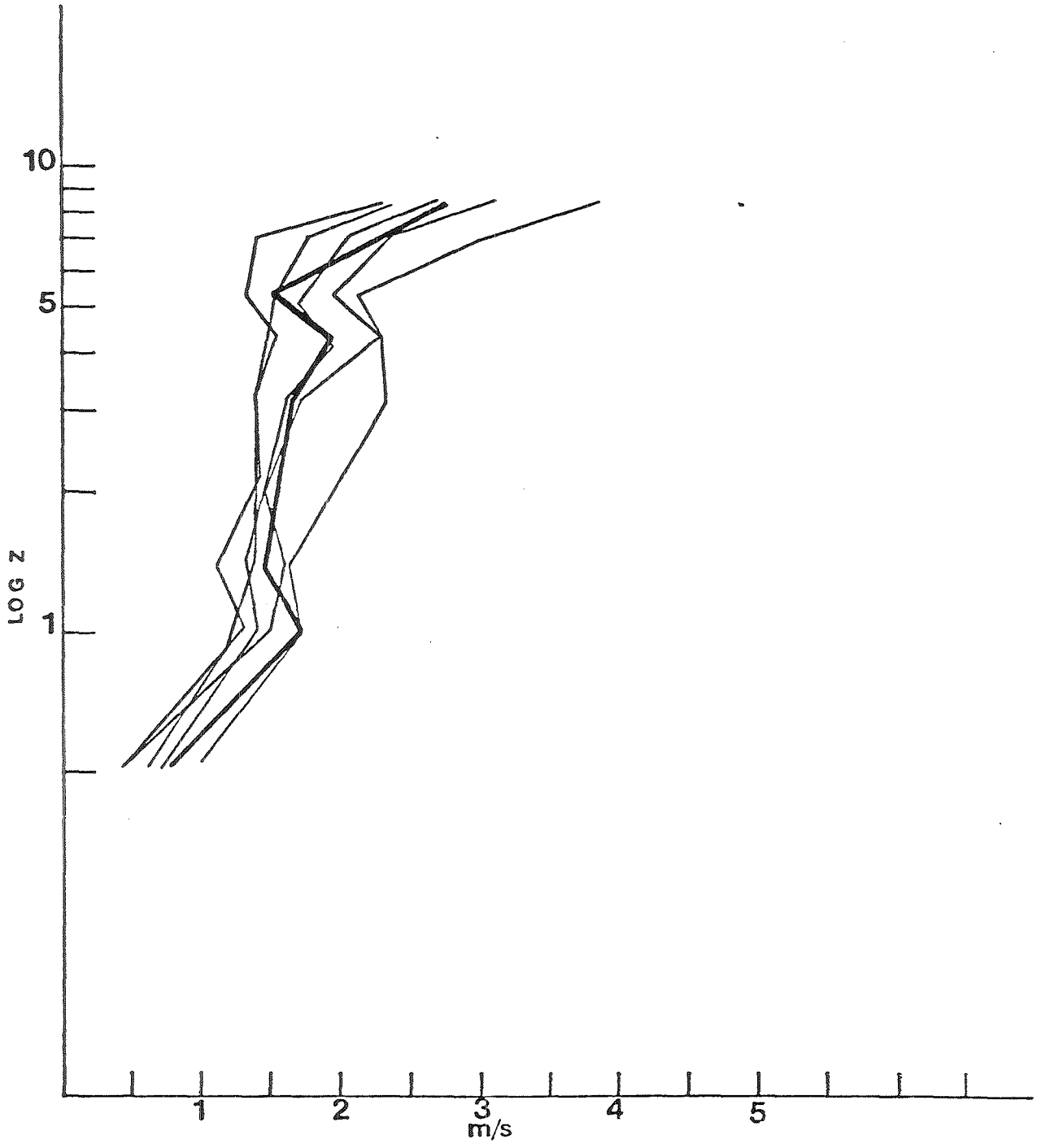

Figure 11b. Windprofiles measured at the W2 profile site. Heavy line is the mean for the measurement period while the lighter lines represent hourly values.

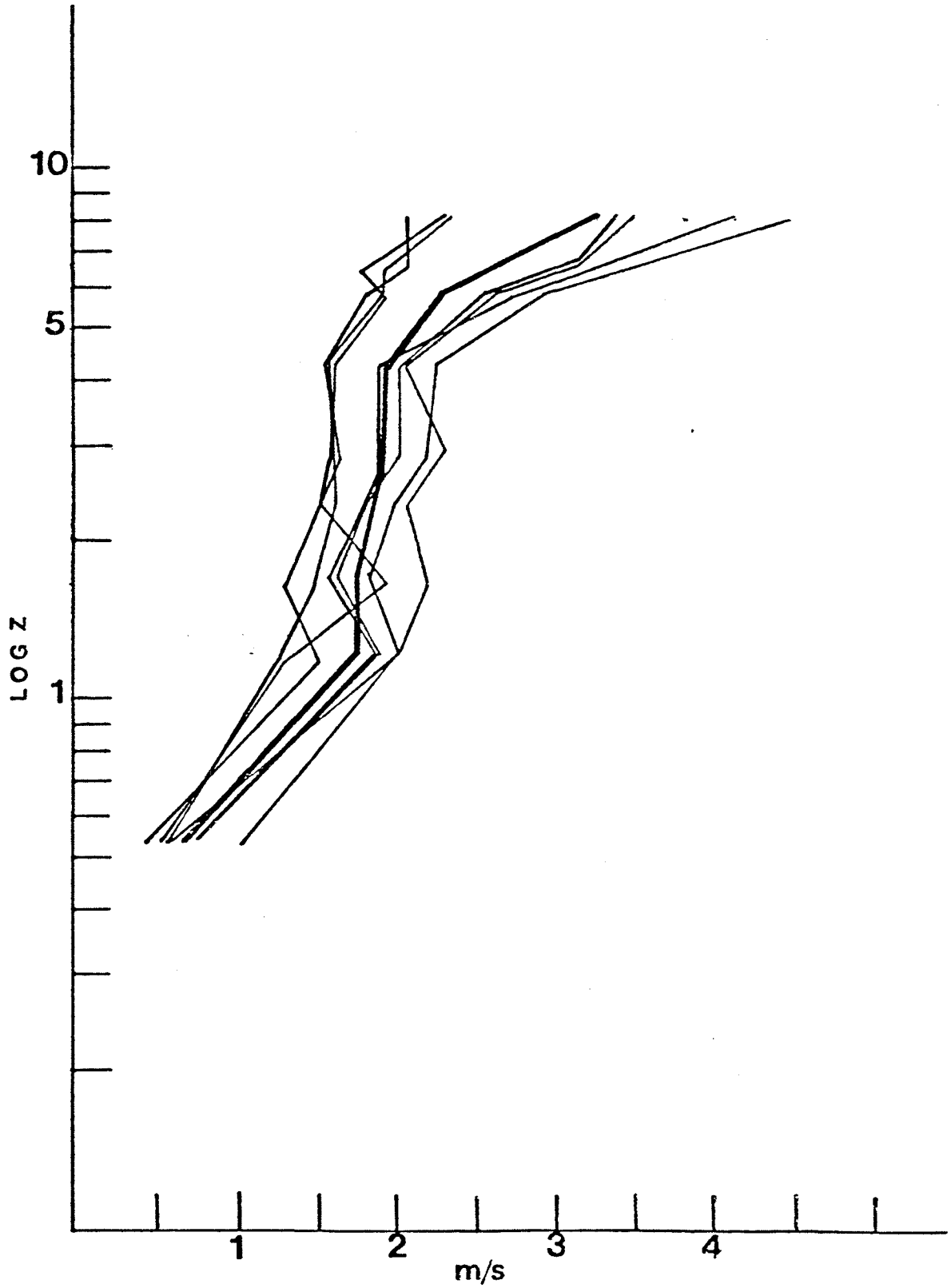

Figure 11c. Windprofiles measured at the W3 profile site. Heavy line is the mean for the measurement period while the lighter lines represent hourly values.

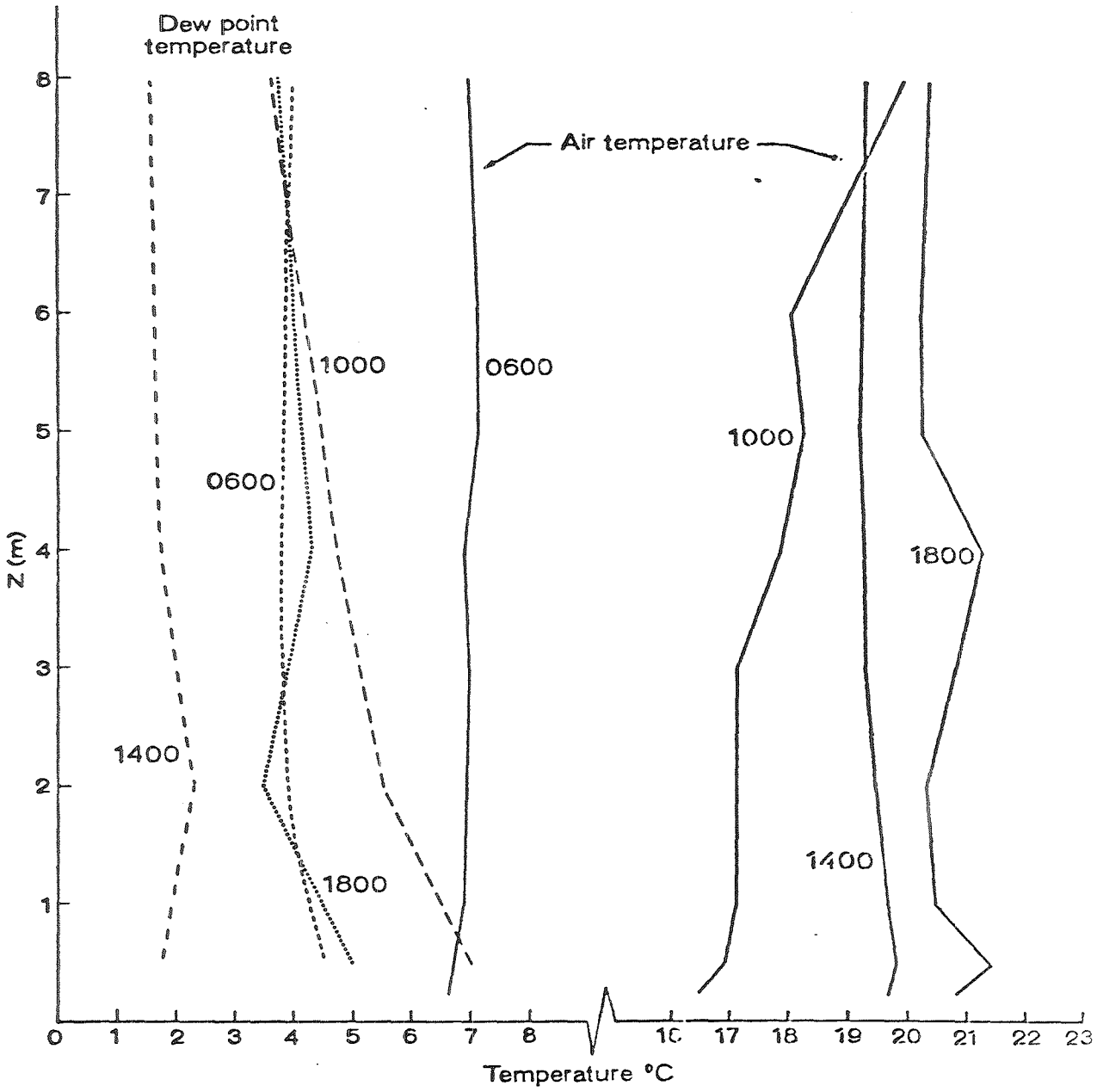

Figure 12a. Mean hourly profiles of air temperature and dew point temperature measured at the W1 profile site on June 4 1977.

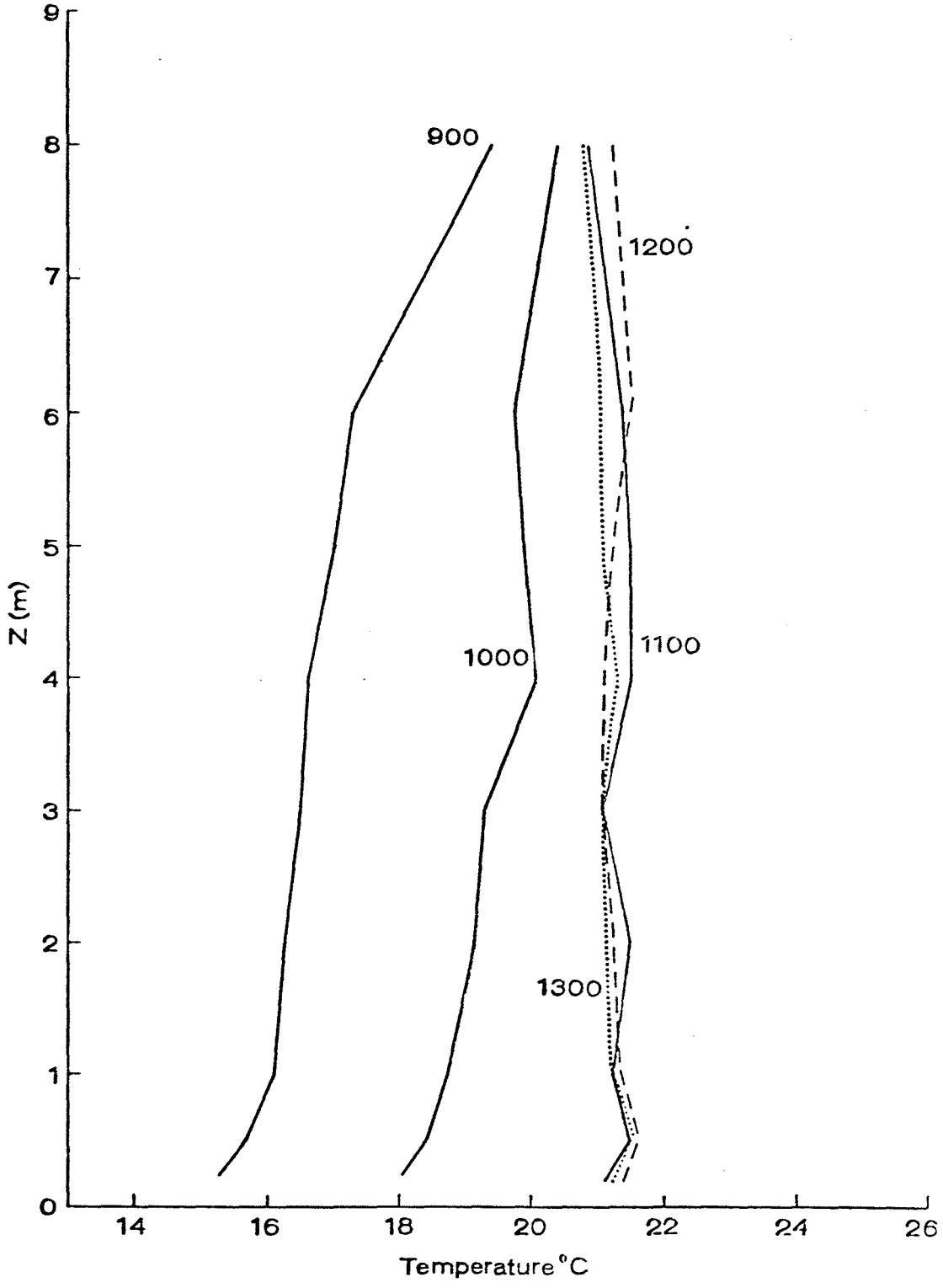

Figure 12b. Mean hourly profiles of air temperature and dew point temperature measured at the W2 profile site on June 24 1977.

of branches. This can be seen at the 0.5 m height at the central tower site (wind profile 1, Fig. 11), at 1 m at the second site, while at the third site there is only a slight indication of this at the 1.2 m height. This phenomenon of "blow through" has also been found to occur in the interior of level forests (Oliver 1975). The fact that our site is a slope with many openings in the canopy makes it possible to have more of these bulges in the profile at heights above the branch-free trunk area. A further explanation of the irregularity of the profile is the horizontal pressure gradient which Jarvis et al. (1976) discuss. These pressure gradients are established by the persistent up and down drafts at varying points in the canopy. It would therefore be difficult, if not impossible, to try to determine exchange coefficients of momentum, heat or water-based, on these profiles.

Further indications of the high degree of mixing which occurs in the canopy are seen in the air and dew point temperature profiles (Figs. 12a and 12b). The profiles drawn are from half hourly means. The gradients in the first set of profiles for June 4 (Fig. 12a) were generally weak, the one exception being the 1000 air temperature profile; but even then the strongest gradient occurred at the top of the canopy. Within the canopy itself the temperature differences were not more than $2^{o}C$. Winds were light (0.7 ms^{-1}) for the 1000 profile and this also partially explains the strong gradient. It is not surprising to see the maximum temperature at the top of the canopy since it is essentially acting like a surface layer with the maximum amount of radiation falling upon it. At 1400 the profile was almost isothermal. Winds had increased by this time to 1.4 ms^{-1} but also the incoming radiation had been reduced with the afternoon buildup of convective cumulus clouds. Following the

dissipation of these clouds in the early evening, temperatures again increased and maximum temperatures were reached at 1800 as opposed to the usual occurrence at 1400. The dew point temperature profiles also exhibited the "isothermal" tendency except at 1000.

Fig. 12b only shows air temperature profiles for the following day. The first profile at 0900 shows a very slight warming from near the surface to 6 m but again the gradient is shallow, only $1^{o}C$; the maximum temperature is again occurring at the top of the canopy. The next profile at 1000 does not show as strong a change from the 6 m level to 8 m, but within the canopy itself the gradient is slightly stronger than the previous hour. The profiles for 11, 12 and 1300 h are very close to isothermal and their uniformity is probably linked to increased windspeeds (2-2.5 ms^{-1}) from the lighter morning winds.

The strongest air temperature profile which was measured was not a vertical one at one site but was the temperature gradient which developed as a result of cold air drainage down the slope. As previously shown in Fig. 5, there are several occasions where the difference between the temperature in the mid and lower screens were as high as $4\text{-}5^{o}C$. Analysis of the data helps determine the necessary conditions to establish the slope temperature gradient. Probably the most important factor is wind. By choosing nights when the difference between the minimum temperatures of the mid slope and bottom screen were at their greatest, one finds that the strongest gradient was developed during periods of very light winds (Table 6). On March 31 the difference in minimum temperatures between the two sites was $5^{o}C$ and the mean windspeed from the time of sunset to just before sunrise was 0.35 ms^{-1}. The next day, April 1, the difference in the minimum was only $0.8^{o}C$ and the winds were

Table 6. Slope Temperature Gradient

DATE	DAILY MIN. TEMP. Mid-Slope	DAILY MIN. TEMP. Bottom Slope	WINDSPEED ms^{-1}
March 31	-8.3	-13.5	.35
April 1	-17.2	-18.0	.82
May 9	8.5	0.6	.56
May 10	12.3	11.0	.48
July 1	4.8	0.1	.36
July 2	8.0	8.3	.57

then 0.8 ms^{-1}. Another example occurred on July 24. The difference in temperatures was 3.5°C and the windspeed was only 0.75 ms^{-1}. The next day, the difference was only 0.6°C and the windspeed was now up to 3.11 ms^{-1}. The radiation balance will also, of course, have a role in determining the extent of the re-radiative cooling. It is interesting to note that on May 9 the temperature difference was 6.9°C and the winds were predictably light, 0.56 ms^{-1}. The next day, May 10, the winds were still just as light during the night, 0.48 ms^{-1}, yet the ΔT_{min} was only 1.3. The possible answer for the lack of cold air drainage on that night was enhanced radiation balance. There was slightly more cloud cover during the night of the 9th and the morning of the 10th than the previous dark period on the 9th. The 9th had only cirrus 1/10 present while the 10th had stratocumulus 2/10, altocumulus 1/10 and cirrus 1/10. As a result there were 380 Wm^{-2} of incoming longwave on the 10th, while the 9th had 340 Wm^{-2}. The extra input of thermal energy towards the surface was probably enough to offset the radiation balance and reduce the amount of radiative cooling. July 1 was another example of the influence of incoming radiation on the re-radiative cooling. On that day the ΔT_{min} was 4.7°C and the winds were light (0.36 ms^{-1}). Cloud conditions during the dark cooling period were stratocumulus 2/10, stratus 3/10 and cirrus 1/10. The next day, July 2, the ΔT_{min} was only 0.3°C, with the winds only slightly greater at 0.57 ms^{-1}. Cloud conditions had greatly increased (SC 9/10), creating a lid to outgoing radiative cooling. Again there were 340 Wm^{-2} of incoming longwave radiation on July 1, while on the 2nd there were 380 Wm^{-2}.

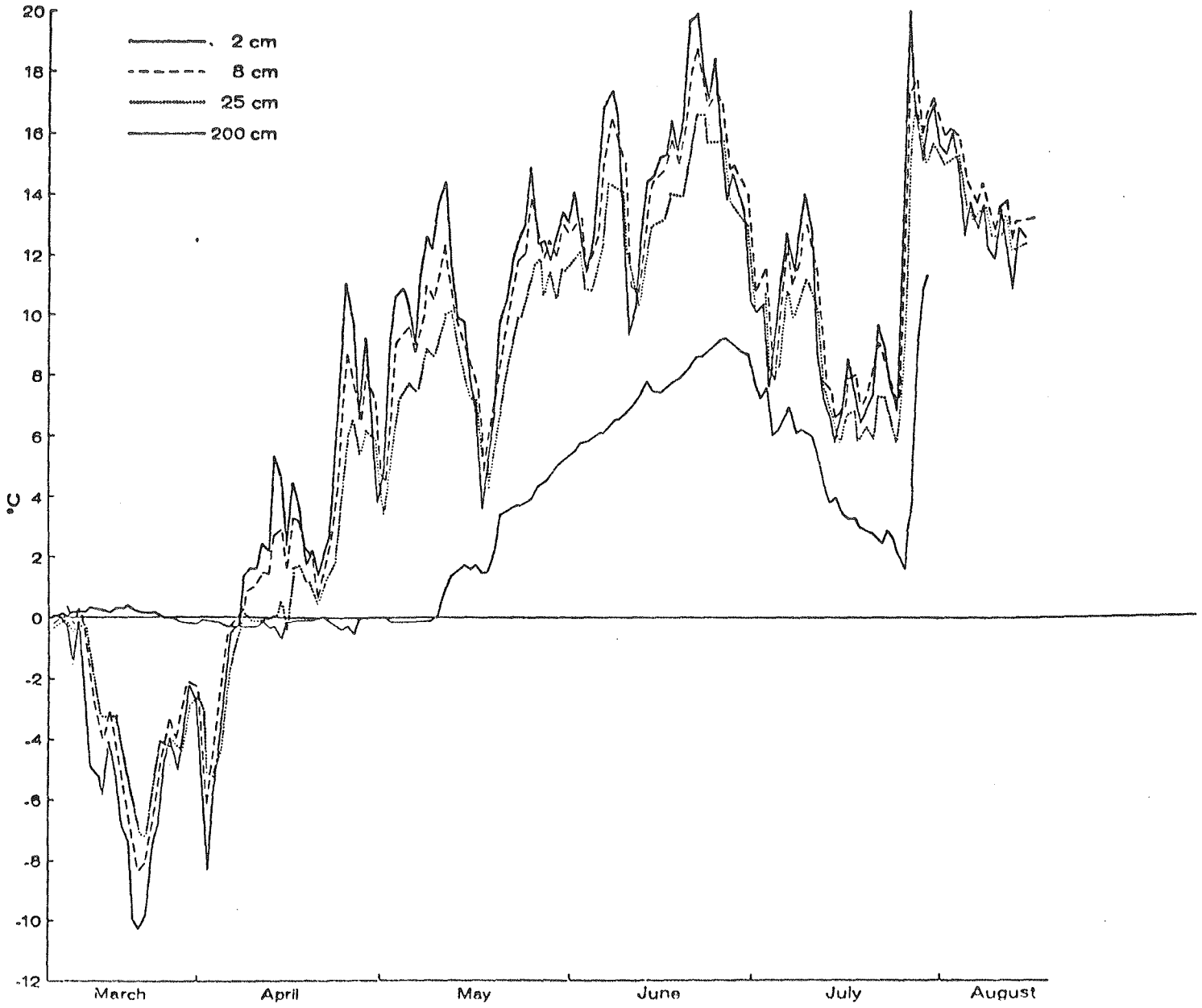

Figure 13. Mean daily soil temperatures at four depths for the 1977 field season.

3.3.4 Soil Temperature and Soil Heat Flow

The soil temperatures for the 1977 field season are shown in Fig. 13. As expected, the variations have similar shapes but smaller amplitudes than the air temperature curve in Fig. 6. The data are shown for 2, 8, 25 and 200 cm soil depths. The top three depths exhibited similar variations but with different absolute values of temperature and some time lag. These top three levels of temperature showed the cold period in early March but the temperatures are approximately half the values of the mean air temperature. The mean daily air temperature fell to almost -24°C during that time while the soil showed -10, -8 and -7°C for the 2, 8, and 25 cm levels, respectively. The 2 cm soil temperature had the greatest variation and extremes since it was closest to the surface. The 8 cm depth was usually 1-2° colder in temperature, while the 25 cm depth was another 1°C cooler. These soil temperatures rose above freezing in the first week of April and then gradually increased with the seasonal warming. At first the soil temperatures of the upper layer were only half of those of the air, but as each new period of warm temperatures was reached, the difference became less until mid-June when mean air temperatures rose to 23.5°C while near-surface soil temperatures reached 20°C. There followed the cooler period from the end of June to the third week in July at which point there was an abrupt increase and then temperatures slowly started to decrease.

The 200 cm depth had a completely different pattern. For the first two and one-half months the temperature remained just slightly above or below the freezing level. This deeper soil level was obviously

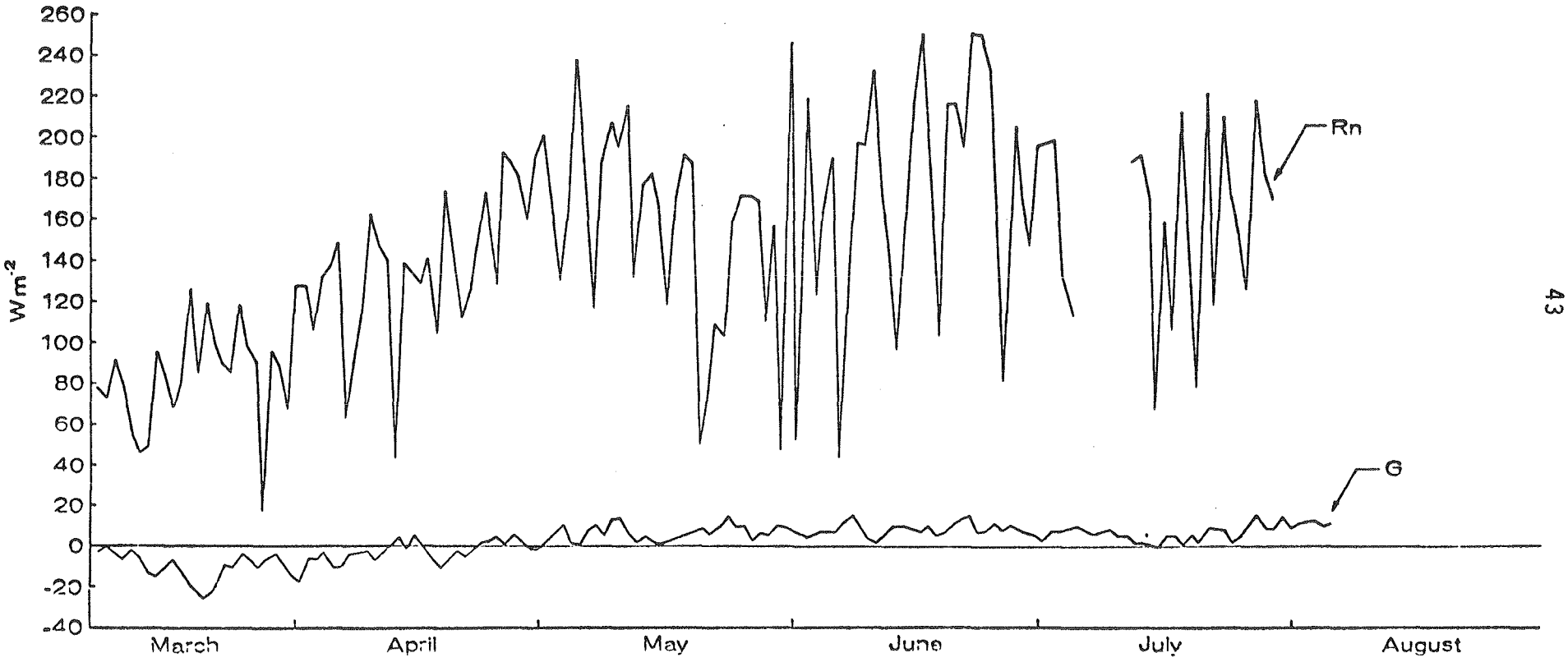

Figure 14 Mean daily values of net absorbed radiation (Rn) and of soil heat heat flux (G) .

below the range of influence of the daily variation of surface temperatures. Even after the temperatures rose above freezing in mid-May, it is obvious from Fig. 13 that the 200 cm level was still below the influence of the daily temperature wave. After rising above the freezing point, soil temperatures at 200 cm increased steadily to a maximum near the end of June. This maximum lagged 3-4 days behind the near surface soil temperature and it was 10°C lower than the maximum near the surface. Following the cool period in July there was a rather rapid increase in temperature. The maximum temperature was still 8°C lower than the near surface temperatures and the lag time was 3-4 days.

The amount of heat flow into the soil is shown in Fig. 14, along with the net radiation. As a rule the soil heat flux is usually only a small fraction of the absorbed net radiation, especially under canopies. According to our measurements over the range of the entire season, the soil heat flux was only 7% of the net radiation. Of interest here is the fact that the net radiation was measured just above the canopy and that if it had been measured above the forest floor under the canopy, it would have been less and therefore the portion of absorbed energy going into soil heat flow would have been in the more usual range of 10-15% of absorbed energy.

On a seasonal basis the soil heat flux was at first negative, indicating that there was a net outflow of heat from the soil towards the surface. This is not surprising since the soil temperatures at greater depths were higher than those near the surface. With the onset of spring and melting of snow at the surface, the soil heat flux became positive and it remained so for the rest of the measurement period varying from 2 to 18 Wm^{-2}.

3.3.5 Precipitation and Interception

The amount of precipitation intercepted by a vegetative canopy is important because it results in the loss of some water to the understory and soil surface, and therefore to the plants themselves. As in the previous field season, we measured the amount of rainfall intercepted by the trees and the results are shown in Figs. 15a and 15b. Fig. 15a is a graph of interception vs. rainfall intensity and as can be seen by the scatter of the points, there was no strong relationship between the two. Kittredge et al. (1941) also found storm intensity to be an inaccurate prediction of canopy interception. The main reasons they state were that storms with light total precipitation were obscured by storms with the same intensity but greater total amounts. Fig. 15b shows the relationship between interception and the total amount of precipitation from the storm. The results were similar to those found in the 1976 field season. Maximum interception occurred with light rainstorms while interception gradually decreased as the total amount of precipitation for the storm increased. It is difficult, therefore to obtain a mean interception value for a jack pine tree. However, by combining all storms and all trees sampled, the mean interception value was found to be 53%, a rather high value. A more useful exercise is to analyze the variation of interception under the canopy. The advantage of this would be to eliminate any problems with prevailing winds and rain shadows which could exist when using a single gauge; this technique would also allow for the variability of tree geometry and branch distribution within a single tree.

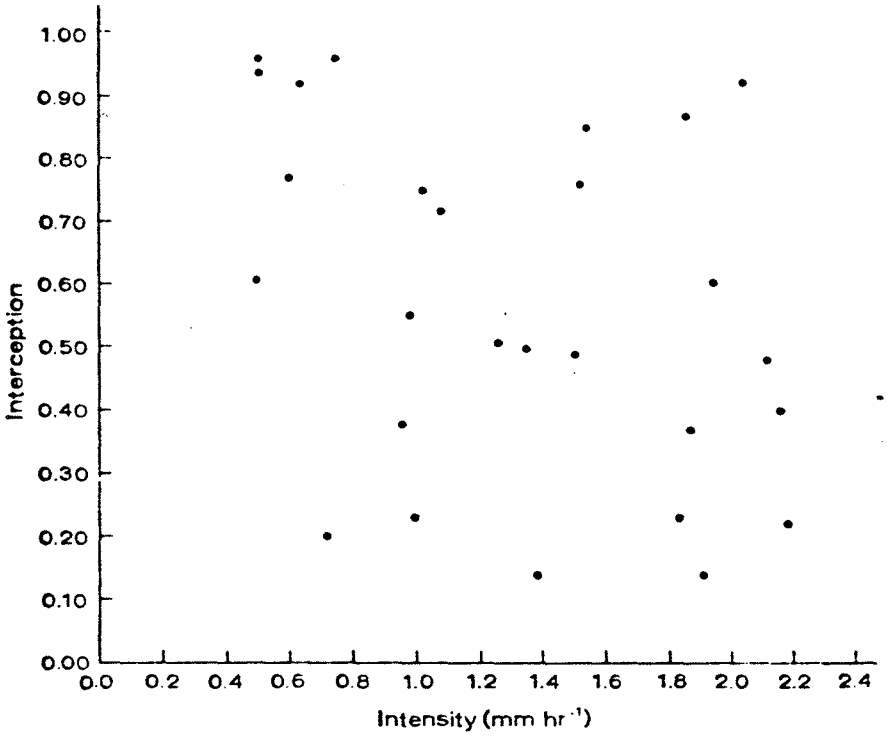

Figure 15a. Precipitation intensity vs. interception by the canopy for all storms during the 1977 field season .

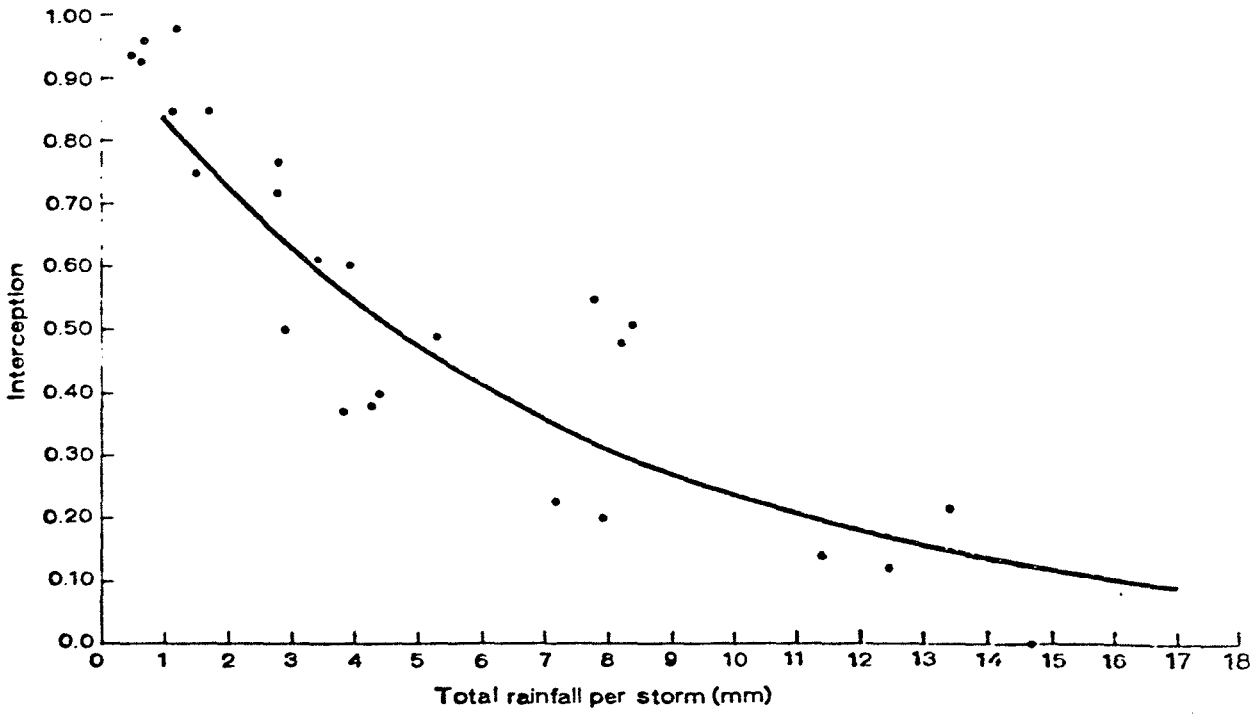

Figure 15b. Total precipitation vs. interception by the canopy for all storms during the 1977 field season.

Table 7. Interception with distance away from tree trunk

Distance from trunk (m)	.25	.5	1.0
Tree 1	.30	.24	.19
Tree 2	.33	.22	.14
Tree 3	.61	.41	.24
Tree 4	.51	.28	.12
Mean	.44	.29	.17

It is believed that the average values of interception shown in Table 7 constitute a more realistic description than that obtained from the gross averaging of all data. In the first case the average values were obtained from gauge networks under single trees while in the second case they were from single gauges. The highest mean value in Table 6 is 44% at the shortest distance from the trunk. This is less than the gross average of 53% obtained from single gauges for all storms and all trees. The large spatial variations are illustrated by values of 29% and 17% at 0.5 and 1.0 m, respectively. By knowing the leaf area distribution, one can calculate a mean distance from the tree trunk beyond which the canopy displays an average distribution of its foliage. This, in combination with storm size, will allow fairly accurate determinations of interception.

3.4 CONCLUSION

This portion of the project has shown the mean climatic characteristics of the Richardson site and described the main micrometeorological and microclimatic features of the jack pine-covered slope.

Long-term temperature records showed that the Richardson Lookout site is generally warmer than Fort McMurray Airport and our sloped, south-westerly exposed research site was obviously warmer as well. The precipitation records indicated that Richardson was generally a drier site than Fort McMurray Airport.

The climate of the two field seasons was discussed. The radiation regime was similar for both years except for August 1977,

which had much less radiation due to the high frequency of cyclonic storms and associated increase in cloud cover. Mean temperature values were generally similar except that the 1977 season was slightly cooler with August being much cooler. The precipitation pattern also reflected the increased storminess of 1977 and there were 28 mm more rain during the 1977 field season.

The greater turbulence of the forest canopy and the exposed nature of the slope combined to create a rather homogeneous environment within the forest canopy. However, by diffusing the concentrations and especially the gradients of temperature, water vapour and wind (momentum) it made it more difficult to locate the actual sources and sinks within the canopy.

The forest floor microclimate was described in terms of soil temperatures and heat flow. The small amount of heat flux into the soil reflected the decrease of radiation because of interception by the canopy. The effects of canopy structure on precipitation interception were also discussed.

The mesoscale temperature characteristics of the slope were described and cold air drainage was found to be present and was fully expressed on clear, calm nights.

With the early termination of this project, climatic data for a stress year were not possible, yet these were required in order to model the effectiveness of jack pine and other species for use in revegetation over long periods of time. An appendix has been added to this section to show how data from a drought-stressed season were obtained.

In conclusion then the forest canopy remains the most complex environment in which to study the exchanges and distribution of microclimatic parameters and much work remains to be pursued. Further work should be initiated in areas of homogeneous cover before going on to the more difficult sloped and hilly terrain areas.

3.5 REFERENCES CITED

Baumgartner, A. 1965. The heat, water and carbon dioxide budget of plant cover: methods and measurements. Methodology of plant ecophysiology. Proceedings of the Montpellier Symposium, p 495-512. Paris, Unesco (Arid Zone Research, XXV).

Bliss, L.C. and D.W.A. Whitfield 1977. Site description. In: Long term prediction of vegetation performance on mined sands. L.C. Bliss (Ed.). Report to the Alberta Oil Sands Environmental Research Programme. Project VE6.1, pp 6-10.

Galoux, A. 1971. Flux et transferts d'énergie au niveau des écosystèmes forestiers. In: Productivité des écosystèmes forestiers, Actes Coll. Bruxelles 1969. UNESCO (Ecologie et conservation, 4).

Gay, L.W. 1972. Energy flux studies in a coniferous forest ecosystem. In: Proceedings - Research on Coniferous Forest Ecosystems. A Symposium (J.F. Franklin, L.J. Dempster and R.H. Waring, eds.). p 243-253. Portland, Oregon.

Hage, K., C. Labine, and G. Reynolds 1977. Micrometeorology. In: Long term prediction of vegetation performance on mined sands. L.C. Bliss (Ed.). Report to Alberta Oil Sands Environmental Research Programme. Project VE6.1, pp 12-38.

Hutchison, B.A. 1979. Forest Meteorology - research needs for an energy and resource limited future. Proceedings of a workshop. Ottawa, 1978.

Jarvis, P.G., G.B. James, and J.J. Landsberg 1976. Coniferous Forest. In: J.L. Monteith (Ed.) Vegetation and the Atmosphere. Vol. 2. Academic Press, New York.

Kittredge, J., H.J. Lougheed, and A. Mazurak 1941. Interception and stemflow in a pine plantation. J. Forestry, 39:505-522.

Landsberg, J.J. and A.S. Thom 1971. Aerodynamic properties of a plant of complex structure. Quart. J. Roy. Met. Soc., Vol. 97, No. 414:565-570.

Landsberg, J.J. and P.G. Jarvis 1973. A numerical investigation of the momentum balance of a spruce forest. J. Appl. Ecol., Vol. 10:645-655.

Longley, R.W. and B. Janz 1978. The climatology of the Alberta Oil Sands Environmental Research Program Study Area. Report for the Alberta Oil Sands Environmental Research Program Project ME 1.0.

Mukammal, E.J. 1971. Some aspects of radiant energy in a pine forest. Archiv. Met. Geophysk. Bioklimt. B, 19:29-52.

Mehlenbacher, A. and D.W.A. Whitfield 1977. Energy and water balance model. In: L.C. Bliss (Ed.). Report to the Alberta Oil Sands Environmental Research Programme. Project VE6.1, pp227-247.

Oliver, H.R. 1975. Ventilation in a forest. Agric. Met. 14:347-355.

Stewart, J.B. and Thom, A.S. 1973. Energy budgets in pine forest. Quart. J. Roy. Met. Soc., Vol. 99, No. 419:154-170.

Thom, A.S., J.B. Stewart, H.R. Oliver, and J.H.C. Gash 1975. Comparison of aerodynamic and energy budget estimates of fluxes over a pine forest. Quart. J. Roy. Met. Soc., Vol. 101, No. 427: 93-105.

Whistance-Smith, R. 1973. Rainfall measurement south of Edmonton, Alberta. A comparison of two network density scales. Unpubl. M.Sc. Thesis, University of Alberta, Edmonton.

Appendix A

Selection of a dry season for modelling purposes.

In order to complete the main predictive aspects of the project, the model needs to be run using data from a dry period. In choosing drought conditions, the plants are put under the worst growing conditions and the survival or death of the plants can be predicted.

All available climatic data for the Tar Sands area were analyzed in order to find typical dry conditions for the region. Monthly precipitation totals and mean daily maximum temperatures for the ten years with lowest precipitation totals in the period April to August are given in Table 1 (Embarras Airport or Fort Chipewan) and Table 2 (Fort McMurray). The five month period was choosen because it essentially represents the growing season. Monthly precipitation totals in the period September to March preceding the ten driest years of Table 1 are shown in Table 3 for Embarras-Fort Chipewyan only.

General Comments:

1. The all-time recorded minimum precipitation was near zero for each of the five months April to August (bottom row, Tables 1 and 2).

2. Thirteen out of the twenty driest April to August periods (Tables 1 and 2) had mean daily maximum temperatures above average. Not much correlation is suggested.

3. Of the fifty-nine months September to March for which data were available preceding the ten driest April to August periods at Embarras-Fort Chipewyan (Table 3), 45 were below the long-term mean precipitation totals. Only 29-30 would be expected by chance. This correlation seems significant.

4. Precipitation amounts and maximum temperatures at Embarras-Fort Chipewyan seem quite different from thos at McMurray. For example, the April to August precipitation of the ten driest years at Embarras-Fort Chipewyan was only 67 percent of that at Fort McMurray on average and maximum temperatures in those years were 3C less than those at McMurray.

Data Selection

Data were available for Embarras (10 years, 1953-1962), and Fort McMurray only (20 years,1953-1972). Therefore data were available only for 1953 in Table 1. For this reason and the other previous comments 1953 was choosen both for a dry April to August period and for a dry single summer month. Some of the characteristics of 1953 were:

(a) The April to August period was the 9th driest in 61 years.

(b) The April to August peiod of 1953 was preceded by below average precipitation in September to March.

(c) The low precipitation amounts of April to August were accompanied by mean daily maximum temperatures well above average (second or third highest of ten years).

(d) The April to June period of 1953 was the second driest on record (1.08 inches vs. 1.04 inches in 1900).

(e) The precipitation in July, 1953 was above average. However it was decided not to replace this with another July because of the complex and subtle interactions among the variables.

With the selection of 1953 as the dry year to run the model, it was a fairly simple matter of extracting the driving variables from the existing data file. The main problem was the lack of radiation data. Since hourly cloud observations for the station were available, radiation values were obtained by comparing cloud conditions at the Richardson site with measured radiation values . This method was just as accurate as if a radiation model was used to create the data base form the observed cloud conditions.

Table 1. Monthly toatal precipitation and mean daily maximum temperatures at Embarras Airport or Fort Chipewyan for the ten years with least total precipitation in the period April to August inclusive based on 61 years of data 1883-1976 (only those years for which precipitation totals were available for each of the five months).

STATION	YEAR	MONTHLY PRECIPITATION (IN.)					TOTAL APRIL TO AUGUST	MEAN DAILY MAX TEMP (^{o}F)					MEAN MAX TEMP.
		A	M	J	J	A		A	M	J	J	A	
PY	1920	0.30	T*	0.90	0.28	1.42	2.90	32.6	54.0	62.9	75.2	69.6	58.9
PY	1923	0.20	1.03	0.02*	0.94	0.95	3.14	33.1	47.4	68.5	71.5	65.0	57.1
PY	1925	1.07	0.46	0.45	1.02	0.64	3.64	42.8	56.5	67.6	75.8	72.1	63.0
PY	1937	0.45	0.89	0.96	0.73	0.86	3.89	45.7	62.0	72.6	80.4*	73.8	66.9
PY	1938	0.29	0.53	1.02	1.28	1.06	4.18	36.3	57.7	71.3	76.6	69.9	62.0
PY	1933	0.85	0.65	0.74	1.34	0.74	4.32	34.8	57.1	66.9	71.8	74.0	60.9
PY	1928	1.27	0.01	1.27	1.05	0.95	4.55	26.5	54.3	67.0	75.6	64.9	57.7
PY	1901	0.70	1.94	0.81	0.21	1.15	4.81	39.6	56.5	62.5	70.1	70.5	59.8
EM	1953	0.19	T*	0.89	2.87	0.89	4.84	41.5	61.3	66.7	73.5	76.7*	63.9
PY	1912	1.06	0.75	2.31	0.58	0.15*	4.85	39.7	M	71.1	M	M	M
LONG TERM MEAN (PY 50 Yrs.)		0.76	0.88	1.36	2.04	1.63	6.67	37.4	54.2	66.0	72.4	68.6	59.7
ALL-TIME RECORD		0.08	T	0.02	0.13	0.15		55.9	67.4	76.6	80.4	76.7	

PY = FORT CHIPEWYAN
EM = EMBARRAS AIRPORT
T = TRACE
M = MISSING DATA

* EQUALS ALL-TIME RECORD .

Table 2. Monthly total precipitation and mean daily maximum temperatures at Fort McMurray Airport for the ten years with least total precipitation in the period April to August inclusive based on 53 years of data 1908-1976 (only those years for which precipitation totals were available for each of the five months).

YEAR	MONTHLY PRECIPITATION (IN.)					TOTAL APRIL TO AUGUST	MEAN DAILY MAX TEMP (°F)					MEAN MAX TEMP.
	A	M	J	J	A		A	M	J	J	A	
1940	0.67	1.95	1.89	0.22	1.19	5.92	51.0	68.1	67.7	77.1	77.0	68.2
1942	0.25	0.28	2.86	1.35	1.34	6.08	47.1	66.7	73.7	77.3	74.1	67.8
1948	0.54	0.47	1.22	2.77	1.14	6.14	34.0	66.6	74.5	75.4	69.5	64.0
1926	0.99	1.70	0.76	1.86	1.38	6.69	51.4	63.9	68,8	78.5	71.2	66.8
1943	0.35	1.21	3.30	0.48	1.65	6.99	55.9	60.5	69.9	79.0	76.4	68.3
1961	0.40	0.42	4.00	1.09	1.15	7.06	41.9	63.5	74.7	75.7	78.1	66.8
1963	0.31	0.63	1.45	2.49	2.22	7.10	48.2	60.8	72.0	76.5	74.6	66.4
1953	1.05	0.09*	1.92	2.15	1.93	7.14	44.5	64.7	66.5	73.1	75.4	64.8
1971	0.77	0.29	2.70	1.91	1.51	7.18	52.8	70.6	72.2	73.4	76.7	69.1
1934	0.61	1.53	1.64	1.98	1.48	7.24	50.5	64.9	68.4	72.9	68.9	65.1
LONG-TERM MEAN	0.82	1.36	2.38	2.98	2.30	9.84	48.0	62.9	70.4	75.2	72.0	65.7
ALL-TIME RECORD	T	0.09	0.69	0.22	0.40		64.6	70.8	78.0	81.6	79.7	

* = ALL-TIME RECORD

T = TRACE

Table 3. Monthly total precipitation September to March inclusive preceding the 10 driest April to August periods at Embarras Airport or Fort Chipewyan.

STATION	YEAR	MONTHLY PRECIPITATION (IN.)							TOTAL
		S	O	N	D	J	F	M	
PY	1919-20	M	0.23	0.85	M	0.60	0.45	0.35	
PY	1922-23	0.99	2.25	1.94	0.60	0.75	0.13	0.30	6.96
PY	1924-25	0.92	0.40	0.60	0.20	M	0.60	1.10	
PY	1936-37	3.60	0.83	0.67	M	0.35	0.90	0.10	
PY	1937-38	0.25	0.22	0.45	1.05	0.40	0.40	0.48	3.25
PY	1932-33	0.75	0.38	1.60	0.50	0.25	1.60	0.85	5.93
PY	1927-28	1.35	1.59	0.43	0.21	0.46	0.35	1.06	5.45
PY	1900-01	0.70	0.51	0.75	0.70	0.58	0.63	M	
EM	1952-53	0.76	1.29	0.68	0.38	0.70	0.43	0.91	5.15
PY	1911-12	0.39	M	M	M	M	M	M	
LONG-TERM (PY 50 Yrs.)		1.50	0.89	0.96	0.85	0.74	0.70	0.71	6.35

PY = FORT CHIPEWYAN
EM = EMBARRAS AIRPORT
T = TRACE
M = MISSING DATA

4. SOIL PHYSICS

A. H. Maclean
Department of Soil Science
University of Alberta

4.1 INTRODUCTION

During 1976 (AOSERP 1978) a considerable amount of field information was acquired on moisture and temperature regimes prevailing in the sand on the sttep Jackpine-covered slope at Richardson tower. This information was supplemented by laboratory determinations of a routine nature together with determinations of relationships between hydraulic conductivity, moisture tension, and moisture content. The purpose during 1977 was to continue field monitoring with emphasis on those areas where understanding was most lacking, namely, moisture infiltration during spring thaw, and moisture tension extremes reached during dry spells in summer.

In the Annual Report for 1976/7, it was shown that the sands at the study sites are generally very low (<2%) in non-sand material, and the sand falls mainly into the medium and fine sand (0.5-0.105 mm) fractions. Bulk densities ranged from 1.35 to 1.45 in the surface Ae horizon to 1.50 to 1.60 in the C horizon. Saturated hydraulic conductivities ranged from 26 to 58 cm/hr while the unsaturated hydraulic conductivity of the C-horizon material from a depth of 75 cm declined rapidly with increase in moisture tension particularly between 30 and 60 mbar. Moisture

Moisture retention data suggested that after initial rapid drainage to a tension of around 60 mbar (6 to 10% moisture by volume) the amount of water available to the vegetation ranges from 95 mm per m depth in the Ae horizon to 58 mm per m in the C-horizon.

Thermocouples showed that the 0°C isotherm penetrated to 2.75 m by early April after which thawing was extremely rapid, being complete by early May. Temperatures in the near-surface soil exceeded 15°C from early June until mid-October.

Moisture tensions were difficult to obtain accurately. Tensiometers failed to respond rapidly enough in these sands to give accurate readings at tensions greater than 100-200 mbar and equipment was not available for many readings with psychrometers. It appeared however that tensions greater than 18 bar did not occur during the growing season.

Moisture content readings were obtained using a neutron probe which was calibrated in materials close to the access tubes. Readings were taken at intervals throughout the year, though inaccuracy occurred in the near-surface in winter because of interception of snow by the "sphere of influence" which is exceptionally large in these low-moisture sands. During the thaw period, readings were again inaccurate because a thin layer of sand which was near-saturated with water lay in contact with sand containing only 3 or 4 percent moisture. When the probe was in the dry material, the sphere of influence intercepted the wet layer and readings were over inflated. Gravi-

metric sampling however provided supplementary information on moisture changes during this period. Since little surface runoff was observed and most of the water in the snowpack could be accounted for as an increase in moisture in the ground, it was assumed that all meltwater entered the soil. The changes in moisture content within 6 m of the ground surface were combined with information on amounts of non-intercepted precipitation to derive cumulative loss curves for the period April to October. The loss consisted of drainage plus evapo-transpiration, but at this stage no attempt was made to calculate drainage separately.

Three water table holes produced evidence for a fairly flat water table surface, supporting the view that the hill contains no core of slowly permeable material.

It was recommended that during the following season, more use should be made of psychrometers for information on tensions, while a more thorough examination of moisture changes over the thaw period should be carried out either using gravimetric sampling or through development of an improved non-destructive method of moisture determination.

4.2 LITERATURE REVIEW

"See previous report"

4.3 MATERIALS AND METHODS

4.3.1 Soils

"See previous report"

4.3.2 Laboratory Methods

4.3.2.1 Routine Analyses. "See previous report".

4.3.2.2 Bulk Density and Core Samples. "See previous report".

4.3.2.3 Hydraulic Conductivity. Saturated hydraulic conductivity was determined by the constant head method (Klute 1965). Rings (2.6 cm diam. 6 cm long) were packed to a bulk density similar to that in the field and saturated with distilled water under vacuum. Because of the high permeability of the sands, it was necessary to minimize flow impedance by using 0.05 mm opening wire mesh screens at both ends of the ring, in place of ordinary filter paper, while loss of fine material was minimized by using microburettes at both inlet and outlet ends of the core which allowed the quantity of water flow to be minimized.

Unsaturated hydraulic conductivity was determined using an apparatus similar to that described by Elrick and Bowman (1964). Cellulose acetate filters of suitable pore size for the required pressure range were used at either end of rings packed similarly to those for saturated conductivity. Pressures were controlled by drilling numerous small holes in the ring wall and enclosing the whole apparatus in a pressurized container.

Unsaturated hydraulic conductivities were also derived from moisture retention curves, using the Millington and Quirk (1961) equations with matching at saturation point (Green and Corey 1971). The determination of moisture retention curves was described in the previous annual report (AOSERP 1978).

4.3.2.4 Moisture Retention. "See previous report".

4.3.3 Field Methods

4.3.3.1 Field Sites and Field Monitoring. Three sites were instrumented in October 1976, one near the top of the hill, one near the middle, and one near the bottom of the hill. Details of the instrumentation at each site are given in the previous annual report. The only changes in 1977 involved the addition of 14 psychrometers to the middle site, at depths of 5 cm(4), 10 cm(6), 15 cm(1), 20 cm(20) and 50 cm(1).

4.3.3.2 Field Methods and Interpretation.

4.3.3.2.1 Soil Temperature

4.3.3.2.2 Moisture Tension

Tensiometers with mercury manometers, similar to those described by Webster (1966) were used to measure tensions at depths to 300 cm below the surface. Psychrometers made by Meryll and also by Wescor Inc. were used to measure tensions in the dry range, in the near surface soil.

4.3.3.2.3 Soil Moisture

A Nuclear Chicago neutron probe was used to measure moisture content. Three 6 m deep aluminum access tubes were present at each of the three sites. Calibration had been carried out by augering holes, inserting an aluminum access tube, taking counts, and saving the augered material for gravimetric determination. At most times of the year, the neutron probe gave satisfactory results, and had the advantage over gravimetric determinations of fairly consistent sample location and minimal site destruction. However, during spring thaw, the probe vastly overestimated total soil water content. At this time, soil almost saturated with water lies in contact with soil which is almost dry. While probe readings taken within the saturated layer should theoretically be fairly accurate, those taken within adjacent dry soil are erroneous, because of the sphere of influence is inversely related to moisture content and expands to include moisture in the wetter soil. During the thaw 1977, gravimetric samples taken within 1 to 2 m of the probe tubes were used to determine the position of wet and dry

layers. Probe readings were used for the wet layers, and gravimetric readings only for the dry zones, where sample errors associated with such readings should have a minimal effect on calculated total water. In the presence of snow cover, snow was removed from some access tubes, to ascertain the amount that near-surface readings should be adjusted for interception of snow by the "sphere of influence". The snow was then returned.

Although a method of measuring soil moisture, based on thermal conductivity was investigated, it was not found to be sufficiently accurate over the desired moisture range to warrant field development, when the project was soon to be terminated.

4.4 RESULTS AND DISCUSSION

4.4.1 Particle Size Analyses

"See previous report"

4.4.2 Bulk Density

"See previous report"

4.4.3 Hydraulic Conductivity

Hydraulic conductivity - moisture content relationships derived from moisture retention curves using the Millington and Quirk equation (1961) are shown (Figure 1). The curves were matched at saturation to the laboratory derived valued (Green and Corey 1971). Laboratory determined hydraulic conductivities

Table 1. Mean annual temperatures at the middle site for two different years, and at all three sites during the period 1 July 1977 to 1 July 1978.

Depth (cm)	Middle site 1 Oct 75-76	Middle site 1 Oct 76-77	Middle site 1 Jul 76-77	Upper site 1 Jul 76-77	Lower site 1 Jul 76-77
100	4.43	4.90	5.28	3.80	4.75
300	4.91	5.12	5.09	4.24	4.72
600	4.98	5.18	5.08	4.18	4.86

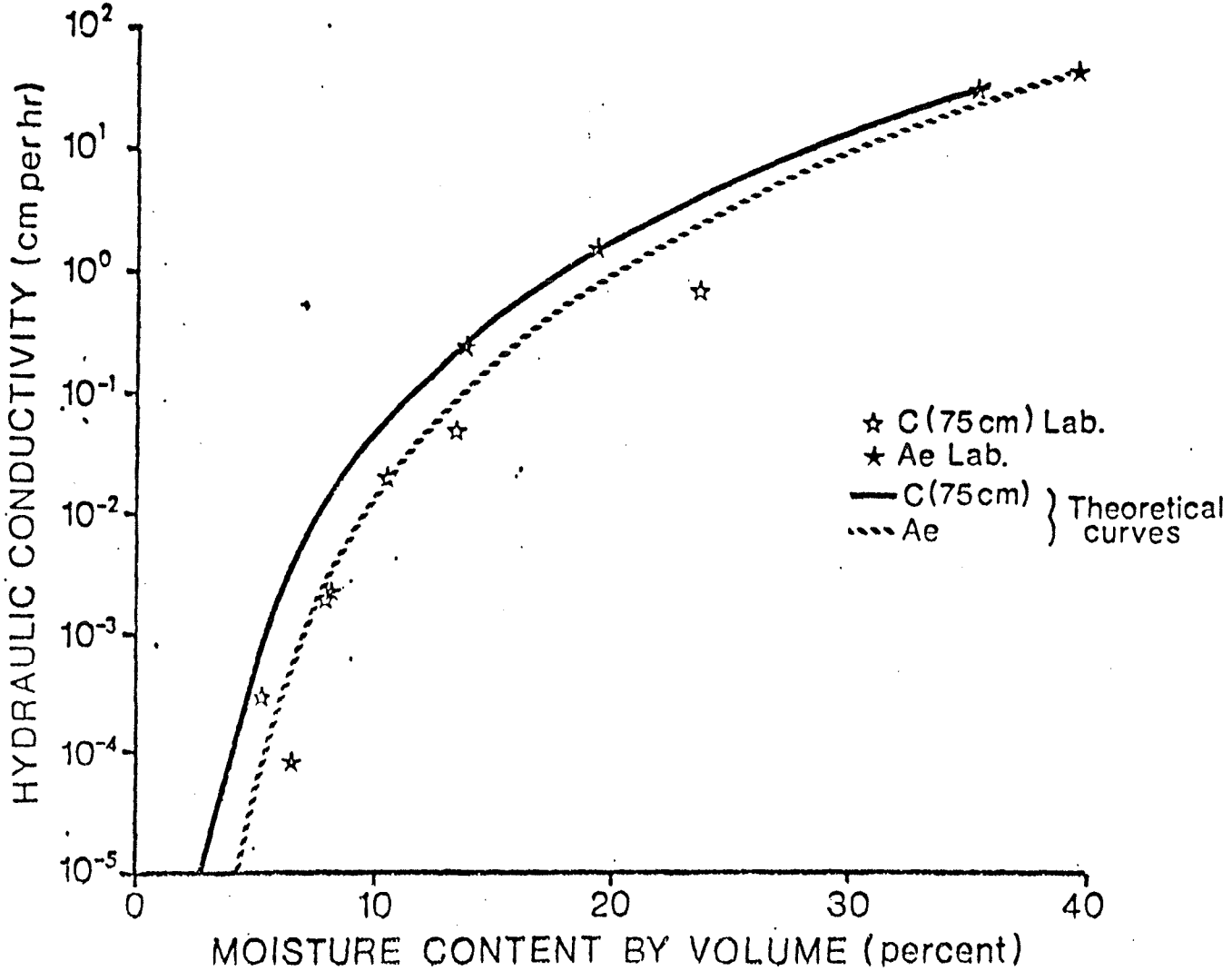

Figure 1. Relationship between hydraulic conductivity and moisture content for two soil horizons, derived from the moisture retention curves, and determined in the laboratory.

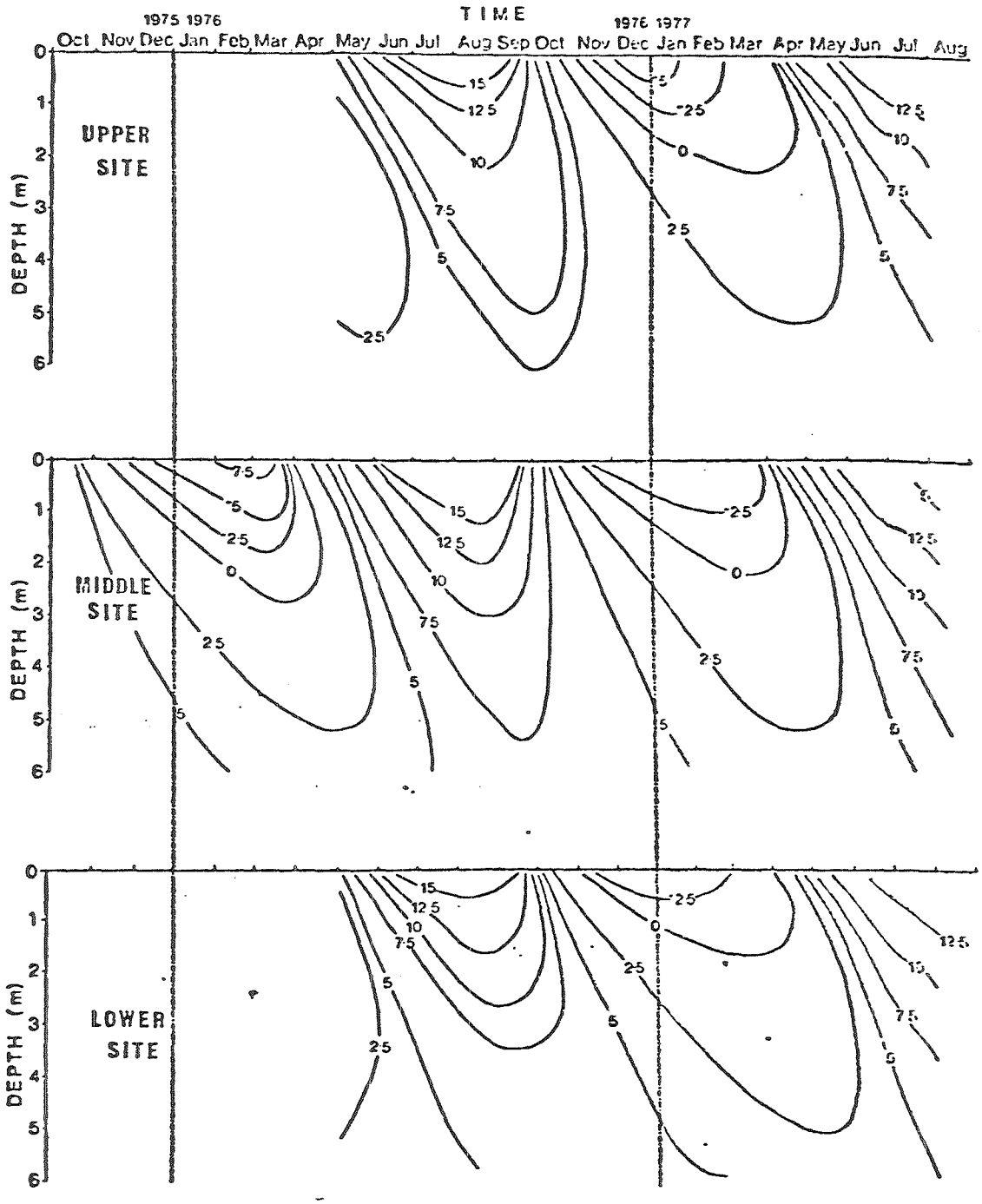

Figure 2. Isotherms in relation to time and depth beneath the ground surface during the whole period of measurement.

are given for comparison and these show a reasonable approximation to the theoretical values.

4.4.4 Moisture Retention

"See previous report"

4.4.5 Ground Temperatures

Changes in ground temperature for all three sites over the whole period are shown (Figure 2). Temperatures differed only slightly between the two years, and were on average (Table 1), a little higher in 1977 than in 1976. The middle site was warmer than the other two sites (Table 1), presumably because it has a steeper slope than the lower site and is less shaded than the upper site.

4.4.6 Moisture Tensions

As in the summer 1976, high moisture tensions (>10 bars) did not appear to persist for any length of time. However, psychrometer readings were only taken occasionally due to the wind-up nature of the project. There was some suggestion of a relationship between moisture tension readings and time of day, peak tensions usually occurring during the afternoon.

4.4.7 Moisture Content

"See previous report"

Table 2. Total water to a depth of 6 metres below the ground surface on March 8th and April 15th 1977 and the expected total water on April 15th assuming all precipitation entered the ground and only a negligable amount of water drained below 6 m.

Location of water	Upper Site	Middle Site	Lower Site
Water (mm) in 6 m soil on March 8	191	242	290
Water (mm) in Snowpack on March 8	14	51	46
Water (mm) Precip. March 8-March 15	22	22	22
Total (above) = water expected in 6 m soil on April 15	227	315	358
Water (mm) found in 6 m soil April 15	161	302	397
Difference	-66	-13	+39

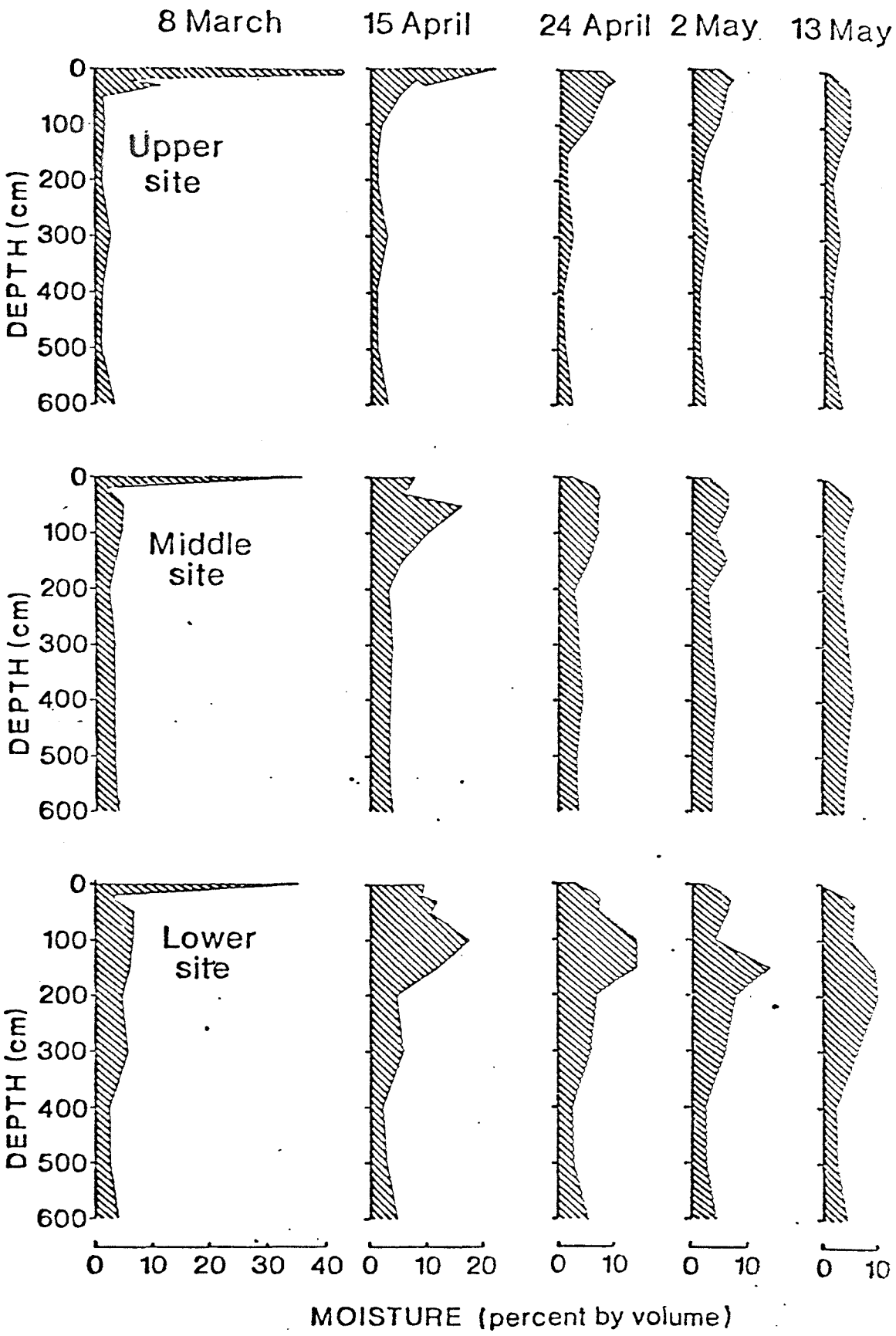

Figure 3. Soil water content profiles at different times following the thaw.

4.4.7.1 Moisture Changes During Thaw. During 1977, particular attention was given to the thaw period. Because the winter was exceptionally mild, considerable thawing had already occurred by early March, leaving the upper site almost bare. The downward movement of water as the season progressed is shown (Figure 3). The graphs suggest that at the upper site, little of the thaw water reaches a depth of 200 cm perhaps due to presence of boulders or other features so that presumably water escapes laterally downhill. Calculations in Table 2, attempt to account for all the water from the snowpack as increase in water held by the soil, (ignoring surface runoff and evapo-transpiration). More water accumulated at the lower site than can be accounted for by meltwater and precipitation, while at the upper site, the reverse is true. Although no significant surface runoff was observed, it seems probable that early in the thaw period, when the surface is near-saturated with water, and vertical movement is impeded by frost, lateral downslope movement of water is considerable, and could account for the extra water at the lower site.

4.4.7.2 Water drainage. Several different ways of estimating vertical drainage rates at the middle site were examined. The most accurate information was at the time of the spring thaw when a large quantity of water moves downwards as a fairly well defined "bulge", into sand that is relatively dry after

the long period of drainage over winter. Drainage at a depth of 300 cm was calculated as the increase in moisture within the 300-600 cm depth limits plus the estimated loss (downwards) from this zone over the same period. At the middle site the movement into this zone was 45 mm between 15 April and 27 May 1977, while loss was estimated at 1 mm bringing total drainage to 46 mm. Similar calculations showed that 42 mm passed the 100 cm depth level by 2 May. At the upper site, only 7 mm was calculated to have passed the 300 cm depth, and only 18 mm to have drained passed the 100 cm depth. At the lower site, little water drained at 300 cm (presumably because of boulders or textural barriers to vertical movement) while 89 mm drained at a depth of 100 cm and presumably escaped laterally downslope.

Outside the thaw period, drainage rates are difficult to calculate. Since hydraulic conductivities had been determined in the laboratory for material from a depth of 75 cm, an attempt was made at calculating drainage at this depth, using tensiometer tensions and field moisture contents obtained over the growing season, in the equation:

$$D = \int_{t_1}^{t_2} (K_\theta + K_\theta \, \partial h/\partial z) \, \partial t$$

(D=drainage, k=hydraulic conductivity, h=suction head in cm water, z=depth in cm, t=time).

The results however varied between 2 and 85 mm in 117 days depending on which moisture values were used, and were

obviously too inprecise. They showed how difficult it is to obtain an accurate measure of water movement in a sand which exhibits such a narrow range of water content, while these water contents correspond to such a relatively broad range of moisture tensions and hydraulic conductivities.

It appeared that the best estimate of drainage should be based on moisture content values at 250 cm, because this was the greatest depth at which moisture tension gradients could be calculated. At this depth, both thermal and moisture tension gradients are small and stable over long periods of time and so errors resulting from interpolation between readings, and response times are minimized. At times of the year when moisture tensions were not available, they were inferred from moisture content using a plot of field moisture and tensions at the same depths (Figure 4). There remained the problem of obtaining an adequate hydraulic conductivity - moisture content relationship for material at a depth of 250 cm. The hydraulic conductivities for material from 75 cm gave results which were obviously too low to explain the fast rate of drainage following the thaw of 1977 and following periods of heavy rainfall such as between June 25th and July 3rd 1977. The assumption was therefore made that the basic shape of the hydraulic conductivity - moisture content curve would be similar at 250 cm to that at 75 cm and the curve was adjusted using a matching factor which brough drainage amounts following

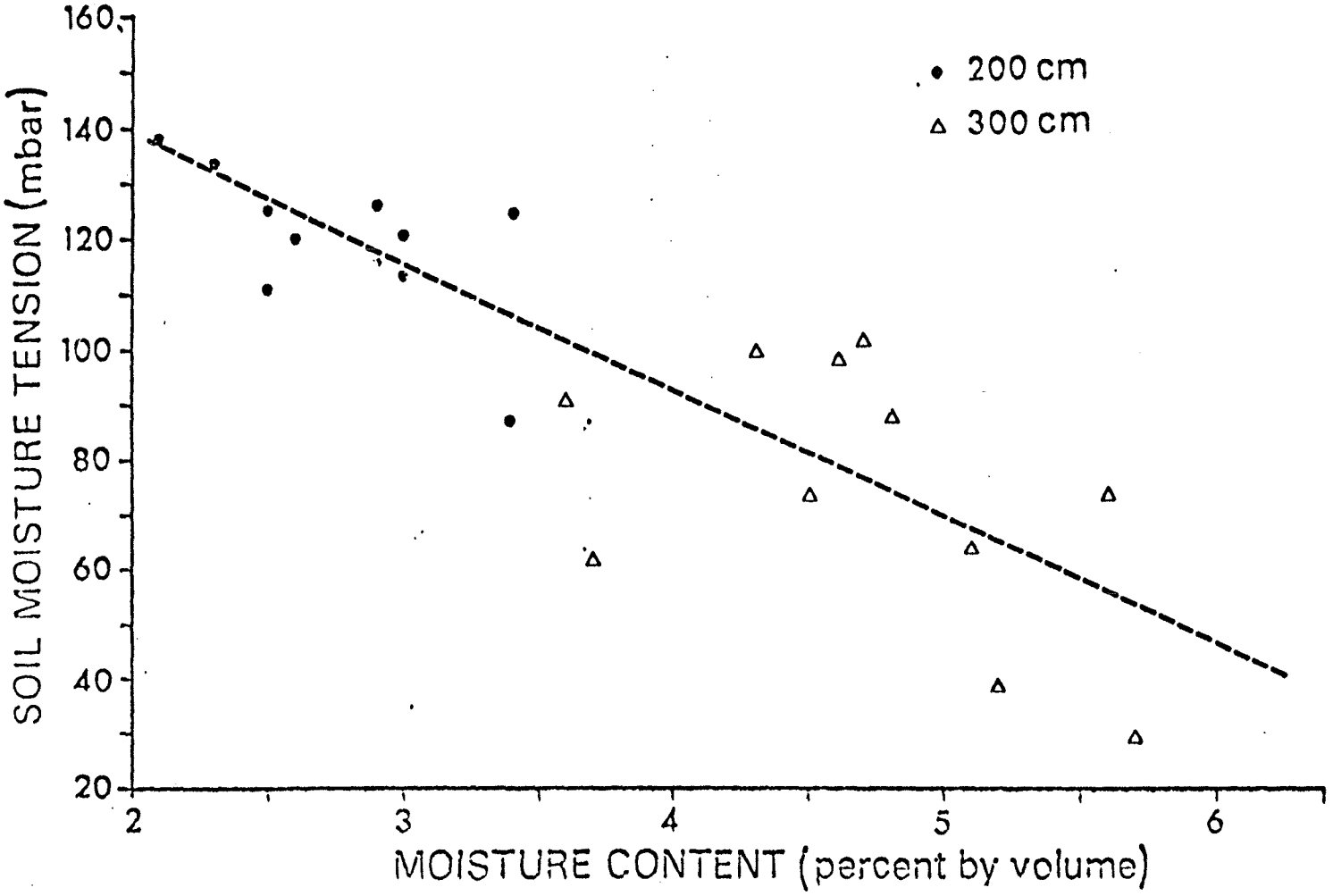

Figure 4. Relationship between field measurements of moisture content and moisture tension, at depths of 200 cm and 300 cm at the middle site.

the 1977 thaw to approximately the same as those calculated from movement of the "thaw bulge", and drainage during short selected periods at other times of the year to those predicted mathematically using the method of Rose et al. (1965). These hydraulic conductivities were then used along with the hydraulic gradients to calculate drainage over the whole two year period of observations except during March to May 1976, when freezing occurred between depths of 200 cm and 300 cm. Drainage for this period had to be estimated graphically by comparing moisture content profiles.

Drainage at a depth of 600 cm was initially calculated using the same hydraulic conductivities as for 250 cm, and assuming that the matric tension gradient at 600 cm was negligable. The hydraulic conductivities were then adjusted by a matching factor to bring the cumulative drainage over two years to the same as at 250 cm (only strictly true over long periods). The theoretical hydraulic conductivities are shown (Figure 5) and calculated cumulative drainage curves are shown (Figure 6).

4.4.7.3 Water Changes Over the Growing Season. Loss in profile moisture has been added to calculated non-intercepted precipitation (plus snowpack meltwater) to give total water loss from the middle site (0-600 cm) over the period March to September 1977 (Figure 7). Calculated cumulative drainage loss from the 600 cm depth and cumulative non-intercepted precipitation are included for comparison. The difference between the drainage and total loss curves should be

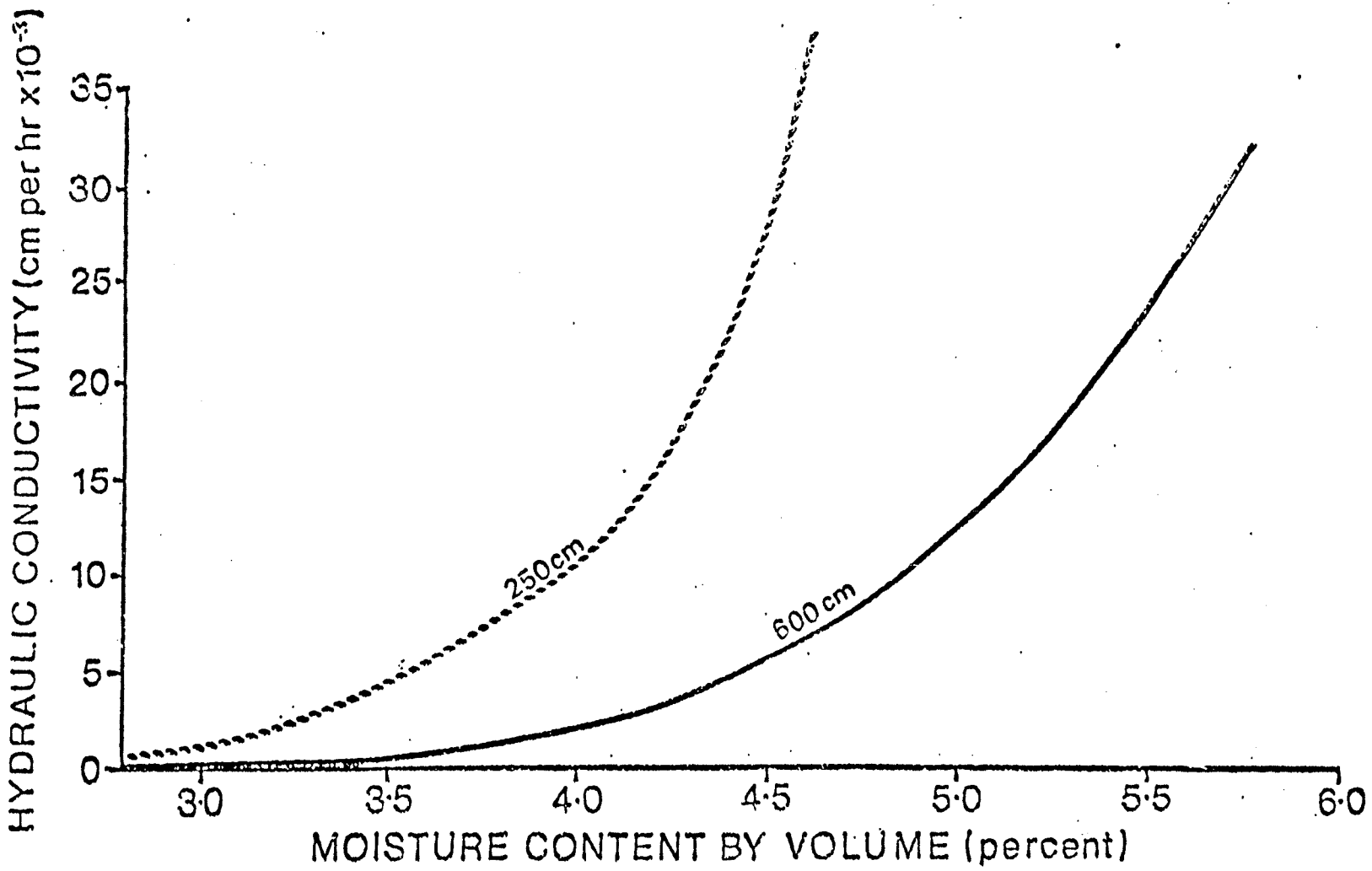

Figure 5. Estimated relationship between hydraulic conductivity and moisture content for sand at depths of 250 cm and 600 cm.

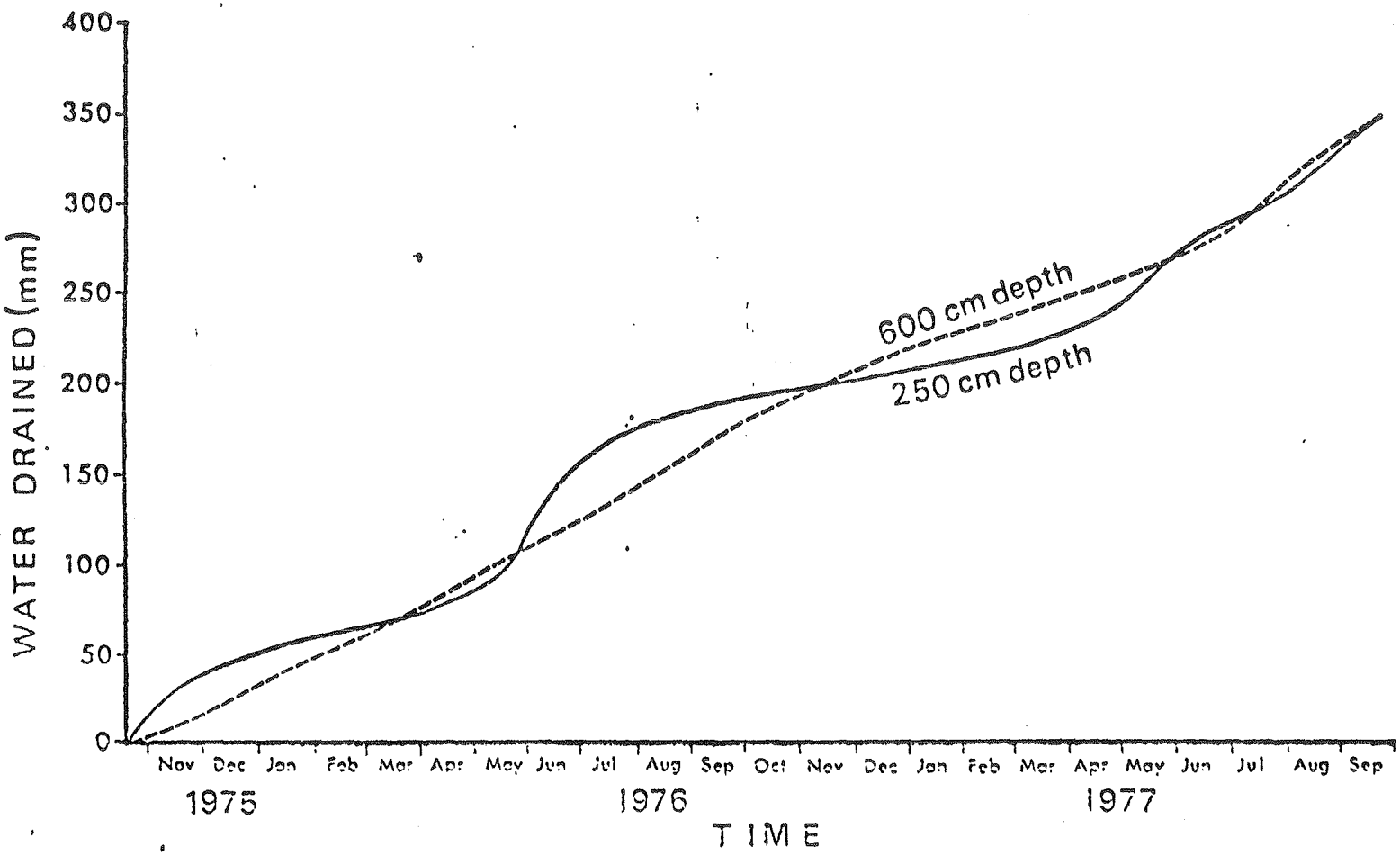

Figure 6. Cumulative water drained at depths of 250 cm and 600 cm at the middle site.

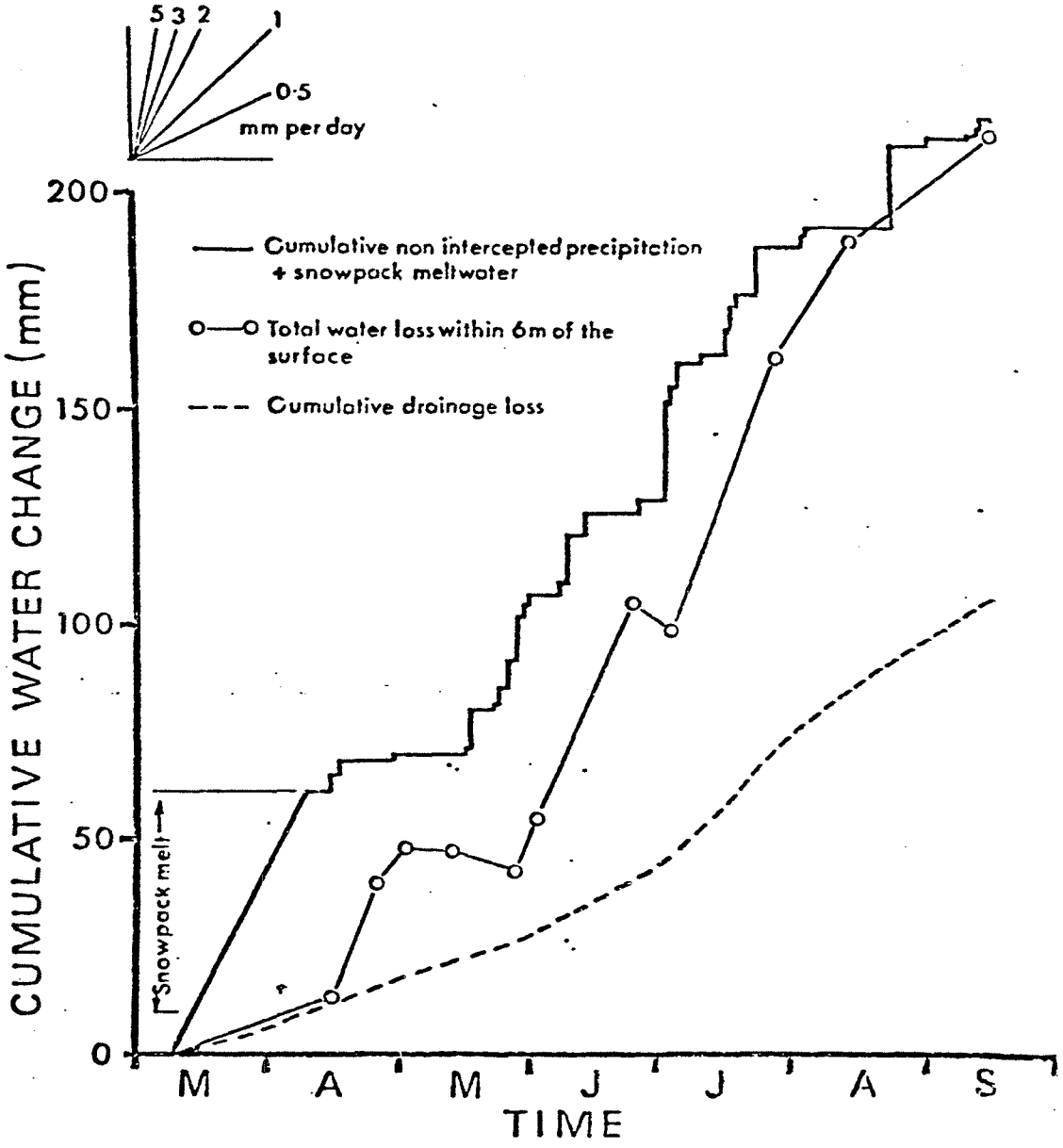

Figure 7. Cumulative total water loss within 6 m of the ground surface during the growing season of 1977 at the middle site, compared with non-intercepted precipitation and calculated cumulative drainage. Slopes corresponding to various loss rates are shown (top).

tree and shrub uptake as presumably only a small component of direct evaporation is included, since evaporation from the lichen layer is incorporated in the calculation of non-intercepted precipitation, and the lichen layer itself should have partly protected the soil surface from direct evaporation. Cumulative loss curves for all three sites are compared in Figure 8. Loss rates at all three sites appear fairly comparable.

4.5 CONCLUSIONS AND RECOMMENDATIONS

Soil temperature profiles for 1977 were similar to those of 1976.

There was a lack of high moisture tensions under the Jackpine, in conformity with the results of 1976.

Analysis of moisture data over the thaw period suggests that although little surface runoff appears to occur, considerable water must move down-slope in near-saturated surface soil while the sub-surface is below freezing.

Calculations suggest that around 167 (year 2) to 195 (year 1) mm water per year drained vertically below the root zone during the project period. This is 47 and 48 percent of total precipitation respectively.

4.6 ACKNOWLEDGEMENTS

"See previous report"

4.7 REFERENCES (ADDITIONAL)

A.O.S.E.R.P. 1978. V.E.6. Annual Report for 1976/77.

tree and shrub uptake as presumably only a small component of direct evaporation is included, since evaporation from the lichen layer is incorporated in the calculation of non-intercepted precipitation, and the lichen layer itself should have partly protected the soil surface from direct evaporation. Cumulative loss curves for all three sites are compared in Figure 8. Loss rates at all three sites appear fairly comparable.

4.5 CONCLUSIONS AND RECOMMENDATIONS

Soil temperature profiles for 1977 were similar to those of 1976.

There was a lack of high moisture tensions under the Jackpine, in conformity with the results of 1976.

Analysis of moisture data over the thaw period suggests that although little surface runoff appears to occur, considerable water must move down-slope in near-saturated surface soil while the sub-surface is below freezing.

Calculations suggest that around 167 (year 2) to 195 (year 1) mm water per year drained vertically below the root zone during the project period. This is 47 and 48 percent of total precipitation respectively.

4.6 ACKNOWLEDGEMENTS

"See previous report"

4.7 REFERENCES (ADDITIONAL)

A.O.S.E.R.P. 1978. V.E.6. Annual Report for 1976/77.

4.8 APPENDIX

APPENDIX TABLE A-1. Ground temperatures (C) at sites at Richardson Tower during 1977.

DEPTH (cm)	UPPER SITE	MIDDLE SITE	LOWER SITE	DEPTH (cm)	UPPER SITE	MIDDLE SITE	LOWER SITE
	6 JANUARY 1977				9 MARCH 1977		
1	-7.7	-5.9	-5.0	1	.1	-.2	.2
2	-7.6	-5.6	-4.9	2	.3	-.2	.2
5	-7.4	-5.2	-4.8	5	-.1	-.1	.1
10	-7.0	-4.8	-4.6	10	-.4	-.3	-.1
20	-6.8	-4.4	-4.2	20	-.7	-.6	-.2
50	-5.2	-3.3	-2.8	50	-1.1	-.7	-.6
100	-3.0	-1.2	-.7	100	-1.3	-.9	-.6
150	-.5	.5	.6	150	-.9	-.5	.0
200	1.0	1.4	1.3	200	-.2	-.2	.5
300	2.7	3.3	2.9	300	.7	1.2	1.4
450	4.2	4.6	4.6	450	2.4	2.4	2.7
600	5.0	6.0	5.6	600	3.5	3.5	3.8
	9 APRIL 1977				16 APRIL 1977		
1	5.6	5.8	.7	1	3.2	1.8	3.5
2	5.1	4.2	.6	2	3.2	1.4	2.5
5	3.6	3.3	.4	5	2.4	1.6	1.6
10	1.4	1.5	.2	10	1.8	1.4	1.0
20	.2	.2	.2	20	1.4	1.1	.6
50	-1.4	.4	-.4	50	-.1	.1	-.1
100	-2.0	.3	-.9	100	-.5	-.2	-.1
150	-1.4	.1	-.4	150	-.6	-.1	-.2
200	-.2	.0	.3	200	-.1	.0	.0
300	.9	-	1.2	300	.6	.8	.8
450	2.0	2.4	2.4	450	2.1	1.7	1.9
600	3.7	3.4	3.5	600	3.2	3.0	3.1
	12 MAY 1977				19 MAY 1977		
1	10.9	9.8	11.5	1	8.6	9.2	9.3
2	10.9	10.0	10.8	2	8.5	8.3	8.0
5	10.6	10.7	10.2	5	7.4	8.0	7.0
10	10.6	10.6	9.6	10	6.5	7.0	6.0
20	10.5	10.6	9.1	20	6.3	6.4	5.2
50	8.5	8.5	7.1	50	6.1	6.5	4.9
100	5.4	5.5	3.5	100	5.1	5.7	3.7
150	2.7	3.2	1.2	150	4.0	4.9	2.8
200	.9	1.7	.5	200	2.8	3.7	2.2
300	.8	-	1.1	300	1.8	2.4	1.6
450	2.1	1.9	2.2	450	2.3	2.4	2.1
600	3.2	3.0	3.1	600	3.3	3.2	3.0

(continued)

4.8 APPENDIX

APPENDIX TABLE A-1. Ground temperatures (C) at sites at Richardson Tower during 1977.

DEPTH (cm)	UPPER SITE	MIDDLE SITE	LOWER SITE	DEPTH (cm)	UPPER SITE	MIDDLE SITE	LOWER SITE
	6 JANUARY 1977				9 MARCH 1977		
1	-7.7	-5.9	-5.0	1	.1	-.2	.2
2	-7.6	-5.6	-4.9	2	.3	-.2	.2
5	-7.4	-5.2	-4.8	5	-.1	-.1	.1
10	-7.0	-4.8	-4.6	10	-.4	-.3	-.1
20	-6.8	-4.4	-4.2	20	-.7	-.6	-.2
50	-5.2	-3.3	-2.8	50	-1.1	-.7	-.6
100	-3.0	-1.2	-.7	100	-1.3	-.9	-.6
150	-.5	.5	.6	150	-.9	-.5	.0
200	1.0	1.4	1.3	200	-.2	-.2	.5
300	2.7	3.3	2.9	300	.7	1.2	1.4
450	4.2	4.6	4.6	450	2.4	2.4	2.7
600	5.0	6.0	5.6	600	3.5	3.5	3.8
	9 APRIL 1977				16 APRIL 1977		
1	5.6	5.8	.7	1	3.2	1.8	3.5
2	5.1	4.2	.6	2	3.2	1.4	2.5
5	3.6	3.3	.4	5	2.4	1.6	1.6
10	1.4	1.5	.2	10	1.8	1.4	1.0
20	.2	.2	.2	20	1.4	1.1	.6
50	-1.4	.4	-.4	50	-.1	.1	-.1
100	-2.0	.3	-.9	100	-.5	-.2	-.1
150	-1.4	.1	-.4	150	-.6	-.1	-.2
200	-.2	.0	.3	200	-.1	.0	.0
300	.9	-	1.2	300	.6	.8	.8
450	2.0	2.4	2.4	450	2.1	1.7	1.9
600	3.7	3.4	3.5	600	3.2	3.0	3.1
	12 MAY 1977				19 MAY 1977		
1	10.9	9.8	11.5	1	8.6	9.2	9.3
2	10.9	10.0	10.8	2	8.5	8.3	8.0
5	10.6	10.7	10.2	5	7.4	8.0	7.0
10	10.6	10.6	9.6	10	6.5	7.0	6.0
20	10.5	10.6	9.1	20	6.3	6.4	5.2
50	8.5	8.5	7.1	50	6.1	6.5	4.9
100	5.4	5.5	3.5	100	5.1	5.7	3.7
150	2.7	3.2	1.2	150	4.0	4.9	2.8
200	.9	1.7	.5	200	2.8	3.7	2.2
300	.8	-	1.1	300	1.8	2.4	1.6
450	2.1	1.9	2.2	450	2.3	2.4	2.1
600	3.2	3.0	3.1	600	3.3	3.2	3.0

(continued)

APPENDIX TABLE A-1. (Continued)

DEPTH (cm)	UPPER SITE	MIDDLE SITE	LOWER SITE	DEPTH (cm)	UPPER SITE	MIDDLE SITE	LOWER SITE
	26 MAY 1977				2 JUNE 1977		
1	12.6	13.9	13.3	1	12.5	13.2	12.5
2	12.6	13.5	13.0	2	12.6	13.1	12.5
5	12.3	13.4	12.7	5	12.3	13.1	12.4
10	11.9	13.1	12.2	10	12.1	13.0	12.1
20	11.2	12.5	11.4	20	11.8	12.9	11.8
50	9.6	10.6	9.6	50	10.6	11.6	10.5
100	7.2	8.2	6.7	100	8.7	9.6	8.2
150	5.1	6.4	4.7	150	6.7	7.9	6.4
200	3.7	4.8	3.6	200	5.1	6.4	5.0
300	2.5	3.3	2.4	300	3.6	4.2	3.2
450	2.4	2.8	2.4	450	2.8	3.2	2.6
600	3.2	3.2	3.0	600	3.3	3.4	3.0
	24 JUNE 1977				1 JULY 1977		
1	18.1	-	20.9	1	15.6	15.1	17.4
2	17.8	-	19.1	2	15.6	14.3	15.8
5	16.2	18.4	17.5	5	13.5	14.1	14.5
10	15.1	17.1	15.9	10	12.0	13.2	13.0
20	14.6	16.4	14.7	20	11.7	12.9	12.0
50	13.8	15.3	13.7	50	12.2	13.6	12.2
100	11.9	13.4	11.6	100	11.5	13.0	11.5
150	9.7	11.7	9.7	150	10.0	12.0	10.2
200	7.8	9.6	8.2	200	8.4	10.3	8.9
300	5.7	6.8	5.7	300	6.4	7.7	6.5
450	3.3	4.9	3.9	450	4.2	5.5	4.3
600	3.5	-	3.4	600	3.7	4.3	3.7
	18 JULY 1977				25 JULY 1977		
1	12.3	12.3	17.0	1	17.3	18.0	20.4
2	12.3	12.4	15.3	2	17.2	17.3	18.9
5	11.9	12.6	14.0	5	15.8	17.2	17.8
10	11.8	12.4	12.9	10	14.9	16.2	16.3
20	12.3	13.0	12.4	20	14.5	15.5	15.0
50	12.9	14.0	12.9	50	13.8	15.0	14.2
100	11.8	13.2	11.7	100	12.3	13.6	12.5
150	10.4	12.2	10.7	150	10.8	12.7	11.1
200	9.3	11.0	9.6	200	9.5	11.2	10.0
300	7.4	8.7	7.7	300	7.7	9.0	7.9
450	5.1	6.7	5.4	450	5.4	7.0	5.7
600	4.0	5.1	4.3	600	4.1	5.1	4.5

(continued)

APPENDIX TABLE A-1. (Continued)

DEPTH (cm)	UPPER SITE	MIDDLE SITE	LOWER SITE
	31 JULY 1977		
1	15.6	15.5	18.3
2	15.5	16.1	17.5
5	14.5	15.4	16.8
10	14.0	15.2	15.5
20	14.2	15.5	14.5
50	14.3	15.7	14.2
100	13.1	14.5	13.0
150	11.6	13.5	11.9
200	10.3	11.9	10.6
300	8.2	9.5	8.4
450	5.8	7.7	6.3
600	4.5	5.8	4.9
	21 SEPTEMBER 1977		
1	-	17.6	-
2	-	-	-
5	-	12.5	-
10	-	11.8	-
20	-	10.5	-
50	-	10.5	-
100	-	9.9	-
150	-	9.5	-
200	-	9.5	-
300	-	8.8	-
450	-	7.8	-
600	-	6.5	-

DEPTH (cm)	UPPER SITE	MIDDLE SITE	LOWER SITE
	15 AUGUST 1977		
1	-	14.3	-
2	-	14.1	-
5	-	-	-
10	-	13.0	-
20	-	12.6	-
50	-	-	-
100	-	-	-
150	-	12.3	-
200	-	11.8	-
300	-	-	-
450	-	8.2	-
600	-	6.4	-

APPENDIX TABLE A-2.Moisture tension readings (bars) from psychrometers during 1977.

PSYCH NO	DEPTH (cm)	DATE AND TIME JUN 1 1515	JUN 1 1840	JUN 3 0950	JUN 3 1250	JUN 3 1625	JUN 3 2010	JUN 4 0600	JUN 4 1000	JUN 4 1430	JUN 4 2120
31	5	6	2	–	–	–	0	0	0	0	0
35	5	–	–	–	–	–	–	–	–	–	–
208	5	–	–	–	–	–	–	–	–	–	–
204	10	8	5	0	–	0	0	0	0	0	0
18	10	13	10	0	0	5	0	0	0	0	0
117	10	10	4	0	–	0	–	–	0	0	0
129	10	7	5	0	–	0	0	0	0	0	0
110	10	–	–	–	–	–	–	–	–	–	–
239	10	7	1	0	0	0	0	0	0	0	0
160	15	15	15	0	0	9	10	0	0	14	11
236	20	–	17	0	–	0	5	0	0	0	9
229	20	–	–	–	–	–	–	–	–	–	–
205	50	–	–	–	–	–	–	–	–	–	–

(continued)

APPENDIX TABLE A-2. (Continued)

PSYCH NO	DEPTH (cm)	DATE AND TIME JUN 5 0925	JUN 5 1220	JUN 5 1550	JUN 5 2200	JUN 6 0830	JUN 23 0930	JUN 23 1830	JUN 24 1000	JUL 1 1745	JUL 20 1815
31	5	0	-	5	0	-	0	18	0	32	0
35	5	-	-	-	-	-	0	5	-	13	0
208	5	-	-	-	-	-	0	0	-	0	0
21	5	-	-	-	-	-	0	6	-	0	8
204	10	0	0	8	3	0	0	5	0	0	5
18	10	0	0	15	11	0	0	13	0	5	13
117	10	0	0	3	0	0	0	0	-	0	0
129	10	0	0	6	2	0	0	0	-	0	5
110	10	-	-	-	-	-		4	-	0	0
239	10	0	0	4	0	0	0	0	-	1	5
160	15	0	7	15	11	0	0	14	0	13	10
236	20	0	0	13	13	0	0	22	0	0	11
229	20	-	-	-	-	-	0	5	-	0	0
205	50	-	-	-	-	-	0	0	-	0	0

(continued)

APPENDIX TABLE A-2. (Continued)

PSYCH NO	DEPTH (cm)	DATE AND TIME JUL 21 0930	JUL 21 1840	JUL 22 1815	JUL 23 1725	JUL 25 1815
31	5	-	-	-	-	9
35	5	-	-	-	-	0
208	5	-	0	-	-	2
21	5	0	4	-	-	8
204	10	0	3	0	0	6
18	10	0	7	6	8	13
117	10	-	0	-	-	2
129	10	0	2	-	-	6
110	10	-	-	-	-	4
239	10	0	2	0	5	8
160	15	0	7	5	0	7
236	20	0	10	9	0	0
229	20	-	-	-	0	0
205	50	-	-	-	-	3

APPENDIX TABLE A-3. Soil moisture (percent by volume), during 1977, obtained with the neutron probe near Richardson Tower.

DEPTH (cm)	JAN 7	MAR 8	APR 15	APR 25	MAY 2	MAY 13/14	MAY 27	JUN 1
				UPPER SITE				
10	15.9	43.2	18.2	8.9	6.1	2.4	9.4	10.5
20	10.5	23.6	17.2	9.8	7.2	3.6	9.1	9.8
30	6.9	11.5	12.4	8.4	6.4	4.2	6.5	7.5
50	4.1	4.8	10.1	7.4	6.0	4.7	4.7	5.6
100	1.5	1.8	1.9	5.3	4.8	4.4	3.8	3.7
150	2.4	1.4	1.2	1.5	2.3	2.7	2.7	2.7
200	1.0	1.2	1.1	1.3	1.2	1.2	1.3	1.2
300	2.5	2.8	2.8	2.7	2.9	2.8	2.8	2.8
400	.9	1.2	1.0	.9	1.1	1.2	1.2	1.1
500	1.1	1.1	1.1	1.4	1.4	1.3	1.3	1.4
600	–	3.3	3.0	2.9	2.6	3.2	3.3	3.4
				MIDDLE SITE				
10	11.1	26.3	7.7	4.4	4.3	2.5	8.1	6.9
20	9.6	26.5	10.4	6.7	5.4	3.9	9.5	8.6
30	9.0	22.8	12.6	7.6	6.6	4.9	9.8	9.4
50	5.9	9.3	15.9	7.3	6.6	5.3	7.4	9.2
100	4.0	4.4	9.7	7.3	4.5	3.9	3.7	3.9
150	2.8	3.3	5.1	5.5	6.2	4.1	3.5	3.4
200	2.7	2.4	3.1	3.0	3.2	3.2	3.0	3.0
300	3.1	3.5	3.7	3.9	3.9	4.7	4.7	4.6
400	3.3	3.4	3.4	4.5	4.7	5.6	5.8	5.6
500	3.5	3.3	3.2	3.3	3.8	4.5	4.8	4.8
600	–	4.0	3.8	3.8	3.9	3.9	4.1	3.7
				LOWER SITE				
10	16.5	26.7	9.1	5.0	4.1	2.1	8.9	7.1
20	11.5	14.4	11.9	6.7	5.8	4.0	12.2	10.1
30	9.2	9.7	13.0	7.7	6.8	5.3	12.8	11.0
50	6.0	6.4	14.4	7.5	6.5	5.7	10.8	10.3
100	5.9	6.3	17.6	14.2	9.1	5.4	5.1	6.0
150	4.1	5.9	11.7	14.2	13.8	9.3	6.3	5.9
200	5.2	4.3	4.6	6.9	8.0	9.8	8.3	8.0
300	5.5	5.7	6.0	5.9	6.0	6.1	6.2	6.1
400	2.3	2.4	2.3	2.5	2.6	2.3	2.5	2.6
500	2.9	2.7	3.0	2.8	2.9	2.8	2.8	2.9
600	–	3.9	4.9	5.1	4.6	4.7	4.7	4.8

(continued)

APPENDIX TABLE A-3. (Continued)

DEPTH (cm)	JUN 3	JUN 4	JUN 5	JUN 25/26	JUL 3	JUL 28	AUG 15	SEP 21
				UPPER SITE				
10	–	–	–	1.9	–	4.3	–	–
20	–	–	–	2.7	–	4.5	–	–
30	–	–	–	2.8	–	3.7	–	–
50	–	–	–	3.5	–	3.5	–	–
100	–	–	–	2.8	–	2.2	–	–
150	–	–	–	2.3	–	2.3	–	–
200	–	–	–	1.2	–	1.2	–	–
300	–	–	–	2.6	–	2.8	–	–
400	–	–	–	1.1	–	1.2	–	–
500	–	–	–	1.4	–	1.5	–	–
600	–	–	–	3.2	–	3.2	–	–
				MIDDLE SITE				
10	8.3	6.9	6.0	3.3	10.7	4.9	3.7	5.1
20	9.6	9.1	8.3	6.7	12.1	6.5	4.3	5.2
30	10.0	9.5	8.8	6.1	11.1	7.3	5.1	6.0
50	9.3	9.2	9.0	6.6	8.3	7.3	5.2	5.9
100	3.9	4.0	4.0	4.4	4.0	4.6	3.9	3.5
150	3.3	3.4	3.3	3.4	3.5	4.1	3.6	3.3
200	2.7	2.9	2.8	2.7	2.7	3.1	3.3	2.9
300	4.5	3.7	4.3	4.1	4.1	4.0	4.1	4.0
400	5.6	5.7	5.4	5.1	5.2	4.7	4.6	4.3
500	4.5	4.7	4.5	4.7	4.6	4.2	4.1	4.2
600	3.8	3.8	4.0	4.2	4.5	4.5	4.1	4.3
				LOWER SITE				
10	–	–	–	4.1	–	5.2	–	–
20	–	–	–	6.3	–	7.2	–	–
30	–	–	–	6.3	–	8.7	–	–
50	–	–	–	6.6	–	8.3	–	–
100	–	–	–	5.9	–	5.9	–	–
150	–	–	–	5.8	–	5.9	–	–
200	–	–	–	7.0	–	7.1	–	–
300	–	–	–	6.1	–	6.2	–	–
400	–	–	–	2.4	–	2.6	–	–
500	–	–	–	2.8	–	2.8	–	–
600	–	–	–	4.3	–	4.4	–	–

5. PLANT PHYSIOLOGY

J. M. Mayo, J. E. Harter, S. Nelson and George Davis
Department of Botany
University of Alberta

5.1 INTRODUCTION

The ecophysiological research on Jackpine was undertaken in order to understand the physiologic adaptation of the major native species capable of stabilizing xeric, nutrient poor sand slopes in the Tar Sands region; and to provide information for the development of the soil-plant-atmosphere model of heat and water flux. A basic assumption was that moisture is a major stress factor for plants growing on sand (nutrients are also a major factor on such sites and nutrient studies proposed originally were removed from the project). The study provides basic information about the adaptations of Jack pine to its environment which may be useful for consideration in selecting species for revegetation of the mined sand. The study site also provides base line data about the behaviour of an ecosystem in an unpolluted region prior to the start up of additional extraction plants. It is in effect a control site in time.

The results reported here constitute an update of those reported previously. (i.e. this report is additional to the previous report and the two are considered additive and will be discussed together). Only methods, results and synthesis not reported earlier are given. The format will follow the previous

report; thus a section in which there is nothing new to report will simply state "See previous report".

5.2 RESUME OF CURRENT KNOWLEDGE

Pereira and Kozlowski (1977) have published a comparison of Jack pine and *Pinus resinosa* with respect to leaf water potential (ψ leaf), leaf resistance (R_L), air temperature and vapor pressure deficit (VPD). This work is of direct interest although limited in scope. Their work agrees, as far as it went, with the present work. It will be discussed later.

Bennett and Rook (1978) report considerable difference in leaf resistance berween two clones of *Pinus radiata* emphasizing the differences in drought hardiness. They indicate the importance of water relations studies for reforestation species selection and the importance of thorough testing even within a species.

Alvin, John and Olsen (1978) report that Jack pine forests can be successfully established using containerized seedlings with minimal site preparation following clear cutting. There is a real possibility of directly revegetating mined sands with climax species using established reforestation techniques.

"See previous report" for other references.

5.3 STUDY AREA

"See previous report"

5.4 MATERIALS, METHODS, AND SOURCES OF DATA

5.4.1 Research Approach

"See previous report"

5.4.2 Photosynthesis

The effect of moisture stress upon net CO_2 assimilation (NA) and dark respiration was studied by witholding water from young greenhouse grown trees over a period of days. These measurements were carried out using a computer controlled Infra-red-gas analyzer (IRGA) system designed by Dr. Whitfield. Recovery from near lethal stress levels was studied. The Jack pine trees studied were grown from seed obtained from the Alberta Forest Service. They were ca. 2 1/2 years old prior to the study. During the drying experiments the plants were kept in a growth chamber adjacent to the IRGA system under the following regimes:

Temperature 20°C

R.H. always >70% or <.7KPa VPD to prevent RH induced stomatal closure

Photoperiod 16 h; varied between 200 $\mu Em^{-2}s^{-1}$ and 600 $\mu Em^{-2}s^{-1}$ PhAR to simulate a daily maximum

NA, water potential (ψ_{leaf}) and water content, were measured periodically as the trees dried the soil in their 7.62 cm pots. When NA reached zero the intent was to rewater the plants and study them through another drying cycle. The same plants were studied through three drying cycles. The first cycle was not as severe as the second and NA was not followed to zero because of equipment malfunction. The second cycle was very severe in that the plants were ultimately stressed to a mean xylem tension of 3.5 MPa which we later realized was near the lethal limit. One of the plants did not recover from this stress and subsequently had started to die when the experiments were completed. The water relations of these plants were studied as described in

the previous report (5.4.3, p. 85). All of the NA measurements were carried out at 20°C, ca 540 $\mu Em^{-2}s^{-1}$ PhAR, and a mean VPD of .91 ± .08 KPa.

5.4.3 Water Potential and Water Content

"See previous report" for the methods used to measure water potential (ψ_{leaf}), the components of water potential ($\psi_\pi + \psi_\tau$), xylem pressure potential (or xylem tension), and water content.

The lethal and sublethal limits of moisture stress were studied by allowing potted (7.62 cm dia.) young (ca. 1 1/2 yrs.) trees to dry for predetermined periods, measuring xylem tension, ψ_{leaf} and $\psi_\pi + \psi_\tau$ then placing the tree in a humid greenhouse, watering and evaluating survival and damage at 3 and 15 weeks. The test plants had received the equivalent of two growing seasons prior to the experiment. During the drying experiments, the trees were kept in a growth chamber (E.G.C., Chagrin Falls, Ohio, U.S.A.) under the following conditions: Photoperiod 14h; 500 $\mu Em^{-2}s^{-1}$ PhAR, 20°C, 75% RH (0.6 KPa VPD). Lights were a mixture of cool white fluorescent 90% and incandescent 10% (based on wattage). Drying times ranged from 4 to 15 days.

Additional information about freezing caused cavitation in the xylem was supplied by Ms. Amanda Wilkinson as part of her M.Sc. thesis dealing with *Ledum groenlandicum*. She subjected Jack pine stems to freezing with liquid nitrogen and evaluated the effects upon water potential and transpiration as described by Hammel (1967).

Additional field studies were made on the variation of xylem tension within the crown in an attempt to determine the gradients of tension up the main stem.

5.4.4 Transpiration and Leaf Resistance (R_L)

"See previous report" for the methods used to measure transpiration rates and R_L. Transpiration was only measured on one occasion during June 1977. The bulk of the 1977 data was taken with a resistance porometer to increase the sample size. The major objective during 1977 was to determine when full stomatal opening occurred. The 1976 data suggested that the stomata were not functional at melt out and it was necessary to try and find out how rapidly minimum R_L values were reached. More data on the effects of VPD upon R_L was sought, particularly on high VPD days, (see Fig. 15 previous report) since stomatal closure under high VPD had been observed.

5.5 RESULTS

5.5.1 Net CO_2 assimilation (NA)

The effects of drying upon the NA of 4 trees are shown in Fig. 1. The first cycle was stopped prior to zero NA because of equipment problems although the trees were dried to somewhat less than -.8 MPa ψ_{leaf}. Even so, NA did not recover to the prestress value of 8 mg CO_2 $dm^{-2}h^{-1}$. NA reached zero in 6 days during the second cycle and ψ_{leaf} was -2.2 MPa at that point. The plants

were dried further to an average xylem tension of 3.5 MPa before being watered. This is very near the lethal limit for Jack pine (see Fig. 5) and in fact one of the plants did not recover. Its leaf water potential only recovered to -1.0 MPa whereas the other 3 plants recovered to -0.5 MPa, the prestress value. Only the results of the trees that recovered are shown in Fig. 1, cycle 3. Day zero, cycle 3, was actually started 10 days after the plants were rewatered thus cycle #3 represents recovery after extreme stress, but not immediately.

5.5.2 Water Potential and Water Content - Laboratory Studies

Water content, water potential and its components were determined for the trees used in the NA studies. The results are given in Figs. 2 and 3. Figure 2 gives the relationship between fresh weight water content and ψ_{leaf}. The linear regression, $\hat{y} = 118.72 + (-1.818X)$ has an r^2 value of 0.71. It should be noted that the water content of well watered trees is low and that a small change in water content results in a large change in ψ_{leaf}; making estimates of ψ_{leaf} highly dependent upon accurate content measurements. Fig. 3 is a Höfler diagram (1920) relating turgor potential (ψ_p) and the combined osmotic and matric potentials ($\psi_\pi + \psi_\tau$) to leaf water content on a dry weight basis. The r^2 value for a linear regression of $\psi_\pi + \psi_\tau$ was 0.64. Osmotic adjustment with water loss is apparent.

A comparison of ψ_{leaf} determined psychrometrically with xylem tension determined by the pressure bomb technique ("see previous report") was carried out during the moisture stress study.

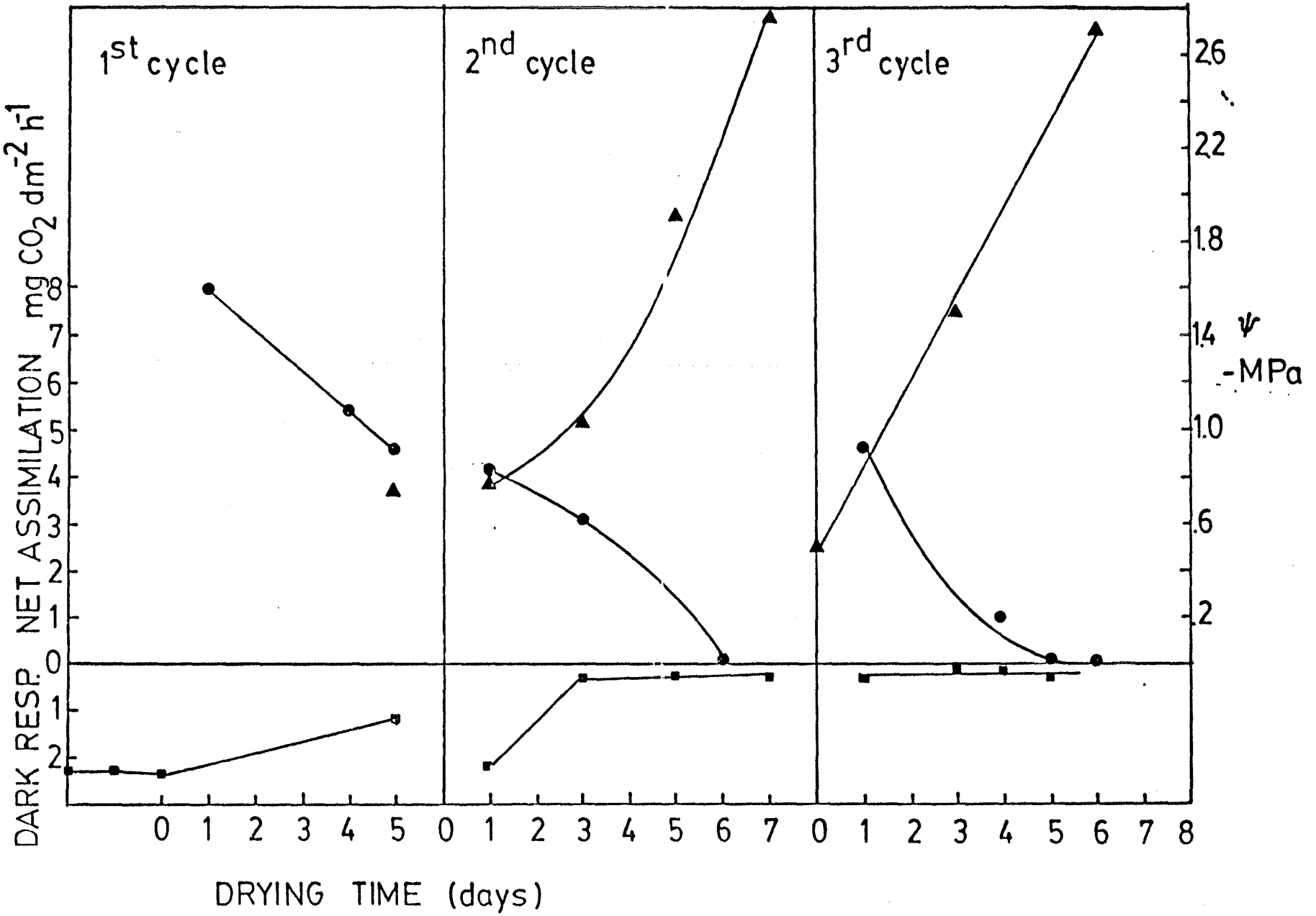

Figure 1. Net CO_2 assimilation (▲), dark respiration (■), and leaf water potential (○) of 2-3 year old Pinus banksiana during 3 succes-

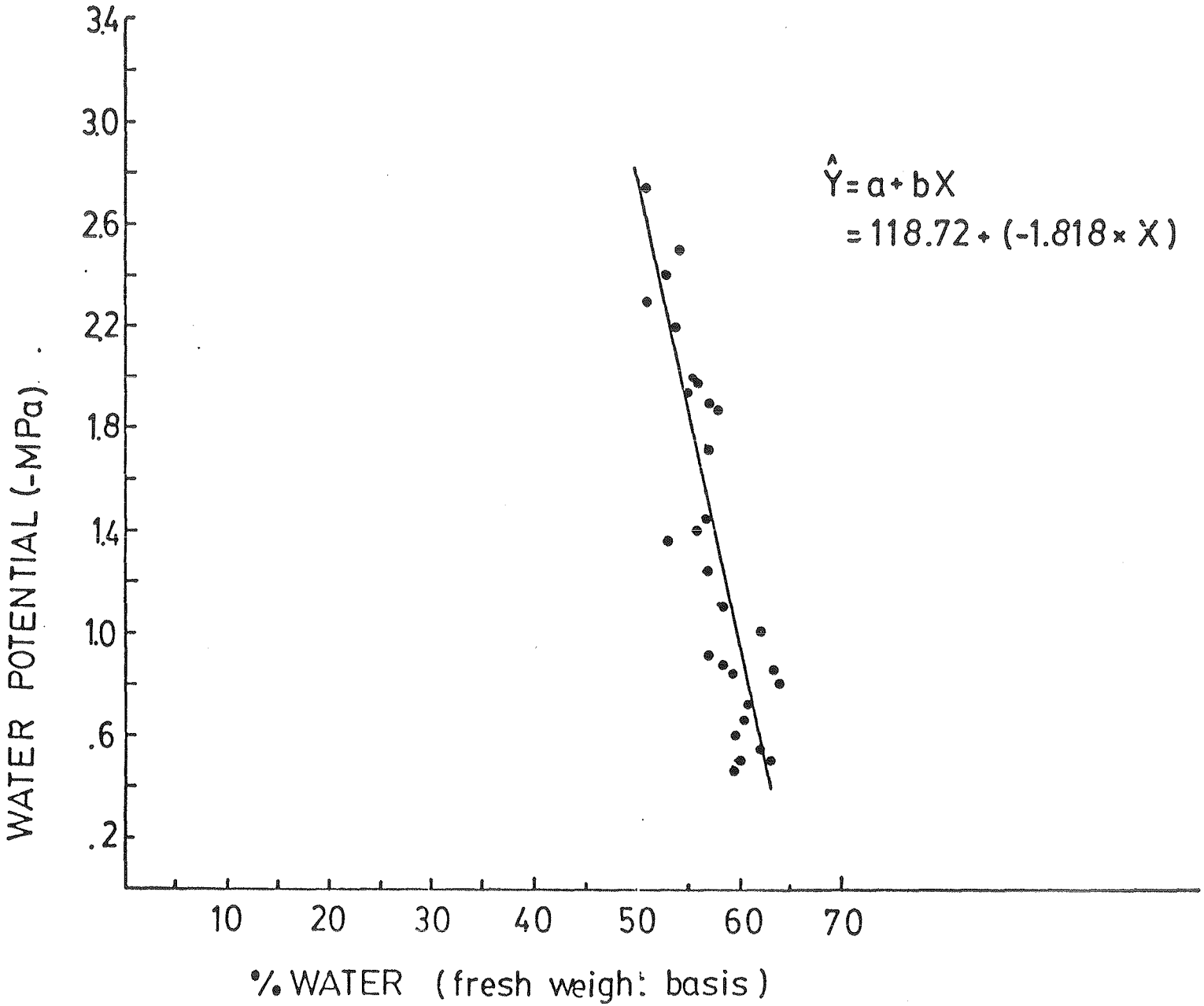

Figure 2. The relationship of leaf water potential (Ψ) and water content of 2 year old Pinus banksiana. Linear regression equation r^2 = 0.71.

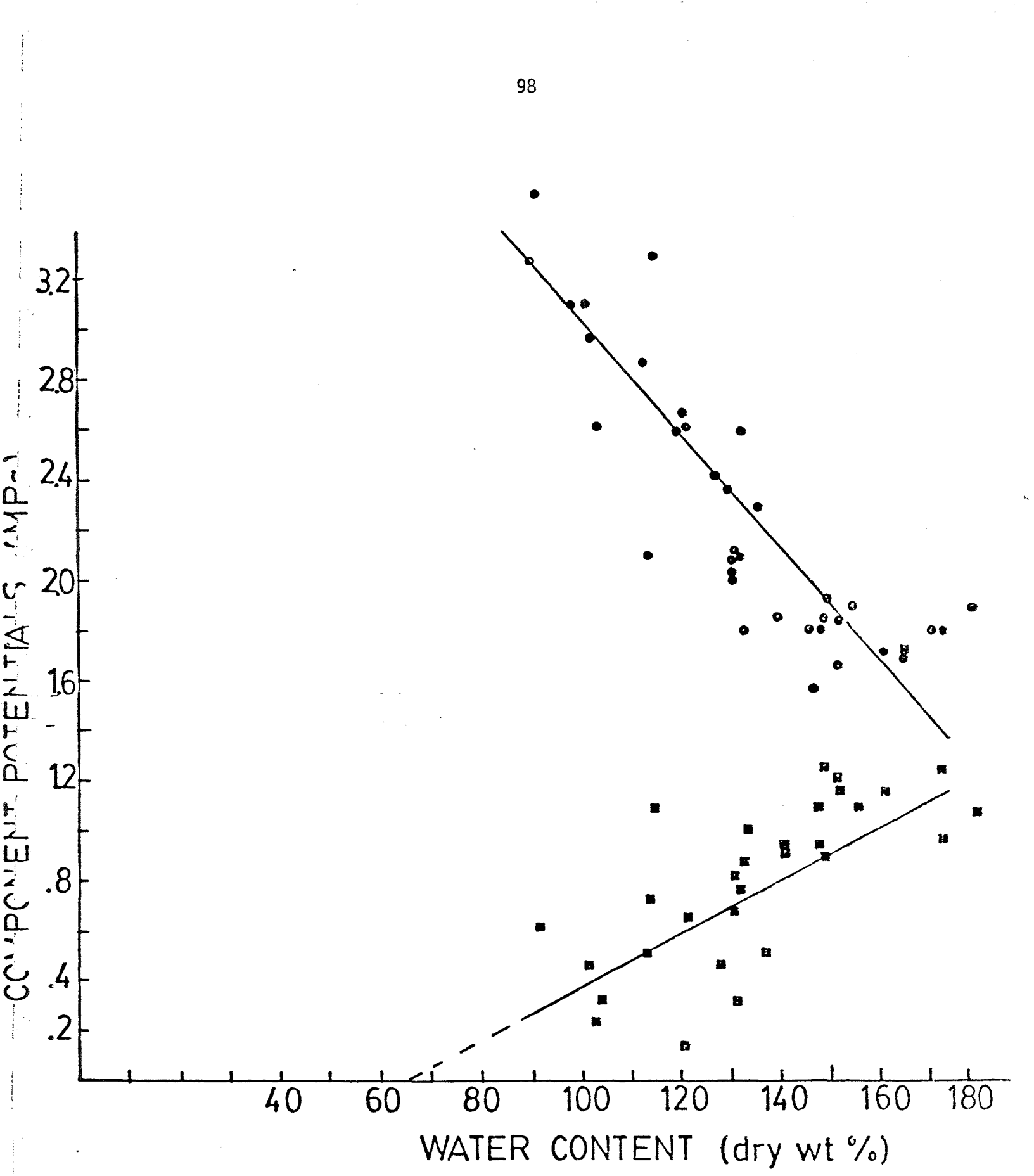

Figure 3. Höfler diagram relation water content, turgor potential (Ψ_p), and the combined osmotic and matric potentials ($\Psi_\pi + \Psi_\tau$) of 2-3 year old *Pinus banksiana*

The results shown in Fig. 4, indicate a considerable difference between the two methods, particularly at very low water potentials. However, these values are considerably lower than any ψ_{leaf} or xylem tensions measured in the field (e.g. Fig. 3 previous report). The correlation between xylem pressure potential and ψ_{leaf} over the 0 to -4.5 MPa range is in fact very good. For the equation:

$$\hat{y} = 3.82 + 0.82X$$

$\hat{y}$ = psychrometric ψ_{leaf}

X = xylem pressure potential (-xylem tension)

$r^2 = 0.88$

Thus, the two methods agree over a wide range and the pressure bomb can be used to estimate ψ_{leaf} even though they do not agree 1:1.

The results of the drying - survival study are given in Fig. 5. The dashed line is the approximate division between minimum damage and severe damage with a high probability of death. It is apparent that xylem tensions of 3.5 MPa to 4.0 MPa will result in severe damage even when the plants are given the best of care after the stress. The results suggest that as drying time increases, the dividing line occurs at higher water potentials. Interestingly enough when the plants were dried to 3.5 MPa ψ_{leaf} during the NA study, one of the plants failed to recover. Thus, there is good agreement between the two studies. Stress symptoms were assessed after 3 weeks in a humid greenhouse where the plants were well watered. They were given a final evaluation at 15 weeks to determine whether or not some of the severely injured plants had

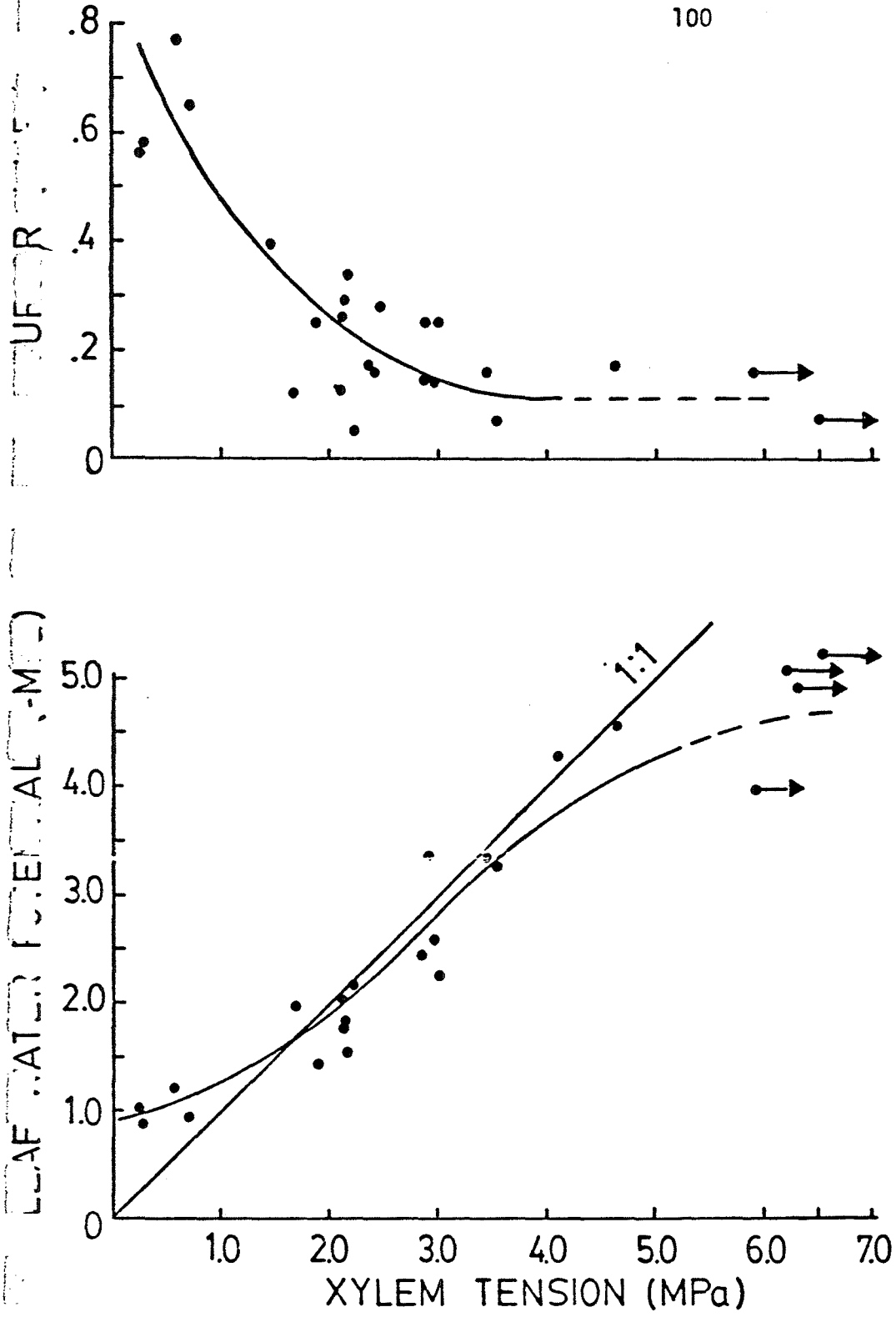

Figure 4. Upper: Leaf turgor (Ψ_p) vs. xylem pressure potential.
Lower: The relationship between xylem pressure potential and psychrometrically determined leaf water potential. (●⟶ indicates that no water was seen at this balancing pressure thus xylem pressure potential is actually lower).

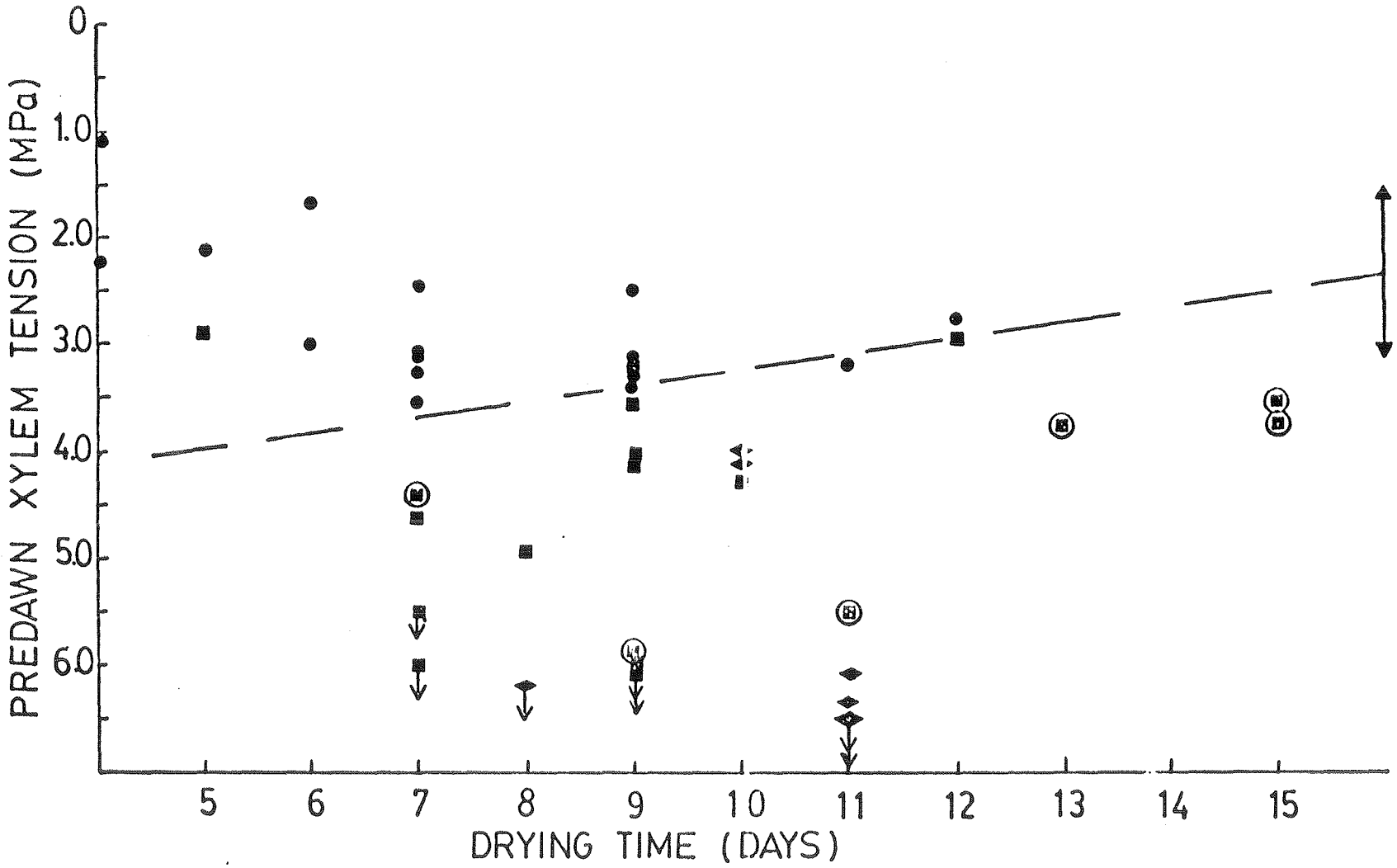

Figure 5. Survival of moisture stressed pinus banksiana.
● = minimal damage after 3 weeks recovery;
■ = severe damage after 3 weeks recovery; Ⓜ = sev dama fter eeks ovel d de
at 15 weeks. ◆ = dead after 3

recovered or died. The following descriptions were used in Fig. 5.

Minimal damage ( ); Perfectly healthy trees to those with a few necrotic spots or bands, often on the 1st year main axis and newer needles.

Severe damage ( ); Extensive necrosis, spots or bands, and/or chlorosis at 3 weeks. Sometimes only the older needles surviving. The younger needles often severely necrotic. After 15 weeks 32% of these plants were dead ( ).

Dead ( ); Dead at three weeks.

The effect of freezing Jack pine stems (with liquid nitrogen) upon transpiration is shown in Fig. 6. The rate of water uptake is the same after freezing as before. Pressure bomb readings of shoots before and after freezing were virtually the same suggesting that Jack pine does not cavitate during the winter when the stems are frozen thus assuring intact water columns upon thawing in the spring.

5.5.3 Water Potential and Water Content - Field Studies

Seasonal psychrometrically determined ψ_{leaf} and $\psi_{\pi} + \psi_{\tau}$ are given in Table 1. These results confirm the previous years report (Table 1 previous report) of year-round high turgor (ψ_{p}) and relatively stable $\psi_{\pi} + \psi_{\tau}$.

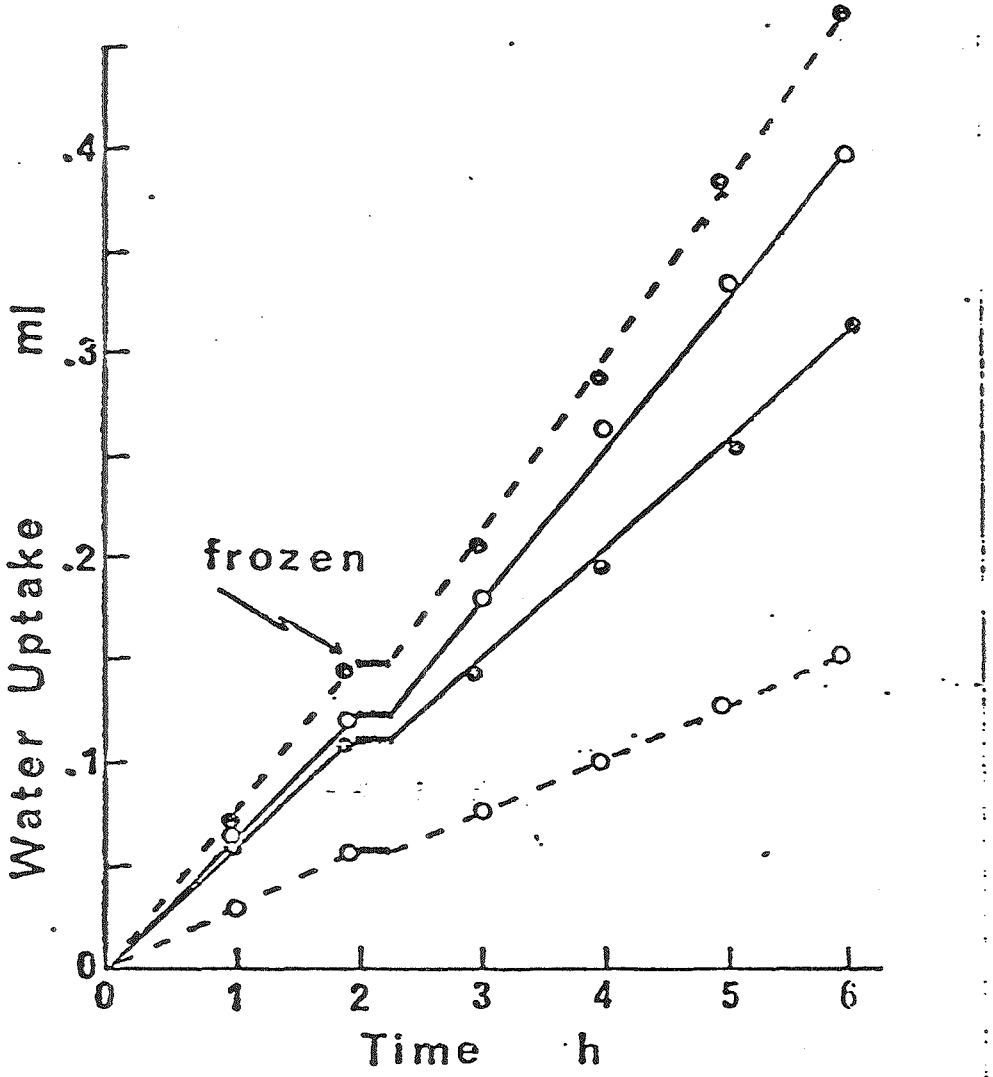

Figure 6. The cumulative water uptake of Pinus banksiana shoots as a function of time. A 2.5 cm section of the stem was frozen with liquid N_2 for 15 minutes at 2h. Taken from Wilkinson (1977).

The Höfler diagram (1920) relating water content to water potential and its components during March 1977 is shown in Fig. 7. This is interesting and unexpected in that over a fairly wide range of water content, ψ_{leaf} is constant as are its components ψ_{ρ} and $\psi_{\pi} + \psi_{\tau}$. (i.e. all of the water potential parameters are insensitive to water content prior to stomatal opening suggesting very elastic cell walls or a high percentage of extra cellular water. Note that the maximum water content is greater than after the onset of stomatal function in April, Figs. 9 and 10, but considerably less than the greenhouse grown plants (Fig. 3).

The relationship between needle water content and ψ_{leaf} for April, May and June is shown in Fig. 8. The 1975-76 needles and the older needles were graphed separately since there appeared to be a difference in the raw data and linear regressions for both groups had r^2 values of 0.8. It is apparent that slight changes in water content resulted in a considerable ψ_{leaf}. Höfer diagrams for the two age class groupings are shown in Figs. 9 and 10. The age classes appear to behave differently and both differ considerably from the greenhouse grown plants (Fig. 3).

Xylem tensions (-xylem pressure potential in the previous report) for the hill transect; top, middle and bottom are given in Figs. 11, 12, 13 and summarized in Fig. 14. Compared with the 1975-1976 (Figs. 3, and 4 previous report) data there was a bit more moisture stress during 1977, up to the termination of field work in July. The lowest xylem tension measured during the entire project was 2.1 MPa during April, 1977 (Fig. 14), but this was only one sample out of several hundred taken.

Table 1. Seasonal leaf water potential (ψ_{leaf}), osmotic and matric potential ($\psi\pi + \psi\tau$), turgor potential ($\psi\rho$), and xylem tension (ψ_{xylem}) of *Pinus banksiana* during 1977. $\bar{x}$ ± confidence intervals. Units are mega Pascals (1MPa = 10 bar).

Date	ψ_{xylem}	ψ_{leaf}	$\psi\pi + \psi\tau$	$\psi\rho$	Notes
9/III/77	.72	- .73±.08	-1.95±.09	1.22±.09	72-76 needles 1000h, no difference between age classes
19/IV/77	.47	- .80±.11	-2.31±.09	1.51±.14	73-76 needles, 0500h, no difference between age classes
19/IV/77	1.15	- .96±.16	-2.41±.12	1.45±.16	73-76 needles, 1050h, no difference between age classes
12/V/77	1.31±.20	-1.72±.14	-3.0 ±.14	1.29±.15	73-76 needles 1415h, no difference between age classes
6/VI/77	--	-1.41±.15	-2.41±.11	1.00±.11	71-77 needles 1315h, no difference between age classes

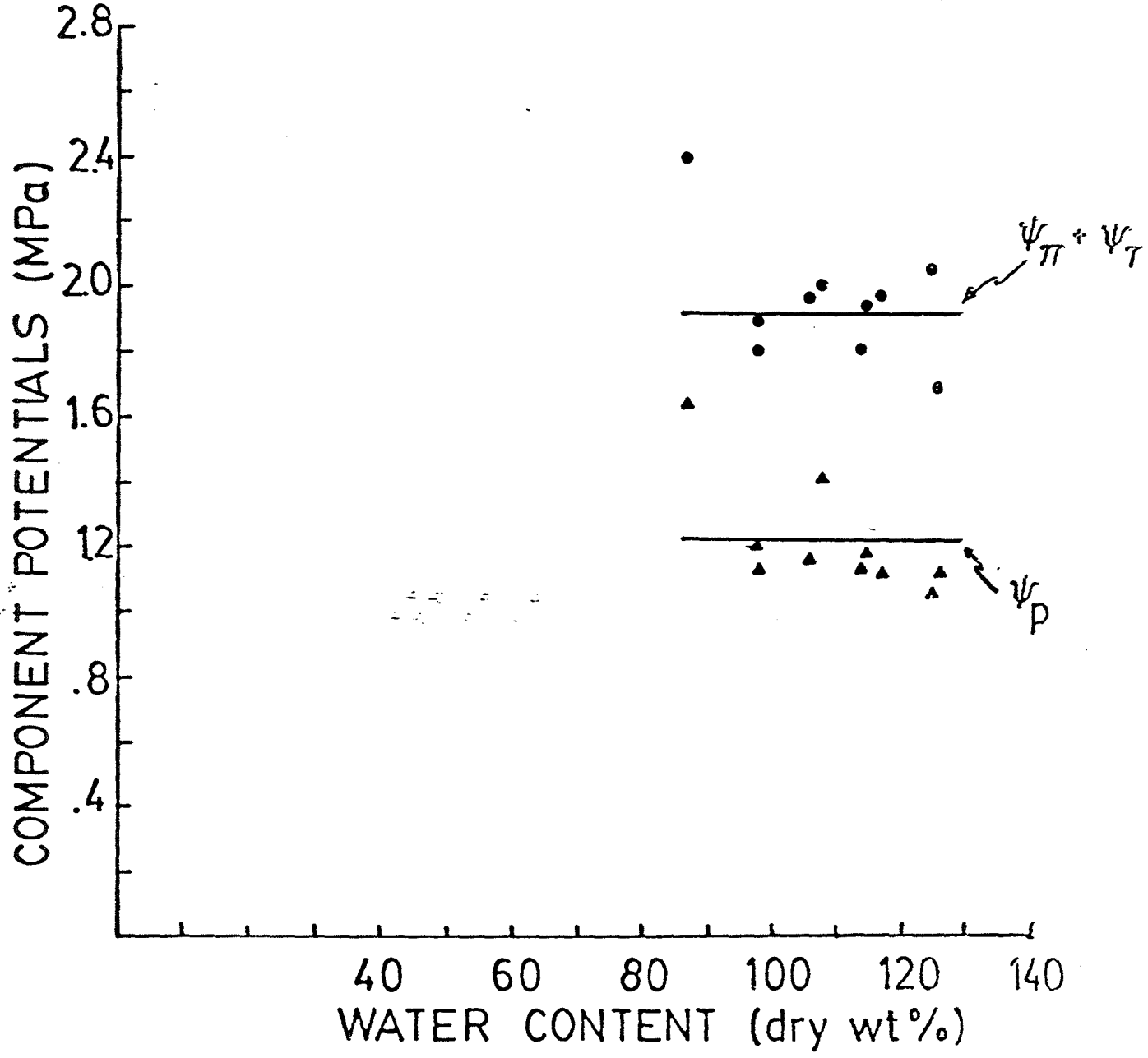

Figure 7. Höfler diagram for all age classes of needles in March 1977, prior to stomatal opening. $\Psi_\pi + \Psi_\tau$ is the combined osmotic and matric potentials. Ψ_p is the estimated turgor potential.

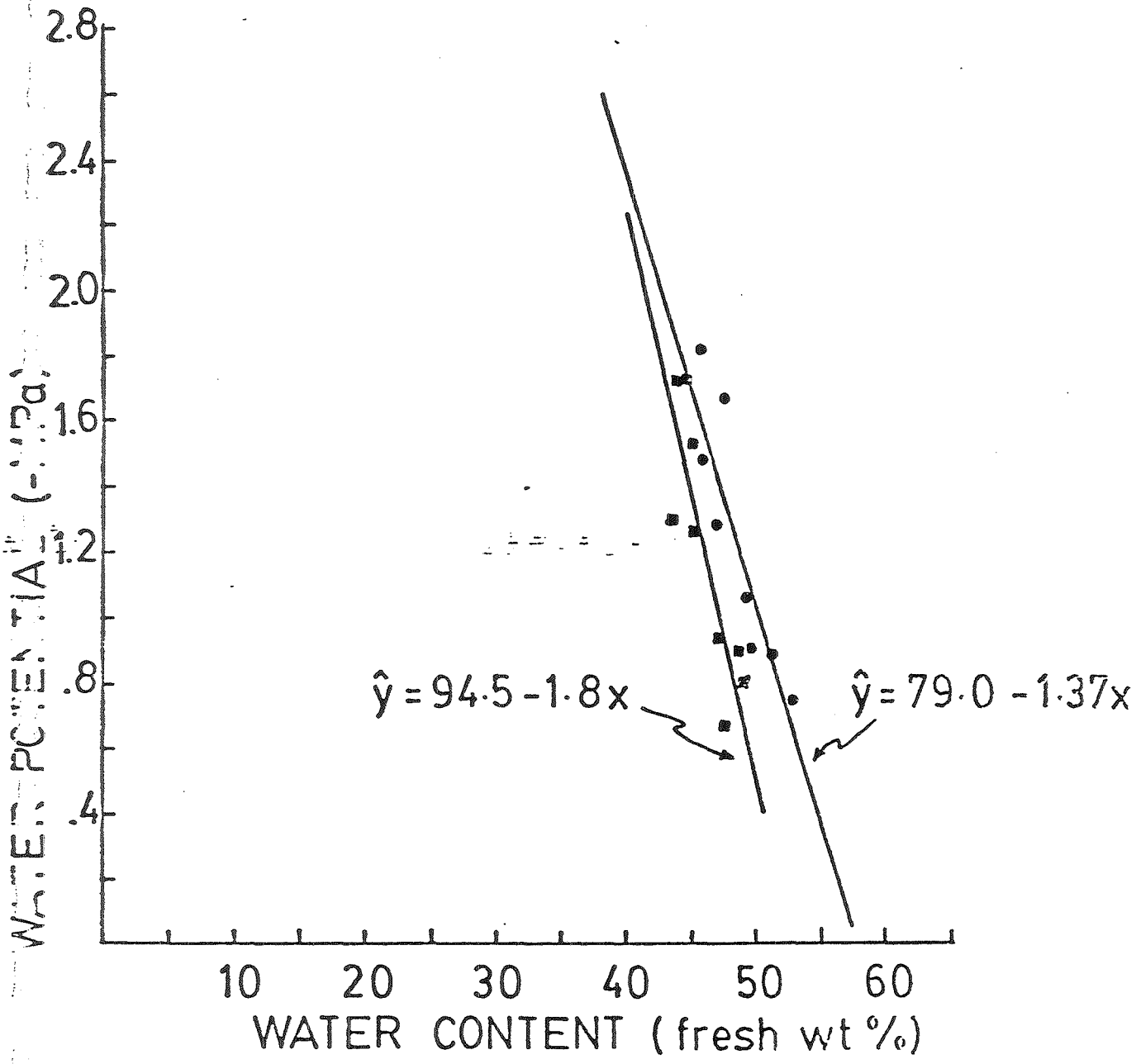

Figure 8. Leaf water potential vs. water content during April, May, June, 1977. The regression line on the right is for the 1975 and 1976 needles (r^2 = 0.8) and that on the left is for 1974 to 1971 needles (r^2 = 0.8).

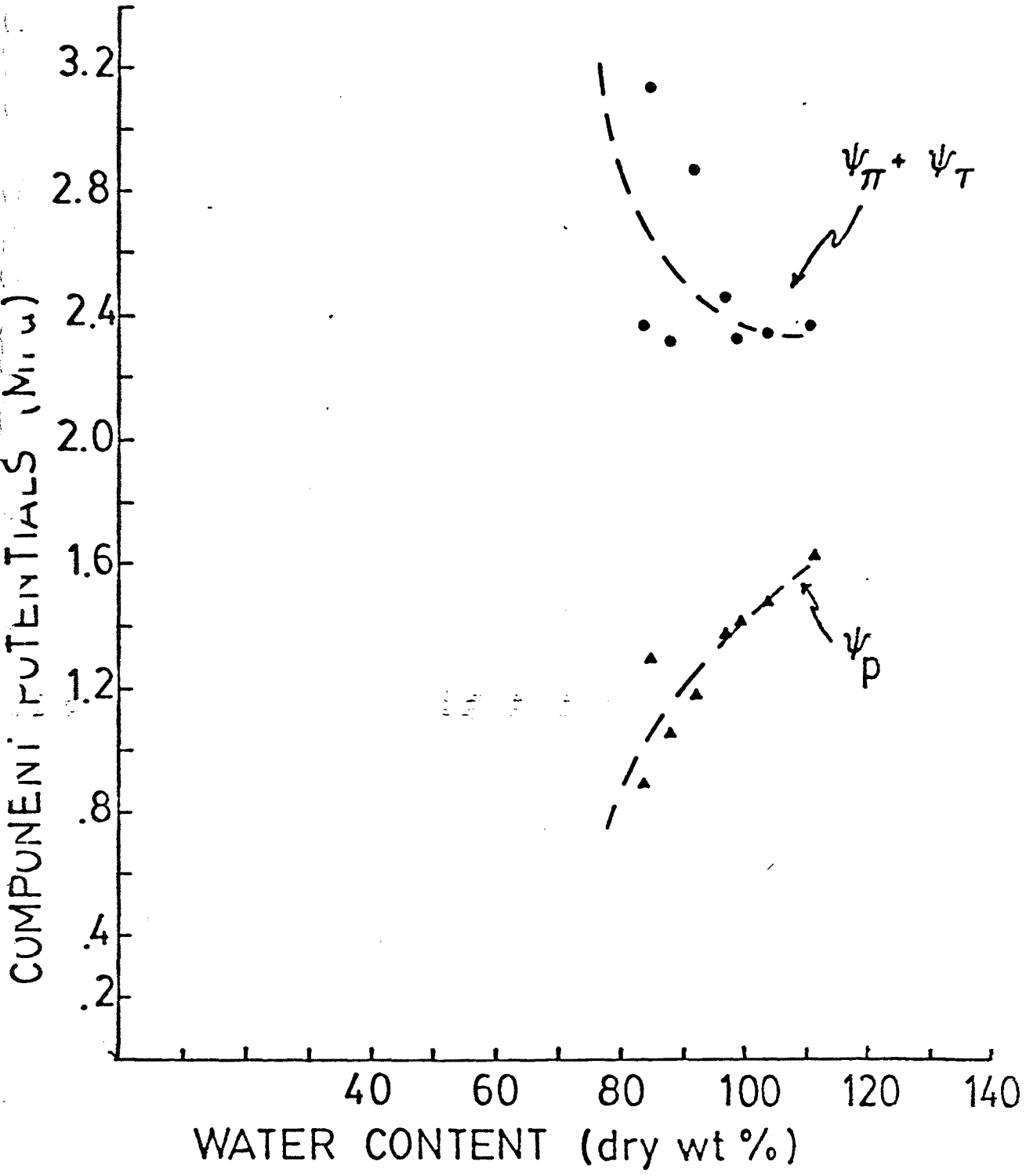

Figure 9. Höfler diagram for 1975-76 needles during April, May, and June, 1977.

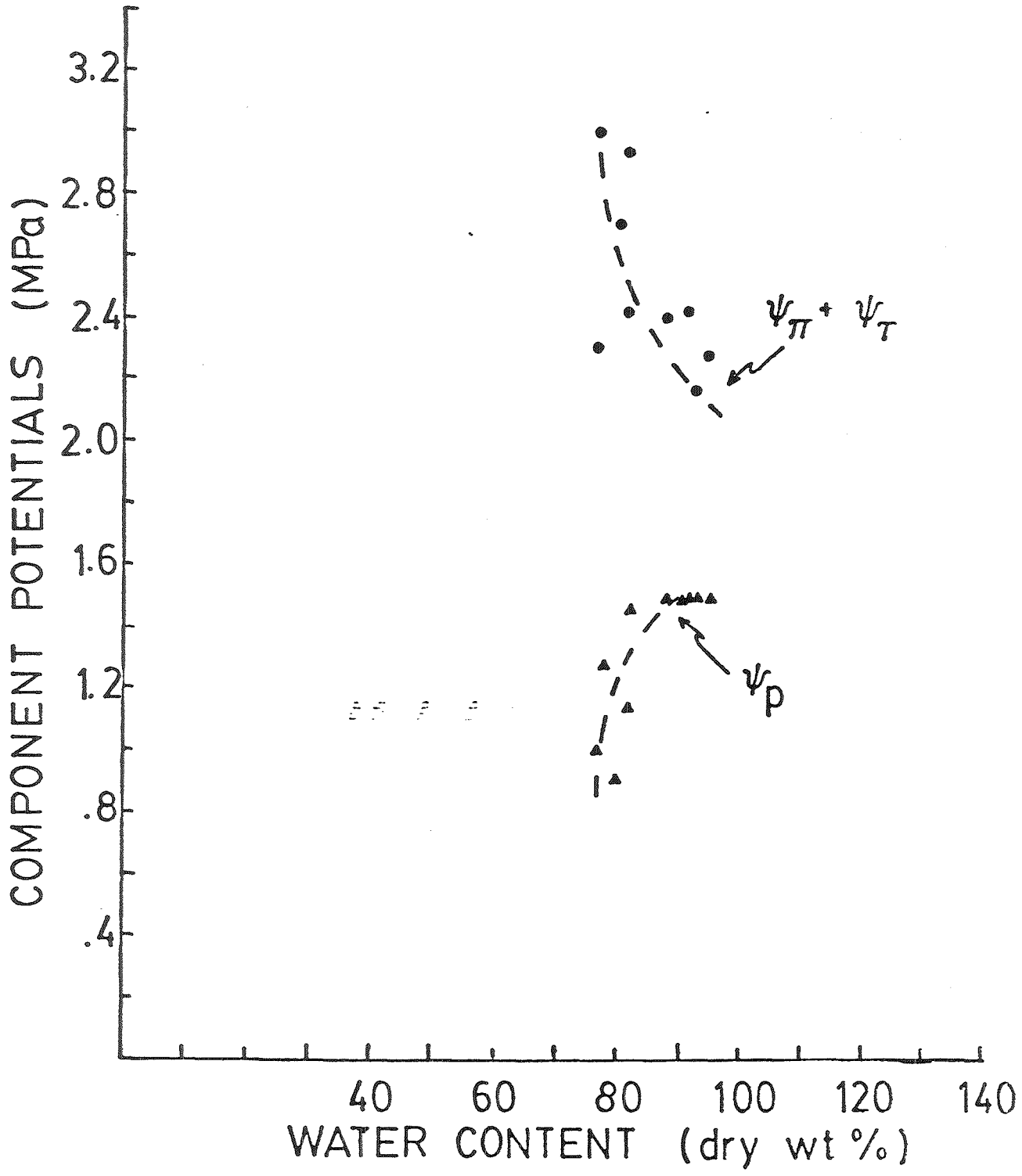

Figure 10. Höfler diagram for 1974-71 needles during April, May, and June, 1977.

The water contents by needle age class during March, April, May and June are summarized in Figs. 15 and 16. These results are similar to the previous report in that maximum content occurs in the spring and declines during the early summer. The reason for a mean increase in June (Fig. 16) is due to the addition of 1977 needles, not shown on Fig. 15.

The relationships between needle water content and xylem tensions in April, May and June are given in Fig. 17. The relationship is poor. Linear regression r^2 values for April, May, and June were respectively 0.11, 0.14, and 0.03. These results agree with the previous report conclusion that the relationship between xylem tension and needle water content is very poor and that it would be very difficult to estimate xylem tension from needle water content. Comparisons of stem water content and xylem tension also were poorly correlated (r^2 = 0.03).

Needle diffusion resistances were measured near noon and 1530h on October 28, 1976. These were the last measurements of 1976. Even though VPD was only 0.6 KPa, soil and air temperatures were above freezing (8.6 and 3.4C respectively) and xylem tension was not particularly high (1.23 MPa), the R_L values were high. The harmonic means were 67.6 scm^{-1} at 1200h and 84.8 scm^{-1} at 1530h; suggesting stomatal closure with the onset of fall dormancy, perhaps due to the short days.

Diurnal measurements of xylem tension and needle diffusion resistance were begun on March 8, 1977 (Table 2, Fig. 18). This was

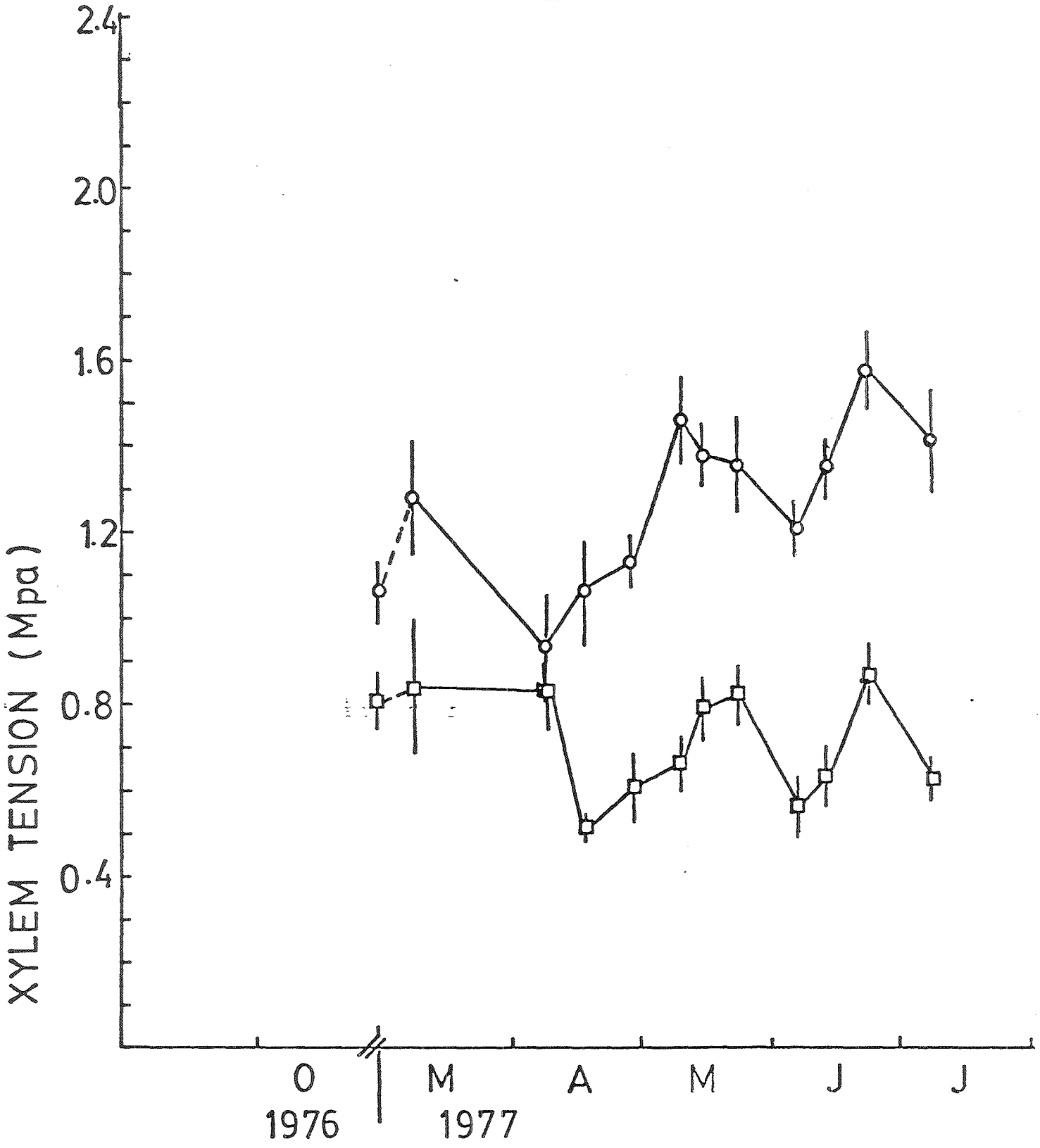

Figure 11. Dawn (□) and midday (o) xylem tensions (-xylem pressure potential) for jack pine at the bottom of the hill transect for October 1976 and spring and summer, 1977. Vertical bars are 95% confidence intervals.

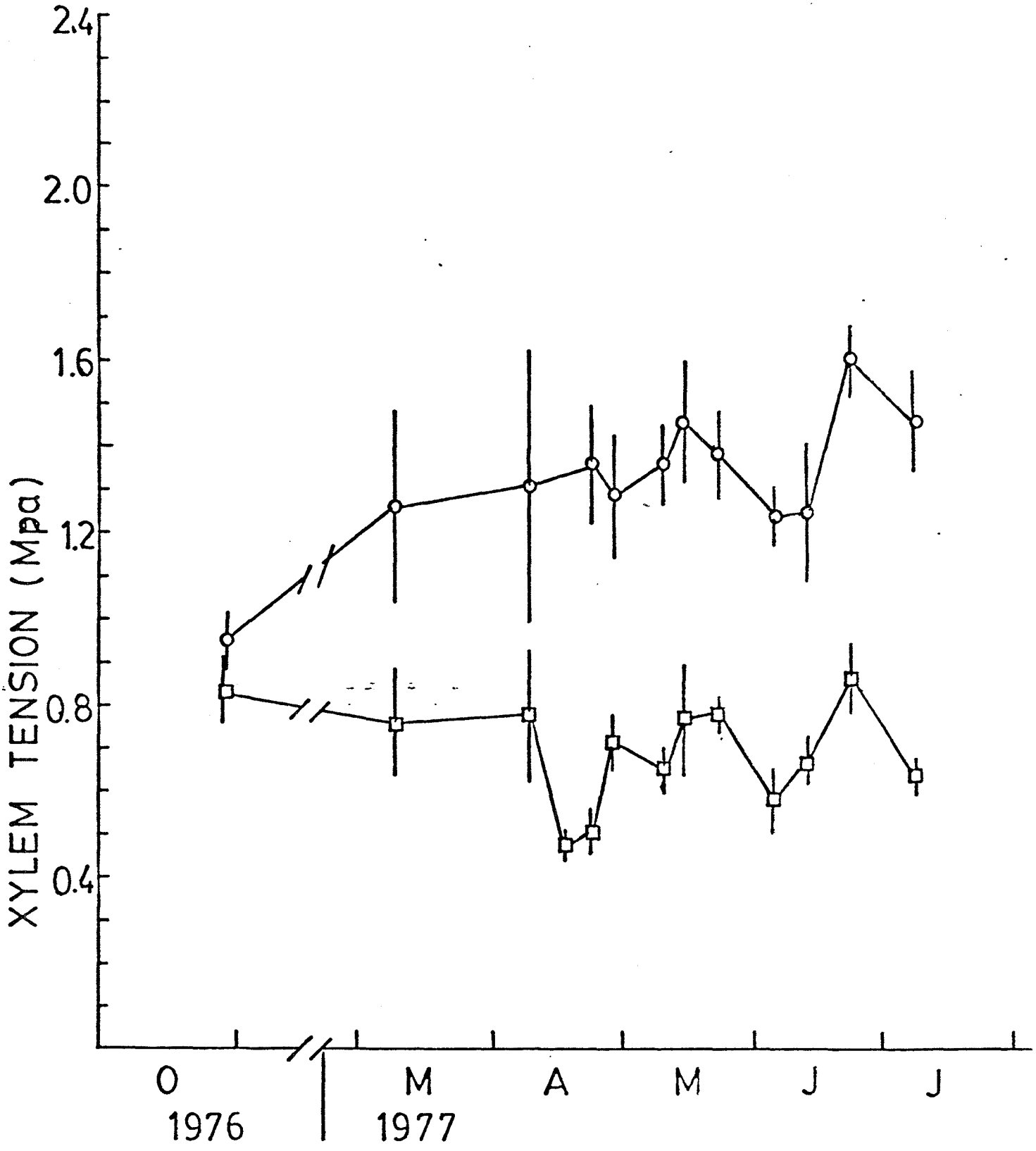

Figure 12. Dawn (□) and midday (o) xylem tensions (-xylem pressure potential) for jack pine at midslope on the hill transect for October 1976 and spring and summer 1977. Vertical bars are 95% confidence intervals

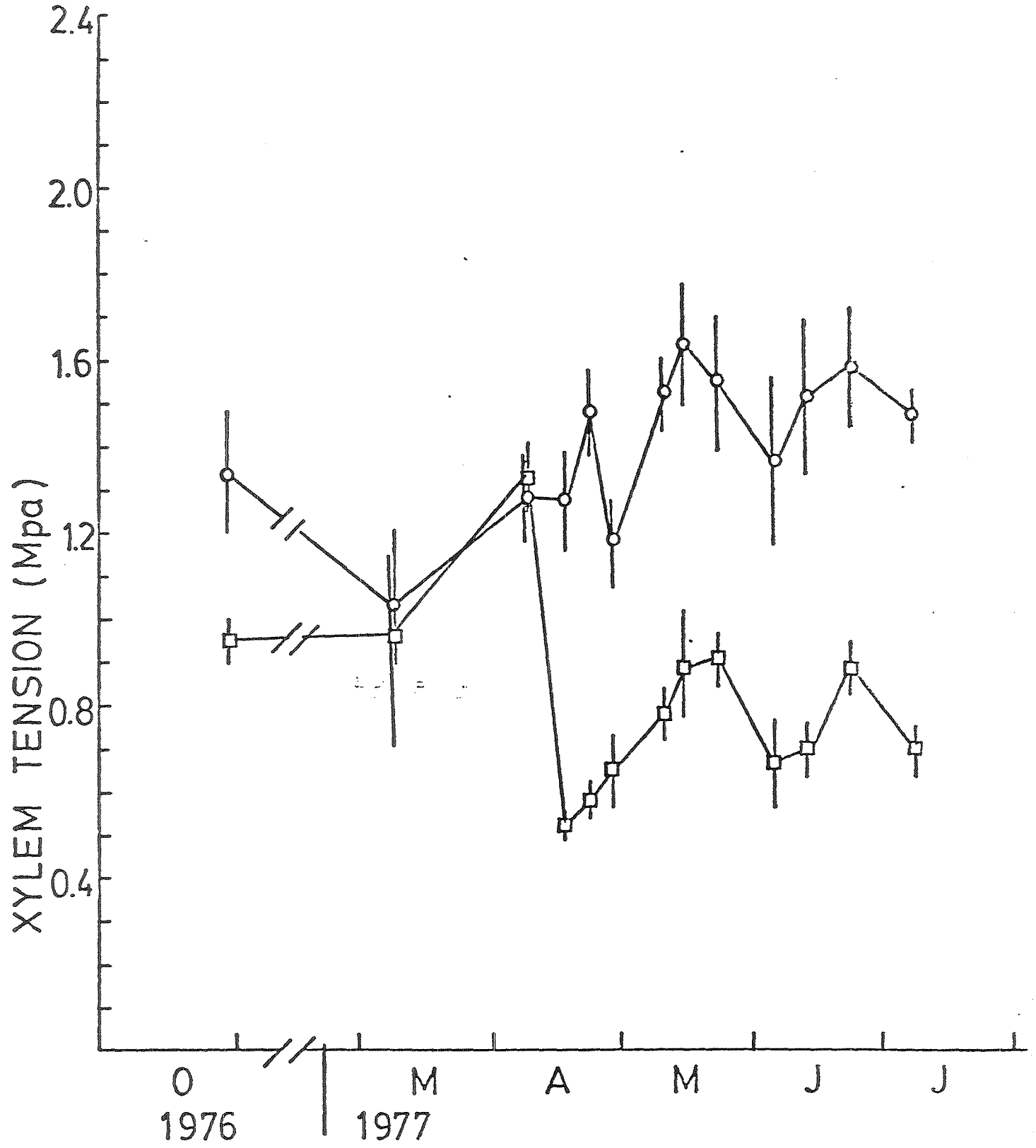

Figure 13. Dawn (□) and midday (o) xylem tensions (-xylem pressure potential) for jack pine at the top of the hill transect for October 1976 and spring and summer 1977. Vertical bars are 95% confidence intervals.

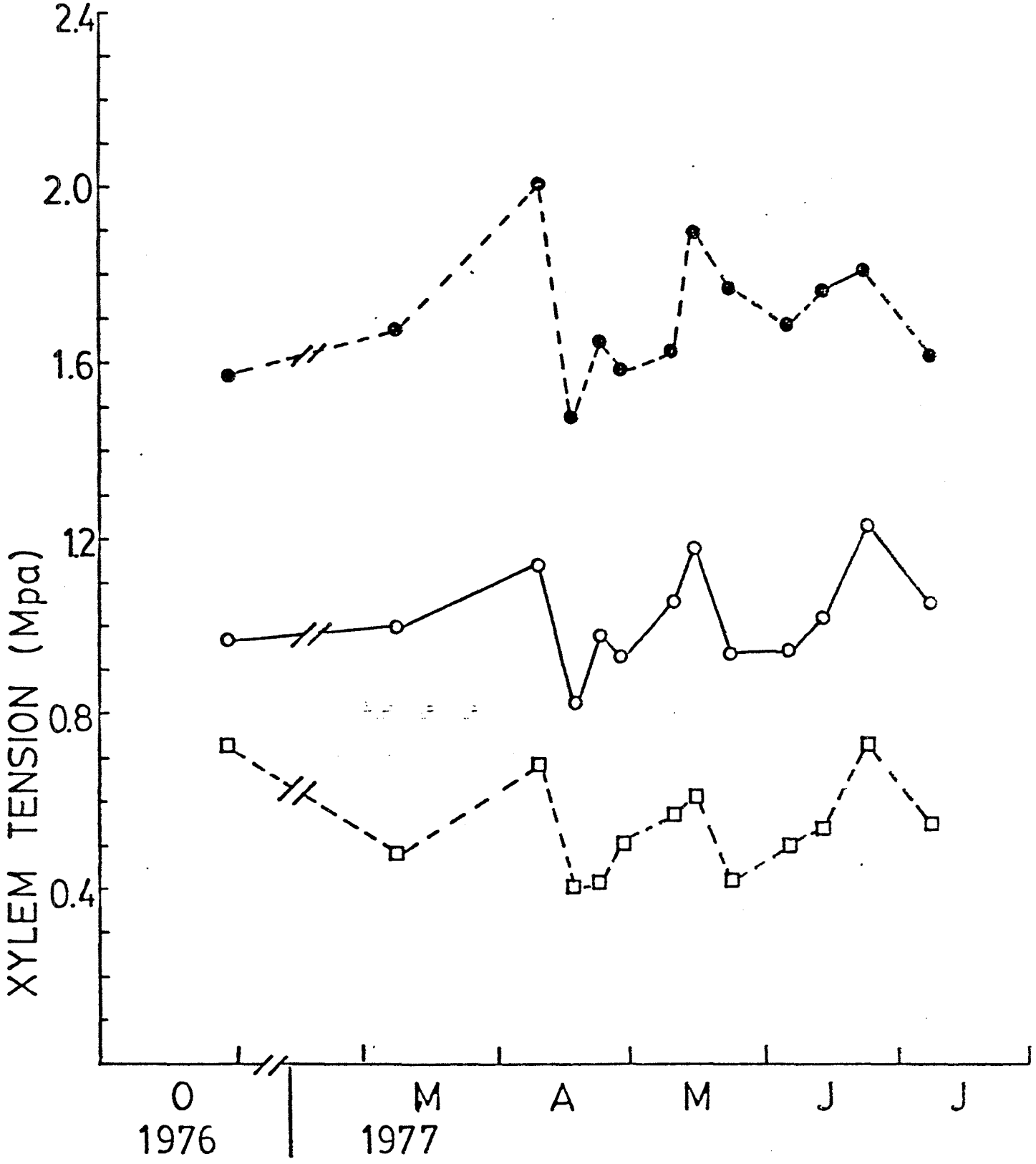

Figure 14. Daily mean (o), absolute maximum (●), and absolute minimum (□) xylem tensions (-xylem pressure potential) for jack pine on the hill transect for October 1976 and spring and summer 1977. Vertical bars are 95% confidence intervals.

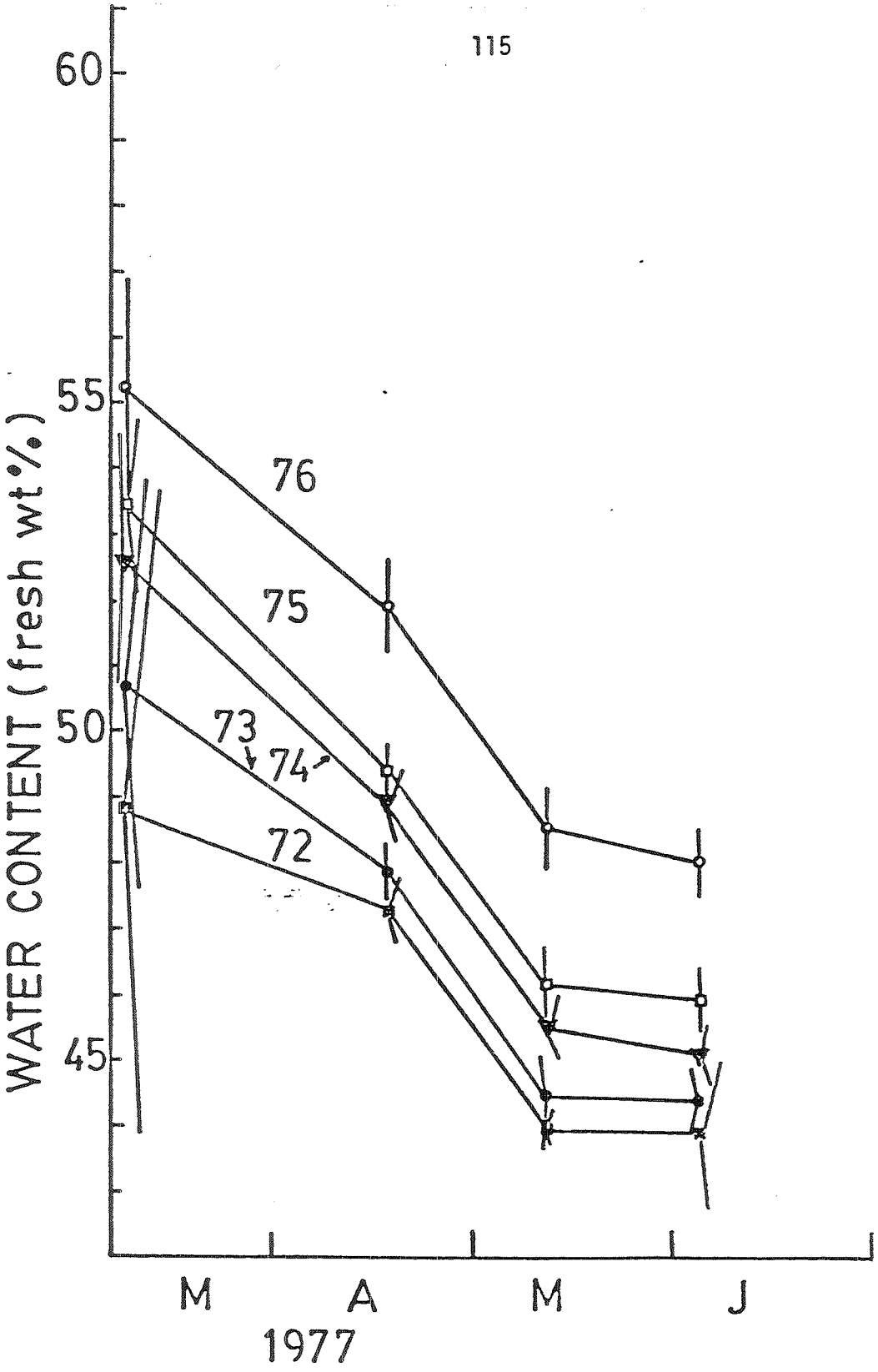

Figure 15. Mean water contents (fresh wt. %) of different age classes of needles during the spring and early summer of 1977. 1977 needles had not begun to develop by the last measurement in June. Vertical bars are 95% confidence intervals.

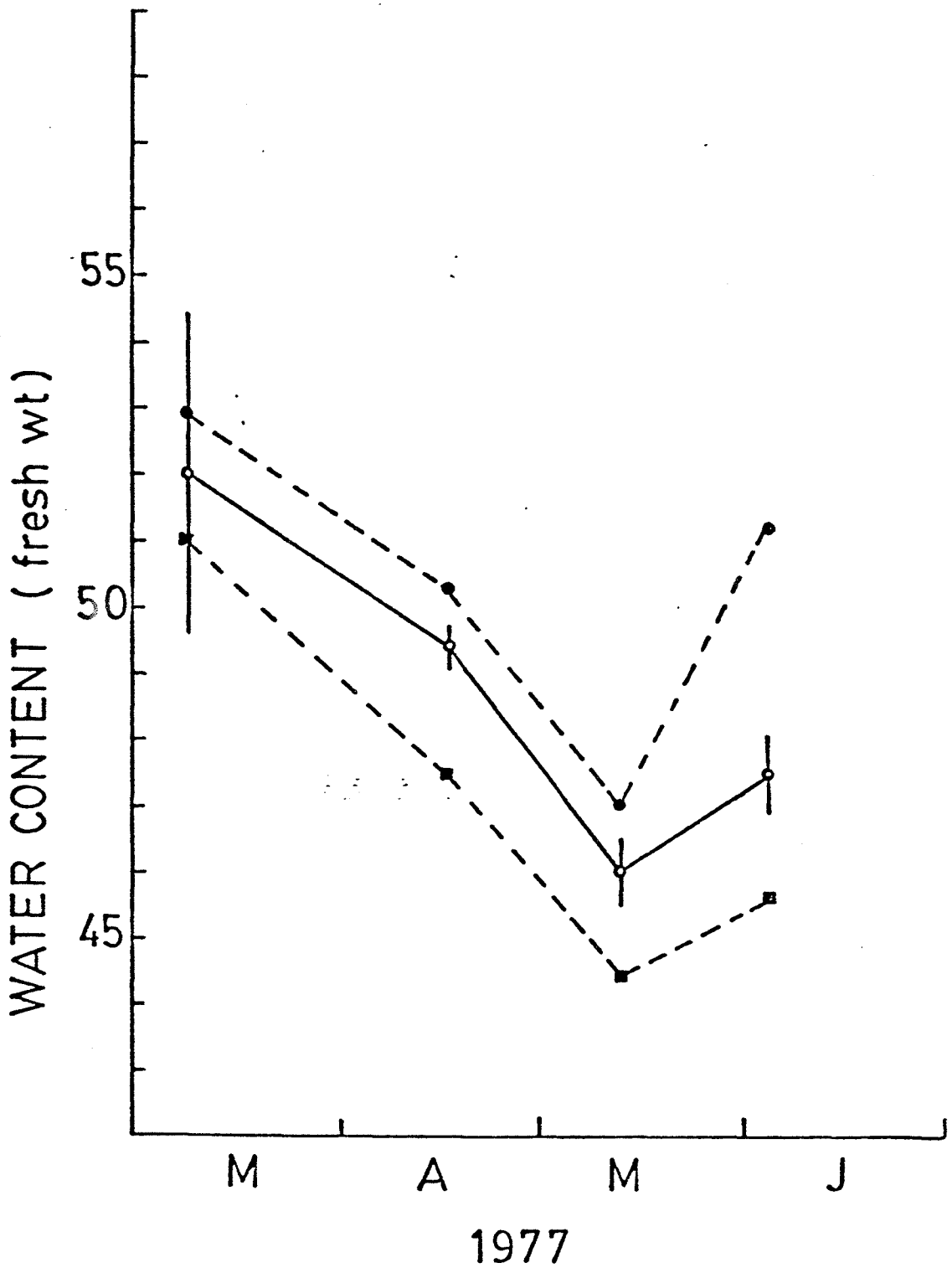

Figure 16. Mean and absolute maximum and minimum water contents (fresh wt. %) of all needle age classes during the spring and summer of 1977. Vertical bars are 95% confidence intervals.

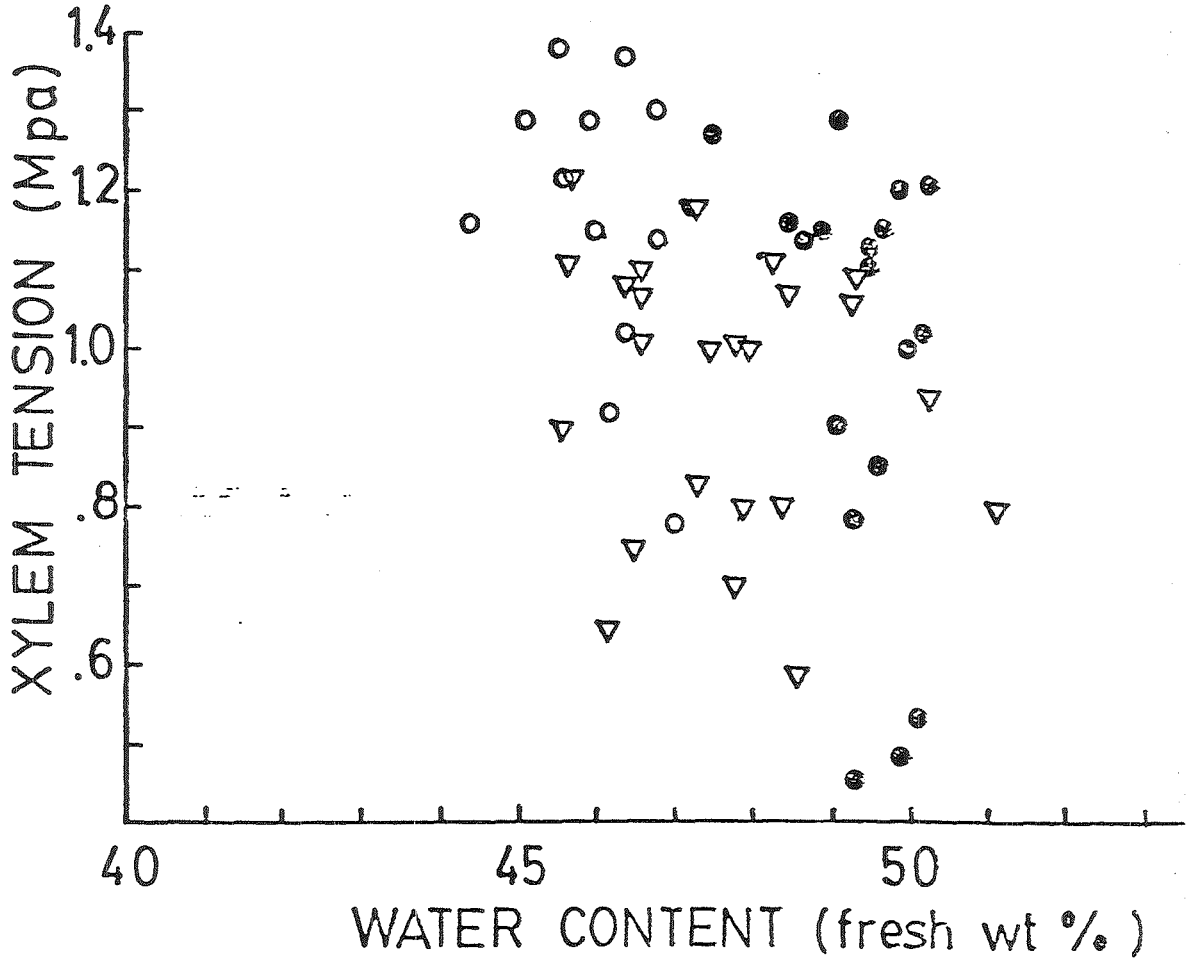

Figure 17. Xylem tension (-xylem pressure potential) vs. mean needle water content for April 15-19, 1977 (●); May, 11-12 (o); June 1-6 (▽). All age classes were averaged.

prior to snow melt, however, air temperatures were above freezing (11°C). Mean leaf resistances were 618, 778 and 428 scm^{-1} at times A, B and C in Fig. 18. The stomata were obviously closed. Xylem tensions varied but were not particularly high. R_L for the various age classes are given in Table 2. All of the values indicate tightly closed stomata. Xylem tensions on the hill transect were followed during the period of snow melt, April 8, 9, and 10 (Fig. 19). Air temperatures at 25°C and leaf temperatures of 27°C were recorded. Needle diffusion resistances were measured at mid afternoon on April 8 and found to be 150 scm^{-1} thus indicating closed stomata. It's not likely that the xylem tensions of 0.9 MPa (Fig. 19) would cause closure since similar tensions were measured in branches with open stomata (e.g. Fig. 11 previous report and Fig. 20).

A full 24 hour study of xylem tension and R_L was carried out April 15 and 16. The results for 3 trees are shown in Fig. 20. There was a definite diurnal opening and closing stomatal response. The mean minimum R_L for 3 trees, all needle age classes was 18 scm^{-1}. Stomatal closure during the afternoon of the 16th was likely due to increasing cloud cover since VPD was relatively low and xylem tensions were not excessively high. Thus, the stomata were not open on April 8, a very warm day, but were functioning by April 15th, however, minimum R_L values were not achieved at this time.

A study on April 18 was undertaken to determine differences of R_L and xylem tension differences within a canopy due to height and sun or shade. Accordingly sun and shade branches were sampled as nearly simultaneously as possible. To speed up the procedure, only 1975 needle leaf resistances were measured. The 1975 needles did not differe significantly from the other age classes and were represented by good healthy needles on all branches within the crown. As Fig. 21 shows, mean xylem tension did not vary throughout the day. Table 3 shows that there was very little difference in xylem tension within the crown. This is not too surprising in that the trees on the site are not large, the canopy is relatively open, and VPD was never very great on that particular day (Fig. 21).

Table 4 is a paired comparison of the xylem tensions of sun and shaded branches at various heights within the canopy throughout the day. The mean difference between branches in the sun and shade isn't great, only 0.031 MPa (.3 bar), however it is statistically significant indicating that branches in the sun will be under more tension than those in the shade. The difference is slight and indicates that in an open stand of small trees samples from branches in the sun and shade can be combined with only a small error. Table 5 is a paired comparison of R_L values for sun and shade branches throughout the day. There is a significant and rather large difference of 9.9 scm^{-1} between branches in the sun and those naturally shaded at the time of sampling. As can be seen in Table 5 there is considerable varia-

Table 2. Needle diffusion resistance (R_L) of Jack pine on March 8, 1977.

Time h	Needle age class	R_{L-1} scm	Air Temperature	Xylem Tension MPa
1010	76	598	2.2°C	1.2
1010	75	642	2.2	1.2
1355	76	1,054	11.0	1.5
1408	75	1,001	11.0	1.5
1430	74	834	11.0	1.5
1435	73	507	11.0	1.5
1440	72	764	11.0	1.5

Table 3. Mean xylem tensions at various heights within the canopy on April 18, 1977.

Height Class	2.5-3.4 m	4-5.2 m	6.5-6.8 m
Sun branches	0.873± .034 MPa	0.868± .041 MPa	0.91± .042 MPa
Shade branches	0.811±0.033	0.824±0.061	0.889±0.034

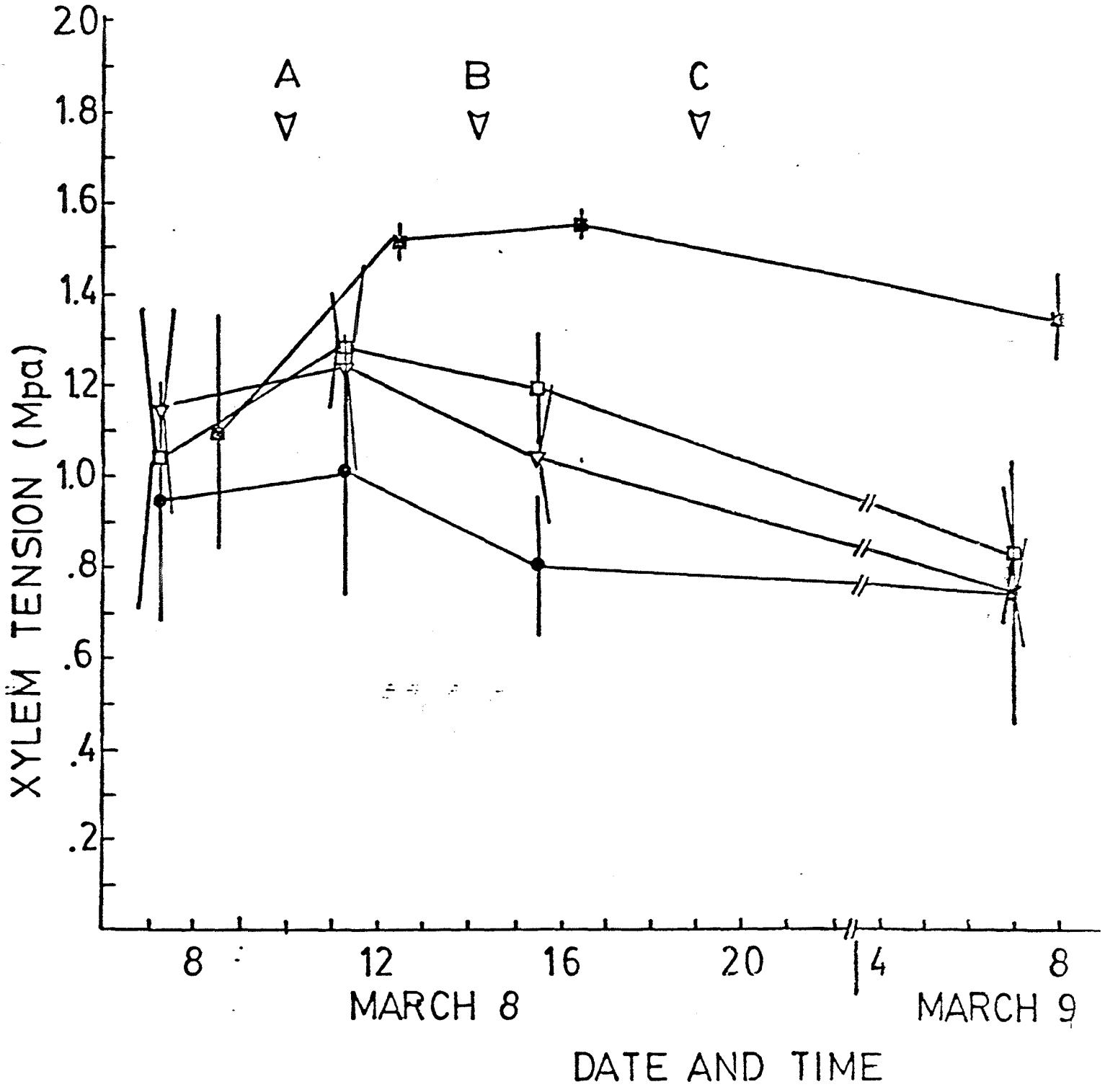

Figure 18. Xylem tensions at the top of the hill (●), middle of the hill (□), bottom of the hill (▽), and near the lab. building (▮) on March 8 and 9, 1977. Mean leaf resistances taken at times A, B, and C were resprectively 618 scm^{-1}, 778 scm^{-1}, and 428 scm^{-1}. Vertical bars are 95% confidence intervals.

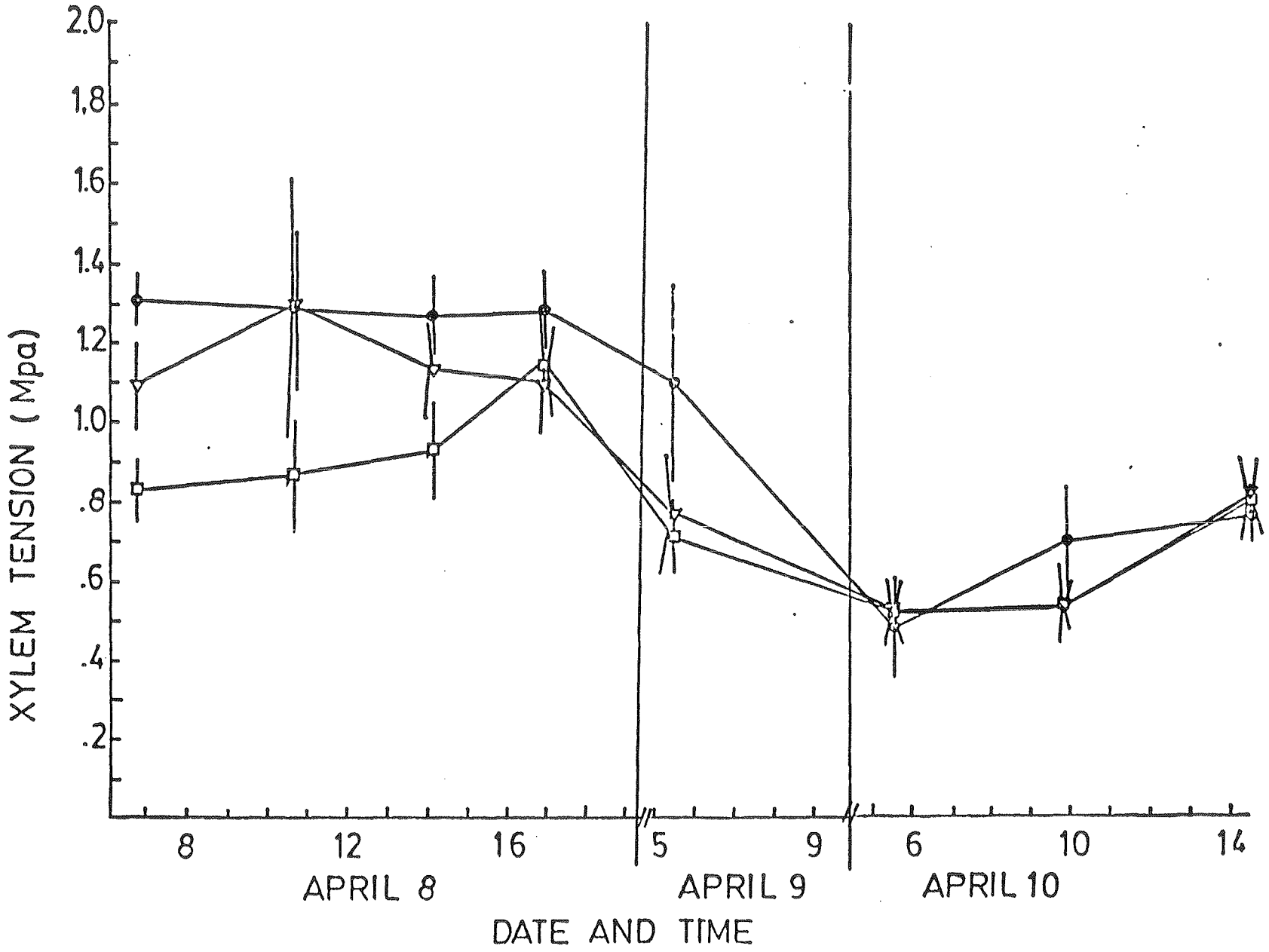

Figure 19. Xylem tensions at the top (●), middle (▽), and bottom (□) of the hill on April 8, 9, and 10. Snow melt occurred during this period.

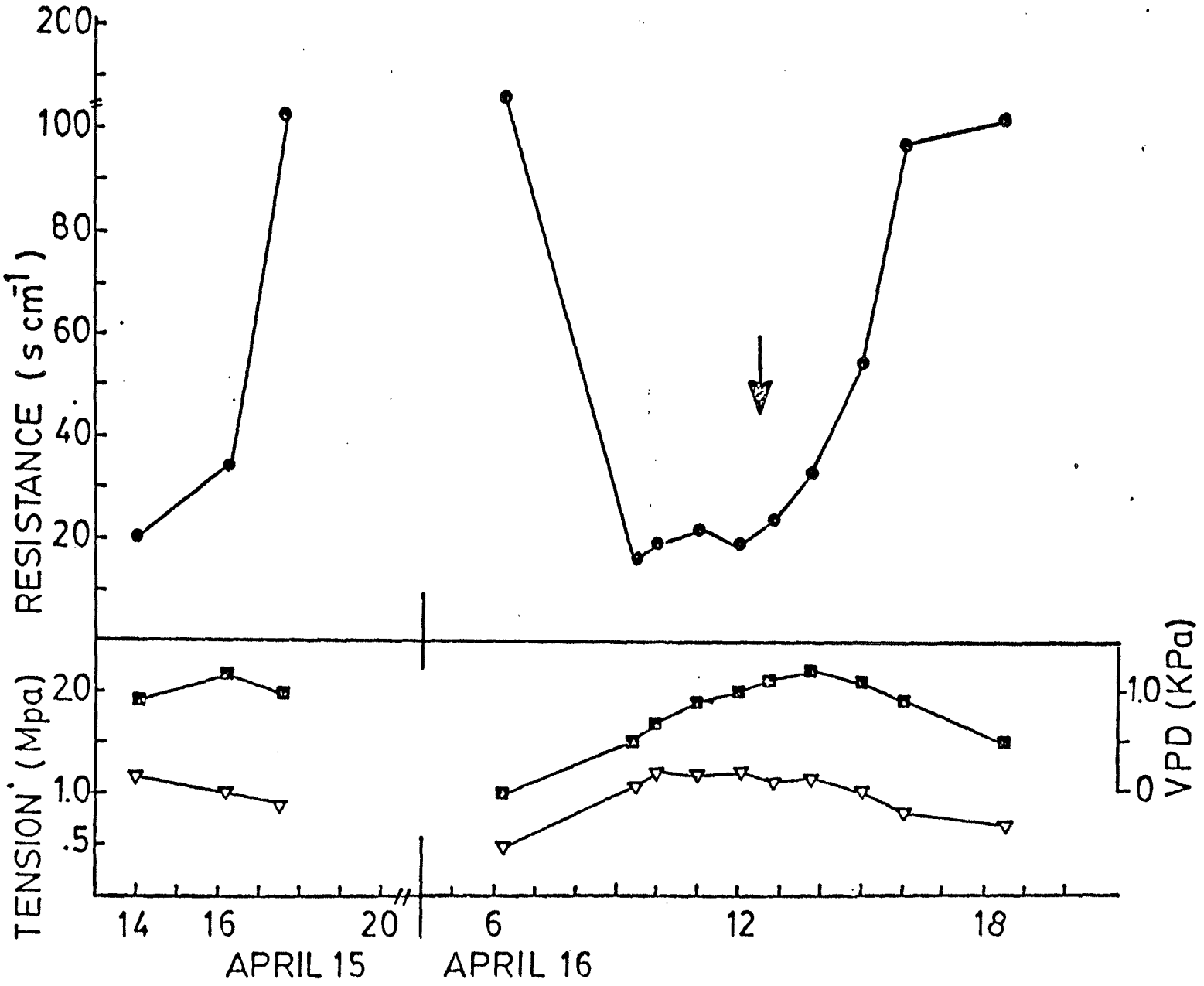

Figure 20. Harmonic mean leaf resistance (●) for all age classes of needles, xylem tension (▽) and vapor pressure deficit (VPD, ■) for three jack pine trees on April 15 and 16, 1977. Approximate hourly means. Arrow indicates in-

Table 4. A paired comparison of xylem tension between branches in the sun and those in the shade at various heights on April 18, 1977.

Time	Height M	XT_{sun}-XT_{shade} MPa
1030	6.5	0.049
1045	5.0	0.030
1100	3.0	0.000
1110	6.5	0.040
1123	3.0	0.040
1130	4.3	0.030
1145	6.5	0.020
1150	3.0	0.070
1205	5.0	0.130
1220	6.5	0.040
1250	3.0	0.050
1300	4.5	-0.050
1315	6.5	0.040
1325	3.0	0.070
1600	3.0	0.020
1610	4.5	0.010
1635	3.2	-0.010
1650	5.0	0.040
1710	6.5	-0.050

$\bar{d}$ = 0.031 MPa

s = 0.020

H°: $XT_{sun} - XT_{shade} = 0$; $t = \frac{0.31}{0.09609} = 3.226^{**}$

$t = \frac{\bar{d}}{\bar{Sd}}$

Reject at the 99% level

Table 5. Paired comparisons of the leaf resistances of sun (Rsu) and Shade (Rsh) branches, April 18, 1977. Units are scm^{-1}.

Time	Rsh	Rsu	Rsh-Rsu
1020	33.1	22.5	10.6
1033	25.8	21.0	4.8
1036	36.8	17.5	19.3
1048	36.1	27.9	8.2
1056	12.7	15.7	-3.0
1103	15.2	11.1	4.10
1106	26.9	15.4	11.50
1110	31.2	12.4	18.8
1118	16.1	10.0	6.1
1126	20.1	10.3	9.8
1128	22.7	12.7	10.0
1140	16.8	13.6	3.20
1142	8.5	14.4	-5.90
1145	12.0	12.1	-0.10
1147	9.6	15.2	-5.6
1155	10.6	11.9	-1.3
1157	79.2	10.4	68.8
1209	100.0	12.3	87.7
1224	14.5	20.7	-6.2
1231	13.2	13.8	-0.6
1246	11.3	14.9	-3.6
1253	11.9	12.0	-0.1
1255	14.6	11.3	3.3
1303	25.9	9.9	16.0
1306	23.3	19.4	3.9
1317	14.1	14.2	-0.1
1320	8.1	19.7	-11.6
1328	14.0	10.4	3.6
1551	27.0	18.0	9.0
1600	21.6	17.5	4.1
1604	19.2	26.8	-7.6
1613	22.8	29.1	-6.3
1615	22.6	17.4	5.2
1625	25.5	20.7	4.8
1628	24.8	22.1	2.7
1640	22.0	27.7	-5.7
1642	114.7	21.5	93.2
1650	75.5	30.4	45.1
1703	21.0	23.4	-2.4
1712	22.8	19.2	3.6

$\bar{d} = 9.93 \pm 7.5\ scm^{-1}$ at 95% confidence limits

$H^\circ: \mu_1 - \mu_2 = 0$

$t = \frac{\bar{d}}{S_{\bar{d}}} = 2.6838$

reject at the .05 level

bility and quite often the R_L of sun leaves exceeds those in the shade. VPD and xylem tensions were not excessive therefore, they were not likely to be the reason for such reversals. The sampling of sun and shade needles means only that the branch was either in the sun or shade at this time of sampling and no accounting for the time in the shade or sun was attempted. Thus, it is possible that some branches had experienced sun or shade for only a few minutes prior to sampling. Nevertheless it is apparent that normal shading within the canopy results in considerable stomatal closure. The mean R_L for sun branches, xylem tension, VPD, and PhAR for April 18 are given in Fig. 21. VPD was quite low throughout the day (<1.0KPa) as were xylem tensions (<1.0MPa). It is not likely that they had much influence upon R_L. The mean minimum R_L was 12 scm^{-1}; considerably lower than on April 15. There was an indication of midday closure at approximately 1600h.

The next study period was May 11 (Fig. 22) when the mean minimum R_L was 2.5 scm^{-1} during the morning hours. These are considerably lower than the R_L on April 18 at comparable VPD and xylem tension. The stomata of the same needle age class opened more fully under comparable conditions. The highest VPD's during a study period were recorded on May 11. Afternoon R_L's were much higher indicating midday closure to VPD. It is doubtful that xylem tension could have caused the increased R_L after 1200h.

Leaf resistance was studied again on June 1 using the transpiration method ("see previous report"). The minimum R_L was 10 scm^{-1} (Fig. 23), higher than the previous study day, May 11, but

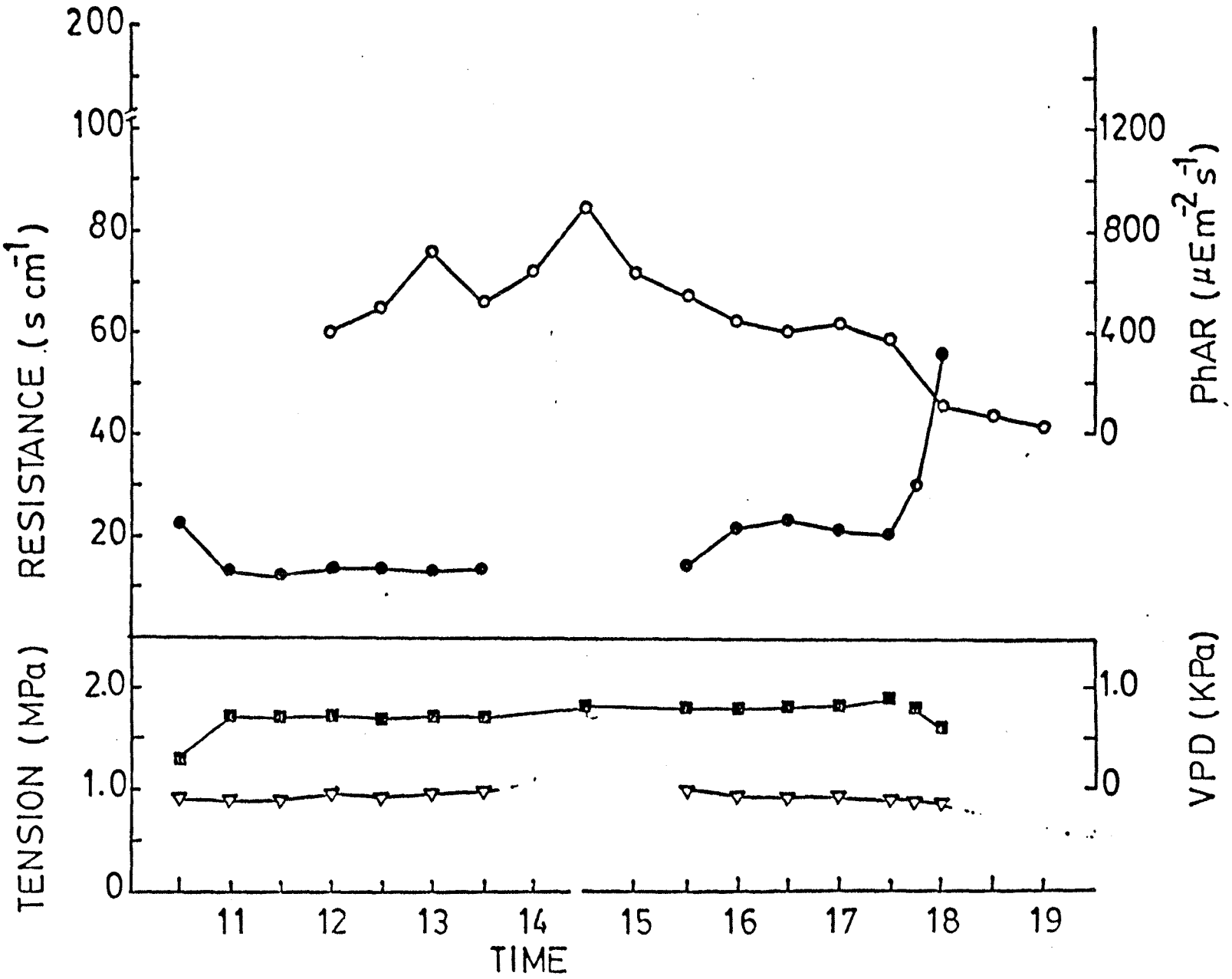

Figure 21. Harmonic mean leaf resistance (⊙) over half hour intervals for 1975 needles, mean xylem

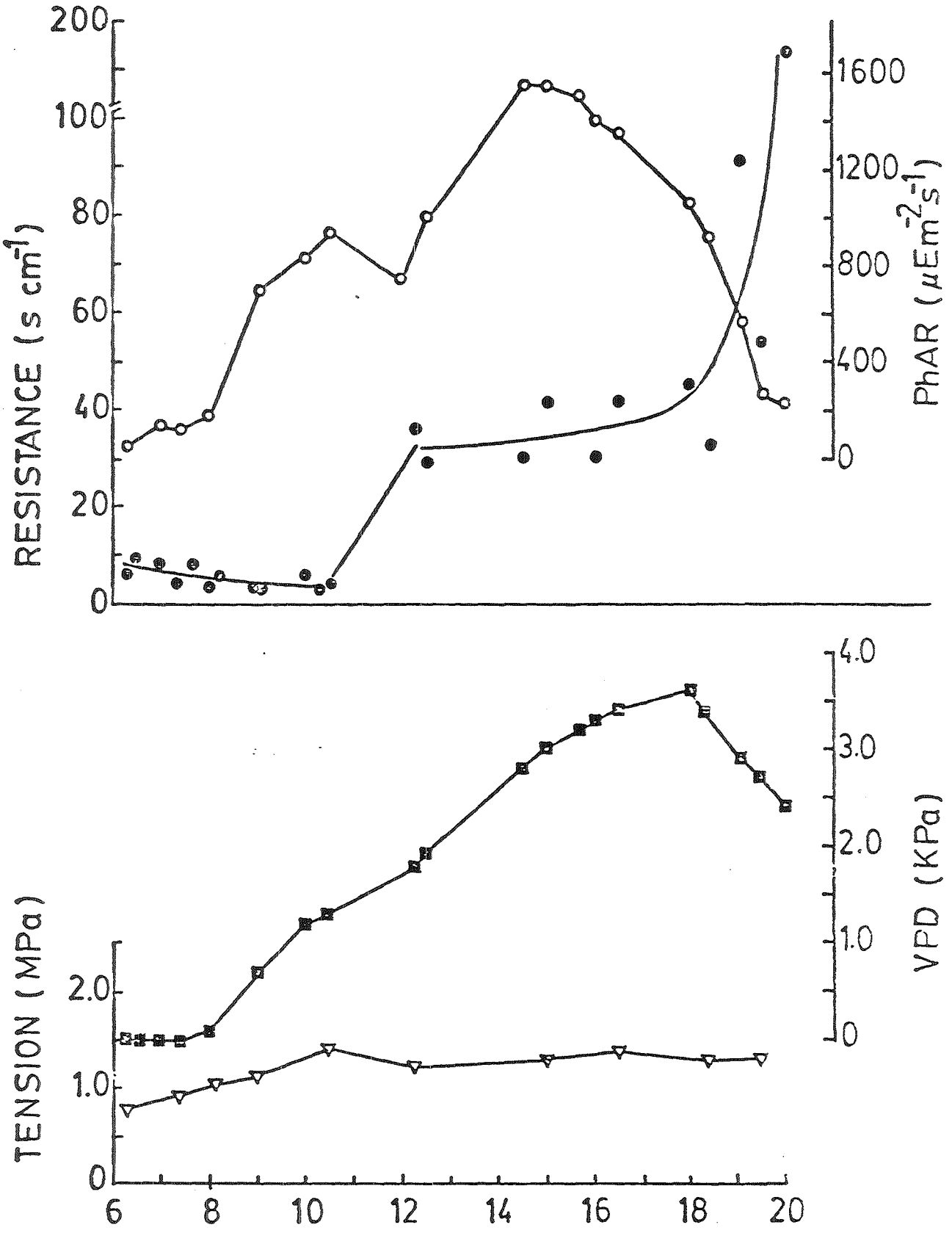

Figure 22. Harmonic mean leaf resistance (●) over half hour intervals for 1975 needles, mean xylem tension (▽), vapor pressure deficit (■), and photosynthetically active radiation (○) for May 11, 1977. Only needles in the sun are recorded.

VPD was nearly 2.0 KPa throughout the day and since the whole branch was studied, some self shading probably occurred resulting in partial closure (see Table 5).

Needle diffusion resistance was next studied on June 3 and 4 (Fig. 24) using the porometer technique ("see previous report"). Minimum resistances of 1.5 scm^{-1} were common. These were considerably lower than those measured June 1 using the transpiration method. VPD was considerably higher on June 1; near 2.0 KPa throughout the afternoon, whereas maximum VPD was below 1.5 KPa on June 3 and 4; except at 1300h on June 4. VPD caused stomatal closure would be expected to be more pronounced on June 1 than June 3 and 4. The 1975 needles did not differ from the harmonic mean therefore the results are comparable with the April 18 results.

During the melt-out period in 1976 it appeared that stomatal functioning was delayed even though air temperatures were relatively high. An effort was made to follow leaf resistance during the spring of 1977 to document the onset of stomatal function. The results are given in Fig. 25 and Table 6. Leaf resistances and xylem tensions were measured from March 8 to June 4. Table 6 indicates the relatively warm temperatures on March 8. There was a very cold period (temperatures as low as -27°C) after March 8, but melt out literally occurred on April 8 when most of the snow on the hill study site melted. As shown in Table 6, air temperatures, VPD and xylem tensions were such that stomatal opening would not be limited. Figure 25 suggests a progressive decrease in minimum leaf resistance associated with progressive warming of the soil at

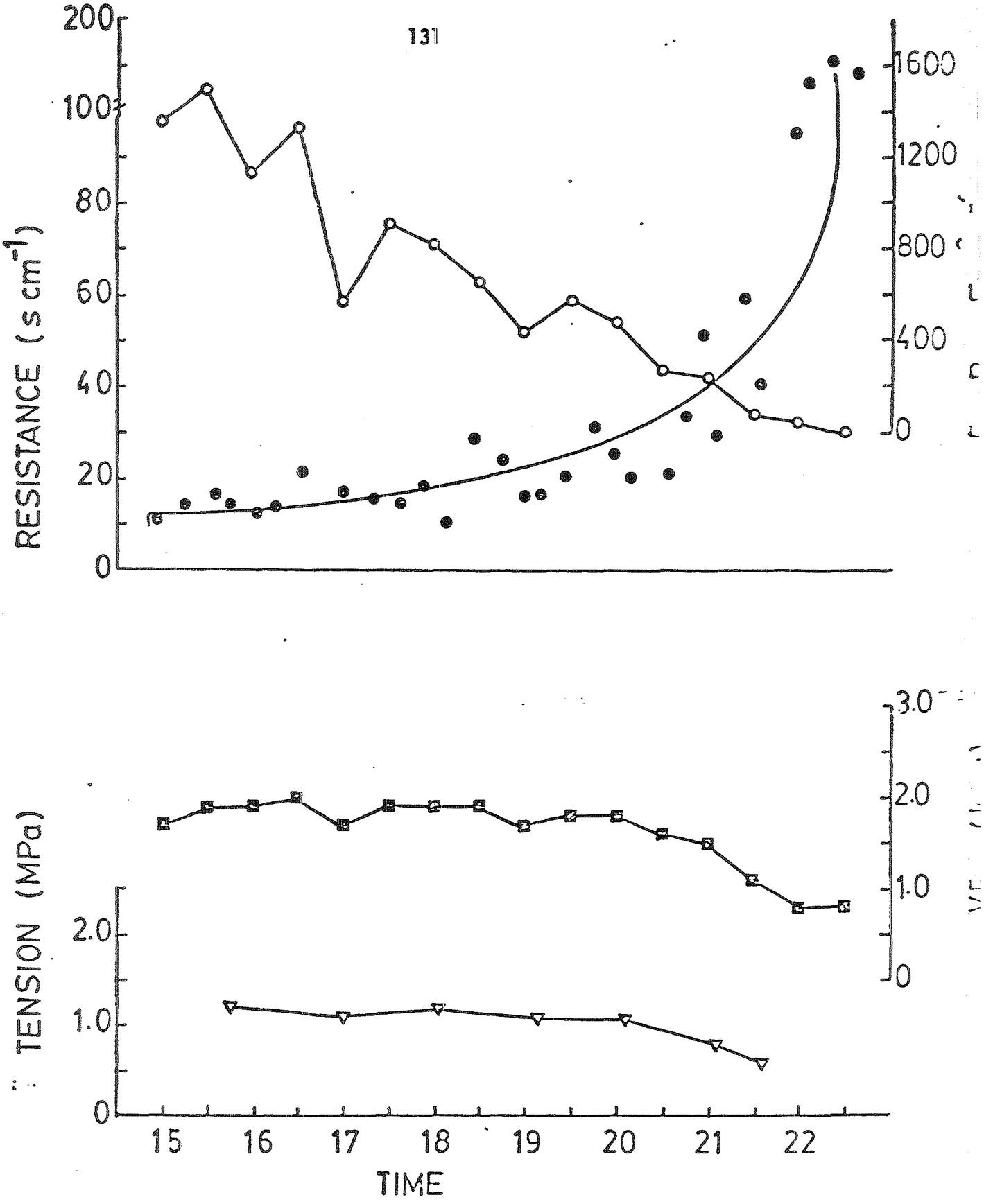

Figure 23. Whole branch (all needle age classes) leaf resistance (●), xylem tension (▽), vapor pressure deficit (⧈) and photosynthetically active radiation (○) for jack pine on June 1, 1977.

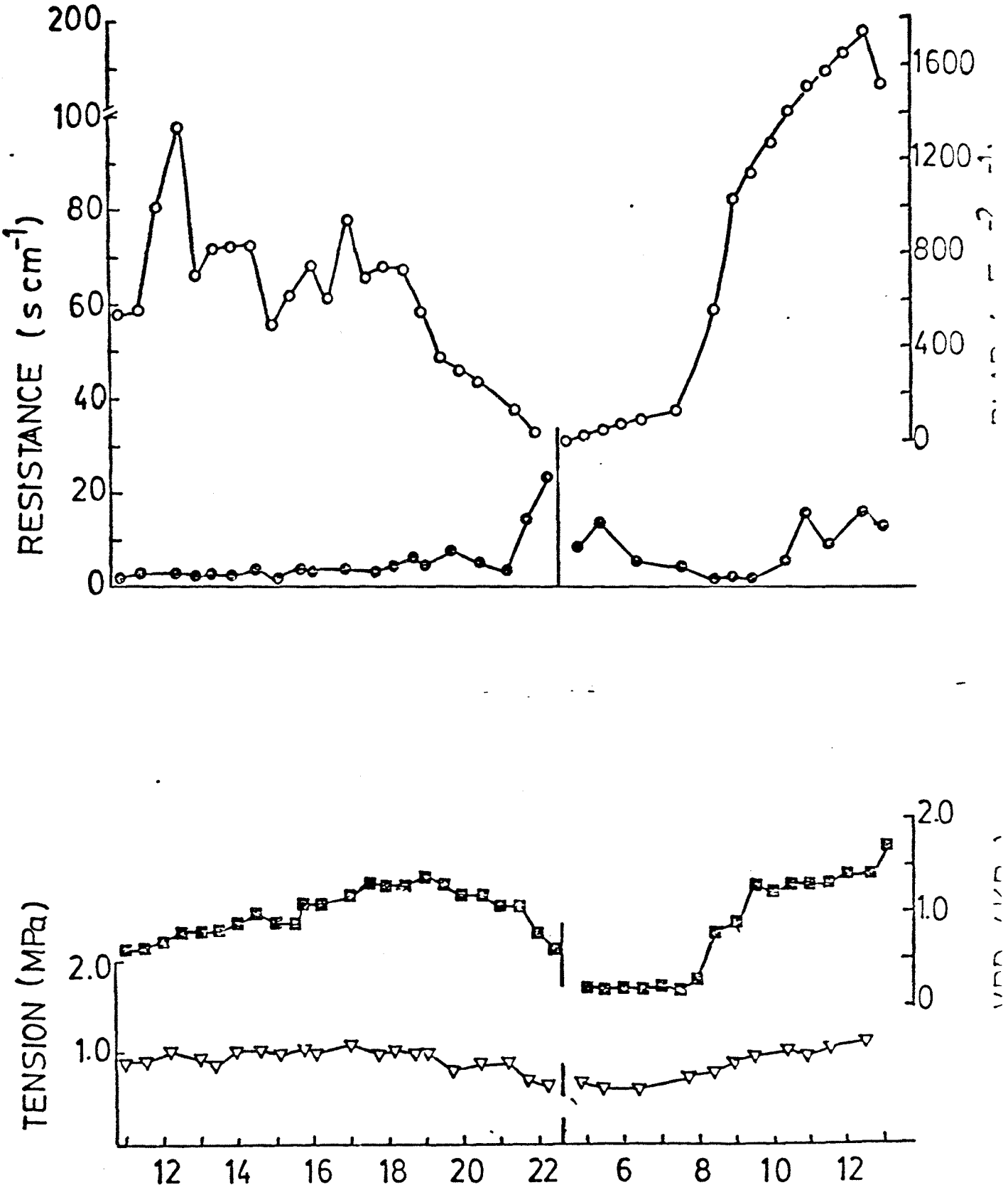

Figure 24. Harmonic mean leaf resistance (●) for all needle age classes, xylem tension (▽), vapor pressure deficit (▣) and photosynthetically active radiation (○) for June 3 and 4, 1977.

25 cm (well within the root zone).

The 1976 results ("see Fig. 15 previous report") indicate that R_L was insensitive to VPD until ca. 1.5 KPa at which time it increased sharply with further dryness. A major objective in 1977 was to confirm and if possible expand those results. Figure 26 summarizes the effect of VPD upon R_L during the April 15 and 16 study period when full stomatal opening (i.e. minimum R_L) had not yet been achieved (Fig. 25). VPD was never particularly high but R_L increased very rapidly at ca. 1.2 KPa. The linear regression r^2 was only .42 well after stomatal opening suggesting a non-linear response. The results of the May 11 and June 3 and 4 study periods confirm the previous years work in that R_L is insensitive to VPD until ca. 1.4 KPa at which time R_L inreases rapidly to 40 scm^{-1}.

The 1977 results extend the 1976 studies because of the very high VPD's on May 11. R_L did not continue to increase, but remained approximately the same, although quite variable (Fig. 27).

5.6 DISCUSSION

Maximum net CO_2 assimilation (NA) of young greenhouse grown trees was 8 mg $dm^{-2}h^{-1}$ prior to the development of any moisture stress (Fig. 1). This is similar to rates for *P. banksiana* reported by Logan (1971), but slightly lower than those reported for comparable lodgepole pine by Dykstra (1974). Legge *et al.* (1978) measured the photosynthetic capacity of

Table 6. Maximum and minimum air temperature, vapor pressure deficit (VPD) and xylem tension during periods of minimum leaf resistance during the spring of 1977.

Date	Air temperature °C maximum	minimum	xylem tension MPa	VPD KPa
March 8	12.6	-0.2	1.10	1.0
April 8	26.6	6.5	1.20	2.3[a]
April 15	14.8	-2.8	1.05	0.5
April 18	10.5	-1.2	0.95	0.7
May 11	34.5	8.8	1.10	0.7
June 4	22.8	8.8	1.00	0.9

[a] even though the VPD on April 8 was high enough to result in partial closure (Fig. 27) it would not have resulted in such complete closure.

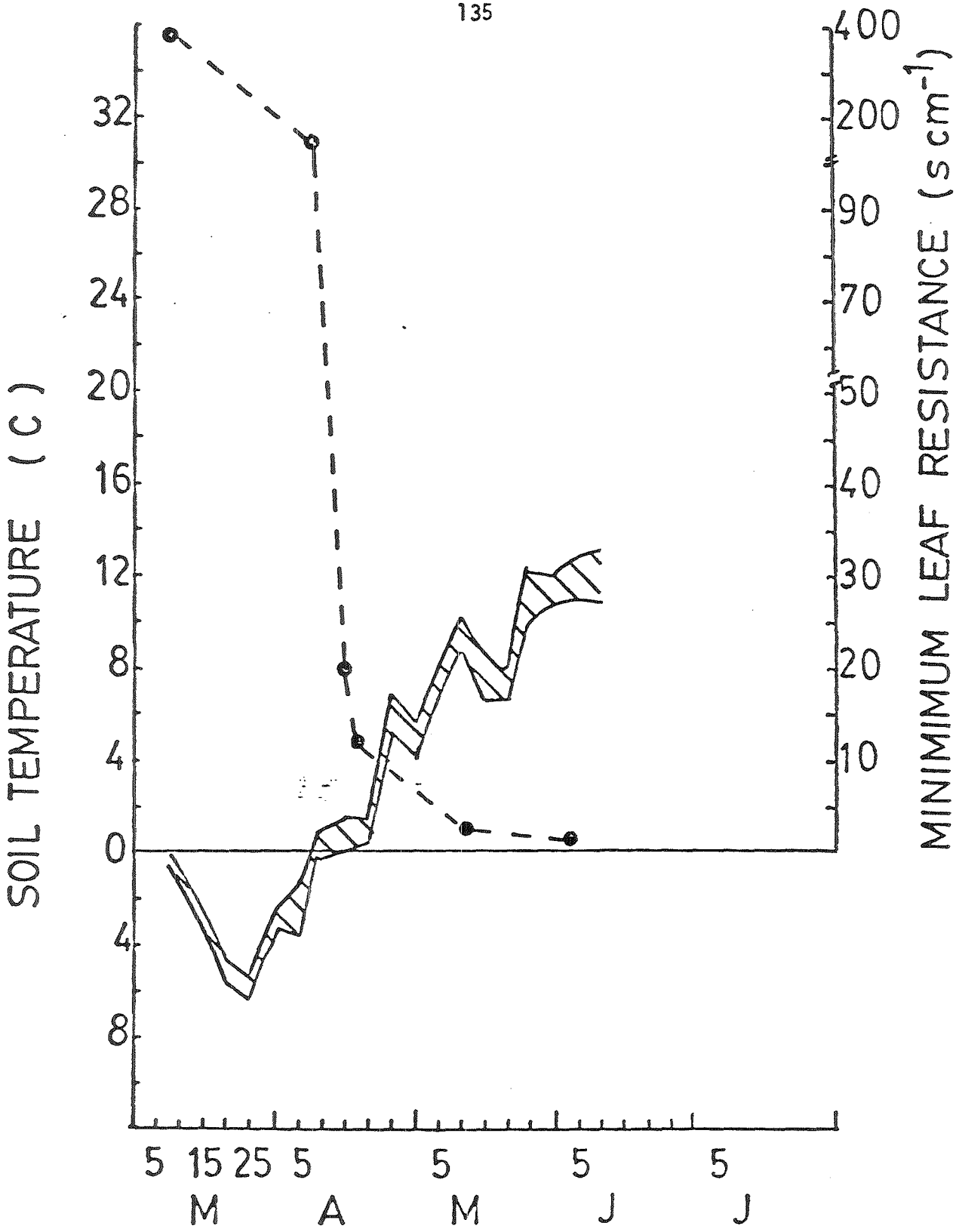

Figure 25. Minimum leaf resistance (⊛) through the spring and early summer of 1977, and soil temperature (max. and min.) at 25 cm. Air temperature, xylem tension, and VPD are given in Table 6.

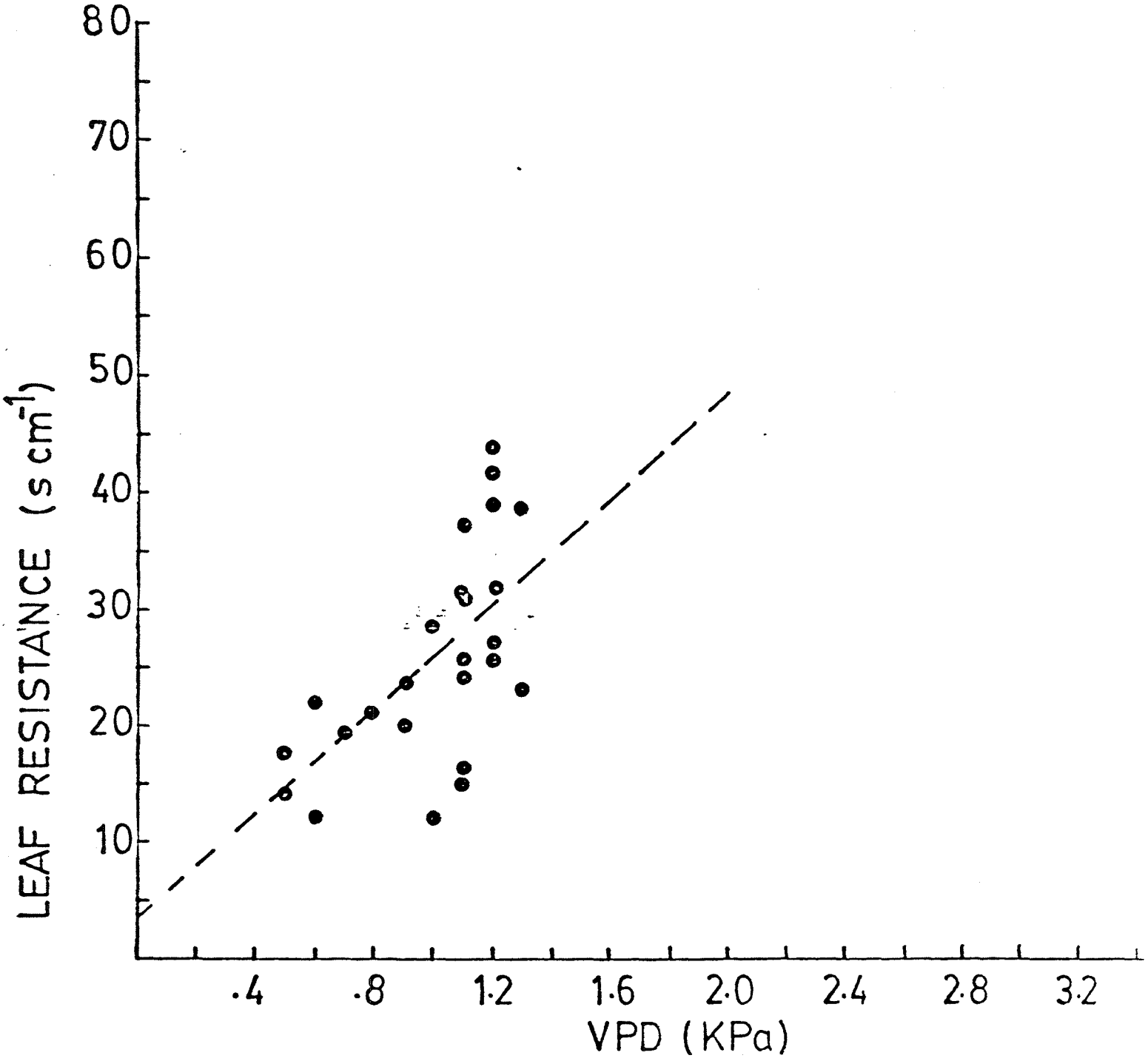

Figure 26. Harmonic mean leaf resistance vs. vapor pressure deficit on April 15-16, 1977. Values are for needles in the sun when PhAR exceeded 200 $\mu Em^{-2}s^{-1}$.

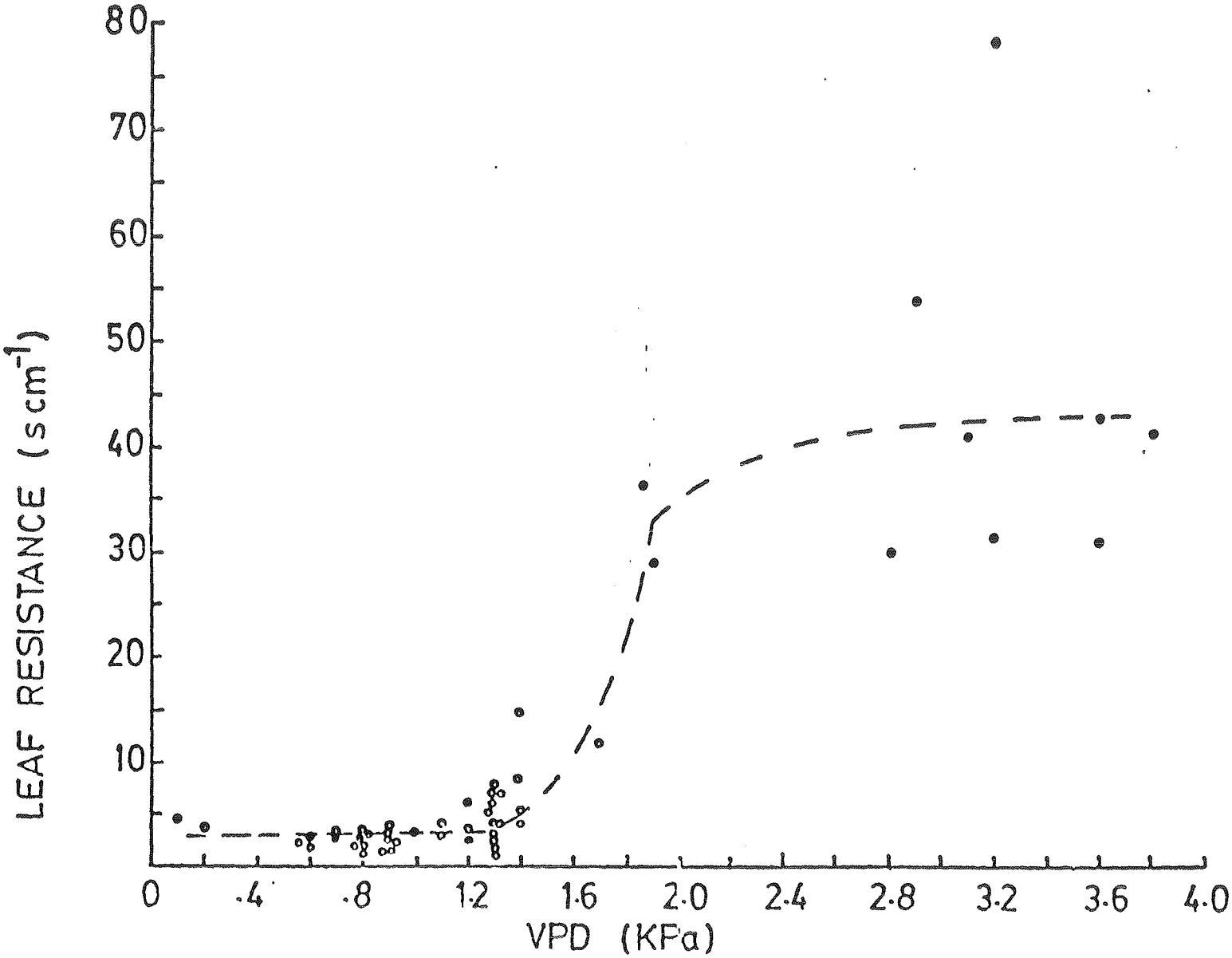

Figure 27. Harmonic mean leaf resistance vs. vapor pressure deficit on May 11 (•) and June 3-4 (∘), 1977. Only needles not shaded when PhAR exceeded 200 $\mu Em^{-2}s^{-1}$

exercised branches from the Richardson site in 1977 and found that the 1976 foliage fixed CO_2 at 6.11 mg $dm^{-2}h^{-1}$ and the 1975 at 3.92 mg $dm^{-2}h^{-1}$, thus the unstressed rate of 8 mg $dm^{-2}h^{-1}$, is not unreasonable nor is the 4.5 mg $dm^{-2}h^{-1}$ rate after stress. After two cycles, the maximum rates of rewatered plants were 4.5 mg $dm^{-2}h^{-1}$ indicating some loss of photosynthetic capacity, perhaps similar to the field conditions. During cycle 2 the plants were dried to an ultimate ψ_{leaf} of -3.5 MPa which is near the lethal limit (Fig. 5) yet CO_2 assimilation capacity did return to the original level indicating considerable ability to recover. NA was zero at -2.2 MPa ψ_{leaf} in both the second and third drying cycles. Dykstra (1974) reported that NA of similarly grown greenhouse lodgepole pine reached zero at -1.5 MPa. Jack pine can continue to fix carbon to a lower ψ_{leaf} perhaps explaining its success on drier sites. Based upon this study, soil water potential induced stress never reduced NA to zero during the 1976-77 study year (Fig. 3 "previous report; Figs. 11, 12, 13, 14). NA would have never been less than 2 mg CO_2 $dm^{-2}h^{-1}$ based upon the xylem tension measurements. This is not to say that NA was not reduced by water relations since VPD induced stomatal closure obviously will reduce carbon fixation (Fig. 27). Even if the photosynthetic capacity isn't particularly great, Jack pine is well adapted to its environment by avoiding ψ_{leaf} through VPD induced stomatal closure, fixing CO_2 to a relatively high xylem tension and being able to recover from the rather severe tensions (-3.5 MPa) of occasional stress.

The relationship between leaf water potential and water content for greenhouse and field plants (Fig. 2 and Fig. 7 respectively) indicates a very rapid decline in ψ_{leaf} with small losses of water thus making it difficult to infer ψ_{leaf} from water content. Maximum water content at high ψ_{leaf} is quite low and the greenhouse material has greater amounts of water at all ψ_{leaf} values indicating just how much "softer" is was. All of the Höfler diagrams (Figs. 3, 9, and 10) show that Jack pine undergoes very rapid osmotic adjustment or concentration as water is lost accompanying the rapid lowering of ψ_{leaf}. This is commonly observed in drought hardy desert species and is considered to be a water conserving mechanism; i.e. as water is lost, ψ_{leaf} drops rapidly resulting in stomatal closure which prevents or reduces further water loss. This is more evident in the field data. Jack pine is adapted to conserving water.

A comparison psychrometric ψ_{leaf} and xylem tension (Fig. 4) using greenhouse grown plants show that one can be used to estimate the other, and the relationship between water content and ψ_{leaf} seems good (Figs. 2 and 8). However, attempts to draw any correlation between xylem tension and needle water content (Fig. 17) have consistently failed to be reliable.

The lethal limit of Jack pine is at least -3.5 to -4.0 MPa ψ_{leaf}. Greenhouse trees (Fig. 4) withstood stress to this level with little apparent damage. Field trees would be at least that drought tolerant. Xylem tensions during the two study years were never close to such a limit with the absolute maximum tension for a

single reading being on the order of 2.0 MPa. The drying study and observations of freshly dug trees in the field suggest that the progression of drought injury is from younger to older needles. The strategy seems to be that photosynthetically mature tissue will be retained at the expense of the immature.

The stem freezing cavitation study (Fig. 6) proves that Jack pine does not cavitate upon freezing and thawing. This was expected, but is an important characteristic since it enables the tree to maintain intact water columns during freeze-thaw periods, particularly in the spring. This is not to say that Jack pine never experiences cavitation. The extreme drying test (Fig. 4), stress that ultimately kills the plant, suggests cavitation may occur. This could explain the discrepancy between psychrometric ψ_{leaf} and pressure bomb measurements. Cavitation occurance would prevent recovery in the greenhouse and pressure bomb readings would be much higher at any given ψ_{leaf} since cavities in the xylem would need to be filled with water from the live tissue during the process of making the pressure bomb reading. This would have the effect of sliding down a Höfler diagram to lower tissue water content and would cause erroneously low xylem tension measurements. Such extremely low xylem tensions were not measured during this project nor on Jack pine x lodgepole hybrids studied at Whitecourt Alta. (Legge *et al.*, 1978). Similar discrepancies have been observed in *Ledum groenlandicum* in the field, a species that readily cavitates (Wilkinson, 1977). The

failure of one of the stressed trees in the NA experiment to recover fully also suggests (but doesn't prove) drought induced cavitation.

Jack pine is quite different in its year-round water relations, compared with other species. The generally accepted paradigm holds that as a plant hardens in the fall; water content, water potential, and osmotic potential all decrease. According to Levitt (1972), "water content is frequently inversely related to hardiness". Water content usually decreases in the fall and may decrease somewhat during the winter (e.g. McKenzie, J. S. *et al.*, 1974; Wilkinson, 1977). Lowered osmotic potentials are also associated with hardening. Wilkinson (1977) reports that for *Ledum* $\psi_\pi + \psi_\tau$ is <-6.5 MPa during the winter and -2.0 MPa in the summer. Courtin and Mayo (1975) have summarized the reported ψ_π values for *Picea engellmanii, Picea pungens, Pinus cembra,* and *Picea mariana.* The differences between summer and winter (winter always lower) are respectively 2.3 MPa, 1.3 MPa, 0.7 MPa, and 4.0 MPa. It should be noted that the smallest difference (0.7 MPa) was in *P. cembra* which grows in Europe where winter conditions are not as severe as in Alberta; where the *Picea mariana* data originated. There is abundant evidence for fall and winter dehydration in trees. The Jack pine at Richardson Fire Tower shows none of the above mentioned changes with hardening. Needle water content is the highest in the late winter, prior to melt out (Fig. 5, "previous report Fig. 14"). The water contents are no different in March 1977 than they were in September 1976, and are much higher than in May and June of both years when water

contents are lowest. The current needles do show a consistent drop in water content through the first summer (Fig. 5 "previous report"), but then fit the pattern described above. The highest xylem tensions occurred during the summer and decreased with the onset of winter (Fig. 3 "previous report"; Figs. 11, 12, 13, and 14). The combined osmotic and matrix potentials ($\psi_\pi + \psi_\tau$) remained virtually unchanged throughout the year, rather than decrease during the fall and winter (Table 1, "previous report"; Table 1). Morning $\psi_\pi + \psi_\tau$ values were ca. -2.4 MPa indicating little change. Maximum turgor potential, estimated as $\psi - (\psi_\pi + \psi_\tau)$, remained high throughout the year (Table 1 "previous report"; Table 1).

The initial R_L measurement in April, 1976 (Fig. 10 "previous report") suggested that Jack pine stomata remain closed during the winter and do not immediately open on warm spring days. R_L on October 28, 1976 showed that the stomata are closed during the fall and slowly become fully operational as the soil warms after snow melt (Table 6, Fig. 17, 19, 20, 21, 22, and 23). Figure 24 shows minimum R_L and soil temperature during the spring. Even though melt out effectively took place on April 8, minimum R_L's weren't observed until late April or early May. Air temperature, xylem tension, and VPD were not likely to be limiting R_L. These results suggest that Jack pine stomata are closed from late fall until late spring regardless of water status, perhaps due to hormonal influences, such as ABA. The results also suggest that stomatal activity is regained slowly during the spring and may be

controlled by soil temperature; perhaps due to cytokinin synthesis in the root system. Jack pine is therefore very resistant to winter and spring drought by virtue of its high leaf resistance.

The 1976 data showed that leaf resistance was relatively insensitive to VPD until ca. 1.6 KPa (Fig. 15 "previous report"). The results for 1977 (Fig. 27) confirm that conclusion. Many more individual measurements were taken during 1977 and on May 11, VPD soared to the highest value (3.8 KPa) during a study period. The conclusion is that given relatively low xylem tensions and PhAR greater than 200 $\mu Em^{-2}s^{-1}$, leaf resistance is insensitive to VPD until ca. 1.4 KPa and that by 1.8 KPa the stomata have nearly closed; resulting in R_L values of 40 scm^{-1}. Further increases in VPD do not result in further closure. Even though R_L varies considerably at the higher VPD's (Fig. 27), there is no doubt of stomatal closure. Pereira and Kozlowski (1977) report minimum leaf resistances of 5 scm^{-1} for Jack pine, which are similar to our results (Fig. 27) and R_L values of 10 scm^{-1} at 1.6 KPa VPD; again similar. They do not show the sharp threshold increase to 40 scm^{-1} even at VPD's of 2.7 KPa. This is perhaps due to the fewer samples reported in their study. Jarvis (1976) reports similar responses to xylem tension and VPD as we do. Fetcher (1976) reports that lodgepole pine R_L is relatively insensitive to xylem tension between 0.9 and 1.7 MPa, but is quite sensitive to VPD. Our results indicate that Jack pine stomata will close on hot-dry days due to VPD, thus tending to prevent high xylem

tension caused stomatal closure difficult to detect; especially since this would happen only under prolonged drought conditions. Conditions which, although possible, did not occur during the two year study.

Jack pine appears to be highly adapted to the sandy, potentially xerix sites on which it grows because:

1) It avoids winter and spring drought by maintaining high leaf resistances during the winter and spring when frozen soils might limit water uptake.
2) It does not cavitate under freeze-thaw conditions thus maintaining xylary water columns.
3) Its stomata are sensitive to atmospheric VPD thus closing prior to xylem tension or ψ_{leaf} induced closure. It therefore tends to conserve soil water by maintaining high R_L (and low transpiration) on hot-dry days. This is important since nearly half of the yearly precipitation may drain out of the root zone (see page).
4) It exhibits considerable osmotic adjustment to water loss thus tending to absorb more water from drier soils.
5) It does not dehydrate upon hardening for winter, thus carrying more tissue water into and through the winter. Winter and spring drought was not a problem during the study.

6) NA is positive down to -2.2 MPa ψ_{leaf} thus allowing carbon fixation under moderate drought stress, and considerable photosynthetic capacity is restored upon drought relief.

7) In the event of extreme drought, the more mature photosynthetically active tissue is retained at the expense of the younger (non self-sufficient) tissue, and death does not occur until -3.5 to 4.0 MPa.

5.6.1 Implications of Jack Pine Physiology for Oil Sands Revegetation

While recognizing that the results of study of Jack pine are not absolutely definitive concerning revegetation of the mined sand; two important facts should be kept in mind: 1) The Jack pine lichen woodland is the major vegetation type that stabilizes dry, infertile sandy soils, particularly the steeper slopes, in the Ft. MacMurray region of Alberta; 2) The ecophysiologic characteristics of Jack pine suggesting that it is well adapted to xeric, nutrient poor sites should be born in mind when selecting potential revegetation species. This is not to say that only similar plants are suitable for revegetation of the mined sands, but that short term success of species with radically different physiologic characteristics must be viewed with caution. Jack pine provides a standard of comparison which should not be ignored. The following characteristics suggest just how well it is adapted to its habitat in northern Alberta.

1) Low nutrient requirements - Jack pine has low amounts of N, P, K, Ca, and Mg compared with aspen, red pine, and white spruce on similar soils (Alban, Perala, and Schlaegel, 1978) and according to Morrison (1973) is less N, P, K, Ca, and Mg demanding than white pine, red pine or white spruce. He goes on to say: "Presumably then, it is this low nutrient requirement which enables Jack pine to maintain acceptable growth rates on sites of low fertility". Unless fertilization is carried out indefinately and/or cation exchange capacity is improved dramatically through substrate ammendments, species (such as Jack pine) with low nutrient requirements are essential. It is known, however, that Jack pine will respond to fertilization (e.g. Weetman and Algar, 1974; Morrison, Winston and Foster, 1977) and can even benefit from sewage effluent (Tolsted, 1976); it is also sensitive to fertilizer and too much will reduce growth (McClain and Annson, 1975). Thus fertilizer in amounts conducive to good growth of agronomic grasses (e.g. George *et al.*, 1973) may actually reduce seedling growth of Jack pine, black spruce and white spruce, i.e. agronomic grasses may not be good nurse crops for these trees.

2) Resistance to winter and spring moisture stress - by entering the winter fully hydrated with closed stomata (Fig. 14, Fig. 5 "previous report"), Jack pine experiences little of the winter dehydration reported for other conifers such as

Engleman Spruce and black spruce (Courtin and Mayo, 1975) or Douglas Fir (Salo, 1974). The stomata remain tightly closed until well after melt-out (Fig. 25) and temperatures are high enough for photosynthesis but cold soils prevent or slow water uptake. Jack pine does not cavitate upon freezing and thawing (Fig. 6), thus maintaining intact water columns and avoiding cavitation enhanced stress. Other species such as grasses or deciduous trees avoid winter and spring stress by shedding their leaves, but they do this at the apprent expense of higher nutrient requirements.

3) Avoidance of summer moisture stress by VPD sensitive stomata - Jack pine tends to avoid summer moisture stress because on hot-dry days, its stomata will close in response to VPD regardless of how high soil and leaf water potential might be (Fig. 26). This characteristic, plus the lichen layer barrier to evaporative water loss ("previous report", p. 187) means that the Jack pine-lichen woodland will in fact conserve soil moisture during protracted hot-dry periods by reducing transpiration water loss before soil water potential can cause stomatal closure via water loss from the system. It is a conservative system. Most stands of agronomic grasses (e.g. *Bromus inermis*) do not behave this way.

4) Photosynthetic capacity under moisture stress - in the event of prolonged drought, Jack pine can fix carbon

positively to -2.2 MPa leaf water potential (Fig. 1). This is considerably lower than many other species (exclusive of strictly desert plants). For example net CO_2 fixation is zero at: -1.5 MPa in *Pinus contorta* (Dykstra, 1974); -1.1 MPa is lobolly pine (Brix, 1962); and -1.4 MPa in noble fir and -1.6 MPa in Pacific silver fir (Hinckley, 1971).

5) A relatively high lethal limit to moisture stress - in the event of prolonged drought, Jack pine can survive extended periods of drought during which leaf water potentials as low as -3.5 MPa occur. This is considerably lower than any values measured in the field during the study, and it is considerably lower than stresses tolerated by most agronomic species although good evidence on lethal limits is lacking, and there are difficulties in comparing results from experiments carried out under different conditions (Levitt, 1972).

The conclusion is that *Pinus banksiana* is very well adapted to nutrient poor sites, avoiding winter dessication, conserving soil moisture, and tolerant of drought should prolonged periods without precipitation occur.

5.7 REFERENCES CITED

Alban, David H., Donald A. Perala, and Bruce E. Schlaegal. 1978. Biomass and nutrient distribution in aspen, pine and spruce stands on the same soil type in Minnesota. Can. J. For. Res. 8(3): 290-299.

Bennett, K. J. and D. A. Rook. 1978. Stomatal and mesophyll resistances in two clones of *Pinus radiata* D. Don known to differ in transpiration and survival rate. Aust. J. Plant Physiol. 5: 231-238.

Brix, H. 1962. The effect of water stress on the rate of photosynthesis and respiration in tomato plants and loblolly pine seedlings. Physiol. Plant 15: 10-21.

Courtin, G. M. and J. M. Mayo. 1975. Arctic and alpine plant water relations. In Physiological Adaptation to the Environment, F. John Vernberg (Ed.), In text Educational Publishers, N.Y. p. 201-221.

Dykstra, G. F. 1974. Photosynthesis and carbon dioxide transfer resistance of lodgepole pine seedlings in relation to irradiance, temperature and water potential. Can. J. For. Res. 5: 55-60.

Fetcher, Ned. 1976. Patterns of leaf resistance to lodgepole pine transpiration in Wyoming. Ecology 57(2): 339-345.

George, J. D., C. L. Rhykerd, C. H. Noller, J. E. Dillon, and J. C. Furus. 1973. Effect of N fertilization on dry matter yield, total N, N recovery, and nitrate-N concentration of three cool-season forage grass species. Agron. Journ. 65: 211-218.

Hammel, H. T. 1967. Freezing of xylem sap without cavitation. Plant Physiol. 42: 55.

Hinckley, Thomas Metcalf. 1971. Plant water stress and its effect on ecological patterns of conifer species. Ph.D. Thesis, University of Washington, Seattle, Washington, U.S.A.

Höfler, K. 1920. Ein schema fur die osmótische Leistung der Pflanzenzelle. Ber. Deutsch. Bot. Ges. 38: 288-298.

Jarvis, P. G. 1976. The interpretation of the variations in leaf water potential and stomatal conductance found in canopies in the field. Phil. Trans. R. Soc. Lond (B) 273: 593-610.

Legge, A. H., D. R. Jaques, G. W. Harvey, H. R. Krouse, H. M. Brown, E. C. Rhodes, M. Nosal, H. U. Schellhase, J. Mayo, A. P. Hartgerink, P. F. Lester, R. G. Amundson and R. B. Walker. 1978. Sulphur gas emissions in the Boreal Forest: The West Whitecourt Case Study. Environmental Sciences Centre, Kananaskis, The University of Calgary.

Logan, K. T. 1971. Monthly variation in photosynthetic rate of Jack pine provenances in relation to their height. Can. J. For. Res. 1: 256-261.

Levitt, J. 1972. Response of Plants to Environmental Stresses. Academic Press, New York.

McKenzie, J. S., D. J. Weiser, and P. H. Li. 1974. Changes in water relations of *Cornus stolonifera*. Mich. Plant Physiol. 53: 783-789.

McClain, K. M. and K. A. Armson. 1975. Growth responses of pine and spruce seedlings to regimes of soil moisture and fertility. Soil Sci. Soc. of Amer. Proc. 39(1): 140-148.

Morrison, I. K. 1973. Distribution of elements in aerial components of several natural Jack pine stands in northern Ontario. Can. J. For. Res. 3(2): 170-179.

Pereira, J. S. and T. T. Kozlowski. 1977. Water relations and drought resistance of young *Pinus banksiana* and *P. resinosa* plantation trees. Can. J. For. Res. 7(1): 132-137.

Salo, David John. 1974. Factors influencing photosynthesis in Douglas Fir. Ph.D. Thesis, University of Washington, Seattle, Wa., U.S.A.

Tolsted, D. N. 1976. Sewage effluent spray increases diameter growth of Jack pine. U.S. DA Forest Service. Research Note, North Central Forest Expt. Sta. No. NC-207.

Wilkinson, Amanda Jane. 1977. Physiological aspects of cold hardiness of *Ledum groenlandicum*. M.Sc. Thesis, University of Alberta, Edmonton, Alberta.

6. HEAT PULSE VELOCITY INVESTIGATIONS IN JACK PINE

R. H. Swanson
Federal Forestry Laboratory
Edmonton

"See previous report"

7. TREE GEOMETRY AND OPTICAL PROPERTIES OF LEAVES

D. W. A. Whitfield, J. M. Mayo, John Harter
Sherman Nelson, and Alan Mehlenbacher
Department of Botany
University of Alberta

"See previous report"

8. INVESTIGATIONS ON THE ROLE OF LICHENS IN THE JACK PINE-LICHEN FOREST ECOSYSTEM

D. C. Lindsay
Department of Botany
University of Alberta

"See previous report"

9. MYCORRHIZAE IN JACK PINE STANDS AT THE RICHARDSON FIRETOWER SITE

R. M. Danielson
Department of Biology
University of Calgary

9.1 INTRODUCTION

This report covers only information gathered since the previous report including some taxonomic revisions of the symbionts collected at the Richardson site. In order to determine the importance of any particular combination of symbiont and host it is necessary to determine the abundance or frequency of occurence in the field. Toward this end efforts were made to culture specific fungi isolated from sporocarps and inoculate sterile root systems to form mycorrhizae. If the mycorrhizae produced were distinctive in appearance then direct evaluations could be made of natural root systems with regard to specific host-symbiont relationships.

In that droughty conditions were initially assumed to be critical in the Jack pine-lichen woodland studied, preliminary experiments were conducted on the water relations of the mycorrhizal fungi. It has been suggested that mycorrhizae formed by certain fungi may aid the host in water uptake and increase drought tolerance (Trappe, 1977). Thus the selection of symbionts may influence the success of any revegetation scheme where the plants are expected to experience severe stress.

The major study area is described in detail elsewhere in this report. Collecting of sporocarps of potential mycorrhizal fungi was also done in mature jack pine stands on level terrain between the

airstrip and the major study site (a distance of about 5 km), alongside the road between the two sites and on an area burned in 1970 and regenerating to jack pine forest.

9.2 SPECIES OF MYCORRHIZAL FUNGI ASSOCIATED WITH JACK PINE WITH NOTES ON SELECTED SPECIES

"See previous report"

9.3 DIRECT ISOLATION OF SYMBIONTS FROM MYCORRHIZAE

"See previous report"

9.4 IDENTIFICATION AND ABUNDANCE OF SPECIFIC MYCORRHIZAL TYPES

"See previous report"

9.5 METHODS

9.5.1 Methods in All Experiments - 1st Year

"See previous report" (including all preliminary work under 9.5.2 and 9.5.3).

9.5.2 Pure Culture Synthesis of Jack Pine Mycorrhizae

Preliminary techniques in large test tubes were described in the previous report. The mycorrhizal syntheses reported here followed the general procedure used by Zak (1976a). Syntheses were considered positive when a Hartig net or a Hartig net and an external mantle were present on hand cut sections and the symbiont could be recovered on MMN agar. One liter erlenmeyer flasks were partially filled with 420 ml vermiculite, 30 ml peat moss and 275 ml MN nutrient solution (Zak, 1976a) and autoclaved for 30 minutes. Jack pine seeds were soaked in cold running water for 24 hr and surface

sterilized by exposure to 30% H_2O_2 for 30 minutes. The seeds were placed on MMN agar plates and allowed to germinate. Contaminant free seeds with radicles 2-3 cm long were planted in the vermiculite-peat substrate. Each of five replicate flasks was then inoculated with 10 ml of a mycelial suspension from liquid cultures. One set of flasks was left uninoculated. Each culture was checked for viability and purity by plating on MMN agar plates. The flasks were placed in a growth chamber with an 18 hr light - 6 hr dark cycle. Temperature of the substrate did not exceed 22°C. After 6-12 months the roots were examined for infection and contamination. Attempts were also made to synthesize mycorrhiza with *Hydnellum peckii* and *Elaphomyces granulatus*, two species which could not be cultured. Pieces of the basidiocarp of *Hydnellum* were surface sterilized in alcohol, flamed and placed beside roots of established pine seedlings. *Elaphomyces* ascocarps were surface sterilized, broken open and a spore suspension added to the synthesis flasks.

9.5.3 Pure Culture Synthesis of Bearberry

The synthesis precedure was the same as with jack pine. The number of tests that could be attempted was severely limited by the very low germination rate of the bearberry seeds. Scarification and stratification procedures used by Zak (1976b) and a warm stratification followed by a cold stratification (T. Laidlaw, Pers. Comm.) all failed to give satisfactory germination. Thus each of ten flasks were planted and each inoculated with one of the fungi previously tested with jack pine. Criteria for mycorrhizal formation were the same as with jack pine.

9.5.4 Pure Culture Synthesis of Isolates from Surface Sterilized Mycorrhizae

In the previous report 82 species groups were isolated from surface sterilized mycorrhizal tips. Only 11 of the 82 taxa could be related by cultural appearance to known mycorrhizal symbionts. It was thus unknown if a majority of these groups represented mycorrhizal fungi or were non-target, saprophytic fungi. In order to test the mycorrhizal forming ability, one representative of each of 18 groups was randomly chosen for synthesis trials in pure culture. Inoculum was prepared in vials containing MMN solution and broken glass fragments to fragment the mycelium (Zak, 1976a) so it could be injected aseptically onto the root system. Seedlings were grown in 150 x 25 mm test tubes in the vermiculite-peat-MN substrate as described in the previous report. The tubes were placed in a growth chamber and the roots examined for infection after three months. Infection was determined by visual examination and confirmed by examining hand-cut sections of the roots.

9.5.5 Growth of Mycorrhizal Fungi at Different Water Potentials

In order to determine if different mycorrhizal fungi were adapted to low water potentials (ψ) they were grown on solid media adjusted to a series of osmotic levels with either NaCl or sucrose. The basal medium was MMN agar used by Mexal and Reid (1973) which they reported to have a water potential of -1.6 bars. In the first test NaCl was used as the osmoticum and in the second sucrose was used to determine if there were specific ion effects of the NaCl. The desired molality values for NaCl were taken from a table in Kozlowski (1968). Osmotic coefficients and water activity values

for sucrose were obtained from Robinson and Stokes (1955). Intermediate values not given in the tables were obtained from a linear regression between water activity and molality or water activity and water potential. Water potentials at 25°C were calculated by the formula by Griffin (1972): $\psi = -24.7\ VM\emptyset$, where V = ions/molecule, M = molality and $\emptyset$ = osmotic coefficient. Water activity (a_w) was converted to ψ by the formula given by Griffin (1969) with

$a_w = {}^{P}/_{PO} : \psi = \frac{RT \ln a_w}{10^6 M}$, which simplifies to: $\psi = 1374.5\ (\ln a_w)$.

Plates were inoculated with either one or two agar discs taken from the margin of colonies growing in MMN medium. Three replicate plates were used with NaCl and four with sucrose. The inoculated plates were sealed with parafilm and placed in plastic bags to reduce moisture losses. Radial colony growth was measured at 10 day intervals.

9.6 RESULTS

9.6.1 Mycorrhizal Fungi Collected from Sporocarps

Additional collections made at the Richardson site require the revision of the list of fungi presented in the previous report. In the revised list 57 species are considered to be symbionts of Jack pine (Table 1). Many or most of these may also be associated with bearberry. Observations on their abundance and distribution were covered in the previous report.

9.6.2 Synthesis of Jack Pine Mycorrhizae

Fourteen species of fungi successfully formed mycorrhizae with jack pine in synthesis flasks. All but two of these were native

to the Richardson area. One of these was an isolate of *Pisolithus tinctorius* obtained from D.H. Marx and was isolated from a southern pine. The other was an isolate from lodgepole pine in the Kananaskis region of Alberta. It is unusual in that it forms ectendomycorrhizae. Its identity is unknown although the absence of clamp connections on the hyphae and an intolerance to benolate suggests it might be an ascomycete.

In addition to those combinations described here *Suillus sibericus*, *Tricholoma zelleri* and *Cenococcum graniforme* also formed typical ectomycorrhizae with jack pine in synthesis flasks. All the flasks inoculated with *Hydnellum* and *Elaphomyces* become contaminated and mycorrhizae were not formed. At the termination of the experimental period thousands of spores of *Elaphomyces* could be seen in contact with the pine roots with no evidence of germination. Descriptions of the mycorrhizae formed by the other fungi follows. Colour notations followed by an asterisk are according to Henderson *et al.* (1969).

9.6.2.1 *Astraeus hygrometricus + Pinus banksiana* FORM: dicotomous becoming coralloid and branching twice or three times, rarely pinnate, elements stout and generally short. COLOUR: vinaceous buff* or whitish becoming nearly livid vinaceous* at times or brown vinaceous*. MANTLE: compact, on close inspection with a sparce network of darker hyphae overlaying the dominantly pallid mantle hyphae. MYCELIAL STRANDS: very abundant, well defined with radiating hyphae, extending for long distances into the substrate. Outer layer of cells of the rhizomorphs rounding up and with thickened walls giving a cellular outer rind when well developed, inner portion

of longitudinally arranged hyphae. ANATOMY: ectomycorrhizal with a Hartig net extending to the endodermis, mantle compact and thick. CULTURAL FEATURES: See *A. hygrometricus* + *A. uva-ursi.* DISTINCTIVE CHARACTERS: The compact dicotomous to coralloid form, vinaceous tint and the abundant vinaceous tinted rhizomorphs are the best field characters. In culture, the dark brown colony with a halo of dark bro n pigments formed a few millimeters from the colony margin is distinctive.

9.6.2.2 *Tricholoma flavovirens* + *Pinus banksiana* FORM: Simple and monopodial or more commonly irregularly branched once or twice, elements long and narrow, projecting up to 10 mm. COLOUR: pale livid vinaceous* to livid vinaceous* or pallid if mycelium sparce. MANTLE: compactly felty or with abundant floccose hyphae. MYCELIAL STRANDS: abundant and originating from the mantle hyphae, fairly well formed, ultimately branching into fine strands, colour same as mantle. ANATOMY: Hartig net well developed, no intracellular hyphae, mantle 20-30 µm thick, all elements compact and well defined, extramatrical hyphae 2-3 µm diameter, smooth, hyaline, simple septate. CULTURAL FEATURES: very slow growing, hyaline. DISTINCTIVE CHARACTERS: The vinaceous colour, the loose and irregular branching and the abundant mycelial strands are distinctive.

9.6.2.3 *Tricholoma pessundatum* + *Pinus banksiana* FORM: simple to dicotomous, elements moderately long and slender. COLOUR: pale brown or pure white when external mycelium not stripped away. MANTLE: a dense, felty mass of white mycelium permeating and clinging to the substrate. MYCELIAL STRANDS: Absent

although with abundant mycelium loosely aggregated around the lateral and short roots. ANATOMY: ectomycorrhizal with a well developed mantle and Hartig net. CULTURAL FEATURES: Slow growing, variable, ranging from pure white to brown in the same colony. DISTINCTIVE CHARACTERS: The mass of pure white mycelium which makes the substrate very difficult to dislodge in a cylinder about 1 cm in diameter is the best field character. However, other species of *Tricholoma* that ere not tested may have a similar development of superficial mycelium.

9.6.2.4 *Suillus tomentosus* + *Pinus banksiana* FORM: simple, dicotomous or in compact coralloid clusters 2-4 mm broad, becoming subtuberculate with numerous tips covered with a felty layer of mycelium which completely obscures the individual tips. COLOUR: white and glistening from air trapped in the loose outer hyphal becoming vinaceous* tinted or brown vinaceous*; when bruised becoming buff* when young or brown vinaceous* to sepia* when mature. MANTLE: loose textured with abundant floccose hyphae. MYCELIAL STRANDS: common but not extending far from the mycorrhizae, originating from the mantle, hyphae radiating out from the length of the strands; white, brown tinted or vinaceous brown*. ANATOMY: with Hartig net extending to the endodermis, mantle 20-40 µm thick. Hyphae 2-2.5(4) µm diameter, septa simple, walls smooth or heavily encrusted with vinaceous* crystals. DISTINCTIVE FEATURES: include the subtuberculate form, the vinaceous tint, the abundant crystalline material on the hyphae and the abundant mycelial strands.

9.6.2.5 *Scleroderma macrorhizon + Pinus banksiana* FORM: dicotomous or occasionally branched twice, branches short or long. COLOUR: pure white, becoming pale brown when compressed. MANTLE: surface matted, unpol shed, abundant loose hyphae becoming floccose with age. MYCELIAL STRANDS: abundant, up to a dozen originating from each tip, white, short and not extending far into the medium. ANATOMY: Mantle 30-60 m thick, Hartig net well developed, no intracellular hyphae. Hyphae 4 m diameter, hyaline, clamped, very slightly roughened. CULTURAL FEATURES, slow growing, deep floccose and hemispherical, pure white; reverse straw becoming apricot to sienna at the center; a small amount of straw coloured diffusible exudate present. DISTINCTIVE FEATURES: best identified by comparison with known isolates in culture.

9.6.2.6 *Pisolithus tinctorius + Pinus banksiana* FORM: dicotomous becoming symetrically double dicotomous all elements short and stout, rarely projecting more than 3 mm; rarely with long elements. COLOUR: vinaceous buff* to fawn* after wetting, pale vinaceous buff* to vinaceous buff* *in situ*, matrix of hyphae trapping air to give a glistening appearance. MANTLE: appressed tomentose, relatively smooth, MYCELIAL STRANDS: abundant, originating from the mantle. ANATOMY: typically ectomycorrhizal. CULTURAL FEATURES: Growth rapid, deeply floccose and filling the petri dishes to the top, aerial hyphae easily stripped from the agar, olivaceous brown*, reverse same as above, becoming umber with age. Diffusible pigments lacking. DISTINCTIVE FEATURES: include to the stout brown coralloid structures and the extremely rapid growth in culture.

9.6.2.7 *Lactarius chelidonium + Pinus banksiana* FORM: simple becoming dicotomous, and branching dicotomously up to three times and forming coralloid clusters; elements long, entire cluster 2-7 mm long; elements considerably inflated. COLOUR: highly variable even on the same root segment, cream or buff* becoming pale fulvous*, fulvous* or sepia*, often unevenly tinted greyish green* with age. MANTLE: smooth, unpolished, nearly glabrous. In profile mantle nearly translucent and appearing as a hyaline halo. MYCELIAL STRANDS: well defined but indifferentiated, hyaline, greyish green* or darkgreen with the colour changing abruptly. Often fused to the lateral roots, never seen directly attached to the mycorrhizal tips. ANATOMY: Hartig net well developed, no intracellular hyphae. Mantle a dense layer 20-25 µm thick, hyphae with simple septa. CULTURAL FEATURES: Growth slow, sparse aerial hyphae but abundant erect fascicles which radiate out from the centre, colour variable, hyaline becoming saffron* and finally green, reverse pale saffron, no diffusible pigments. DISTINCTIVE FEATURES: The green colour, when present, of the mycelial strands and mycorrhizal, the glabrous mantle, the halo effect in profile and the clampless hyphae are the best guides for field identification. Other closely related species of *Lactarius* also result in a green colour (Zak, 1976b).

9.6.2.8 *Laccaria laccata + Pinus banksiana* FORM: short dicotomous becoming branched two to three times and forming compact coralloid clusters. COLOUR: whitish to page cream *in situ*, after washing may be fulvous. MANTLE: floccose with white hyphae, finely tomentose after washing. MYCELIAL STRANDS: absent.

ANATOMY: Mantle 15-30 µm thick, compact; Hartig net well developed, no intracellular hyphae; hyphae clamped. CULTURAL FEATURES: Growth rapid, aerial hyphae sparce, pigments lacking. DISTINCTIVE FEATURES: The combination of white coralloid form, rapid growth in culture and absence of pigments appear to be the best guide in identification.

9.6.2.9 *Bankera fuligineo-alba + Pinus banksiana* FORM: dicotomous or branched two oo four times, branching somewhat irregular, elements long forming a loose coralloid structure, primary element long, 2-6 mm; total structure projecting up to 10 mm. COLOUR: whitish, pale hazel* or fulvous* depending on the amount of loose mycelium; if whitish becoming fulvous* to umber* when compressed. MANTLE: varying from nearly glabrous to densely covered with wefts of white hyphae. MYCELIAL STRANDS: absent when young, abundant with age and originating from the mantle, well formed, 60-70 µm diameter. ANATOMY: Hartig net one to two cells deep, mantle about 15 µm thisk. Hyphae hyaline, smooth 1.5-2 µm diameter, simple septate. Extramatrical hyphae with abundant chlmydospore-like units, terminal or intercalony globose, 5-6 µm diameter, walls slightly thickened and pale brown. DISTINCTIVE CHARACTERS: None macroscopically although the hyphal swellings may be an aid in identification.

9.6.2.10 *Coltrichia perennis + Pinus banksiana* FORM: simple or dicotomous with long elements, occasionally branched twice but never coralloid. COLOUR: rusty tawny becoming fulvous black when old. MANTLE: with abundant hyphae radiating out, hyphae appearing stiff or becoming tangled and floccose, fulvous* to cinnamon* in colour; mantle nearly glabrous when dark and old.

MYCELIAL STRANDS: absent. ANATOMY: typically ectomycorrhizal with the Hartig net extending to the endodermis and with a well developed mantle 40-60 μm thick. BASIDIOCARPS imperfectly formed either in the presence or absence of a mycorrhizal host. Hyphae becoming aggregated into a pad of mycelium and a fertile poroid hymenophore produced. Stipe not formed. CULTURAL FEATURES: growth slow, colony floccose, fulvous*, reverse rusty tawny* to bay*, diffusible pigments lacking, septa simple. DISTINCTIVE FEATURES: See under *Arctostaphylos*.

Unknown ectendomycorrhizal fungus + *Pinus banksiana*. FORM: simple to dicotomous with long elements up to 7 mm long, occasionally with constricting rings. COLOUR: fuscous black* with the end portions concolouress or bay*, meristematic region whitish. MANTLE: glabrous, shiny, lacquered appearance, very few free hyphae. MYCELIAL STRANDS: absent. ANATOMY: Mantle essentially absent, net-like arrangement between tanninized outer vertical cells; when present, surface hyphae tightly appressed. Hartig net extending to the endodermis, first two layers of cortical cells filled with coiled hyphae. CULTURAL FEATURES: hyphae pallid becoming pale brown, unusually straight and rigid, septa simple, initially with infrequent branches. DISTINCTIVE FEATURES: This combination is most readily recognized by the ectendomycorrhizal status and the appearance of young colonies with stiff bristle-like hyphae. It is also unusual in that the fungus will not grow on benolate-amended media.

9.6.3 Synthesis of Bearberry Mycorrhizae

Although only a limited number of bearberry plants were established in flasks due to the very low germination rate of bearberry seeds, eight fungi were confirmed as potential mycorrhizal symbionts.

Some of the flasks became contaminated but the symbionts were all recovered on benolate-amended MMN agar at the termination of the incubation period. All of the fungi tested also formed ectomycorrhizae with jack pine under similar conditions. With bearberry the infections were all of the ectendomycorrhizal type with no fungal penetration beyond the first layer of cortical cells. Bearberry roots collected in the field had mycorrhizae identical to those formed by *Tricholoma flavovirens, Suillus tomentosus* and *Lactarius chelidonium* as well as *Cenococcum graniforme*. The morphology and colour of the bearberry mycorrhizae strongly resembled those formed by the same fungi with jack pine. The major difference was the tendency for mycorrhizal roots of bearberry to branch at nearly right angles producing a cross-like configuration with some symbionts. Brief descriptions of the ectendomycorrhizae formed with bearberry follows.

9.6.3.1 *Astraeus hygrometricus* + *Arctostaphylos uva-ursi* FORM: coralloid, branching dicotomously or not, if the latter, clusters irregular in appearance; elements robust, about three times the diameter of uninfected roots; clusters projecting up to 7 mm. COLOUR: pallid with a vinaceous* tint, this colour overlaying the compact cinnamon* to umber* mantle; often a sparce network of umber* hyphae interlaced over the dominant pallid hyphae. MYCELIAL STRANDS: abundant, well defined, originating from the mantle, vinaceous buff* to vinaceous*, up to 60-80 µm diameter. Outer layer of cells rounding up and walls thickened, individual cells up to 30 µ diameter. Hyphae 2-5 µm, clamped, walls hyaline to ochraceous becoming finely roughened and encrusted. ANATOMY: ectendomycorrhizal, first cortical layer filled

with hyphae; mantle 30-50 μ thick. CULTURAL FEATURES: Growth moderately rapid, floccose, snuff brown* to cigar brown*; reverse purplish chestnut* to nearly fuscous black* in the center, outer protion bag* to pale snuff brown*. Diffusible pigments abundant, ochraceous, forming distinct dark ring with age. DISTINCTIVE CHARACTERS: are the same as with jack pine.

9.6.3.2 *Coltrichia perennis* + *Arctostaphylos uva-ursi* FORM: simple becoming branched at right angles, occasionally subpinnate, elements moderately long; simple forms projecting 1-2 mm, these branched three times 2-3 mm. COLOUR: rusty tawny* becoming blackish. MANTLE: densely covered with brown mycelium which radiated out into the substrate, hyphae stiff and untangled. MYCELIAL STRANDS absent. ANATOMY: ectendomycorrhizal, Hartig net one cell deep, outer layer of cortical cells filled with hyphae, mantle well developed, 4-5 cells thick. BASIDIOCARP FORMATION: primordial pads of interwoven hyphae formed against the wall of the flasks, hymenophore are not developed. DISTINCTIVE FEATURES: were the brown to dark brown colour of the mycorrhizae, the abundant bristly mantle hyphae, hyphae with pigmented walls, the absence of clamps and formation of basidiocarp primordia.

9.6.3.3 *Lactarius chelidonium* + *Arctostaphylos uva-ursi* FORM: dicotomous becoming loosely clustered coralloid structures with long elements, branching irregular, occasionally subpinnate; projecting up to 8 mm elements, brittle and breaking cleanly. COLOUR: saffron*, pale fulvous* or snuff brown*, a few tips dark green*, most commonly snuff brown*. MANTLE: smooth, glabrous, transleucent and appearing as a halo in profile, occasionally appearing reticulate from the Hartig net. MYCELIAL STRANDS: rare, well developed, hyaline or dark green. ANATOMY: ectendomycorrhizal,

Hartig net extending one cell deep, outer layer of cortical cells packed with hyphae, mantle dense, 20-30 µm thick. Hyphae simple septate, smooth. DISTINCTIVE CHARACTERS: were the green colour (when present), glabrous and transleucent mantle and the long elements in a coralloid form.

9.6.3.4 *Rhizopogon rubescens* + *Arctostaphylos uva-ursi* FORM: simple becoming cross-like with right-angle branching, occasionally pinnate; total structure 1-2 mm long. COLOUR: white *in situ*, after washing ochraceous to fulvous*. MANTLE: floccose with hyaline mycelium reticulate or not. MYCELIAL STRANDS: occasional, well defined, abundant loose mycelium along entire length, frequently branched at narrow angles, white to vinaceous buff. Hyphae simple septate, 1.5-4 µm diameter, roughened or with abundant crystalline material. ANATOMY: ectendomycorrhizal, hyphae occupying the first layer of cortical cells; mantle 20-30 µm or very thick, 50-100 µm. CULTURAL FEATURES: Growth moderate, white floccose and developing buff to pale brown colours; reverse fluvous becoming rusty tawny to bay, straw near margin. Diffusible pigments abundant, pale luteus*.

9.6.3.5 *Tricholoma flavovirens* + *Arctostaphylos uva-ursi* FORM: simple or occasionally with an irregular branch, elements 2-3 mm long. COLOUR: tinted vinaceous* to vinaceous*, fulvous when old. MANTLE: densely surrounded by floccose mycelium, surface shiny from interwoven mycelium, air frequently trapped in the mantle. MYCELIAL STRANDS: absent. ANATOMY: ectendomycorrhizal, Hartig net extending one cell deep, outer layer of cortical cells filled with hyphae, mantle 20-30 µm thick. Hyphae simple septate 3-4 µm diameter. DISTINCTIVE CHARACTERS: were the vinaceous colour, abundant extramatrical mycelium and simple form.

9.6.3.6 *Suillus sibiricus* + *Arctostaphylos uva-ursi* FORM: simple becoming subpinnate with one or rarely two pairs of opposing tips, branch angle slightly less than 90°, elements moderately long, projecting up to 3 mm. COLOUR: saffron* becoming pale fulvous* or hazel*. MANTLE: finely floccose, unpolished, mycelium white, appearing reticulate or not. MYCELIAL STRANDS: abundant, very well defined and appearing almost root-like, branching frequently; 20-40 (60) µm diameter; hyaline to brick. Hyphal walls hyaline to pale ochraceous, abundant resin-like deposits on the walls resulting colours ranging from sienna* to rusty tawny* (500X). Hyphae 1.5-6µ diameter, septa simple. ANATOMY: ectendomycorrhizal, hyphae occupying the first layer of cortical cells, mantle 10-15 µ thick. CULTURAL FEATURES: Growth moderately fast, low floccose, outer portion white, center yellow brown with or without bay exudate; reverse rusty tawny* with straw* margin. Diffusible pigments sparce, pale luteus*.

9.6.4 Synthesis of Mycorrhizal with Jack Pine and Isolates from Surface Sterilized Mycorrhizal

Results of this experiment showed that surface sterilazation of mycorrhizae with H_2O_2 and plating on a benolate ammended medium was highly selective for mycorrhizal symbionts. Sixteen of the 18 randomly chosen isolates formed ectomycorrhizae with pine in the vermiculite-peat substrate. This indicates that a majority (89%) of the 82 species groups truely represented mycorrhizal fungi. Of the two that failed to infect the r ts one was very slow growing and one very rapid. Three of the random isolates could be matched with isolates from basidiocarps and formed mycorrhizae typical for the respective species. Five of the 18 species formed mycelial strands in the synthesis tubes thus not indicating a strong selective pressure for this morphological feature. Only

four of 16 mycorrhizal types were distinctive enough in morphology and colour to permit identification in the field. These included two unknowns, and *Astraeus hygrometricus* and *Rhizopogon rubescens*. Nine fungi formed what can be described as non-descript types, i.e. whitish and bruising reddish brown. This type was the most common one observed in the field and the synthesis results indicate that it was formed by a large number of fungi rather than by a dominant symbiont.

9.6.5 Growth of Mycorrhizal Fungi at Different Water Potentials

Each isolate tested on both osmotica was able to grow at higher water potentials on sucrose than on NaCl (Table 2). This suggests that NaCl is unsatisfactory for determining minimal values for growth but relative tolerance of the different fungi was much the same on the two media. Most species were capable of growth at -15 bars on NaCl and -24 bars on sucrose. *Pisolithus* and *Cenococcum* were the most tolerant to low water potentials as both could grow at -48 bars on sucrose but not at -78 bars. *Laccaria* was the most sensitive of those fungi tested failing to grow on -10 and -15 bars on NaCl and sucrose amended media respectively. *Scleroderma* and *Rhizoposom* w e both highly sensitive to NaCl but much less so to sucrose.

9.7 DISCUSSION

Despite the apparent simiplicity of the vascular flora at the Richardson Site, the mycorrhizal associations are complex and varied. From fruit body occurrence alone greater than 57 species of fungi were associated with jack pine within a limited area with relatively uniform soil conditions. The large variety of symbionts was further substantiated by direct observation of mycorrhizae and cultural studies. These techniques failed to indicate that any one or several species of fungi dominated the below ground symbiotic system. The fungal partner of only a minority of the mycorrhizae observed in the field could be identified. The inability to match cultures from the dominant sporocarps to isolates from mycorrhizae appears to be the usual situation in some forest systems (Lamb and Richards 1970; Riffle 1973; Zak and Bryan 1963). However, Harvey *et al.* (1976) have reported that one morphological type of mycorrhizae dominated a mature douglas fir-larch forest in Montana.

The only previous report of pure culture synthesis with jack pine was with *Thelephora terrestris* and *Pisolithus tinctorius* (Marx and Bryan 1970). Of the 14 species which formed mycorrhizae with pine in this study, only *Suillus tomentosus, Astraeus hygrometricus, Lactarius chelidonium, Tricholoma flavovirens, Cenococcum graniforme* and *Pisolithus tinctorius* produced structures distinctive enough to be recognized in the field. Synthesis tests with the unknown isolates showed that a variety of fungi produced the common non-descript type that dominated field samples. Therefore, direct observations of root systems may allow quantification of certain species but other techniques are necessary to identify and quantify species which produce mundane

mycorrhizae. It should be noted that in culture several basidiocarp isolates of *Suillus tomentosus* differed from the description given by Pantidou and Graves (1966). Clamps were very rare under all circumstances and occurred only on large diameter hyphae (5-6 μm).

It has been suggested that the hydnums were very likely mycorrhizal associates of conifers but confirmation has been lacking due to their stringent growth requirements. *Bankera fuligineo-alba* in this study is the first confirmation of a hydraceous fungus as a mycorrhizal symbiont.

From the occurrence of fruit bodies, it would appear the hydnums become important only in mature forests and in localized areas. *Hydnellum peckii* frequently was observed forming fairy rings indicating a slow, progressive growth from a inoculum point. Hintikka and Naykki (1967) estimated that *Hydnellum ferrugineum* grew about 3 cm per year and was never found in disturbed areas or young stands, the same pattern that was observed at the Richardson site. Thus the hydnums occupy small islands of the forest root system in mature stands apparently limited to these sites by an extremely slow growth rate.

Mycorrhizal synthesis by *Coltrichia perennis* with jack pine also represents the first confirmation of a mycorrhizal role of the terrestrial, stipitate polypores. In contrast to the hydnums, *Coltrichia* was typically found on bare disturbed soils. In that the mycorrhizae produced by *Coltrichia* are distinctive in appearance, they must be relatively rare or localized in occurrence as they were not observed on natural root systems. The ability of this fungus to produce a fertile hymenophore both in the absence and presence of a suitable host is very unusual for a mycorrhizal fungus. Additional field observations should be made in the vicinity of basidiocarps to confirm its ability to form mycorrhizae in natural systems.

The only previous report of the synthesis of ectendomycorrhizae with bearberry is that of Zak (1976b). As in Zak's study the synthesis results found here strongly suggest that certain conifers and bearberry share many or most of the same symbionts. In other species of *Arctostaphylos* Thiers (1975) has found several boletes that are apparently restricted to the ericaceous host. The close association of bearberry and jack pine at the Richardson site did not allow one to determine from sporocarp distribution the bearberry associates in the field. Mycorrhizae collected at the site were identical to those formed aseptically by *Tricholoma flavovirens, Suillus tomentosus* and *Lactarius chelidonium*. Isolates from these mycorrhizae which were surface sterilized in H_2O_2 closely matched isolates from sporocarps. Additional isolates from other bearberry mycorrhizae could not be matched with sporocarp cultures.

All of the synthesized bearberry mycorrhizae were of the arbutoid type with the first tier of cortical cells filled with hyphae. All of the mycorrhizae synthesized by Zak (1976b) were also of this ectendo-type. In contrast field samples were both of the ecto- and ectendo-types. The factors determining the anatomical type and their significance are far from clear at this point. Of four plants sampled in the fall, two were ectomycorrhizal and two dominantly but not exclusively ectendomycorrhizal. Mycorrhizae formed by *Cenococcom graiforme* and *Tricholoma tovovirens* on different plants were ecto-on one, ectendo-on the other. Seven plants were sampled the following spring and of 36 mycorrhizae sectioned only three were of the ecto-type. The following fall 40 root samples of 20 plants were collected from mature stands and the burned area and 150 roots sectioned. All of the infections

were of the ectendomycorrhizal type. Mejstrick and Hadac (1975) reported that the ecto-type of infection was much more common than the ectendo-type in an isolated patch of bearberry in Czechoslovakia. From the observations in this study the causes of the two anatomical types does not appear to be due to differences in symbionts but perhaps rather to season and physiological state of the host.

It has been suggested that mycorrhizae may aid the host plant in water uptake and thus increase drought resistence (Trappe 1977). However, experimental evidence on ectomycorrhizae is completely lacking and little is known of the ability of mycorrhizal fungi to grow at low water potentials. Mycorrhizae could function to increase drought tolerance in ways other than simply increasing the range of water potentials in which water can be taken up by the plant. Mycorrhizae, particularly those with well developed rhizomorphs, may function as pipelines to increase the volume of soil being exploited and move water from a as of high water potential to the roots where the water potential is low. Mycorrhizae are known to increase the longivity of feeder roots (Harley 1969), and they may also aid in survival during short periods of stress such as drought. Roots infected with the appropriate symbionts would then be able to respond to favourable moisture conditions once the droughty period had passed. These and other potential functions of the ectomycorrhizal remain to be evaluated.

In this study maximum linear growth occurred at the highest water potentials used with both NaCl and sucrose. In contrast Mexal and Reid (1973) found maximum growth of *Cenococcum* in liquid cultures to occur at -15 bars. Uhlig (1972), who also used liquid cultures,

found that five of the six mycorrhizal fungi he tested including *Tricholoma pessondatum*, grew best between -34 and -58 atm. Working with the root pathogen *Phytophthora cinnamomi* Sterne *et al.* (1976) found that the method of culture affected responses to osmotic potential. However, in their work *Phytophthora* was more tolerant to low water potentials on solid media than in liquid culture. Griffin (1972) concluded that linear extension was a satisfactory method to use in studies of water potential. Differences in the osmoticum used and cultural methods make comparisons between studies difficult. However, the data given here illustrates that some fungi e.g. *Cenococcum*, are much more tolerant to low water potentials than other fungi such as *Laccaria*. It may be common in forest nurseries (Sinclair, 1974; Trappe & Strand 19 9) and further investigations should be made to determine if *Laccaria* infested seedlings are more adversely affected by drought than seedlings invected with other mycorrhizal fungi.

Experiments on the water relations of the mycorrhizal fungi were of a preliminary nature only. Behaviour in culture where the transition from a high ψ to a low ψ is abrupt unlike the gradual transition in nature when the fungus is in a symbiotic situation may lead to erroneous conclusions. The question whether a good performer in pure culture behaves in a similar manner when mycorrhized remains to be tested.

9.8 CONCLUSIONS

"See previous report".

9.9 FUTURE RESEARCH

"See previous report".

9.10 ACKNOWLEDGEMENTS

"See previous report", and we express our appreciation to A.H. Smith for identifying some of the *Lactarius* species and to H.D. Thiers for help with the boletes.

9.11 REFERENCES CITED

Griffin, D.M. 1969. Soil water in the ecology of fungi. Ann. Rev. Phytopath. 7: 289-342.

Griffin, D.M. 1972. Ecology of soil fungi. Syracuse Univ. Pr.

Harley, J.L. 1969. The Biology of Mycorrhizae. Leonard Hill, London.

Harvey, A.E., M.J. Larsen & M.F. Jurgensen. 1976. Distribution of ectomycorrhizae in a mature Douglas fir/larch forest soil in Western Montana. For. Sci. 22: 393-398.

Henderson, D.M., P.D. Orton & R. Watling. 1969. British fungus flora-Agarics & Boleti: Introduction. Royal Botan. Gar., Edinburgh.

Hintikka, V. & O. Naykki. 1967. Notes on the effects of the fungus *Hydnellum* ferrigineum (Fr.) Karst. on forest soil and vegetation. Comm. Inst. For. Fen. 62(2): 1-22.

Kozlowski, T.T. 1968. Water deficits and Plant Growth. Academic Press.

Lamb, R.J. & B.N. Richards. 1970. Some mycorrhizal fungi of *Pinus radiata* and *P. elliottii* var. *elliottii* in Australia. Trans. Brit. Mycol. Soc. 54: 371-378.

Marx, D.H. & W.C. Bryan. 1970. Pure culture synthesis of ectomycorrhizae by *Thelephora terrestris* and *Pisolithus tinctorius* on different conifer hosts. Can. J. Bot. 48: 639-643.

Mejstrick, V.K. & E. Hadac. 1975. Mycorrhiza of *Arctostaphylos*. Pedobiologia 15: 336-342.

Mexal, J. and C.P.P. Reid. 1973. The growth of selected mycorrhizal fungi in response to induced water stress. Can. J. Bot. 51: 1579-1588.

Pantidou, Maria E. and J.W. Groves. 1966. Cultural studies of boletaceae. Some species of *Suillus* and *Fuscoboletinus*. Can. J. Bot. 44: 1371-1392.

Riffle, J.W. 1973. Pure culture synthesis of ectomycorrhizal on *Pinus ponderosa* with species of *Amanita, Suillus* and *Lactarius*. For. Sci. 19: 242-250.

Robinson, R.A. and R.H. Stokes. 1955. Electrolyte solutions. Academic Press, NY.

Sinclair, W.A. 1974. Development of ectomycorrhizae in a Douglas fir nursery: I. Seasonal characteristics. For. Sci. 20: 51-56.

Sterne, R.E., G.A. Zentmyer and F.T. Bingham. 1976. The effect of osmotic potential and specific ions on growth of *Phytophthora cinnamomi*. Phytopathology 66: 1398-1402.

Thiers, H.D. 1975. California Mushrooms: A field guide to Boletes. Hafner Press, NY.

Trappe, J.M. 1977. Selection of fungi for ectomycorrhizal inoculation in nurseries. Ann. Rev. Phytopathol. 15: 203-222.

Uhlig, S.K. 1972. Investigations on drought resistance of mycorrhiza forming fungi. Zentralbl. Bakt. Parwitenk. Infekt. Hyg. Abt. 2, 127: 124-132.

Zak, B. 1976a. Pure culture synthesis of pacific madrone ect-endomycorrhizae. Mycologia 68: 36a-369.

Zak, B. 1976b. Pure culture synthesis of bearberry mycorrhizae. Can. J. Bot. 54: 1297-1305.

Zak, B. and W.C. Bryan. 1963. Isolation of fungal symbionts from pine mycorrhizae. For. Sci. 9: 270-278.

Table 2. Growth of mycorrhizal fungi at different osmotic levels adjusted with either NaCl or Sucrose.

ecies and Culture number	Ψ -bars	Osmoticum					
		NaCl			Sucrose		
		10 da	20 da	30 da	10 da	20 da	30 da
		Radial Growth (mm) ± S.E.					
solithus	1.6	28.1 ± 2.2	55.5 ± 1.8	67.8 ± 1.4	23.9 ± .5	39.1 ± .2	--
tinctorius	6.1	16.7 ± 1.6	47.0 ± 2.8	66.8 ± 1.4	15.0 ± .58	39.5 ± 0	--
	10.6	15.0 ± 1.9	44.0 ± 2.7	62.5 ± 1.3	--	--	--
	15.0	12.2 ± .8	35.5 ± 1.4	53.8 ± 1.4	9.7 ± 1.2	23.3 ± 2.5	--
	24.4	0	0	0	3.2 ± .2	9.6 ± 1.7	--
	48.0				.5 ± 0	1.6 ± .1	--
ococcum	1.6	.5	7.5	11.6	.5 ± 0	3.1 ± .8	5. ± (
graniforme	6.1	.5	6.2	10.2	1.6 ± .36	5.6 ± .5	11.5 ±
26	10.6	.5	1.5	8.5	--	--	--
	15.0	Tr	1.0	5.9	1.3 ± .4	5.3 ± .4	10.2 ±
	24.4	0	0	0	.6 ± .2	3.2 ± .7	8.2 ±
	48.0				.3 ± .2	.5 ± .2	1.0 ± (
illus	1.6	11.0 ± .4	24.6 ± .5	41.7 ± 1.4	3.7 ± .1	9.5 ± 0	15.7 ±
tomentosus	6.1	9.3 ± .5	20.0 ± .5	31.8 ± .7	4.3 ± .5	10.1 ± 1.4	16.5 ±
715	10.6	4.3 ± .5	15.0 ± .9	24.8 ± 1.1	--	--	--
	15.0	0	.8 ± .4	10.5 ± 1.1	3.2 ± .2	8.1 ± .4	15.2 ±
	24.4	0	0	0	1.0 ± .3	3.6 ± .5	6.6 ±
	48.0				0	0	0

Continued

Species culture number	Ψ -bars	Osmoticum					
		NaCl			Sucrose		
		10 da	20 da	30 da	10 da	20 da	30 da
		Radial Growth (mm) ± S.E.					
S illus	1.6	10.0 ± 1.2	25.8 ± 1.9	43.5 ± .3	--	--	--
sibericus	6.1	4.0 ± .4	18.7 ± 1.6	33.2 ± 2.2	--	--	--
2467	10.6	2.8 ± .2	14.3 ± .7	24.8 ± .8	--	--	--
	15.0	0	7.7 ± .7	18.3 ± 1.6	--	--	--
	24.4	0	0	0	--	--	--
	48.8				--	--	--
I ccaria	1.6	23.0 ± 2.1	55.7 ± 1.5	72.0 ± 2.1	10.3 ± 1.2	30.8 ± .9	--
laccata	6.1	Tr	23.5 ± 3.6	28.7 ± 6.2	5.8 ± 1.3	19.6 ± 3.3	--
2456	10.6	0	0	0	--	--	--
	15.0	0	0	0	0	0	
	24.4	0	0	0			
	48.0						
A traeus	1.6	12.9 ± .3	28.6 ± .8	38.8 ± 1.2	3.3 ± .2	13.0 ± .4	24
hygro-	6.1	8.6 ± .4	20.3 ± .8	34.0 ± .9	2.9 ± .2	10.7 ± .7	23.3 ±
m tricus	10.6	Tr ±	13.7 ± .8	24.1 ± .6	--	--	--
2168	15.0	0	6.0 ± .4	9.6 ± .4	2.3 ± .1	5.1 ± .4	7.7
	24.4	0	0	0	Tr	1.6 ±± .2	3.7
	48.0				0	0	0

C- tinued

S ies cu ture n ber	Ψ -bars	Osmoticum					
		NaCl			Sucrose		
		10 da	20da	30 da	10 da	20 da	30 da
		Radial Growth (mm) ± S.E.					
Tricholoma	1.6	14.2 ± .2	28.2 ± .9	34.8 ± .7	1.7 ± .1	3.7	.5 ± 4.7 ±
p sundatum	6.1	8.6 ± .3	20.1 ± .3	24.7 ± .4	1.0 ± .1	2.2	.2 ± 3.2 ± 0
2476	10.6	0	15.3 ± .3	15.0 ± .3	--	--	--
	15.0		.5	4.7 ± 1.2	.6 ± .1	2	6 ± 2.(
	24.4	0	0	0	Tr	1.4	.2 ± 2.7 ± .:
	48.0				0	0	0
Tricholoma	1.6	.2	8.8	11.8	--	--	--
vavirens	6.1	Tr	5.7	7.5	--	--	--
2458	10.6	Tr	5.7	8.7	--	--	--
	15.0	0	0	0	--	--	--
	24.4	0	0	0	--	--	--
	48.0						
Tricholoma	1.6	6.2	11.7	21.4	--	--	--
leri	6.1	.5	11.4	20.7	--	--	--
2491	10.6	0	8.2	15.0	--	--	--
	15.0	0	.5	4.7	--	--	--
	24.4	0	0	0	--	--	--
	48.0						

inued

es ulture um er	Ψ -bars	Osmoticum							
		1 da	20 da	30 da	10 da		20 da		30 da	
		Radial Growth (mm)			S.E.					
cleroderma	1.6	6.9	16.7	29.0	2.0	.4	4.0	.4	9.4	.1
ac orhizan	6.1	0	0	0	1.1	.4	1.9	.7	5.1	.
782	10.6	0	0	0	--		--		--	
	15.0	0	0	0	.4	.1	1.8	.4	2.5	
	24.4	0	0	0	.3	.2	.5	0	--	
	48.0				0		0		0	
actarius	1.6	8.4	17.2	24.2	--		--		--	
h lidonium	6.1	6.3	12.1	16.2	--		--		--	
2454	10.6	4.6	9.2	10.9	--		--		--	
	15.0	Tr	Tr	Tr	--		--		--	
	24.4	0	0	0	--		--		--	
	48.0									
hizopogon	1.6	11.5	39.3	46.0	Tr		10.3	1.8	18.2	2.
escens	6.1	0	0	2.2	Tr		14.3	1.2	25.8	
	10.6	0	0	0	--		--		--	
	15.0	0	0	0	Tr		9.0	.4	22.0	2
	24.4	0	0	0	0		1.1	.6	7.1	2.
	48.0						0		0	

Continued

Species culture number	Ψ -bars	Osmoticum					
		NaCl			Sucrose		
		10 da	20 da	30 da	10 da	20 da	30 da
		Radial Growth (mm) ± S.E.					
Unknown	1.6	9.5	16.0	17.8	--	--	--
L-89	6.1	9.0	15.5	17.1	--	--	--
	10.6	3.1	12.8	15.8	--	--	--
	15.0	0	0	0	--	--	--
	24.4	0	0	0	--	--	--
	48.0				--	--	--
Hebeloma	1.6	--	--	--	1.5	6.1 ± .1	11.9 ± .
s	6.1	--	--	--	2.0	3.6 ± .2	10.2 ± 1.
587	10.6	--	--	--	--	--	--
	15.0	--	--	--	.1	1.3 ± .5	4.5 ± .
	24.4	--	--	--	0	0	0
	48.0						
Coltrichia	1.6	--	--	--	3.0 ± .5	6.1 ± 1.0	11.2 ± .
p mnis	6.1	--	--	--	2.8 ± .5	6.7 ± .4	11.2 ± .
443	10.6	--	--	--	--	--	--
	15.0	--	--	--	2.0 ± .5	5.3 ± .5	9.0 ± .
	24.4	--	--	--	.4 ± .1	3.7 ± .3	6.0 ± .
	48.0	--	--	--	0	0	0

Prof. Dr. Hans ADAM, Zoologisches Institut der Universitaet, Akademiestrasse 26, A-5020 Salzburg (Austria)

Administrative Bibliothek des Bundeskanzleramtes, Ballhausplatz, A-101 Wien

10. ENERGY AND WATER BALANCE MODEL

A. Mehlenbacher and D. W. A. Whitfield
Department of Botany
University of Alberta

"See previous report"

11. RADIATION MODEL AND MEASUREMENTS

D. W. A. Whitfield, C. Labine and A. L. Mehlenbacher
Department of Botany
University of Alberta

11.1 INTRODUCTION

This report describes a mathematical model of radiation exchange in the Jack pine-lichen woodland studied by VE 6.1, and a series of measurements taken to compare with the theory.

A central aim of VE 6.1 was to develop mathematical models of energy and water exchange of a forested hillside, and to use these models to understand the ability of the trees to survive under drought stress on an unfavorable southwest-facing site. The interactions of both solar and terrestrial radiation with the vegetation is an important part of energy exchange, and a model of these processes was a prerequisite for the larger model.

The natures of both the site and vegetation type introduce complexities into the model. The site is a steep hillside, while most detailed radiation models have been applied to flat sites; the leaves are doubly clumped into tufts on branch ends and into discrete trees, often well separated from their neighbours. Thus the situation is greatly different from the ideal simple case of a horizontally random distribution of intercepting surfaces. The model is based on an innovative technique in which a Monte-Carlo simulation is used to calculate

the interceptions of light rays with idealized tree outlines, following which the usual theory of interception by randomly located elements is applied along the ray paths within trees.

The output of this model is compared with a series of measurements of radiation profiles, made on the hillside site.

This report is meant to entirely replace the previous one (Mehlenbacher and Whitfield 1977). Its main body describes the model rather sketchily, with many details relegated to appendices. This is done in an attempt not to overwhelm the reader with mathematics.

SI units are used throughout this report, except where indicated.

11.2 PREVIOUS WORK

When the radiation intercepting elements (leaves, branches) are randomly distributed horizontally, a ray has a probability of penetrating to some depth without interception given by

$$P = e^{-F_c} \qquad [1]$$

where F_c is the silhouette leaf and branch area per unit soil area in the layer above the level of interest. This result has been long known; the theory is reviewed by Norman (1975).

When Eqn. 1 is applied to the direct solar beam, P gives the fraction of horizontal area, at the level of interest, which is illuminated by the sun. When sky, or diffuse radiation is being considered, Eqn. 1 is used to compute radiation penetration separately from different directions, and the result is appropriately averaged to yield overall diffuse penetration.

The computation of F_c is often complex, depending on element area, number, shape and orientation, and direction of the ray.

Unfortunately, vegetation is rarely so ideally distributed that Eqn. 1 can be used simply. Considerable literature is devoted to various methods of accounting for non-randomness of location, which may take the form of either clumping or uniform dispersal. Nilson (1971) pointed out that Eqn. 1 is the zero term in the Poisson distribution, and extended the scope of radiation models to include positive and negative binomial distributions. These distributions are empirical in that they contain an arbitrary

parameter which must be adjusted to make the distribution fit the data.

For a sitka spruce plantation, Norman and Jarvis (1975) considered the clumping of needles into shoots and shoots into whorls using the Poisson distribution. Brown and Pandolfo (1969) analytically computed interception by identical cylindrical shapes that are regularly arranged on a flat surface.

Tanaka (1968) used a Monte-Carlo computer technique to compute interception by a tobacco plant community and Oikawa and Saeki (1972) used this technique to explore penetration in square-planted communities. This and other techniques for handling non-random distributions is reviewed by Monsi, Uchijima and Oikawa (1973).

Once Eqn. 1, or some other approach, has been used to calculate solar beam and diffuse penetrations (and thus, interceptions), there remains the problem of the scattering of intercepted radiation. This very difficult problem has been approached in many ways, reviewed briefly by Norman (1975).

11.3 MODEL STRUCTURE

We set out to compute the fate of the direct solar beam and diffuse radiation, both interception and scattering, for visible and near infrared wavelengths, in a jackpine forest on a hillside.

The situation is idealized as follows:

(a) the hillside is a flat plane, of slope α_s from the horizontal and azimuth ω_s (azimuthal direction from true north of a normal to the slope). Figure 1 illustrates this geometry.

(b) the trees are randomly located with their trunks vertical and thus at an angle α_s to a normal to the slopes.

(c) tree heights are random, with the empirical distribution shown in Figure 2.

(d) each tree is in the shape of a cylinder capped with a cone. The cylinder radius is linearly related to tree height. Several cone apex half-angles (α_t) are considered.

(e) all vegetational elements (needled branches, bare live branches, dead branches and cones) are randomly distributed within the above tree shape, with a uniform distribution horizontally, and the empirical vertical distributions shown in Figure 2.

Appendix A describes our determination of stand and tree geometry parameters, and the coordinate system used in the model,

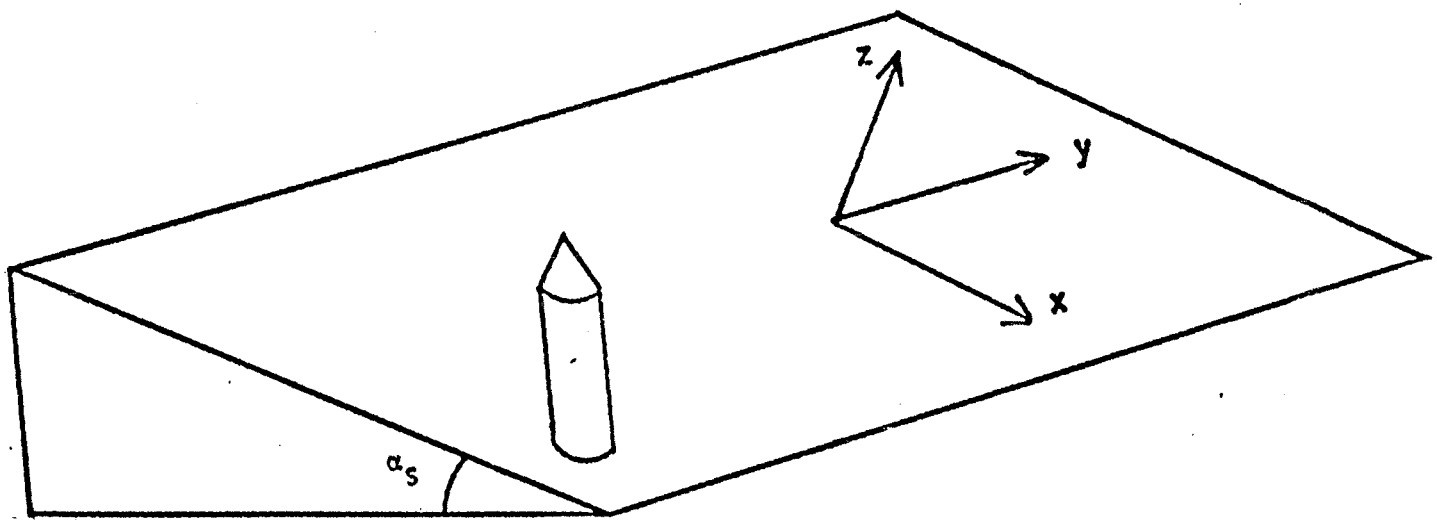

Figure 1. The idealized hillside used in the model, showing the hillside co-ordinate system, hill slope, and an idealized tree outline.

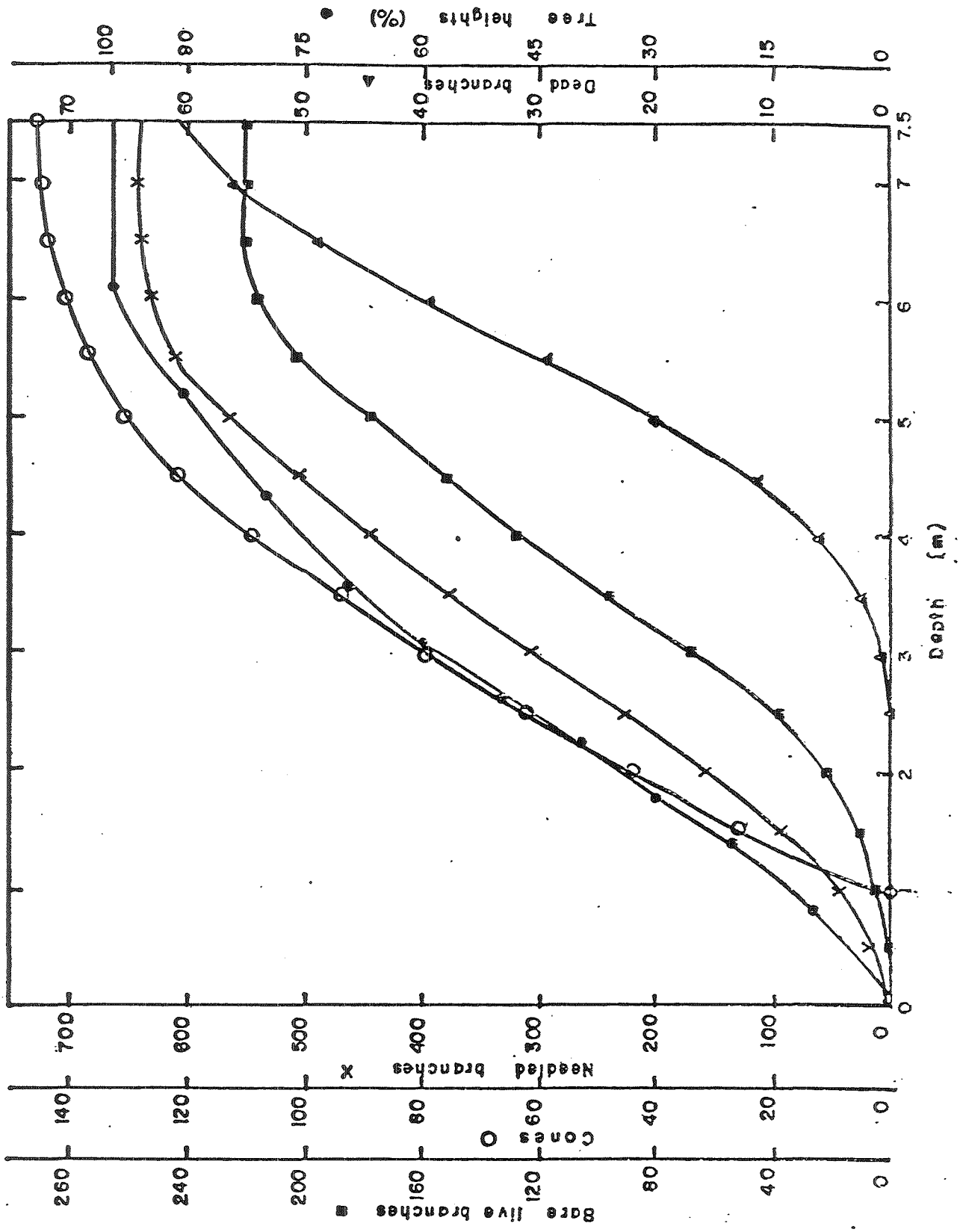

Figure 2. Distributions of elements with depth in the canopy, accumulated from the top down, expressed as average numbers per tree.

called the hillside system, is described in Appendix B.

The only symmetry in the problem is a reflection in a plane perpendicular to the hillside, aligned up and down the slope. Thus, we consider azimuthal angles $o \leq \phi \leq \pi$, and zenith angles $o \leq \eta \leq \pi/2$.

11.3.1 Interception Probabilities

First, a "numerical forest" was generated. Over a surface area of 30 m (across the slope) by 33 m (up and down slope), 650 trees were located by calls to a random number generator. Their heights were determined by other calls to the generator, with height distribution adjusted to fit that of Figure 2.

Next, the paths of a large number of light rays through the forest were considered, and the lengths of these rays passing through tree outlines were calculated and given the symbol $L_i^j(\eta, \phi)$, where i is the height slice (i = 1 to 15, numbered from the top down), j is the ray number, and η and ϕ designate the direction of ray origin. The origin points of the rays were chosen randomly over a 10 x 10 m area at 7.5 m from the ground at the "up-ray" corner of the forest. We used 500 rays per η, ϕ pair. Appendix C contains details of the pathlength calculations.

The maximum pathlength of a ray through a 0.5 m vertical distance is 0.5/cos z m. Where two trees overlap, some L_i^j's could exceed this value, but we imposed it as an upper limit, to account for the expected thinning in the region of the overlap.

Once the values of $L_i^j(\eta, \phi)$ were calculated, noninterception probabilities for the elements followed:

$$P_i^k(\eta, \phi) = \frac{1}{N_j} \sum_{j=1}^{N_j} e^{-\rho_i^k \bar{A}^k(\eta, \phi) L_i^j(\eta, \phi)} \qquad [2]$$

where the superscript k refers to element type, N_j is the number of rays considered, i and j are used as defined above, ρ is volume

density within the tree outline and $\bar{A}$ (n, ϕ) the average projected area of an element viewed from n, ϕ. Eqn. 2 is just an elaboration of Eqn. 1.

The projected areas are determined from the assumption that the elements are all cylindrical in shape (for needled branches the cylinder encloses the needles to their tips). Appendix D gives the details. In the case of cones, which are idealized as spheres, the projected area is simply 6.79×10^{-4} m^2 from any direction.

Tree trunk interception was handled differently: they were idealized as vertical cones, with the height distribution indicated in Figure 2, and a fixed apex angle (β_t) determined from field data. Then

$$P_i^t(z) = e^{-(\rho^t \sum_{j=1}^{i} g_j^i A_j^i (n)/\cos n)} \qquad [3]$$

where ρ^t is the stand density ($0.66\ m^{-2}$), g_j is the proportion of trunks reaching above level i and $A_j^i(n)$ is the area, projected from zenith angle n, of trunks in the height classes j projected onto level i. Pathlength from canopy top to level i is $1/\cos n$. In this formulation, the trunks are assumed to be perpendicular to the slope, so that viewing azimuth is irrelevant. This is a crude approximation, but is justified because trunks contribute in only a minor way to total interception.

The above calculations yield the probabilities that a ray from direction n, ϕ will not be intercepted by a given element type to the bottom of level i. The overall probability of non-

interception is given by

$$\hat{P}_i(\eta, \phi) = P_i^n(\eta, \phi)\ P_i^c(\eta, \phi)\ P_i^b(\eta, \phi)\ P_i^d(\eta, \phi)\ P_i^t(\eta) \quad [4]$$

where the superscripts n, c, b, d, and t refer to needled branches, cones, bare live branches, dead branches and trunks, respectively.

From $\hat{P}_i(\eta, \phi)$ we proceeded to determine the penetration of diffuse or sky radiation. This requires averaging, with appropriate weighting, over the hemisphere:

$$\bar{P}_i = \frac{\int_0^{\pi/2} d\eta \int_0^{\pi} d\phi\ r(\eta, \phi)\ \hat{P}_i(\eta, \phi) \sin\eta \cos\eta}{\int_0^{\pi/2} d\eta \int_0^{\pi} d\phi\ r(\eta, \phi) \sin\eta \cos\eta} \quad [5]$$

where $r(\eta, \phi)$ is the relative brightness of the sky in the direction η, ϕ. In our case, we took $r = 1$ in calculating $\bar{P}$. This assumes that the sky is uniformly bright. See Appendix E for details of the numerical procedure used to evaluate Eqn. 5. What turns out to be a small correction to $\bar{P}$ is produced by setting $r = 1$ for the part of the hemisphere occupied by sky and $r = 0$ for that occupied by the flatland forest below the hill. The result is called $\tilde{P}_i$.

11.3.2. Scattering

The previous section explains our calculations of penetration of direct sunlight and diffuse sky light into the forest. Now we consider the fate of this radiation once it is intercepted by vegetational elements. In this treatment we follow Norman and Jarvis (1975) with a few notational changes. Figure 3 illustrates the terms used. E_m and E'_m are the diffuse fluxes above the layer m, F_m and F'_m are the contributions to diffuse flux arising within layer m due to scattering of the intercepted direct solar beam, B_m. Then

$$E_j = \tau_i E_i + \rho_i E'_j + F_i \qquad [6]$$

and

$$E'_i = \tau_i E'_j + \rho_i E_i + F'_i \qquad [7]$$

where τ_i and ρ_i are the transmissivity and reflectivity, respectively, of the layer i, assumed to be the same from below as above. This pair of equations may be written out for each of the 15 vegetational layers. At the ground surface

$$E'_{16} = \rho_g E_{16} \qquad [8]$$

At this point, the problem is conveniently divided into two parts: the scattering of radiation arriving at the canopy top as diffuse sky radiation, and the scattering of intercepted solar beam. In the former case we set $E_1 = 1$, $F_i = 0$, $F'_i = 0$ for all i, and arrive at 31 equations in 31 unknowns (E'_1, E_2, E'_2, ... E_{15}, E'_{15}, E_{16}, E'_{16}), which can be solved by standard methods for linear systems, or the fast algorithm described by Norman and Jarvis (1975). The second

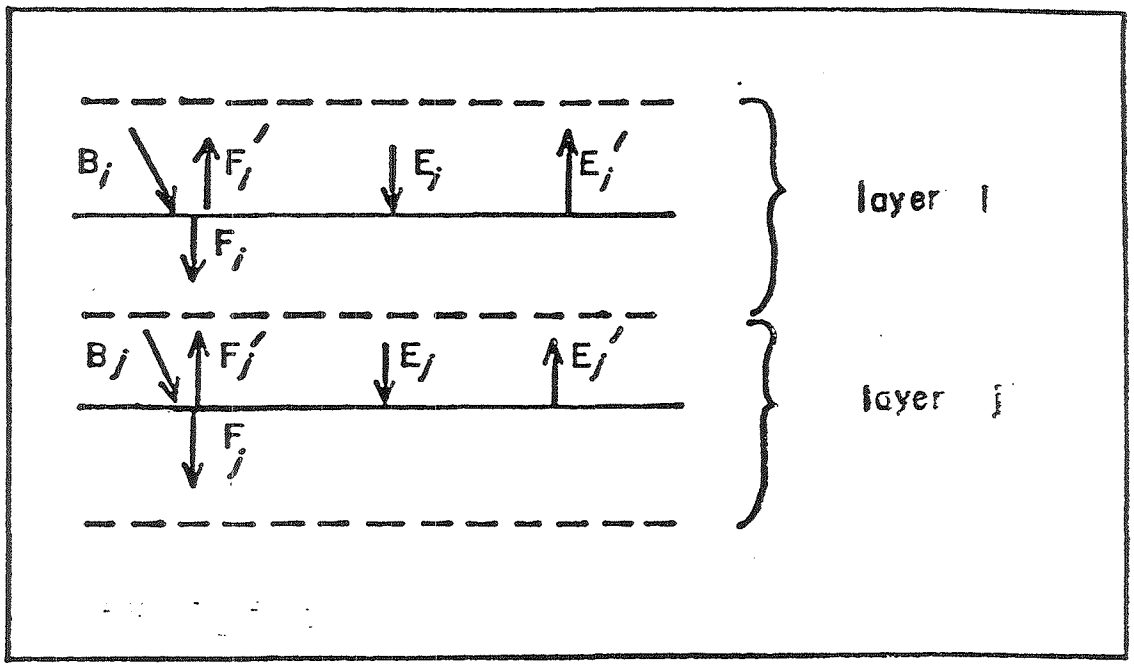

Figure 3. The symbols used in scattering calculations. The downward (E) and upward (E') diffuse fluxes apply to layer tops, while upward (F') and downward (F) scattering due to solar beam (B) interception are considered as originating in the layers.

case, scattered solar beam, is not so simple; first, F_i and F_i' must be determined (as described below), and although setting $E_1 = 0$ again yields 31 equations in 31 unknowns, the fast algorithm is unstable and a standard Gaussian elimination procedure must be used.

We thus have reduced the computation of scattering to the determination of layer coefficients for transmission and reflection, and to evaluation of beam scattering contributions. Note that in what follows we assume all diffuse radiation is isotropic, and do not follow Norman and Jarvis (1975) in their accounting for its angular distribution. This seems to be justified in our open canopy where the sky diffuse contribution dominates scattered.

The diffuse penetration to the bottom of layer i is $\bar{P}_i$. Then the open space transmissivity of layer i is

$$\tau_i^o = \frac{\bar{P}_{i+1}}{\bar{P}_i} \qquad [9]$$

To this must be added the effect of diffuse radiation which is intercepted and reflected or transmitted down. The scattering of diffuse radiation is treated by Norman and Jarvis (1975) in their Appendix A. They show that if scattering elements are oriented randomly and all surfaces of a given element type have the same properties, 1/4 of reflected radiation is forward scattered and 3/4 back scattered. Of that transmitted, 3/4 is forward and 1/4 backward. Thus

$$\tau_i = \frac{\bar{P}_{i+1}}{\bar{P}_i} + \frac{1}{4}\left[\rho^t \tilde{I}_i^t + \rho^c \tilde{I}_i^c + \rho^b \tilde{I}_i^b + \rho^d \tilde{I}_i^d + \rho^n \tilde{I}_i^n\right] + \frac{3}{4}\tau^n \tilde{I}_i^n \qquad [10]$$

and

$$\rho_i = \frac{3}{4}\left[\rho^t \tilde{I}_i^t + \rho^c \tilde{I}_i^c + \rho^b \tilde{I}_i^b + \rho^d \tilde{I}_i^d + \rho^n \tilde{I}_i^n\right] + \frac{1}{4}\tau^n \tilde{I}_i^n \qquad [11]$$

where $\tilde{I}_i^k$ is the fraction of diffuse radiation incident on layer i which is intercepted by element type k, and ρ^k and τ^k are the reflectivity and transmissivity of element type k, respectively. Then if we designate by $I_i^k(\eta, \phi)$, the fraction of canopy top radiation from η, ϕ which is intercepted by element type k in layer i,

$$I_i^k(\eta, \phi) = \frac{(P_{i-1}^k(\eta, \phi) - P_i^k(\eta, \phi))\,(\hat{P}_{i-1}(\eta, \phi) - \hat{P}_i(\eta, \phi))}{\sum_{j=n,c,b,d,t}(P_{i-1}^j(\eta, \phi) - P_i^j(\eta, \phi))} \qquad [12]$$

For the top layer, i = 1, the P_o's and $\hat{P}_o^i$'s are unity. Then $I_i^k(\eta, \phi)/\hat{P}_{i-1}(\eta, \phi)$ is the fraction of radiation from η, ϕ, incident on the top of level i which is intercepted in level i by element type k, and

$$\tilde{I}_i^k = \frac{\int_o^{\pi} d\phi \int_o^{\pi/2} d\eta \; I_i^k(\eta, \phi)/\hat{P}_{i-1}(\eta, \phi) \sin\eta \cos\eta}{\int_o^{\pi} d\phi \int_o^{\pi/2} d\eta \; \sin\eta \cos\eta} \qquad [13]$$

The numerical procedure used in evaluating this expression was the same as that described for $\bar{P}$, described in Appendix E.

At this point, the τ_i's and ρ_i's may be evaluated and the scattering of incident diffuse radiation treated completely. To consider the scattering of intercepted solar beam, we must evaluate the F_i's and F_i''s. Again, we make use of Appendix A of

Norman and Jarvis (1975):

$$R_i = \rho^t \tilde{I}_i^t + \rho^c \tilde{I}_i^c + \rho^b \tilde{I}_i^b + \rho^d \tilde{I}_i^d + \rho^n \tilde{I}_i^n \quad [14]$$

$$F_i = (1 - f_w(n)) R_i + f_w(n) \tau^n \tilde{I}_i^n \quad [15]$$

$$F_i' = f_w(n) R_i + (1 - f_w(n)) \tau^n \tilde{I}_i^n \quad [16]$$

where $f_w(n)$ is tabulated by Norman and Jarvis for weighted average scattering. We reproduce this as Figure 4.

The above scattering calculations were done twice, for visible and near infrared wavelengths. Details will be found below. The output of these calculations is a series of tables of the scattered radiation above each level, including the ground surface, downward and upward, originating from direct solar beam and diffuse sources for visible and infrared wavelengths. The next section describes how these are combined to calculate downward flux from sun position and measured beam and diffuse fluxes. Output also includes tables of radiation absorbed, which will be used in energy balance calculations.

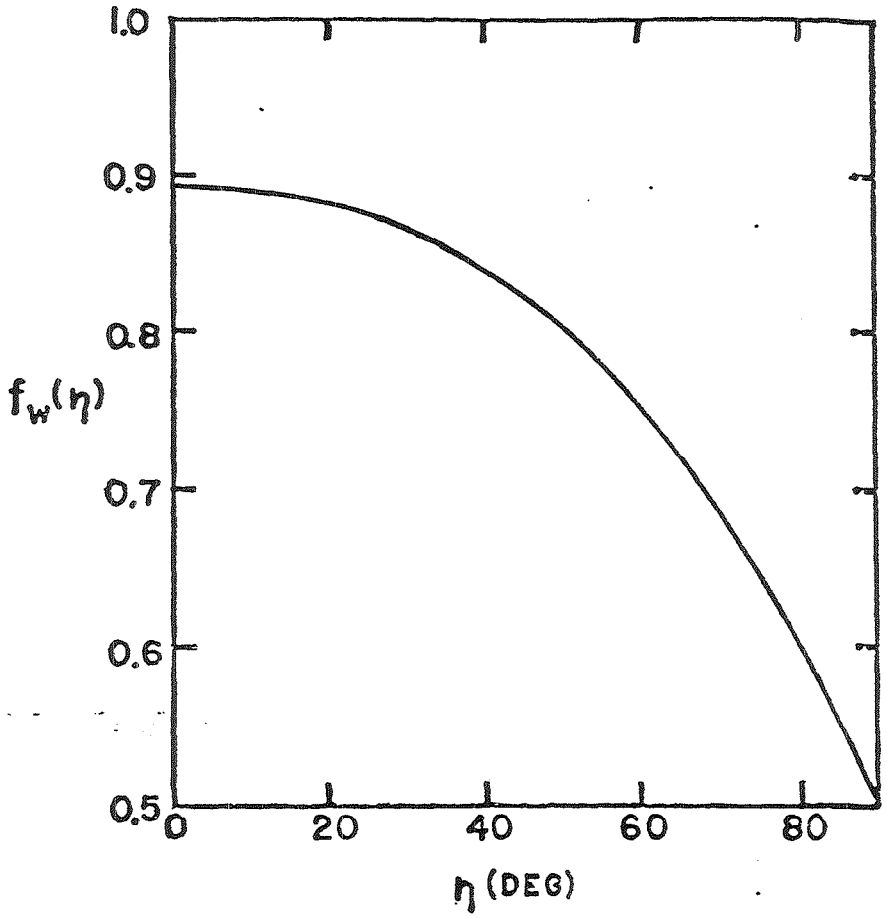

Figure 4. The average proportion of radiation which is scattered upward when intercepted by randomly oriented surfaces, as a function of incident zenith angle (Norman and Jarvis, 1975).

11.3.3 Calculation of Total Downward Fluxes

As will be described in the next section, the measurements with which the results of this model will be compared consist of downward visible and near infrared fluxes, measured by horizontally mounted, cosine corrected sensors, averaged along horizontal transects at several levels in the forest canopy.

The first step in this calculation is partition of incoming radiation into four components by two ways of division: direct vs. diffuse, visible vs. near infrared. The measured quantities were total all-wave, diffuse all-wave and total infrared. Then the diffuse all-wave (S_d) may be divided between visible and infrared components.

$$S_d^v = 0.7\ S_d \qquad [17]$$

$$S_d^r = 0.3\ S_d \qquad [18]$$

which follows Ross (1975). The beam components then follow directly from the above and the measured total all-wave (S_t) and total infrared (S_t^r)

$$S_b^r = S_t^r - S_d^r \qquad [19]$$

$$S_b^v = S_t - S_d - S_b^r \qquad [20]$$

Then, given the sun position, η, ϕ, we can write down the desired downward fluxes at the bottom of canopy level i as fractions of their values at the canopy top (V_i for visible, R_i for infrared):

$$V_i = \{\varepsilon [S_b^v (E_i^{bv} (n, \phi) + \hat{P}_i (n, \phi) + S_d^v E_i^{dv} (n, \phi)] + (1 - \varepsilon) [S_b^v E_i^{'bv} (n, \phi) + S_d^v E_i^{'dv} (n, \phi)]\}/(S_b^v + S_d^v) \quad [21]$$

and

$$R_i = \{\varepsilon [S_b^r (E_i^{br} (n, \phi) + \hat{P}_i (n, \phi) + S_d^r E_i^{dr} (n, \phi) + (1 - \varepsilon) [S_b^r E_i^{'br} (n, \phi) + S_d^r E_i^{'dr} (n, \phi)]\}/(S_b^r + S_d^r) \quad [22]$$

where ε is the weighted proportion of the horizontal sensor's hemisphere which sees downward scattered radiation. This enters into the calculation because of the angle α_s between the hillside normal and a normal to the sensor. The value of ε for $\alpha_s = 22°$ is 0.9633.

This completes our description of the model structure to the point where the computations may be compared with measured radiation penetrations.

11.4 RADIATION MEASUREMENTS

Hage, Labine and Reynolds (1977) described the instrumentation used to monitor various components of incoming radiation on top of the hill above our study plots. Here we are concerned with the determination of solar radiation penetration into the forest canopy on the hillside.

The method used was similar to that of Norman and Jarvis (1974). We established vertical towers ca. 20 m apart, 9 m high, aligned across the slope. At chosen heights, wire pairs, 15 cm apart in a horizontal plane, were stretched taut between the towers. A teflon-skidded sled, 18 cm x 18 cm, bearing horizontally mounted sensors, was towed at a uniform speed along the wires from tower to tower. A data acquisition system periodically recorded the signal from the mounted sensors and from similar sensors mounted horizontally atop one of the towers. The sled speed and recording interval were such that readings were made approximately every 2.0 cm along the transects.

Two different sensors were used, both manufactured by the Lambda Instruments Corp. One sensor, model LI-190S, responds nearly equally to photon numbers in the wavelength band 400-700 nm., with nearly zero response outside this band. The other, model LI-220S responds to band about 70 nm wide around 780 nm. The sensors were terminated by appropriate resistors supplied by the manufacturer.

In our processing of the data lagger output, we computed for each set of readings the ratio of sled sensor to tower sensor

values, and averaged these ratios along the transects. These average values are the basic data for comparison with model output.

Two transect stations were used with four levels run at one and three at the other.

11.5 MODEL RESULTS AND COMPARISON WITH MEASUREMENTS

Here we first present some output from the radiation model, and then make comparisons with the measured profiles.

Representative results from the penetration part of the model are shown in Fig. 5. Figure 5a compares the effects of the various intercepting elements and illustrates the variation of P^{η} with η. The first and most important thing to note from this figure is the dominant role of needle clumps compared to other elements. Also apparent are the almost total lack of interception in the top meter of the canopy and the effects of element height distributions (Fig. 2); cones have their influence near the top of the canopy, dead branches near the bottom. In Fig. 5b, the overall impact of all elements is illustrated. Note the effect of slope angle, in that for $\eta = 20°$, rays from $\phi = 0°$ are much more attenuated than from $\phi = 180°$; this is reduced for greater values of η. Also shown in this figure is the integrated attenuation from a uniformly luminous sky ($\bar{P}$).

Although they have not been mentioned to this point, we performed two other sets of calculations, representing (i) a horizontally random canopy (no clumping into trees), and (ii) a canopy of flat-topped trees having the same height, density and spacing as the pointed trees. These models differ from the one so far described only in the horizontal distribution

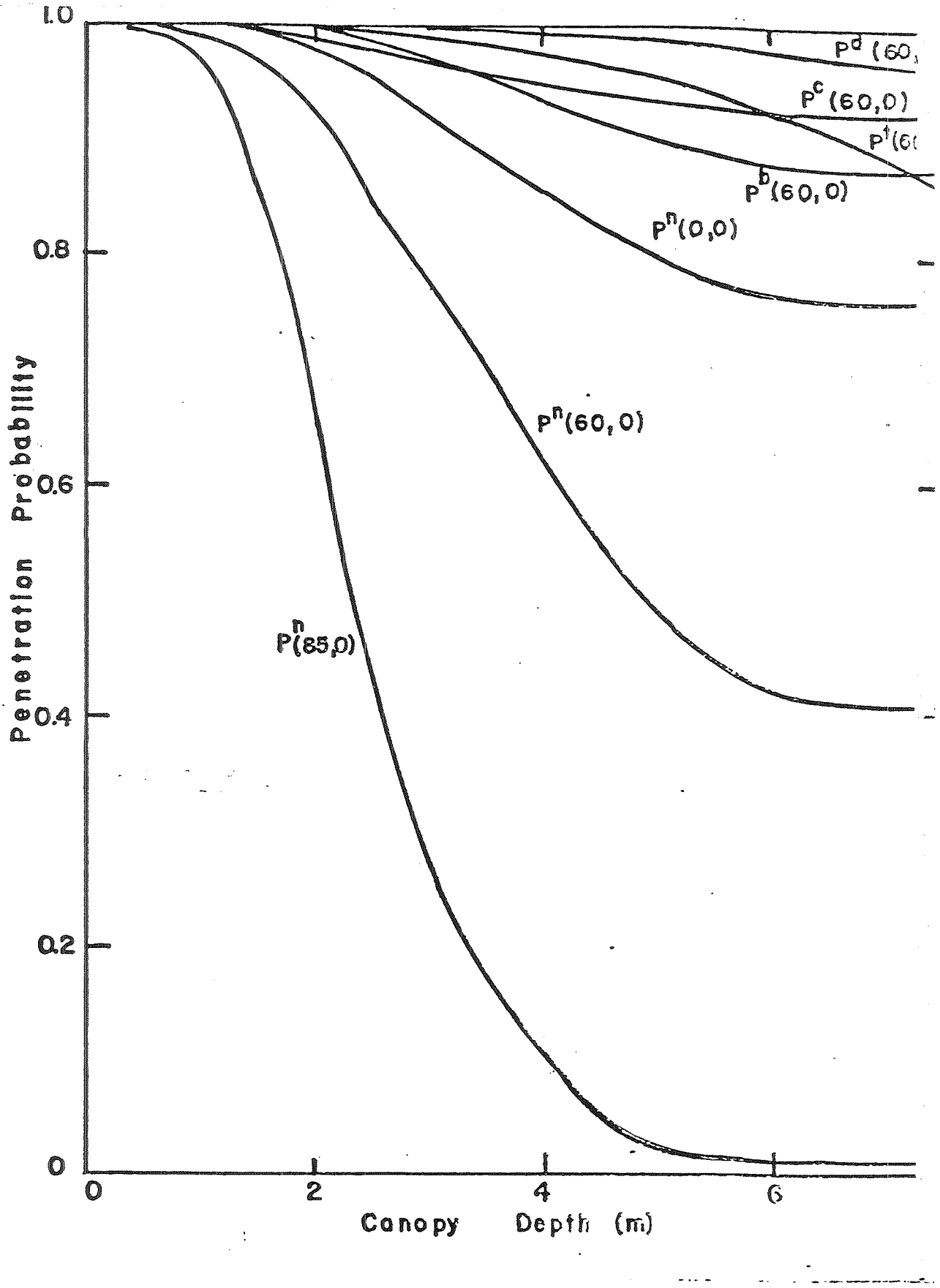

Figure 5. (a) Some typical results from the penetration probability model, showing the probabilities of non-interception by each element type at an incident zenith angle of 60° and additionally for needle clumps at n = 0° and 85°, all for ϕ = 0.

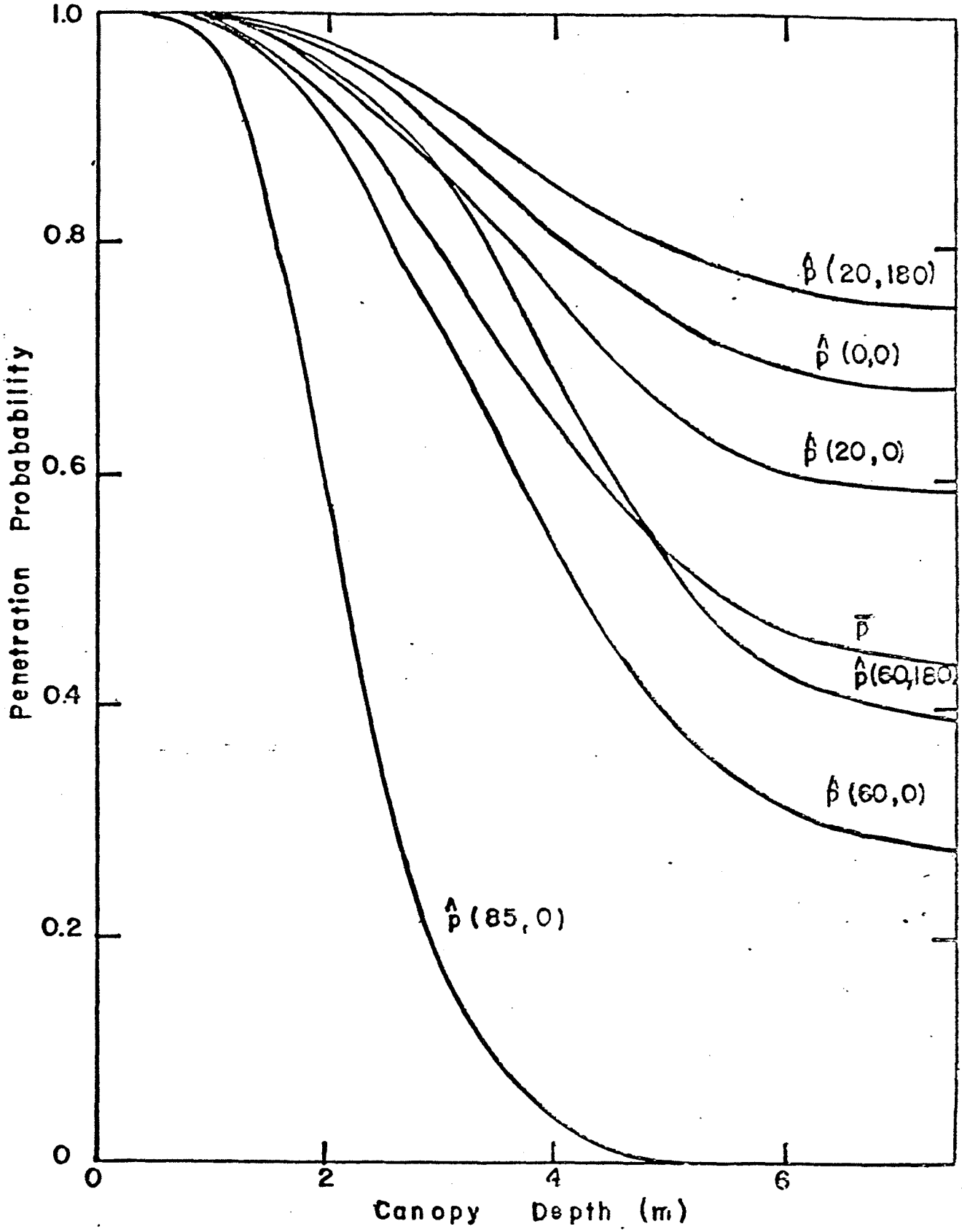

Figure 5 (b). Overall penetration probabilities ($\hat{P}$) for a variety of incident directions, and average pen penetration for sky radiation ($\bar{P}$).

of elements. Pertinent output from this calculation is illustrated in Fig. 6. Comparison with the corresponding curves of Fig. 5b reveals considerable differences, mainly in the degree of attenuation in the upper canopy. The two clumped models show the same rate of attenuation deep in the canopy, as expected.

The behaviour of scattered radiation is revealed in Fig. 7, for some typical cases. The difference between visible and near-infrared scatter is due entirely to needle optical characteristics, as detailed in Appendix F.

As described above, our measurements of radiation interception were made by moving sensors horizontally through the forest canopy; each transect required about 10 minutes, and between transects the sled had to be hauled back and repositioned, and a side-by-side comparison made with output from the tower top sensors. Consequently, solar position changed during the course of one set of measurements, and in making computations to compare with the data, the model had to be run separately for times corresponding to the centre of each transect. In Fig. 8, we superimpose one set of measurements on the output of the three models.

Rather than repeat this sort of presentation for each of the data sets, we compare predicted and measured value for the three models (Fig. 9). In this figure, we indicate those points taken in the morning, as separated from afternoon. The main result is that our primary model accounts reasonably well for

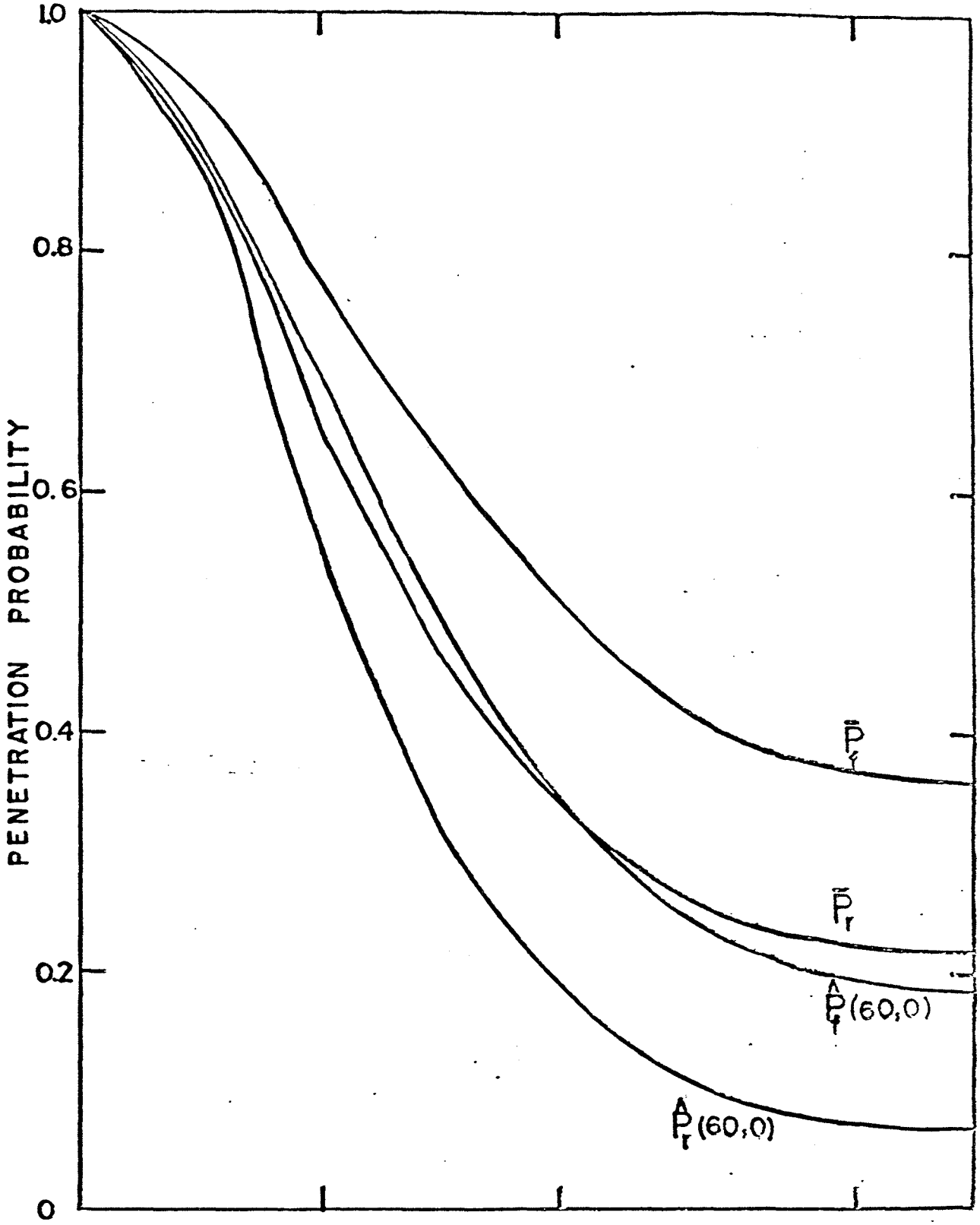

Figure 6. Penetration probabilities for the random model ($\hat{P}_r$ and $\bar{P}_r$) and flat-topped tree model ($\hat{P}_f$ and $\bar{P}_f$).

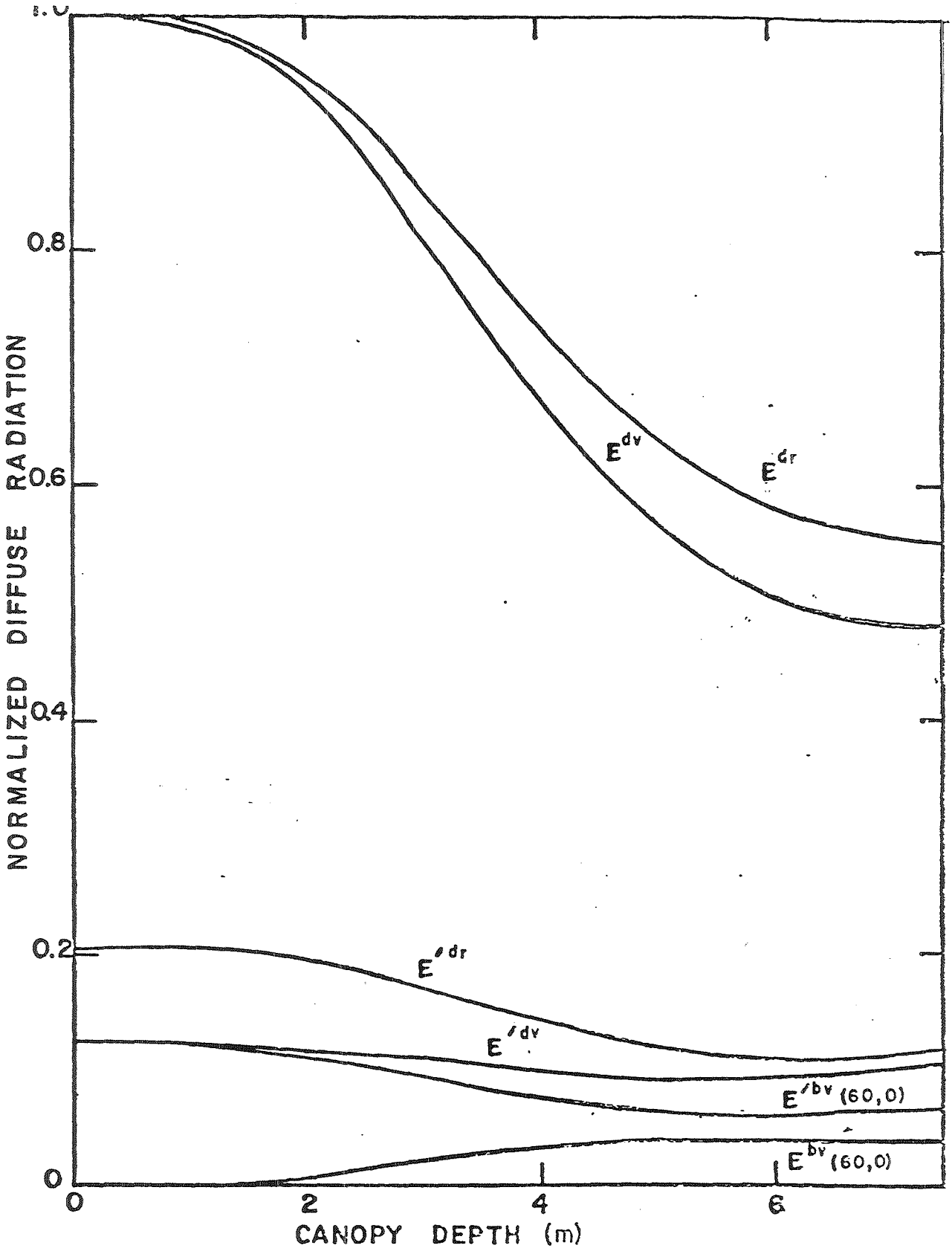

Figure 7. Some typical results from the scattering model. The superscripts d and b refer to radiation originating as sky diffuse and solar beam, respectively, r and v refer to near infrared and visible radiation respectively, and the unprimed and primed values are downward and upward fluxes, respectively.

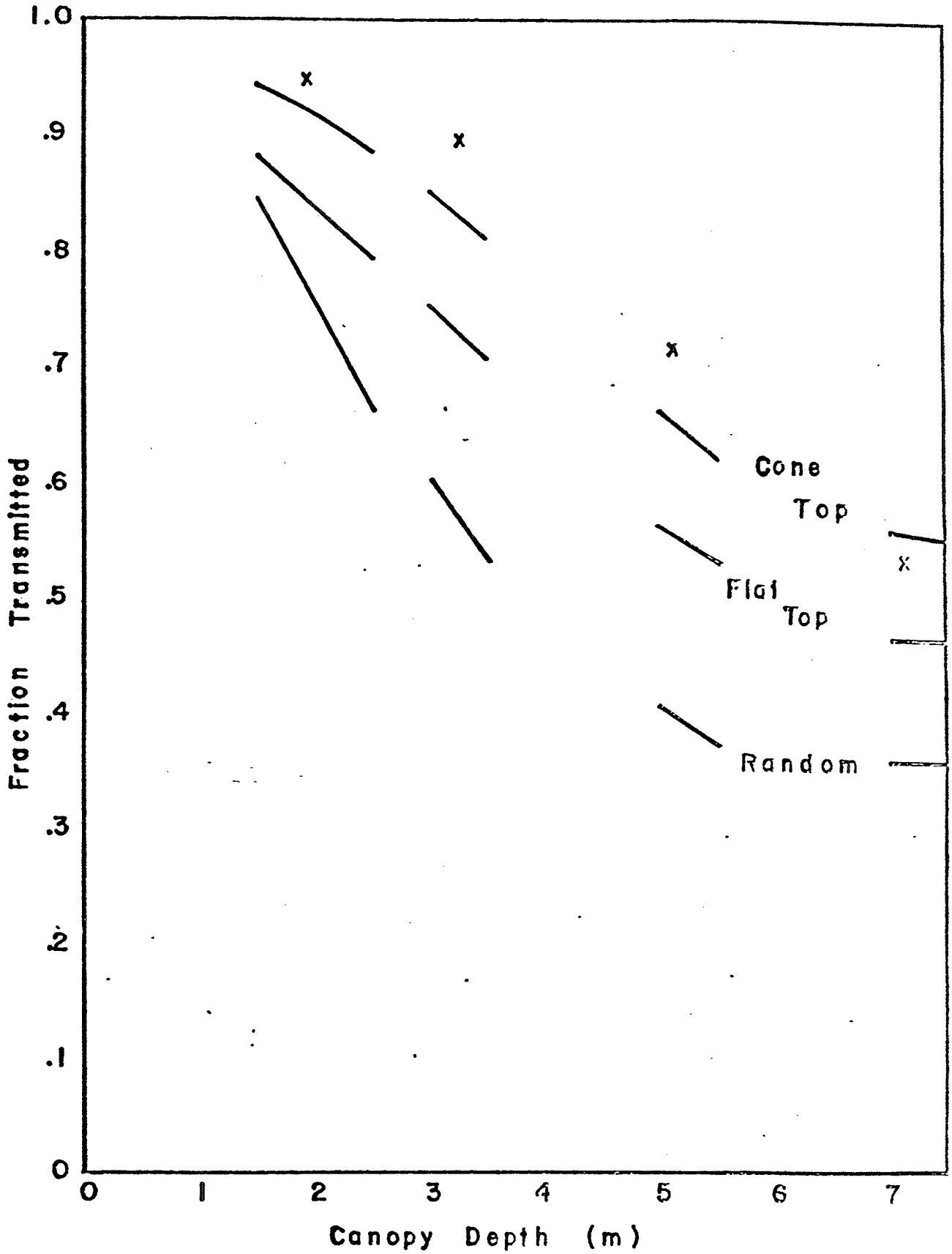

Figure 8. The comparison of one set of measurements with predictions of the three models. The x marks are average values of visible radiation penetration along horizontal transects, given as ratios to radiation incident above the canopy.

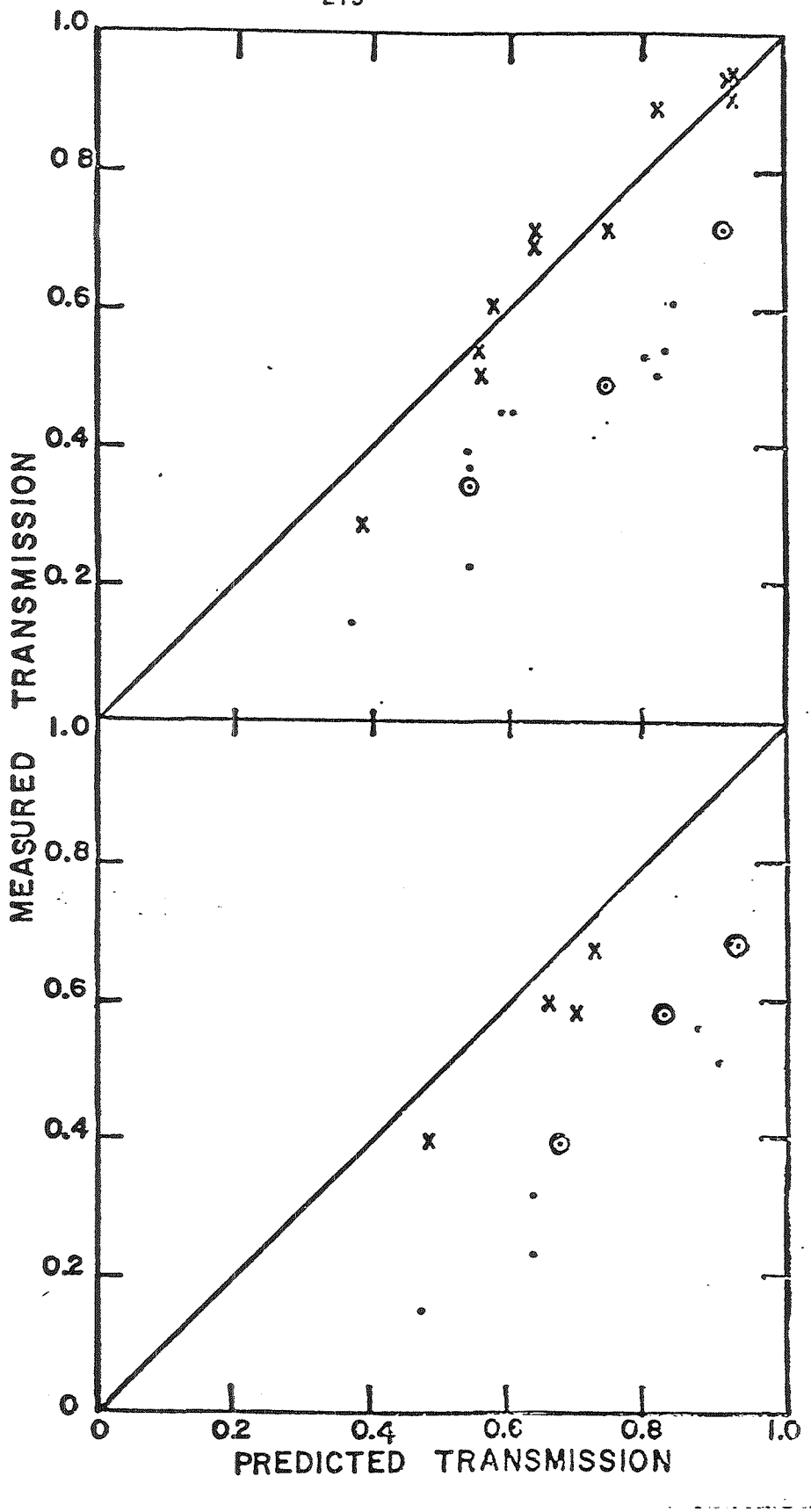

Figure 9. Comparison of radiation attenuation measurements with predictions of the three models. In each case the upper panel refers to visible light and the lower to near infrared. The x symbols designate afternoon readings, the dots morning readings and the circled dots readings made with the sun below the hill limb. (a) Cone-topped tree model.

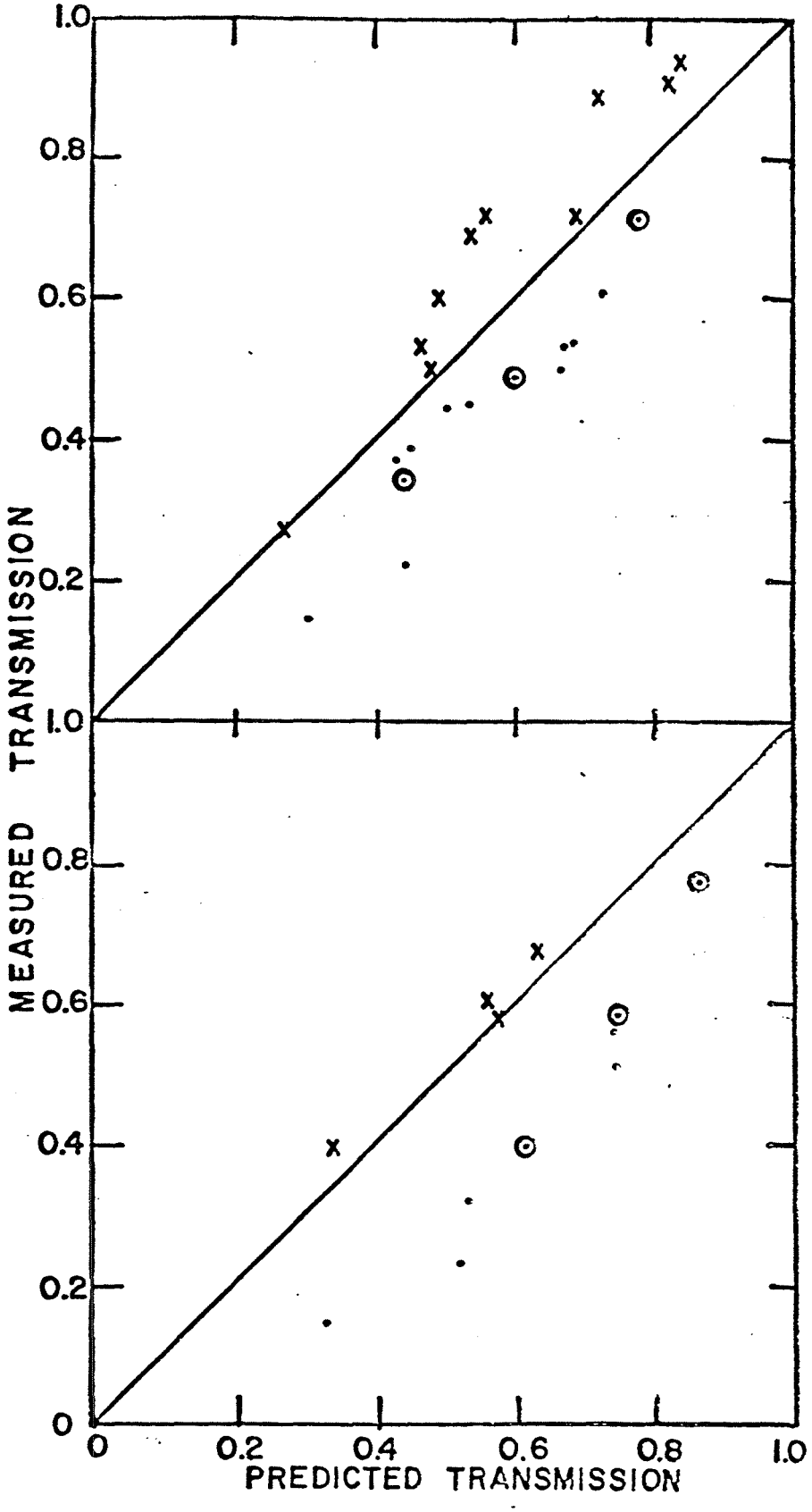

Figure 9 (b). As in Fig. 9(a), for flat-topped trees.

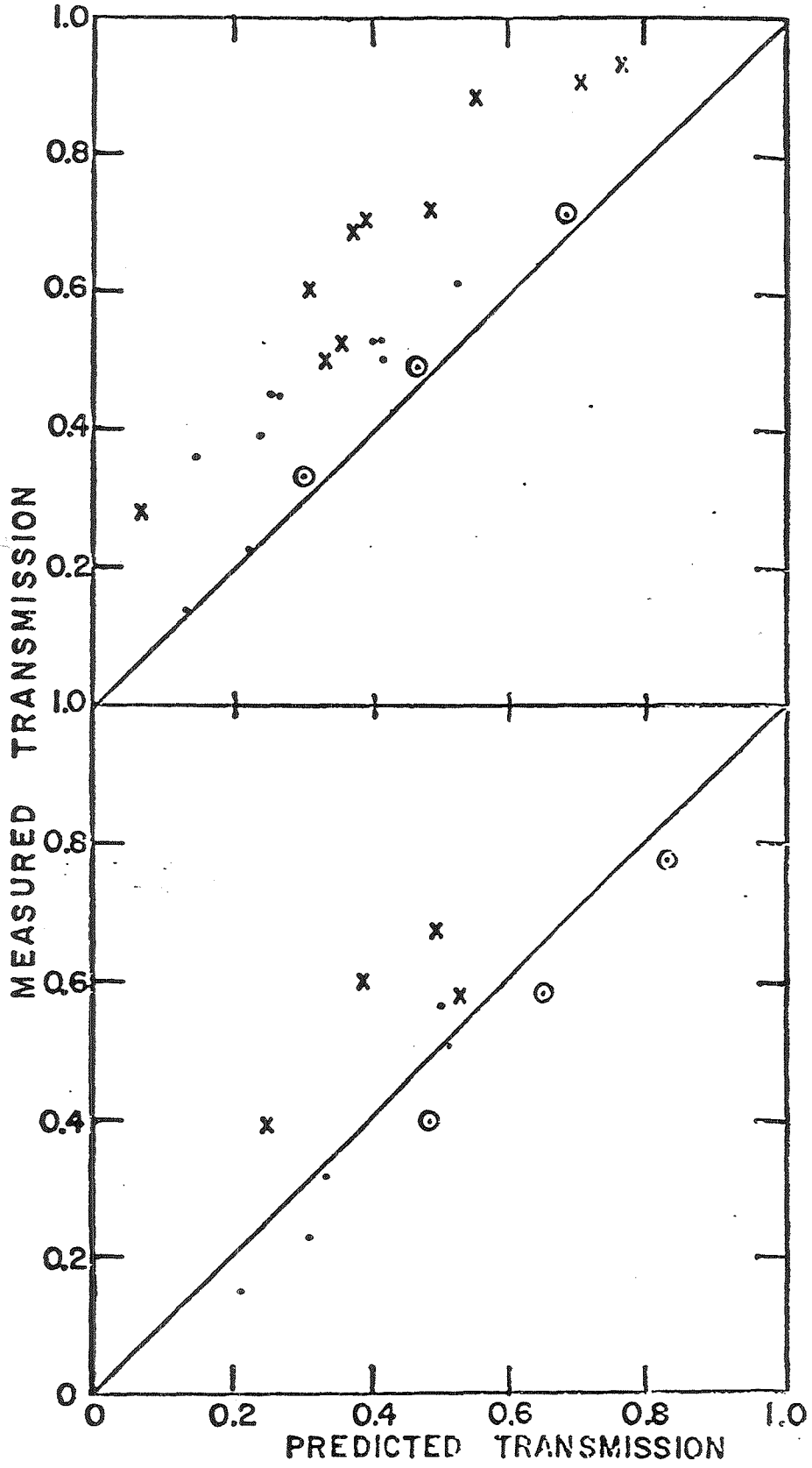

Figure 9 (c). As in Fig.9(a), for random element distributions.

afternoon measurements, while the morning ones seem to fit between the flat-topped and random models. This conclusion will be explored in the next section.

Also indicated in Fig. 9 are the results of measurements of sky radiation attenuation, made in early morning with the sun behind the hill. Note that the random model best accounts for these results.

11.6 DISCUSSION AND CONCLUSIONS

Our main model is free of tuning parameters: there are no unknown or empirical parameters which are to be adjusted to produce a good fit to the data. One could feel free to vary a few parameters which are subject to measurement uncertainty, but no reasonable twiddling would modify the results as much as going to the flat-topped or random model. These really are new models, which have built into them considerably different assumptions of gross canopy geometry. Thus, the observation of good fit to the main model for afternoon measurements and not for morning ones should be explained in terms of canopy geometry. In fact, there is an aspect of this geometry which has not yet been accounted for, and that is the azimuthal asymetry of element location, discussed by Whitfield et al. (1977). In that paper there is demonstrated a pronounced aggregation of needle clumps in the southwest quadrant w.r.t. the tree trunk. We used the same to construct Fig. 10, which indicates the radial and azimuthal arrangement of needle clumps. Also indicated on this figure are the slope azimuth, and the ranges of sun azimuth for the morning and afternoon measurements. It is apparent that the tree shape, seen from the sun direction, is very different for the two sets of measurements. We suggest that it is probably as a consequence of such asymetry that we find the ability of the models to fit the data varying through the day. A test of this conjecture would require construction of a new model with asymetrically

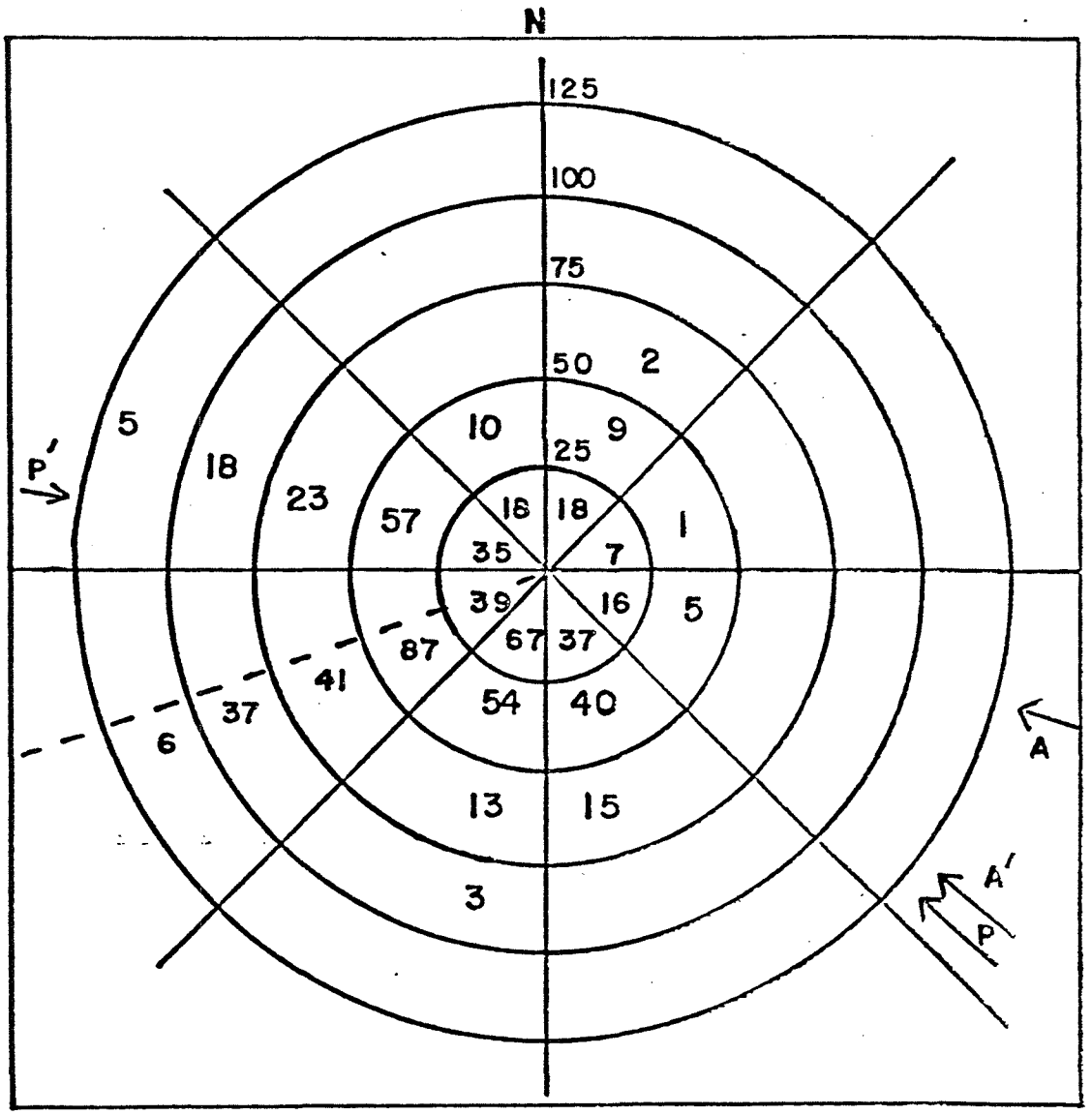

Figure 10. The numbers of needled clumps in various azimuthal and radial positions with respect to the trunk, for the intensively harvested tree. The arrows labelled A and A' delimit the sun azimuth for morning measurements and P and P' that for afternoon ones. The dashed line indicates hill azimuth direction. The circle radii are given in centimetres.

shaped trees, which is beyond the scope of this project.

That the random model best accounts for the diffuse attenuation measurements is probably due to the discrepancy between our assumption of a uniformly luminous sky and the real situation in which a preponderance of the sky radiation comes from near the sun direction, which in this case would be from near the horizon of the hillside system.

For the purpose of driving the energy and water balance model, we propose that the radiation interception calculated by assuming flat-topped trees will be adequate.

11.7 ACKNOWLEDGEMENTS

We wish to thank George Reynolds, Janet Marsh and George Davis for invaluable assistance with the field measurements and Paul McCourt and Arun Kumar for programming. J. Mayo and J. Harter laboured mightily to collect tree geometry data, and Murray Hunt constructed and operated the integrating sphere.

11.8 REFERENCES CITED

Birkebak, R. and R. Birkebak. 1964. Solar radiation characteristics of tree leaves. Ecology 45: 646-649.

Bliss, L. C. and D. W. A. Whitfield. 1977. Site description. In Long term prediction of vegetation performance on mixed sands. L. C. Bliss, ed.

Brown, P. S. and J. P. Pandolfo. 1969. An equivalent-obstacle model for the computation of radiative flux in obstructed layers. Agr. Meteorol. 6: 407-421.

Clark, P. J. and F. C. Evans. 1954. Distance to nearest neighbour and measure of spatial relationships in populations. Ecology 35: 445-453.

Hage, K., C. Labine and G. Reynolds. 1977. Micrometeorology. In Long term prediction of vegetation performance on mixed sands. Pp. 12-30. Report to Alberta Oil Sands Environmental Research Programme. Project VE6.1.

List, R. J. 1949. Smithsonian Meteorological Tables. Sixth Edition. Smithsonian Institution Press, Washington. 527 pp.

Mehlenbacher, A. L. and D. W. A. Whitfield. 1977. Radiation model. In Long term prediction of vegetation performance on mixed sands. L. C. Bliss, ed.

Monsi, M., Z. Uchijima, and T. Oikawa. 1973. Structure of foliage canopies and photosynthesis. In Ann. Rev. Ecol. and Systematics. R. F. Johnston, ed. Annual Reviews Inc., Palo Alto. 424 pp.

Nilson, T. 1971. A theoretical analysis of the frequency of gaps in plant stands. Agr. Meteorol. 8: 25-38.

Norman, J. M. 1975. Radiative transfer in vegetation. Pp. 187-206. In Heat and mass transfer in the biosphere. I. Transfer processes in plant environment. D. A. deVries and N. H. Afgan, eds. Scripto Book Co., Washington. 540 pp.

Norman, J. M. and P. G. Jarvis. 1974. Photosynthesis in sitka spruce. III. Measurements of canopy structure and interception of radiation. J. Appl. Ecol. 11: 375-398.

Norman, J. M. and P. G. Jarvis. 1975. Photosynthesis in sitka spruce. V. Radiation penetration theory and a test case. J. Appl. Ecol. 12: 839-878.

Oikawa, T. and T. Saeki. 1972. Light regime in relation to population structure - an experimental approach based on the Monte Carlo simulation model. Rep. 1971 IIBP/PP Photosynthesis Level III Group, Tokyo, pp. 107-116.

Ross, J. 1975. Radiative transfer in plant communities. In Vegetation and the Atmosphere. Vol. 1. Principles. J. L. Monteith, ed. Academic Press, London, New York and San Francisco. 278 pp.

Tanaka, S. 1968. Estimation of sunlit leaf area in tobacco community by Monte Carlo method. (1) Estimation on direct sunlight of a plant. Environ. Control Biol. 7: 12-16. (In Japanese).

Whitfield, D. W. A., J. M. Mayo, J. E. Harter, S. Nelson and A. Mehlenbacher. 1977. Tree geometry and optical properties of leaves. In Long term prediction of vegetation performance on mixed sands. L. C. Bliss, ed.

APPENDIX A.

STAND AND TREE GEOMETRY PARAMETERS USED IN THE MODEL

Bliss and Whitfield (1977) describe the study site and some characteristics of the trees. Whitfield et al. (1977) give some data on tree geometry and leaf optical properties. This appendix summarizes and extends these results, and puts them into the forms used in the model.

Average tree density on the study plots is .63 stems m^{-2}. In the plots used for radiation transits there is an average of .71 m^{-2}. We used .66 m^{-2} for the model. Randomness of tree location was tested over a 10 x 20 m block by the method of Clark and Evans (1954). Accepting only stems of dbh $\geq$ 0.01 m, no departure from random spacing could be detected.

Hillside slope (22°) was determined by surveying a transect upslope through the study plots with a level and surveyor's rod. Hill azimuth was measured with a magnetic compass as 250° from true north.

Whitfield et al. (1977) describe the results of an intensive harvesting of one tree, in which the locations, lengths, diameters, masses and orientations of all elements were determined. This data set was used to compute size (Table A.1) and orientation (Table A.2) distributions. Seed cones are idealized as being spherical, of radius 1.47 cm. To determine distributions with height, and number of elements per tree, Mayo and Harter (pers. comm.)

Table A.1. Distributions of element numbers by length and diameter for the intensively harvested tree described by Whitfield et al. (1977).

Element Type	Length (cm)	Diameter (cm) 1.0-1.9	2.0-2.9	3.0-3.9	4.0-4.9	5.0-6.0
Needled branch	0 - 2.08	22	0	14	15	8
	2.09- 4.36	0	35	44	7	0
	4.37- 9.14	15	81	1	0	2
	9.15- 19.12	16	1	0	0	0
	19.13- 40.00	24	0	17	3	48
		0.2 -0.276	0.277-0.382	0.383-0.529	0.530-0.733	.734-1.016
Bare live branch	2.57- 5.46	105	22	159	0	56
	5.47- 11.62	26	9	0	0	5
	11.63- 24.73	0	0	1	0	0
	24.74- 52.63	0	3	4	5	0
	52.64-112.00	10	6	96	0	14
		0.169- .231	.232- .318	.319- .437	.438- .600	.601-0.826
Dead branch	3.0 - 8.99	12	24	0	3	8
	9.00- 13.15	0	0	0	0	0
	13.16- 27.57	0	2	1	1	0
	27.58- 57.75	4	3	6	0	7
	57.76-121.0	9	9	0	9	4

Table A.2. Distribution of element numbers by orientation angles for the intensively harvested tree described by Whitfield et al. (1977). The angular coordinate system is referred to the hillside. The zenith angle, η, is measured from a normal to the slope and ϕ, the azimuth, is measured clockwise, as viewed from above, with ϕ = 0 downslope.

η (deg.)	ϕ (deg.)							
	0-45	45-90	90-135	135-180	180-225	225-270	270-315	315-360
				a. Needled branch				
0- 20	17	32	27	64	32	18	10	8
20- 40	7	30	76	160	41	10	9	4
40- 60	0	7	32	32	8	4	2	0
60- 80	1	1	3	8	3	1	1	0
80-100	0	1	6	1	0	1	0	0
100-120	0	0	1	1	2	0	0	0
120-140	1	1	0	0	1	0	0	0
140-160	0	0	0	0	0	0	0	0
160-180	0	0	0	0	0	0	0	0
				b. Bare live branches				
0- 20	12	19	13	27	10	10	12	6
20- 40	23	44	29	32	11	12	11	13
40- 60	23	30	18	9	4	6	16	12
60- 80	16	18	8	5	3	2	9	14
80-100	8	11	2	6	1	3	7	3
100-120	4	2	4	1	1	4	3	2
120-140	0	1	1	1	0	0	1	0
140-160	0	0	0	0	0	0	0	0
160-180	0	0	0	0	0	0	0	0
				c. Dead branches				
0- 20	14	8	11	18	10	2	7	2
20- 40	14	27	23	29	13	10	10	11
40- 60	11	22	21	8	3	4	5	9
60- 80	19	27	8	4	3	5	6	11
80-100	11	13	8	3	6	7	8	6
100-120	7	3	5	3	4	1	4	0
120-140	0	0	0	0	1	0	1	0
140-160	0	0	0	0	0	2	0	0
160-180	0	0	0	0	0	0	0	0

undertook less intensive samplings in which the spatial positions and orientations of all elements on 11 trees were measured. The sample of trees was randomly selected, and we consider it to be representative of the stand. Figure 2 illustrates the results of this study, averaged over the random sample, and put into the form of distributions accumulated downward. The tree height distribution was determined from the survey reported in Bliss and Whitfield (1977).

Tree outline shape was also determined from Mayo and Harter's personally communicated results, from which maximum element radius from the trunk was taken as a function of height. Hand fitting of the idealized tree shape (a cylinder topped with a cone) to the data yielded an estimate of 12° for the cone angle (side to axis) and the following relationship of cylinder radius to tree height (meters)

$$R = -0.0883 + 0.0757\ H \text{ meters} \qquad [A.1]$$

Calculations in the model are performed for 0.5 m intervals, from 7.5 m to the ground surface, measured perpendicular to the ground. The volume densities of intercepting elements, by height slice and within tree outlines, are required for the penetration calculations. To get these, we combined tree height distribution of Figure 2, Eqn. A.1 for cylinder radius, and the cone shape described above to determine average tree volume per height slice. Then these volumes were divided by the average numbers of elements per tree for the height slices.

APPENDIX B.

COORDINATE SYSTEMS AND THE CALCULATION OF SOLAR POSITION

Several coordinate systems were used in model calculations. Some of these are described here, together with equations for transformations among them, and equations for sun position. Other coordinate systems and transformations are described as needed in Appendix C.

The transformations described here are based on the cosine law of spherical trigonometry.

Solar position is first calculated as declination (δ) and hour angle (h), from the formulae (in radians)

$$\delta = \delta_o \cos\left(\frac{2\pi}{365}(D-172)\right) + \delta'(D) \qquad [B.1]$$

and

$$h = \frac{2\pi}{\varepsilon_4}(H - 1.398 + \varepsilon) \qquad [B.2]$$

where δ_o is maximum declination (23.45°), D is day number in the year, δ' is a correction table which we generated by comparing the first term of Eqn. B.1 with an ephemeris of the sun (List, 1949), H is hour of the day (DST) and ε is the "equation of time", tabulated in List (1949). In DST, mean solar noon occurs at 13.398 hours. In this system, somewhat unconventionally, h is zero at solar noon.

Next, we used a system oriented to true north and to the horizontal. Direction in this system is specified as η' (angle from the vertical), and ϕ' (azimuth from true north).

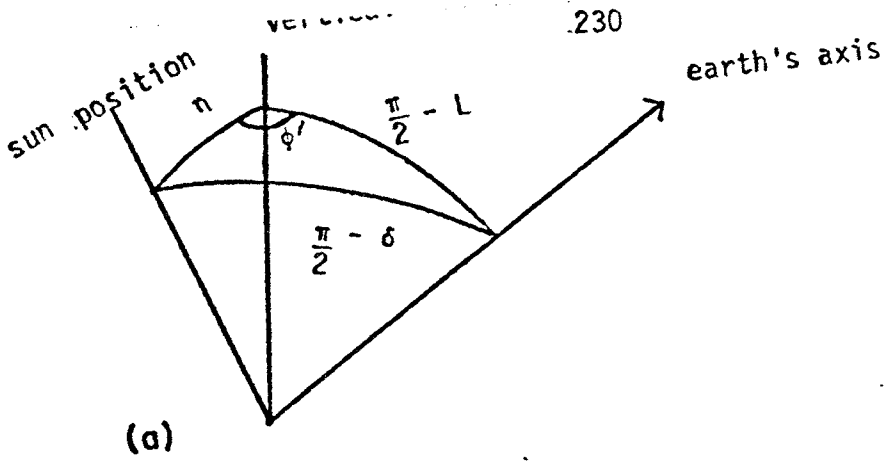

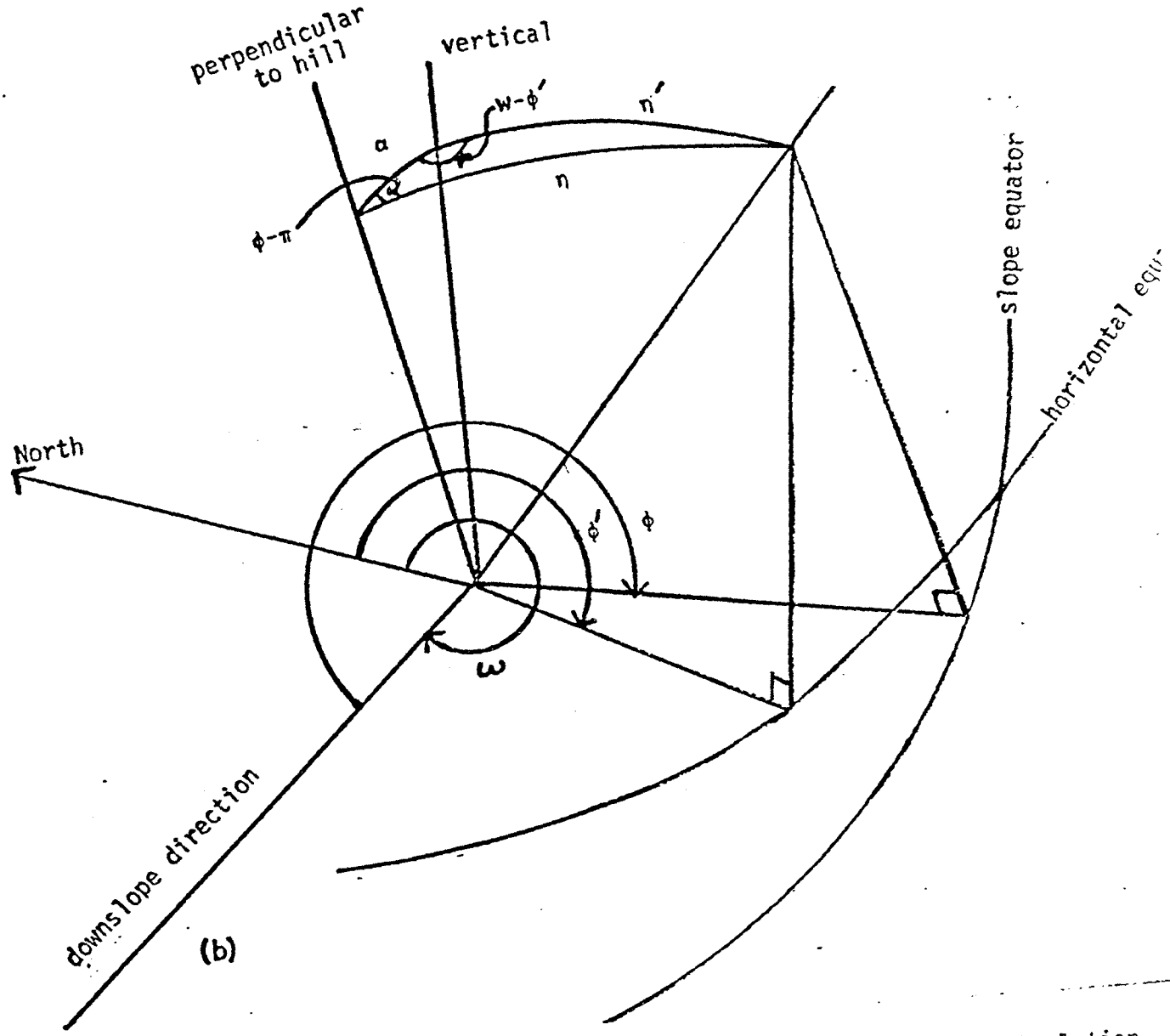

Figure B.1. Spherical triangles for (a) sun position calculation and (b) transformation to hillside co-ordinates. The symbols are defined in the text.

Figure B.1a shows the spherical triangle relating this system to the sun's declination and hour angle. The transformations are:

$$\cos \eta' = \cos (\pi/2 - L) \cos (\pi/2 - \delta) + \sin (\pi/2 - L) \sin (\pi/2 - \delta) \cos (h - \pi) \quad [B.3]$$

and $$\sin \delta = \cos (\pi/2 - L) \cos \eta' + \sin (\pi/2 - L) \sin \eta' \cos \phi' \quad [B.4]$$

where L is the study site latitude. Eqn. B.3 is evaluated directly for cos η', and Eqn. B.4 is rearranged before evaluating for cos ϕ':

$$\cos \phi' = \frac{\sin \delta - \sin L \cos \eta'}{\cos L \sin \eta'} \quad [B.5]$$

Penetration calculations were performed w.r.t., a system oriented to the hillside, with η measured from a perpendicular to the hill and ϕ, the azimuth, measured clockwise from a line running down the hill. This is called the hillside system. The relevant angles and spherical triangle are illustrated in Figure B.1b. The transformations are:

$$\cos \eta = \cos \eta' \cos \alpha + \sin \eta' \sin \alpha \cos (\omega - \phi') \quad [B.6]$$

and $$\cos \eta' = \cos \eta \cos \alpha + \sin \eta \sin \alpha \cos (\phi - \pi) \quad [B.7]$$

where ω is the azimuth of the downslope direction from true north and α is the slope angle from horizontal. Again, Eqn. B.6 is evaluated for cos η and Eqn. B.7 is solved for cos ϕ before evaluation:

$$\cos \phi = \frac{\cos \eta \cos \alpha - \cos \eta'}{\sin \eta \sin \alpha} \quad [B.8]$$

APPENDIX C.

CALCULATION OF INTERCEPTION POINTS OF RAYS WITH TREES, AND THE CONSEQUENT WITHIN-TREE PATHLENGTHS.

In this appendix we describe the calculations performed to determine the points at which rays intersect tree outlines in the numerical forest.

We start by considering a ray entering the forest top, at 7.5 m above the ground. Here we are in a hillside coordinate system, with height measured perpendicular to the slope, and the trees slanting at α_s to the vertical. The ray has a direction η_b, ϕ_b, and point of entry, x_{bs}, y_{bs}. Then its path projected onto the x-y plane is

$$y = y_{b_s} + (x - x_{b_s}) \tan (\pi - \phi_b) \qquad [C.1]$$

where x is positive downslope, and y across.

To account for the possibility of a ray leaving the numerical forest edge before striking the ground surface, we perform a wrap-around at the edges, as follows: a series of x,y pairs, each value 0 or ± 30 m, was generated, such that when these values were used to displace the forest block, the beam was always in the forest before it reached the ground. The procedure for generating the displacements is best illustrated in a flow chart, Fig. C.1. In what follows, all interception calculations were performed for each displacement as well as the original forest location.

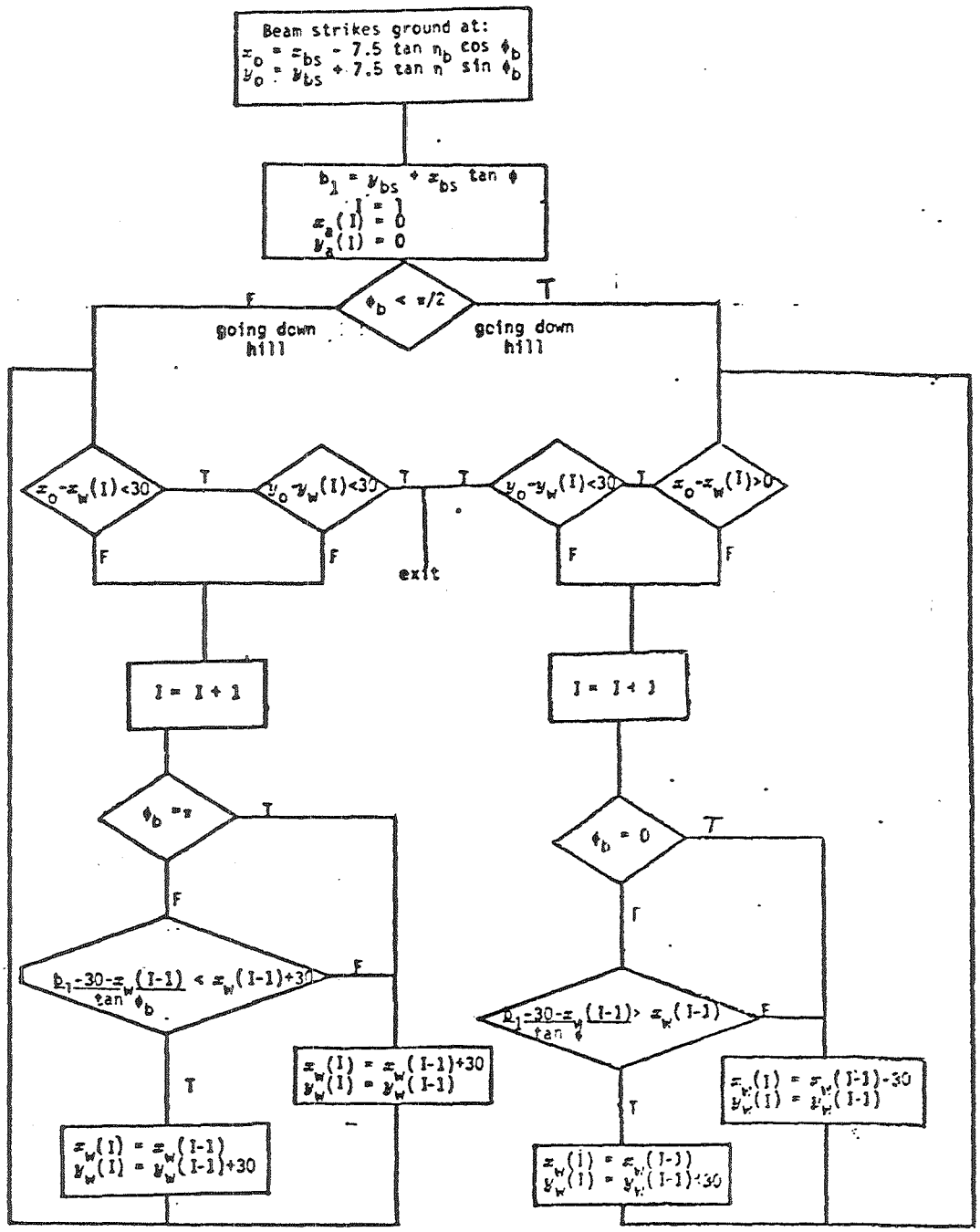

Figure C.1. Flow chart for the algorithm which calculates plot displacements required to keep the beam from passing a plot edge before striking the ground surface.

To reduce the amount of more complex calculation required later, the program first scans all trees in the forest to detect close encounters, and enters their indices into a table. To detect these potential intersections, we consider projected onto the x-y plane a circle large enough to enclose the projected tree. A tree (treated as a cylinder) of height h_t has a projected midpoint at $x_t - \frac{h_t}{2} \sin \alpha_s$, y_t and its total projected length in the x direction is $h_t \sin \alpha_s + 2r_t$, where r_t is tree cylinder radius. Thus, a circle of radius $\frac{h_t}{2} \sin \alpha_s + r_t$, centered at the projected midpoint, completely encloses the tree's projection. We used for h_t and r_t the values for the largest tree. Substituting into Eqn. C.1 the y coordinate of the tree, and subtracting the resulting x value from the circle center x coordinate one gets

$$\Delta x = \frac{y_{b_s} + x_{b_s} \tan \phi_b - y_t - (x_t - \frac{h_t}{2} \sin \alpha_s) \tan \phi_b}{\tan \phi_b} \quad [C.2]$$

If $|\Delta x| < (r_t + \frac{h_t}{2} \sin \alpha_s) \sin \phi_b$, the projected ray path and circle intersect, and the tree must be considered in detailed calculations. When $\phi_b = 0$ or $\phi_b = \pi$, the above calculation is simplified to determining if $|y_t - y_{b_s}| < r_t$.

Detailed interception calculations for each tree are carried out in a special coordinate system, x''', y''', z''', with origin at the tree axis where the tree top cone and cylinder intersect, with z''' aligned with the tree axis and y''' parallel to y. Figure C.2 illustrates this system and the sequence of

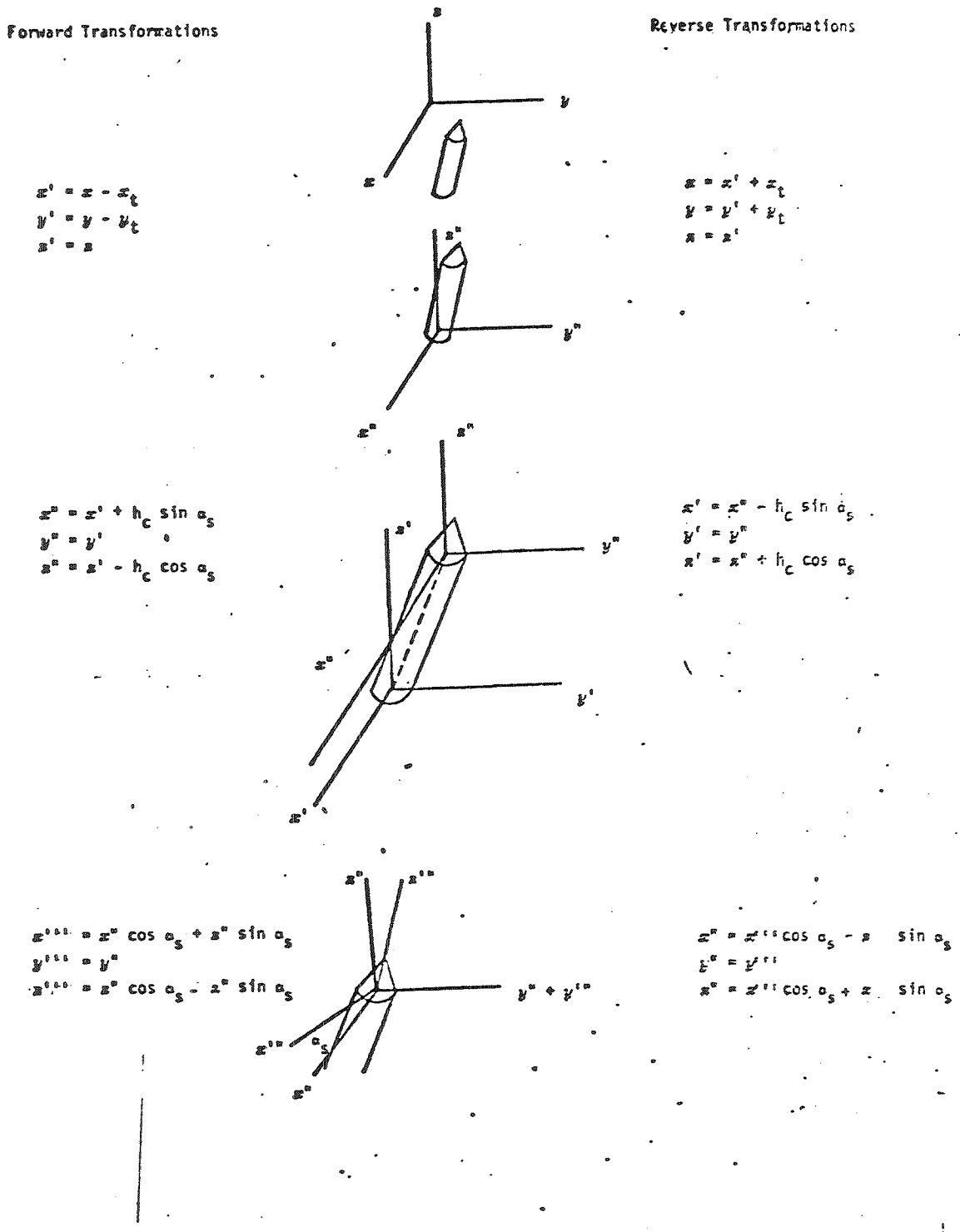

Figure C.2. Co-ordinate systems and transformations used in beam-tree interception calculations.

transformations from it to the hillside system and back. In these transformations, h_c is the height of the cylinder part of the tree, and

$$h_c = h - r_t \cos \alpha_t \qquad [C.3]$$

where α_t is the cone apex half-angle, and is a constant parameter of the model.

In the hillside system, the beam equations are:

$$x = x_{b_s} - (z_{b_s} - z) \tan \eta_b \cos \phi_b \qquad [C.4]$$

$$y = y_{b_s} + (z_{b_s} - z) \tan \eta_b \sin \phi_b \qquad [C.5]$$

where $z_{b_s} = 7.5$ m, is beam starting z coordinate. In the tree system, the cone equation is:

$$(x''')^2 + (y''')^2 = (r_t - z''' \tan \alpha_t)^2 \qquad [C.6]$$

and the cylinder equation is:

$$(x''')^2 + (y''')^2 = (r_t)^2 \qquad [C.7]$$

Using the transformations of Figure C.2, Eqns. C.4 and C.5 are converted to the tree system and substituted into Eqn. C.6 and C.7. After a few pages of algebra, one gets, for the cone interception:

$$z'''^2 (C_2^2 + C_4^2 - \tan^2 \alpha_t) + z''' (2C_2C_3 + 2C_4C_5 + 2r_t \tan \alpha_s) + C_3^2 + C_5^2 - r_t^2 = 0. \qquad [C.8]$$

where $C_1 = \cos \alpha_s - \sin \alpha_s \tan \eta_b \cos \phi_b$ [C.9]

$$C_2 = \frac{\sin \alpha_s + \cos \alpha_s \tan \eta_b \cos \phi_b}{C_1} \qquad [C.10]$$

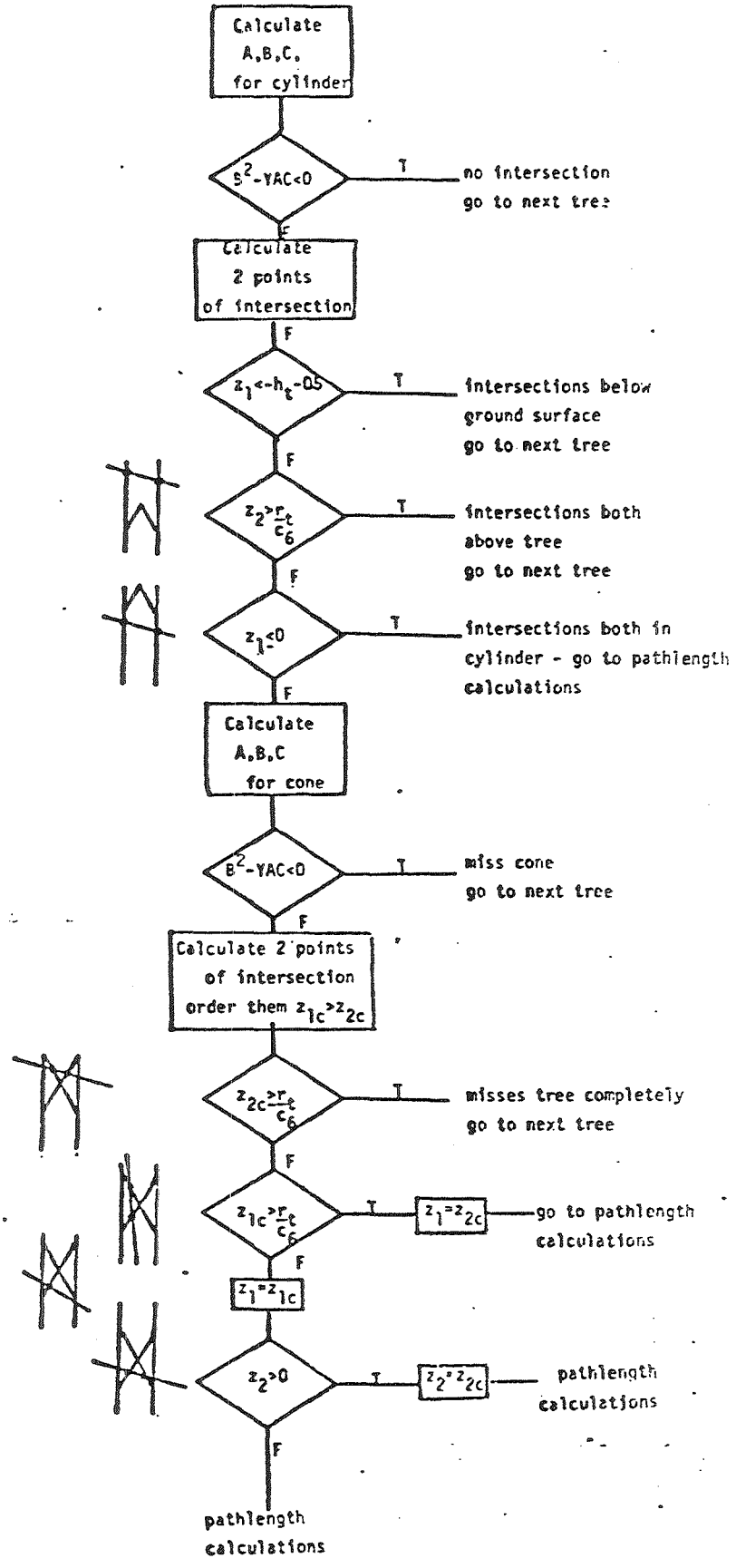

Figure C.3. Flow chart for the algorithm which calculates interception points of beams with tree outlines, together with explanatory diagrams.

$$C_3 = \frac{h_c \sin \alpha_s - (z_{b_s} - h_c \cos \alpha_s) \tan \eta_b \cos \phi_b + x_{b_s} - x_t}{C_1} \quad [C.11]$$

$$C_4 = - \tan \eta_b \sin \phi_b [C_2 \sin \alpha_s + \cos \alpha_s] \quad [C.12]$$

and $$C_5 = \tan \eta_b \sin \phi_b [-C_3 \sin \alpha_s - h_c \cos \alpha_s + z_b] + y_{b_s} - y_t \quad [C.13]$$

Eqn. C.8 applies to the cylinder interception as well, when $\tan \alpha_t = 0$. If the quadratic Eqn. C.8 has real roots, there are two interceptions of the beam with the cone or cylinder. Computing

$$A = C_2^2 + C_4^2 - \tan^2 \alpha_t \quad [C.14]$$

$$B = 2C_2C_3 + 2C_4C_5 + 2r_t \tan \alpha_s \quad [C.15]$$

and $$C = C_3^2 + C_5^2 - r_t^2 \quad [C.16]$$

and using the logic laid out in flow chart form in Figure C.3, the intersection points were determined, if they occurred, as x_1''', y_1''', z_1''', and x_2''', y_2''', z_2'''. These were transformed to the single primed system of Figure C.2 to yield x_1', y_1', z_1' and x_2', y_2', z_2'. Then if $z_1' < 0$, the interception is below ground and counts as a non-interception. If $z_2' < 0$, the beam strikes the ground surface before leaving the tree outline, and a new lower intersection point, at the ground surface, must be calculated

$$\rho = \frac{z_1'}{z_1' - z_2'} \quad [C.17]$$

$$x_2' = x_1' + \rho\,(x_2' - x_1') \qquad [C.18]$$

$$y_2' = y_1' + \rho\,(y_2' - y_1') \qquad [C.19]$$

$$z_2' = 0. \qquad [C.20]$$

Now the total within-tree pathlength, for this tree, was calculated:

$$\tilde{L} = (x_1' - x_2')^2 + (y_1' - y_2')^2 + (z_1' - z_2')^2 \qquad [C.21]$$

and divided up among the horizontal layers it passed through. Then the calculations of Eqns. C.2 through C.21 were repeated for other trees. When all trees were considered for a given ray, the exponential function of Eqn. 2 in the main text was calculated, and a new ray chosen.

APPENDIX D.

PROJECTED AREAS OF ELEMENTS

Each element is viewed as a cylinder of diameter d and length L (except trunks and cones). Then if α is the angle between the cylinder axis and the viewing direction, the projected area is

$$A(\alpha) = d\,\ell \sin\alpha + \pi\,(d/2)^2 \cos\alpha \qquad [D.1]$$

If, in the hillside coordinate system, the element is viewed from η, ϕ, and the cylinder axis has an orientation of $\hat{\eta}$, $\hat{\phi}$, the value of α is easily calculated from the cosine law of spherical trigonometry:

$$\cos\alpha = \cos\hat{\eta}\cos\eta + \sin\hat{\eta}\sin\eta\cos(\phi-\hat{\phi}) \qquad [D.2]$$

For needled branches, the cylinders are partially transparent, due to gaps between the needle projections. Mehlenbacher and Whitfield (1978) give results for the opaque fraction Ω as a function of α. This is reproduced here as Figure D.1, with slight changes. The curve drawn through the data points on this figure is represented in the model by a quadratic. For other elements, $\Omega = 1.0$.

Taking into account the observed distributions of elements (Appendix A) over length and diameter, $f^k(\ell, d)$, and over orientation angles, $F^k(\hat{\eta}, \hat{\phi})$, the average projected area is

$$\bar{A}^k(\eta, \phi) = \sum_{M_\ell=1}^{N_\ell} \sum_{M_d=1}^{N_d} \sum_{M_\eta=1}^{N_\eta} \sum_{M_\phi=1}^{N_\phi} f^k(\ell, d)\, F^k(\hat{\eta}, \hat{\phi})\, A(\alpha)\, \Omega(\alpha) \qquad [D.3]$$

where ℓ, d, $\hat{\eta}$, $\hat{\phi}$ are taken at discrete intervals, of numbers N_ℓ, N_d, N_η and N_ϕ, respectively.

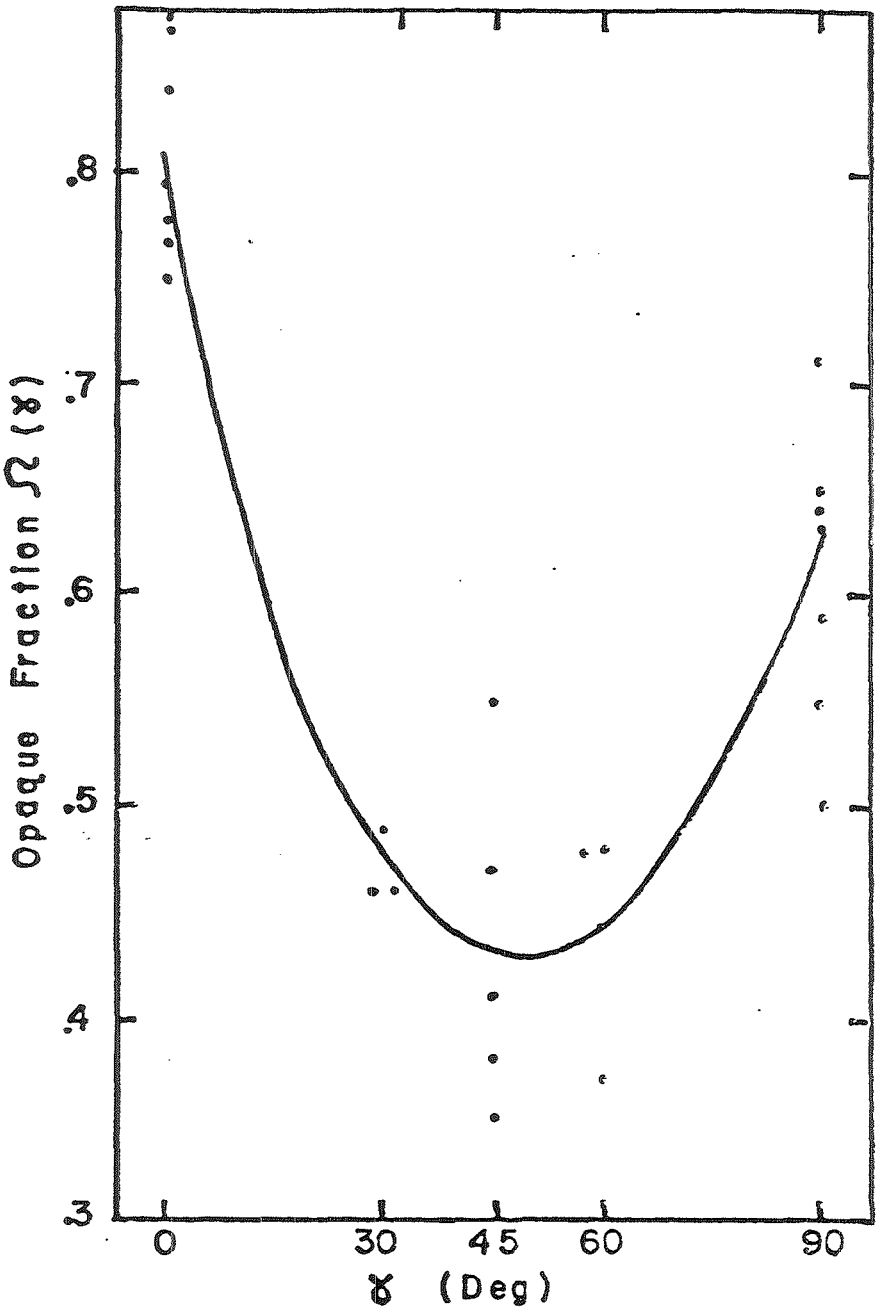

Figure D.1. Measurements of the fraction of needle clump outline occupied by needles or branch when viewed from various angles from the clump axis. The points are individual measurement results and the curve is that used in model calculations.

Note that our treatment of needle clump gaps is equivalent to Norman and Jarvis' (1975) handling of shoot gaps and whorl gaps. They take the 0^{th}, 1^{st},...i^{th}... terms of a Poisson distribution series as representing the probability of altogether missing an element, passing through a gap in one but missing others,... passing through gaps in i elements but missing others... However, when their series are summed, it turns out that they reduce to simple exponential attenuation by elements having the area of the element projected outline multiplied by the gap fraction.

APPENDIX E.

NUMERICAL EVALUATION OF THE INTEGRALS DETERMINING DIFFUSE RADIATION PENETRATION

The problem treated in this appendix is that of evaluating

$$\frac{\int_0^{\pi/2} d\eta \int_0^{\pi} d\phi \; r(\eta, \phi)\, \hat{P}_i(\eta, \phi) \sin\eta \cos\eta}{\int_0^{\pi/2} d\eta \int_0^{\pi} d\phi \; r(\eta, \phi) \sin\eta \cos\eta} \qquad [E.1]$$

given tabulated values for $\hat{P}_i$ and a function or table for r. This is Eqn. (5) in the main text. We called the result $\bar{P}_i$ when $r = 1$, for all source angles.

Values of $\hat{P}_i$ were available at discrete points on the grid: $\phi = 0, 20, 40, \ldots 180°$ and $\eta = 0, 10, 20, \ldots 70, 75, 80, 85, 90°$.

The denominator is easily evaluated analytically when $r = 1$, and yields a value of $\pi/2$. To evaluate the numerator, we linearly interpolate $\hat{P}$ between tabulated values, so

$$\int_0^{\pi} d\phi \int_0^{\pi/2} d\eta \; \hat{P}_i(\eta, \phi) \sin\eta \cos\eta \approx \frac{F_i(0) + F_i(10)}{2} + \ldots + \frac{F_i(180)}{2} \qquad [E.2]$$

where $$F_i(\phi) = \int_0^{\pi/2} \hat{P}_i(\eta, \phi) \sin\eta \cos\eta \, d\eta \qquad [E.3]$$

$$= \int_0^{10} + \int_{10}^{20} + \ldots + \int_{60}^{70} + \int_{70}^{75} + \int_{85}^{90} \qquad [E.4]$$

and $$\int_{\eta_1}^{\eta_2} \hat{P}_i(\eta, \phi) \sin\eta \cos\eta = \int_{\eta_1}^{\eta_2} (a + b\eta) \sin\eta \cos\eta \, d\eta \qquad [E.5]$$

$$= a \int_{\eta_1}^{\eta_2} \sin\eta \cos\eta \, d\eta + b \int_{\eta_1}^{\eta_2} \eta \sin\eta \cos\eta \, d\eta \qquad [E.6]$$

$$= \frac{a}{2} \left[\sin^2 \eta\right]_{\eta_1}^{\eta_2} + b \left[\frac{\eta}{2} \sin^2 \eta - \frac{\eta}{4} - \frac{\cos\eta \sin\eta}{4}\right]_{\eta_1}^{\eta_2} \qquad [E.7]$$

$$= \frac{a}{2} (\sin^2 \eta_2 - \sin^2 \eta_1) + \frac{b}{2} (\eta_2 \sin^2 \eta_2 - \eta_1 \sin^2 \eta_1)$$

$$+ \frac{b}{4} (\eta_1 - \eta_2 + \cos\eta_2 \sin\eta_2 - \cos\eta_1 \sin\eta_1) \qquad [E.8]$$

where integration by parts was used in the second to last step. Also, after a few lines of algebra

$$a = \frac{\eta_2 \hat{P}_i(\eta, \phi) - \eta_1 \hat{P}_i(\eta_2, \phi)}{\eta_2 - \eta_1} \qquad [E.9]$$

and

$$b = \frac{\hat{P}_i(\eta_2, \phi) - \hat{P}_i(\eta_1, \phi)}{\eta_2 - \eta_1} \qquad [E.10]$$

When we treat the case of $\Gamma = 1$ for sky and $\Gamma = 0$ for the part of the hemisphere occupied by flatland forest below the hill, the calculations are more complex. We start with

$$\bar{P} = \frac{\int_0^{\pi} d\phi \int_0^{\bar{\eta}(\phi)} \hat{P}_i(\eta, \phi) \sin\eta \cos\eta \, d\eta \, d\phi}{\int_0^{\pi} d\phi \int_0^{\pi/2} \sin\eta \cos\eta \, d\eta \, d\phi} \qquad [E.11]$$

where $\bar{\eta}$ is defined by the horizontal in the downslope direction, so

$$\bar{\eta} = \tan^{-1}\left(\frac{\cot\alpha}{\cos\phi}\right) \text{ for } 0 \leq \phi < \pi/2 \qquad [E.12]$$

$$\bar{\eta} = \pi/2 \text{ for } \pi/2 \leq \phi \leq \pi \qquad [E.13]$$

Eqn. E. 12 is deduced by applying the cosine law to the spherical triangle of Fig. E.1:

$$\begin{aligned} \cos\eta' &= \cos\eta\cos\alpha_s + \sin\eta\sin\alpha_s\cos(\pi-\phi) \\ &= \cos\eta\cos\alpha_s - \sin\eta\sin\alpha_s\cos\phi \end{aligned} \qquad [E.14]$$

The horizon is defined by $\cos\eta' = 0$, and E. 12 follows immediately.

To carry out the numerical integration, the procedure outlined above for $\bar{P}_i$ is used, with the exception that $\bar{\eta}$ is substituted for η_2, when $\bar{\eta} < \eta_2$, in Eqn. E.8, but not in Eqn. E.9 or E.10.

The results of this calculation, compared with that of $\bar{P}_i$ are indicated in Fig. E.2. Near canopy top there is a difference

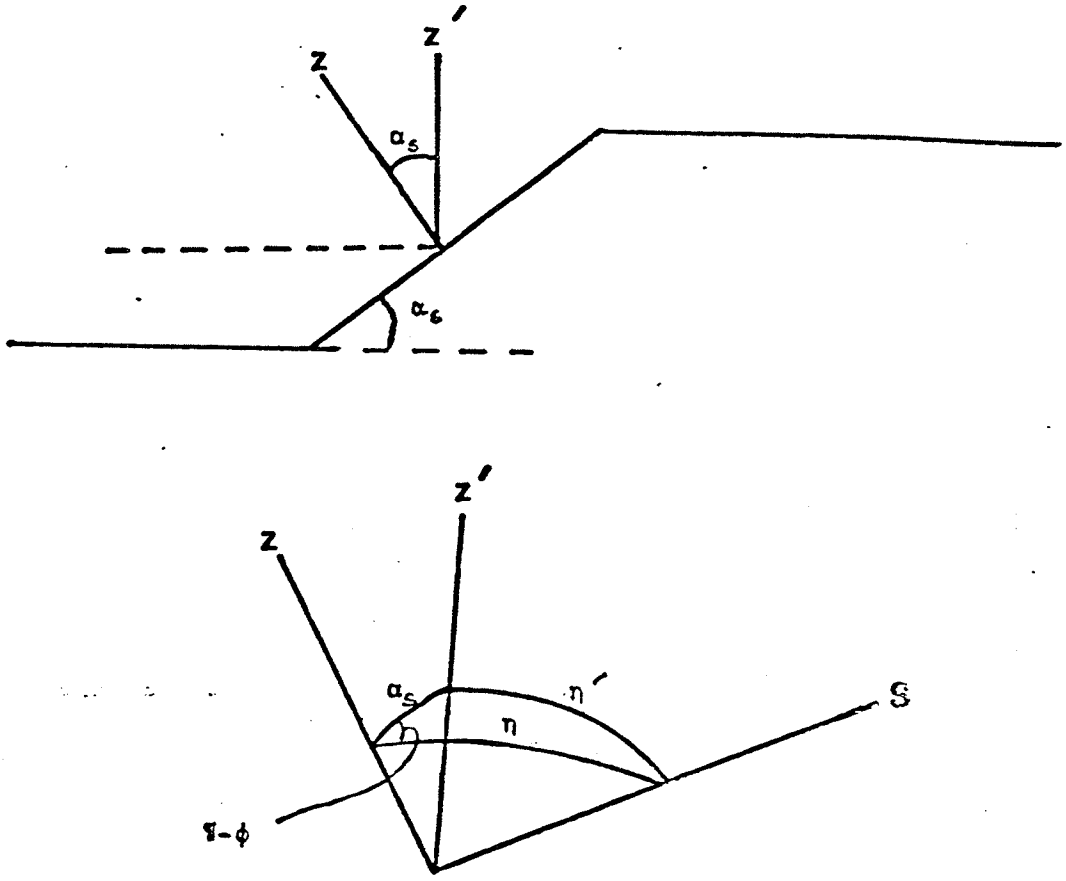

Figure E.1. Top: The hillside slope, showing the flat-land below the slope, and the perpendicular axes in two reference systems.
Bottom: The spherical triangle used in calculating $\bar{\eta}$, which is the downslope horizon in the primed system.

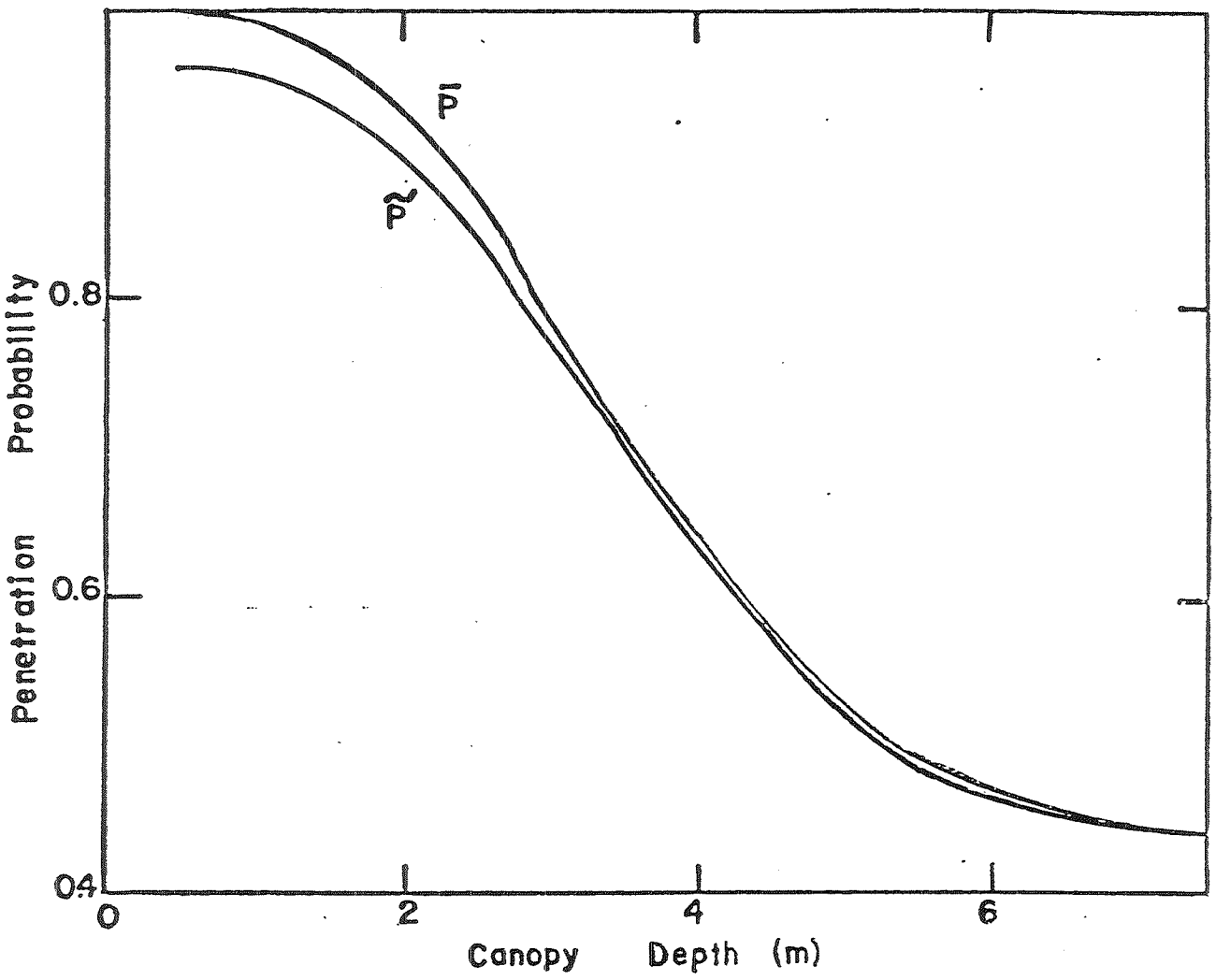

Figure E.2. A comparison of $\bar{P}$, which is the average penetration probability for diffuse sky radiation, ignoring the presence of the flat-land below the slope, and $\tilde{P}$ which is based on the assumption of zero flux from flat-land forest.

of about 4%, which declines rapidly into the canopy as high source n's contribute less to the result. We regard this difference as insignificant in the overall, and deal only with $\bar{P}_i$ in further calculations.

APPENDIX F

Element Optical Characteristics

The scattering submodel requires, as input, values for the reflectivity, transmissivity and absorptivity of the scattering elements and of the ground surface. Only needles have non-zero transmissivity.

We undertook measurements of needle properties which entirely supercede those reported by Whitfield et al. (1977). We constructed an integrating sphere, following Birkebak and Birkebak (1964), based upon the substitution method. The detector was an ISCO spectroradiometer connected to the sphere by a bundle of optical fibres. The sample was a set of needles laid so closely together as to allow no detectable spaces between them.

The results of three separate measurements are presented in Fig. F1, showing a typical abrupt change in properties between visible and infrared wavelengths. The arrow indicates the wavelength of peak response of the infrared sensor used in our penetration measurements. From these measurements, we took the values for needle properties indicated in Table F1.

The reflectivities of other elements are much less critical in determining the behaviour of scattered radiation, and we were content to accept rough estimates, based on literature (e.g. Norman and Jarvis, 1975).

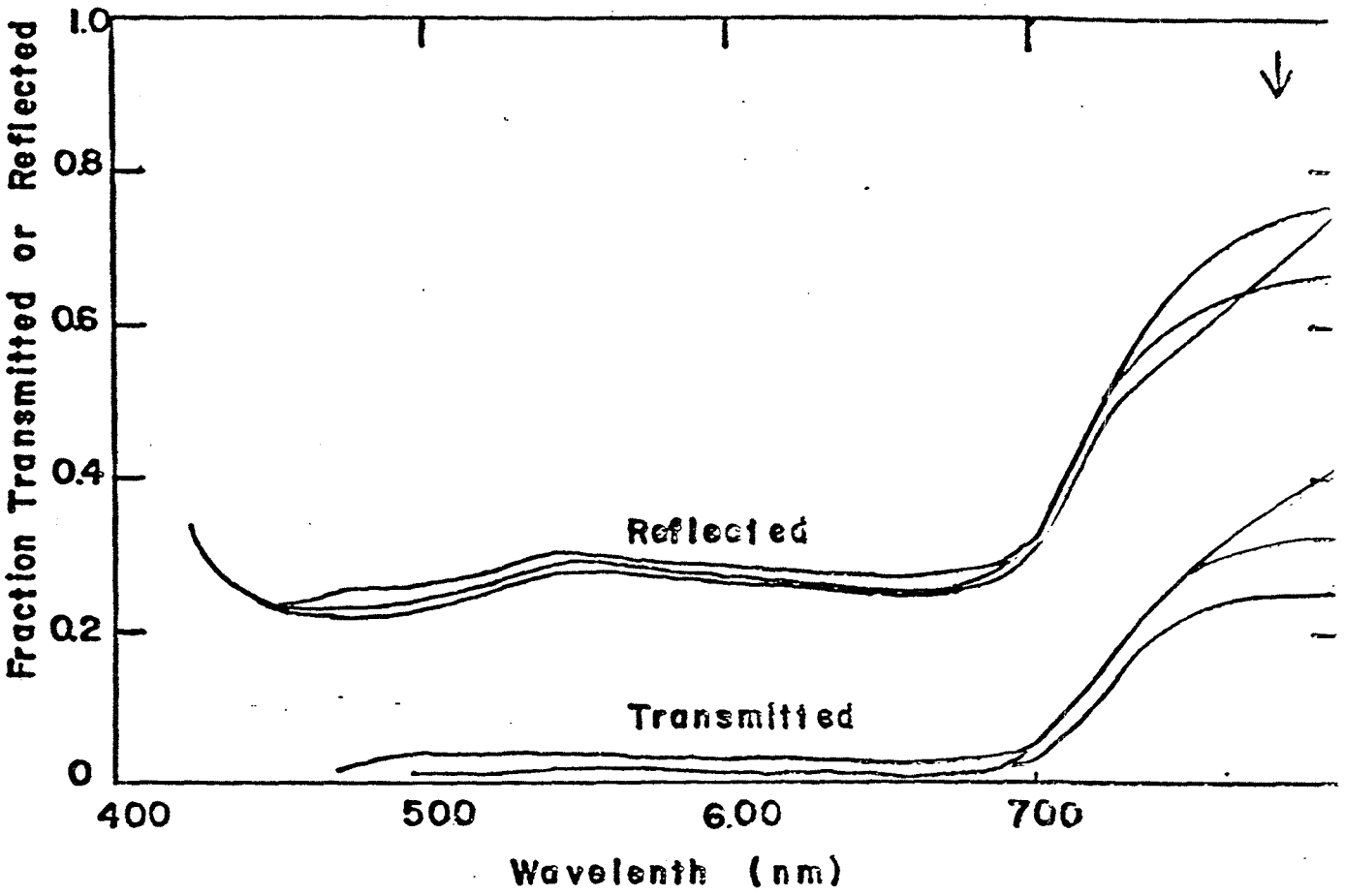

Figure F.1. Three separate measurements, by the substitution method with an integrating sphere, of reflectivity and transmissivity of jackpine needles, as functions of wavelength.

Table F1. Optical properties of the elements.

Element type	Visible		Infrared	
	τ	ρ	τ	ρ
Needle	.03	.28	.25	.45
Trunk	0	.05	0	.05
Cone	0	.1	0	.1
Live Branch	0	.05	0	.05
Dead Branch	0	.05	0	.05
Ground Surface	0	.2	0	.2